Elastic properties of triglycine sulphate

Dunk, Alan

Award date:
1987

Awarding institution:
University of Bath

ELASTIC PROPERTIES OF TRIGLYCINE SULPHATE

Submitted by

Alan Dunk

for the degree of PhD

of the University of Bath

1987

ProQuest LLC
789 East Eisenhower Parkway
P.O. Box 1346
Ann Arbor, MI 48106-1346

ACKNOWLEDGEMENTS

This was perhaps the most pleasurable part of the thesis to write (it's the last bit!) and at which stage I can express my thanks to several people who have helped or contributed unwittingly to the hopefully, successful completion of this project.

My unreserved thanks go to to my supervisor Professor G.A. Saunders for his boundless enthusiasm and helpful advice. His patience during my sporadic writing sessions was appreciated.

I also extend my thanks to E. Lambson for his help with the experimental equipment, to W. Lambson for the preparation of the crystal samples and also to B. Draper for his advice.

I also would like to thank my fellow postgrads for the various useful discussions and for their frendship. Without them my time at Bath would not have been so enjoyable. I will not name names, there has been to many of you !

ABSTRACT

The properties of a number of the adiabatic elastic stiffness constants of triglycine sulphate (TGS) have been determined over the temperature range 20 to 65 °C from measurements of the ultrasonic wave velocities in selected directions. Ten out of the thirteen elastic stiffness constants have been determined, the exceptions being c_{12},c_{13} and c_{25}. In the region of the ferroelectric phase transition (T_c = 49°C) anomalies are observed in the elastic stiffness constants, with that of c_{33} being the most pronounced.

The temperature derivatives of the elastic stiffness constants show different characteristics in the ferroelectric phase as compared to those in the paraelectric phase. For c_{11},c_{33} and c_{66} the temperature derivative magnitude is decreased in the paraelectric phase, while for c_{13},c_{15},c_{35} and c_{46} the temperature derivative changes sign and becomes positive. The magnitudes of the temperature derivatives for c_{44} and c_{22} are observed to be the same on both sides of the transition.

A method has been developed for obtaining the hydrostatic pressure derivatives ($\partial C_{IJ}/\partial P$) of the elastic stiffness constants of a monoclinic crystal from the hydrostatic pressure dependences of the ultrasonic wave velocities. This method has been applied to investigate the properties of ($\partial C_{IJ}/\partial P$) over the temperature range 20 °C to 65 °C. The pressure derivatives of the elastic

stiffness constants increase with temperature; all derivatives show an anomaly at the phase transition varying from a slight effect in $\partial c_{22}/\partial P$ to the larger change in $\partial c_{44}/\partial P$.

At room temperature all thirteen of the monoclinic elastic stiffness constants have been determined along with their pressure derivatives. The results are used to describe the elastic behaviour of TGS. Accidental pure mode directions have been found at 9.4° and 106.5° .

CONTENTS

1 ACKNOWLEDGEMENTS

2 ABSTRACT

4 CONTENTS

7 INTRODUCTION

CHAPTER 1: THE CRYSTALLOGRAPHIC STRUCTURE OF TGS

10 1.1 Introduction

10 1.2 Reference axis for TGS

12 1.3 The crystallographic structure

CHAPTER 2: THE DEFINITION AND MEASUREMENT OF ELASTIC CONSTANTS

16 2.1 Introduction

17 2.2 Homogeneous strain

21 2.3 Thermodynamic definition of elastic constants

26 2.4 Propagation of elastic waves in crystals

30 2.5 Hydrostatic pressure derivatives of "effective" SOEC

CHAPTER 3: EXPERIMENTAL METHODS

32 3.1 Introduction

33 3.2 Sample preparation

35 3.3 Transducers

36 3.4 Bonding materials and procedure

37 3.5 Pulse echo overlap system

39 3.6 Hydrostatic pressure system

41 3.7 Measurement of hydrostatic pressure

45 3.8 Temperature controller

47 3.9 Experimental errors and their correction

CHAPTER 4: EVALUATION OF ELASTIC CONSTANTS

51 4.1 Introduction

52 4.2 Determination of the elastic constants

61 4.3 Determination of the elastic constants c_{12}, c_{25} and c_{23}

70 4.4 Consistency checks on measured velocities and obtained elastic constants.

72 4.5 A procedure for determination of the hydrostatic pressure derivatives of the elastic stiffness constants for a monoclinic crystal.

CHAPTER 5: EXPERIMENTAL METHODS

76 5.1 Introduction

77 5.2 Measurement of the elastic properties of TGS at room temperature

79 5.3 Measurement of the temperature dependence of the elastic stiffness constants

82 5.4 Measurement of the temperature dependence of pressure derivatives of elastic stiffness constants

CHAPTER 6: DISCUSSION OF ULTRASONIC PROPERTIES AND ELASTIC BEHAVIOUR OF TGS

84 6.1 Introduction

86 6.2 Theortical models of the phase transition

91 6.3 Discussion of the present results

95 6.4 Elastic properties of TGS

101 APENDIX 1: Determination of the elastic compliances.

105 APENDIX 2: Computer programs

135 REFERENCES

INTRODUCTION

Triglycine sulphate $(NH_2CH_2COOH)_3H_2SO_4$ (abbreviated to TGS) at room temperature is a ferroelectric crystal belonging to the monoclinic system and space group $P2_1$. Ferroelectricty is observed along the direction of the 2-fold polar axis (monoclinic b-axis). At 49 ^oC TGS undergoes a second-order phase transition into a paraelectric, non-piezoelectric phase. The transition temperature is pressure dependent. The phase above the transition has monoclinic symmetry and belongs to the centrosymmetrical class 2/m. TGS has proved to be a popular material to work with as it is a convenient model system for the study of a second order ferroelectric phase transition and perhaps more importantly good quality crystals are easily grown. It has a number of technological applications, in particular as the pyroelectric sensing element in infrared vidicon cameras.

Previous experimental work concerned with the measurement of the physical properties of TGS can clearly be split into two main groups. The first group is concerned with the measurement of the magnitude of selected physical properties over a wide temperature range (or even just at one selected temperature). The second area of work is concerned with measuring a particular property very accurately over a narrow temperature range centred on the phase transition. The experimental data is then used either to confirm the predictions made by a specific model, or in some cases

used to suggest whether a particular model provides a comprehensive enough physical picture. The present work falls into the latter category and provides the most comprehensive experimental data to date on the elastic properties of TGS over the temperature range 20 to 65 °C.

Experimentally the elastic stiffness constants have been obtained using standard pulsed ultrasonic techniques, while their pressure derivatives have been found from the pressure-induced changes in the ultrasonic wave velocities. For a monoclinic crystal, which is characterized by 13 independent elastic stiffness constants, extraction of the elastic stiffness constants and their pressure derivatives from ultrasonic velocity data is rather complex. However, procedures which can be used to obtain the elastic stiffness constants have been suggested by several workers. A method for finding the pressure derivatives is given here and is used to find them for triglycine sulphate . The second-order elastic stiffness constants of a crystal determine the slopes of the acoustic phonon dispersion curves in long wavelength limit; their hydrostatic pressure dependences provide information on the shift of the mode energies with compression.

Previously the elastic stiffness constants have been measured in both the ferroelectric (Konstantinova et al (1960), Luspin and Hauret (1977) and Tylczynski (1981) and paraelectric phases (Haussuhl and Albers (1977)). There are piezoelectric contributions to the elastic stiffness constants in the ferroelectric phase. These

have been considered in part in a Brillouin scattering determination of the elastic stiffness constants but not in the ultrasonic measurements of Konstantinova et al (1960). Haussuhl and Albers (1977) have found that calculations of the piezoelectric corrections are unsatisfactory and suggest a requirement for high precision determination of the piezoelectric and dielectric constants for TGS under accurately defined dielectric conditions. In view of this, they have restricted their work to a determination of the elastic stiffness constants in the paraelectric phase. The Brillouin scattering measurement of Luspin and Hauret (1977), which include measurements of c_{11}, c_{22} and c_{33} in both phases suggest that the piezoelectric contributions in ferroelectric TGS are not large. Hence in these present measurements of the elastic stiffness constants, piezoelectric stiffening effects have not been taken into account. Results are used to provide a comprehensive picture of the elastic behaviour and its pressure dependences in TGS on both sides of the phase transition.

CHAPTER 1

THE CRYSTALLOGRAPHIC STRUCTURE OF TGS

1.1 Introduction

Triglycine sulphate $(NH_2CH_2COOH)_3H_2SO_4$, usually abbreviated to TGS, at room temperature is a ferroelectric crystal belonging to the monoclinic class with space group $P2_1$. The polar axis lies along the direction of the two fold axis (monoclinic b axis), and the crystal is piezoelectric. TGS undergoes a ferroelectric phase transition at 49°C; the transition temperature is pressure dependent. In the paraelectric phase TGS still possesses monoclinic symmetry but then belongs to the space group $P2_1/m$ which has a centre of symmetry so that TGS is not piezoelectric in this phase. Detailed dielectric and thermal studies of TGS show that the ferroelectric transition is of the second order type; the deviation of the structure from the ferroelectric phase to the paraelectric phase is slight.

1.2 Reference axis for TGS

Two possible orientations for the crystallographic a and c axis have been quoted in the literature. The earliest is due to Wood and Holden (1957), who reported the following lattice constants;

a= 9.15 Å , b=12.69 Å , c=5.73 Å β =105° 40′ 20″

and showed that there are two formula units per unit cell. In a later study Hoshino et al (1959) used a different selection of the a and c axis, claming that

this simplifies the description of the crystal structure; in this axial reference frame the lattice constants are:

$a=9.14\ \mathring{A}$, $b=12.64\ \mathring{A}$, $c=5.73\ \mathring{A}$, $\beta=110^{\circ}\ 23'$

The two axes are related by the transforms $a=a'+c'$, $b=b'$ and $c=-c'$ where the primed axis are those used by Wood and Holden (1957). The relationship between the two axial reference forms is shown in Fig 1.1. In acoustic studies of TGS the monoclinic axis due to Wood and Holden (1957) is used by all workers.

To define a set of three orthogonal axes (x,y,z), which are often more convenient than the crystallographic monoclinic axes in description of the physical properties of the crystal, the standards set out by the Institute of Radio Engineers (IRE) can be used. For a monoclinic crystal the IRE convention is that the axis of symmetry is taken to be the b axis (which is also used as the orthogonal y axis), with the smaller of the other two denoted as the c axis. The rectangular axes y and z will then coincide with b and c respectively with the x axis at an angle of 15° to the a axis in the ac plane (see fig 1.2). This orthogonal (x,y,z) axial set has been used by Tylczynski (1981), Luspin and Hauret (1977).

Konstantinova et al (1960) who made the first recorded determination of the elastic constants of TGS adopted a different reference orthogonally axial set (see fig 1.3), where the x and y axis are in opposite directions to those proposed by the IRE standards. In using the orthogonal reference axis due to Konstantinova et al instead of the IRE recomended axis

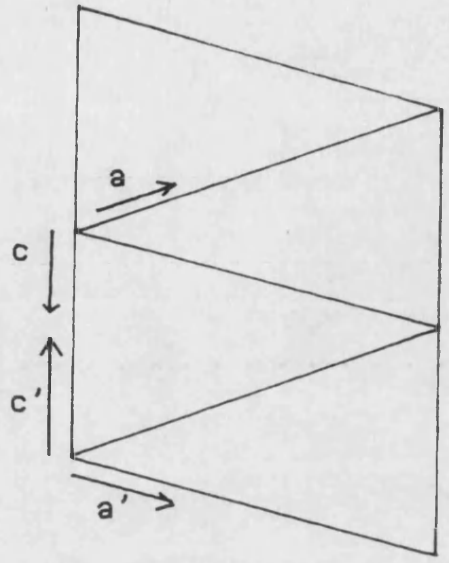

Fig 1.1 Relationship between the unit cell proposed by Wood and Holden (1957) and that of Hoshino et al (1959).

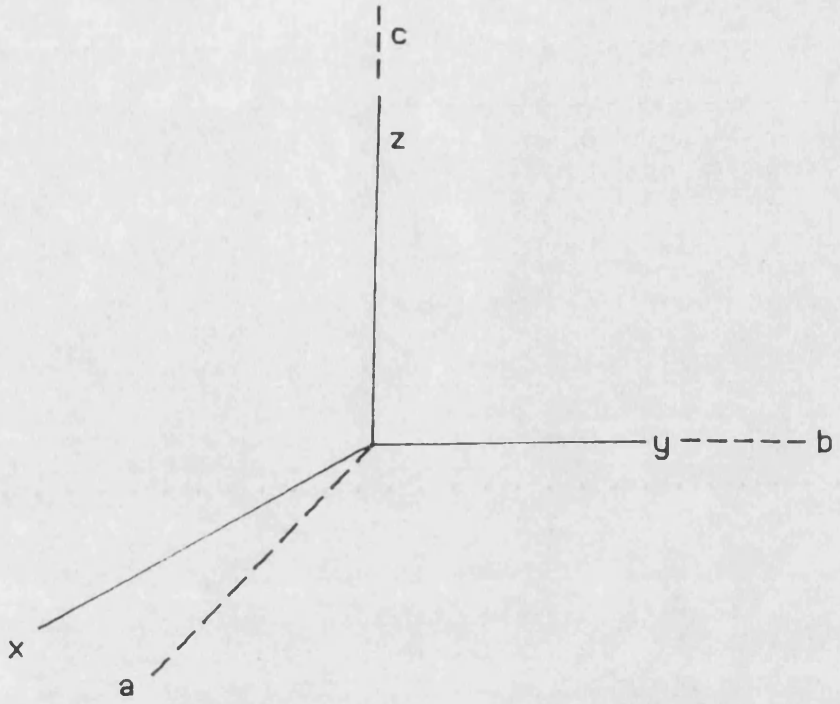

Fig 1.2 Relationship between the orthogonal axis and crystallographic axis as used by Tylczynski (1981) Luspin and Hauret(1977).

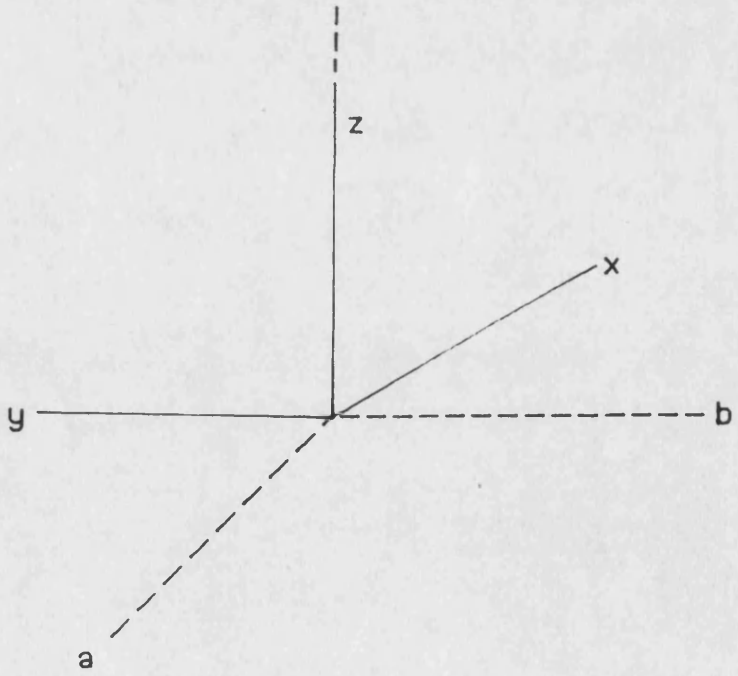

Fig 1.3 Relationship between the orthogonal axis and crystallographic axis as used by Konstantinova et al (1960).

has the effect of reversing the sign of 4 elastic constants ($c_{15}, c_{25}, c_{35}, c_{46}$).

A different orthogonal axial set (see fig 1.4) has been used by Haussuhl and Albers (1977). In their work they adopted the following axis

x//a , y//b , z//a x b

Early on in this work the orthogonally axis of Konstantinova et al was adopted before i was aware of the IRE recommendations. On this discovery i considered it unwise to change to the recommended orthogonal axial set as this ran the risk of introducing confusion over which axial system measurements were taken in.

1.3 The crystallographic structure

The crystal structure of TGS has been examined in detail by Hoshino et al (1959), and was later refined by Itoh and Mitsui (1973). By considering over 2,000 reflections from a scattered x-ray beam, using a fourier synthesis technique, they were able to establish the position of all the individual atoms in the unit cell and their temperature dependence. Fig 1.5 shows the structure of TGS viewed down the c axis, the hydrogen bonds are also indicated (note the axial system is that due to Hoshino et al (1959)).

Before examing the structure of TGS in general, first consider the glycine molecule, NH_2CH_2COOH , which commonly crystallizes in two different forms. One is a structure in which the two carbon atoms and the two oxygen atoms are approximately coplaner, with the

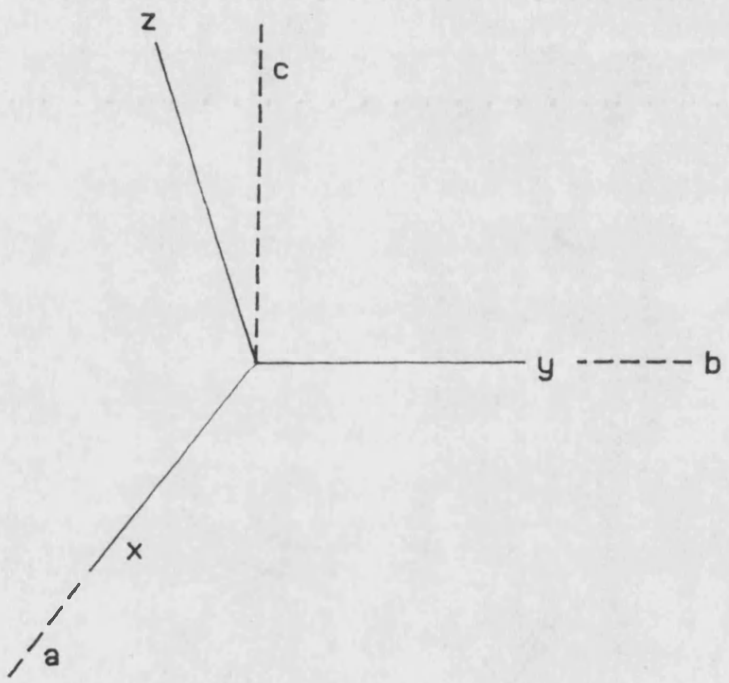

Fig 1.4 Relationship between the orthogonal axis and crystallographic axis as used by Haussuhl and Albers (1977).

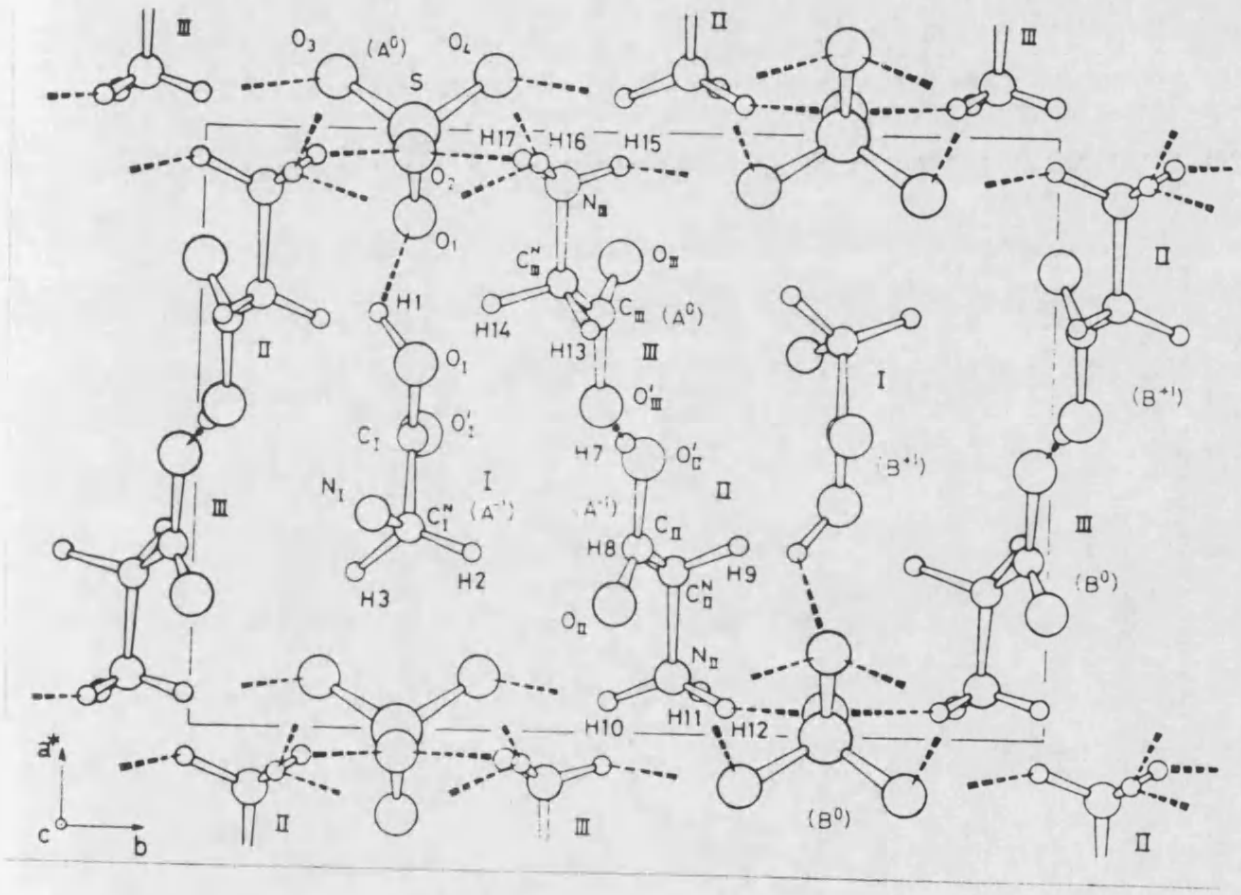

FIG 1.5 Crystal structure of TGS at 19°C (due to Itoh and Mitsui (1973)) viewed along the c-axis. Dashed lines show the hydrogen bonds of which those terminated at half way indicate that the mate of the bond exists in the upper or lower cells.

nitrogen atom significantly displaced out of this plane; while the other form is a structure in which all carbon, nitrogen and oxygen atoms are close to planar. In TGS, which has three glycine groups, two (designated II and III in Fig 1.5) are quasi-planar and one (designated I) is non-planar, where the nitrogen atom is displaced by 0.5 A out of the plane. The two planar glycine molecules II and III are arranged almost perpendicular to the polar b-axis and are in mirror image positions. They are connected by a hydrogen bond between oxygen atoms (O_{II} and O_{III}) which are some 0.25 nm apart. There are other hydrogen bonds in the detailed structure (see the original papers or fig 1.5 for their probable arrangement).

It has been shown by Itoh and Mitsui (1973), that bond distances and angles in glycine I change slightly with temperature, whereas variations in glycines II and III are significant. The atomic positions of glycine I depend significantly upon temperature.

It has been shown that chemically two protons from the H_2SO_4 group are more properly associated with the glycines and the compound is often written as glycine di-glycinium sulphate $(NH_2CH_2COOH)(NH_3CH_2COOH)^{2+}_2.SO^{2-}_4$. The glycine I is more correctly a glycinium ion. The other proton can be thought of as the O_{II}-H-O_{III} proton and resonates between glycine II and glycine III, at least in the paraelectric phase. This suggests that glycine II and III are by nature intermediate in state between glycinium $NH_3CH_2COOH^+$ and glycine zwitter ion $(NH^+_3CH_2COO^-)$. This

description of the glycines II and III is termed glycinium-glycine.

The only strong intermolecular bonding between the glycine I and other molecules is the hydrogen bond through H1 (see fig 1.5), if the NH_3 group is rotating. Glycine I is associated with the reversible dipole. It is by considering the glycine I group that the most convincing evidence is provided that the phase transition is of the order-disorder type. Above the Curie temperature the b-plane through the glycine molecules is a plane of mirror symmetry, and Itoh and Mitsui (1973) found that, if an analysis of the X-ray scattering data is commenced assuming a planar glycine I in the mirror plane, the refined structure shows that all the oxygen, carbon and nitrogen atoms occupy double-minimum sites straddling the mirror plane. In effect this means that above the curie temperature the mirror plane refers only to the average structure, with the glycine molecule under going a thermally activated hopping motion between equivalent potential wells on either side of the b plane. In the paraelectric phase there is no disorder with respect to the glycine II and III molecules.

Near the transition temperature a comparison of the average amplitudes of motion for the heavy atoms show that by far the greatest amplitude is for the glycine I nitrogen atom in the b-direction. This in turn has lead to the suggestion of the possibility of a driving role for the nitrogen double-well instability in the mechanism of the ferroelectric transition. Although the hydrogen

bond may still play an important part, effects of deuteration on the dielectric properties have been found to be small which suggest that this role may be less than a dominant one.

The sulphate ion which sits on the mirror plane has been shown to deviate from tetrahedral symmetry, this is to be expected since there are hydrogen bonds of unequal strength existing between the sulphate oxygens and the other atoms. The shape of the sulphate ion changes only slightly with temperature.

The transition of each atom during the polarization reversal has been investigated by many workers. It has been shown that there is a negligible shift of the sulphur atom. The three glycine groups I,II,III are all participating in the polarization reversal , but the main reversible dipole is that associated with glycine I. With reference to the model of Itoh and Mitsui (1973), it can be seen how polarization reversal takes place with respect to glycine I, and it can be easily recognized that the polarization reversal does not correspond to a simple rotation of the molecule , but to a combination of the shift of the $C-CO_2$ plane along the b-axis (accompanied by a small rotation) and a kind of isomer transformation in glycine I involving the rotation along the $C-C^N$ bond which brings N_I to the opposite side of the $C-CO_2$ plane. As shown in fig 1.5 the only strong intermolecular bonding between the glycine I and other molecules is the hydrogen bond through H1 , if the NH_3 group is rotating. Probably this fact makes the large movement of the glycine I molecule easy.

CHAPTER TWO

THE DEFINITION AND MEASUREMENT OF ELASTIC CONSTANTS

2.1 Introduction

The elastic constants of solids were introduced originally to describe the experimentally observed linear relationship between stress and strain. This relationship is known as Hooke's law (Nye, 1957 , Huntington 1958)

$$\sigma_{ij}=c_{ijkl}\epsilon_{kl} \qquad 2.1$$

$$(i,j,k,l=1,2,3)$$

where σ_{ij} and ϵ_{kl} are second rank stress and strain tensors , while c_{ijkl} is a fourth rank elastic stiffness tensor. The associated elastic constants are termed second order (SOEC). It has been shown that Hooke's law is only valid for infinitesimal strains ; for finite strains the relationship becomes non-linear. If one includes higher order elastic constants in the definition, the non-linear region of the stress-strain relationship observed in practice for finite strains, can be accounted for. This specification of higher order elastic constants has been investigated in detail by Murnaghan (1951) and Wallace (1972).

The elastic constants of a material are dependent on its physical state and the conditions under which they are considered. Therefore the definition of elastic constants is best expressed in thermodynamic terms. Such definition permits elastic constants of any order, whereas only SOEC are required by Hooke's law. The inclusion of higher order elastic constants are required

to describe successfully the non-linear stress-strain region observed for finite strains. The thermodynamic definition of elastic constants is described in this chapter.

2.2 Homogeneous strain

For thermodynamic calculations the crystal is considered to be a homogeneous anisotropic medium, which when subjected to a uniform stress suffers a homogeneous strain.

Consider a body occupying a space, with every particle referenced to a rectangular Cartesian frame. The position P of a particle in the unstrained state is located at (a_1,a_2,a_3) with it's position described by the vector $\underline{a}$. On straining the body this particle moves to a new position Q with coordinates (x_1,x_2,x_3) described by the vector $\underline{x}$. The deformation of the body is known if x_1,x_2,x_3 are known functions of a_1,a_2,a_3

$$x_i=x_i(a_1,a_2,a_3) \qquad 2.2$$

It is assumed that the deformation is continuous, a neighbourhood is transferred into a neighbourhood and that the transformation is one-to-one; ie the functions in 2.2 are single-valued, continuous and have unique inverse for every point in the body

$$a_i=a_i(x_1,x_2,x_3) \qquad 2.3$$

As the strain is homogeneous the vectors $\underline{a}$ and $\underline{x}$ are related by a linear transform according to

$$x_i=\Sigma\ \epsilon_{ij}a_j \qquad 2.4$$

where ϵ_{ij} is the deformation gradient from the unstrained

configuration to the strained configuration. It also follows from the definition of the transform that

$$\alpha_{ij} = \frac{\partial x_i}{\partial a_j} \qquad 2.5$$

The stress induced displacement from $\underline{a}$ to $\underline{x}$ is described by a displacement vector $\underline{u}$, defined by

$$u_i = x_i - a_i \qquad 2.6$$

with displacement gradients given by

$$u_{ij} = \frac{\partial u_i}{\partial a_j} \qquad 2.7$$

Differentiation of equation 2.6 with respect to a_j, and comparison of the result with equation 2.5 leads to the relationship between the transformation coefficients and the displacement gradients.

$$\alpha_{ij} = \delta_{ij} + u_{ij} \qquad 2.8$$

where δ_{ij} is the Kronecker delta

Describing the strain of a body in terms of the displacement gradients u_{ij} is not satisfactory as, if the body is not deformed but undergoes a translation or rotation, the displacement gradients are non-zero and the internal energy of the body remains unaltered. A more useful strain parameter is one which is zero for a body rotation or translation.

This strain parameter is obtained by considering the change in distance between any two points in the body. In the unstrained state consider an infinitesimal line element dS_o, connecting the point $P(a_1, a_2, a_3)$ to a neighbouring point $P'(a_1+da_1, a_2+da_2, a_3+da_3)$. The square

of the length dS_o at PP' in the unstrained configuration is given by

$$dS_o^2 = da_1^2 + da_2^2 + da_3^2 \qquad 2.9$$

On straining, the points P and P' are deformed to $Q(x_1, x_2, x_3)$ and $Q'(x_1+dx_1, x_2+dx_2, x_3+dx_3)$ respectively, the square of the length dS of the new element QQ' is

$$dS^2 = dx_1^2 + dx_2^2 + dx_3^2 \qquad 2.10$$

on differentiating Eq's 2.2 and 2.3

$$dx_i = \frac{\partial x_i}{\partial a_j}\, da_j \qquad 2.11 \qquad da_i = \frac{\partial a_i}{\partial x_j}\, dx_j \qquad 2.12$$

introducing the Kronecker delta δ_{ij}, 2.9 can be rewritten using 2.11

$$dS_o^2 = \delta_{ij} da_i da_j = \delta_{ij} \frac{\partial a_i \partial a_j}{\partial a_l \partial a_m} dx_l dx_m \qquad 2.13$$

and similarly for 2.10 using 2.12

$$dS^2 = \delta_{ij} dx_i dx_j = \delta_{ij} \frac{\partial x_i}{\partial a_l} \frac{\partial x_j}{\partial a_m} da_l da_m \qquad 2.14$$

The difference between the squares of the length elements may be written after several changes in the suffixes for dummy indices either as

$$dS^2 - dS_o^2 = \left(\delta_{lm} \frac{\partial x_l}{\partial a_i} \frac{\partial x_m}{\partial a_j} - \delta_{ij} \right) da_i da_j \qquad 2.15$$

or

$$dS^2 - dS_o^2 = \left(\delta_{ij} - \delta_{lm} \frac{\partial a_l}{\partial x_i} \frac{\partial a_m}{\partial x_j} \right) dx_i dx_j \qquad 2.16$$

The following strain tensors can be defined

$$\eta_{ij} = \frac{1}{2}\left(\frac{\partial x_m \partial x_m}{\partial a_i \partial a_j} - \delta_{ij}\right) = \frac{1}{2}(\alpha_{mi}\alpha_{mj} - \delta_{ij}) \qquad 2.17$$

$$\epsilon_{ij} = \frac{1}{2}\left(\delta_{ij} - \frac{\partial a_m \partial a_m}{\partial x_i \partial x_j}\right) \qquad 2.18$$

so that

$$dS^2 - dS_o^2 = 2\eta_{ij} da_i da_j \qquad 2.19$$

$$dS^2 - dS_o^2 = 2\epsilon_{ij} dx_i dx_j \qquad 2.20$$

where η_{ij} are the elements of the Lagrangian strain (measured in the initial coordinate system), and ϵ_{ij} are the elements of the Eulerian strain, measured in the strained coordinate system.

The tensors η with components η_{ij} is symmetric. From 2.17 it can be seen that if $\eta_{ij}=0$, then α_{ij} represents a body rotation only. In this way the strained state of a crystal may be completely specified in terms of the initial unstrained state and either the transformation coefficients α_{ij} or the displacement gradients u_{ij}.

2.3 Thermodynamic definition of elastic constants

In the following consideration, to simplify matters, it is assumed that there are no other contributions to thermodynamic potentials, including those which arise from magnetic and electric fields.

Brugger (1964) introduced the thermodynamic definitions for higher order elasticity by using the combined first and second laws of thermodynamics ie

$$dU=TdS-dW \qquad 2.21$$

The work dW, is that done by the crystal in changing the configuration from $\underline{a}$ to $\underline{a}+\Delta\underline{a}$ against an applied stress Γ. The applied stress is represented by the thermodynamic stress tensor Γ_{ij} which is an analogous to σ_{ij} used in Hooke's law .

If the surface of the crystal in the initial unstrained configuration $\underline{a}$ is s , with a surface element denoted by ds, the i'th component of force on ds , due to the applied stress is given by

$$f_i=\sum_j \Gamma_{ij}ds_j \qquad 2.22$$

The displacement gradients corresponding to the strain Δa is Δu_{ij}, the displacement of ds in the i direction is

$$\Delta a_i=\sum_k \Delta u_{ik}a_k \qquad 2.23$$

The work done by the crystal against the stress applied to ds is

$$-\sum_i f_i\Delta a_i = -\sum_{ijk} \Gamma_{ij}ds_j\Delta u_{ik}a_k \qquad 2.24$$

Note that the customary convention is that positive stresses are directed outward from the crystal surface. The total work done by the crystal is the integral of this expression over the surface s. This surface integral

is transformed to a volume integral by Gauss's theorem and becomes

$$\Delta W=-\int_S \sum_{i,j,k} \Gamma_{ij}\Delta u_{ik}a_k ds_j=-\int_V \sum_{i,j} \Gamma_{ij}\Delta u_j dV = -\sum_{i,j} \Gamma_{ij}\Delta u_{ij}V(a) \qquad 2.25$$

since Γ_{ij} and Δu_{ij} are constants.

Finally, since Γ_{ij} is symmetric, the anti-symmetric part of Δu_{ij} gives no contribution to the Σ_{ij} in 2.25 , so Δu_{ij} may be replaced by $\Delta\eta_{ij}$ to a first order approximation. Writing the work 2.25 in differential form gives

$$dW=-V \sum_{i,j} \Gamma_{ij}d\eta_{ij} \qquad 2.26$$

If the case of unit mass is considered and ρ_o is the density of the unstrained solid , then rewriting 2.26

$$dW = -(1/\rho_o) \sum_{i,j} \Gamma_{ij}d\eta_{ij} \qquad 2.27$$

From the first and second laws of thermodynamics (2.1)

$$dU=TdS + (1/\rho_o)\Gamma_{ij}d\eta_{ij} \qquad 2.28$$

and for the Helmoltz free energy

$$dF=(1/\rho_o)\Gamma_{ij}d\eta_{ij}-SdT \qquad 2.29$$

In a similar way Brugger (1964) obtained the following potentials for the enthalpy H and Gibbs free energy

$$dH=TdS-(1/\rho_o)\ \eta_{ij}d\Gamma_{ij} \qquad 2.30$$

$$dG=-SdT -(1/\rho_o)\ \eta_{ij}d\Gamma_{ij} \qquad 2.31$$

The potentials and all extensive variables are taken per unit mass and all the above are summed over repeated indices i and j. The thermodynamic tensors Γ_{ij} are given by

$$\Gamma_{ij} = \rho_o \left(\frac{\partial U}{\partial \eta_{ij}}\right)_{s,\eta} = \rho_o\left(\frac{\partial F}{\partial \eta_{ij}}\right)_{T,\eta} \qquad 2.32$$

The subscript η' means that all other components of η_{ij} are held constant while differentiating with respect to η_{ij}.

The state functions U and F must remain unchanged if the body is translated or rotated, without deformation. This rotational invariance suggests that U and F depend on the strained configuration x only through the initial configuration a and the rotational-independent strains η_{ij}. Therefore, the functional dependence may be written:

$$U(x,S)=U(a,\eta_{ij},S) \qquad 2.33$$

and

$$F(x,T)=F(a,\eta_{ij},T) \qquad 2.34$$

As the strains involved are small, it is possible to express the strain dependence of the thermodynamic potentials in the form of a Taylor series expansion about the state of zero strain. For example

$$U(S)=U(S,\eta)-U(S,0)=\left(\frac{\partial U(S,\eta)}{\partial \eta_{ij}}\right)_{\eta=0}\eta_{ij} + \qquad 2.35$$

$$(1/2)\left(\frac{\partial^2 U(S,\eta)}{\partial \eta_{ij}\partial \eta_{kl}}\right)_{\eta=0}\eta_{ij}\eta_{kl} + (1/6)\left(\frac{\partial^3 U(S,\eta)}{\partial \eta_{ij}\partial \eta_{kl}\partial \eta_{mn}}\right)_{\eta=0}\eta_{ij}\eta_{kl}\eta_{mn}$$

but for an unstrained crystal in thermodynamic equilibrium

$$\left(\frac{\partial U(S,\eta)}{\partial \eta_{ij}}\right)_{\eta=0} = 1/\rho_o\ (\sigma_{ij}(\eta))_{\eta=0} = 0 \qquad 2.36$$

As elastic coefficients of order n (n> 2) are defined thermodynamically as the n'th partial derivatives of the appropriate thermodynamic potential with respect to the Lagrangian strains, evaluated at zero strain (or with respect to the tensions, evaluated at zero tension).The

energy density can be written as

$$\rho_o U(S) = (1/2) c_{ijkl}\eta_{ij}\eta_{ik} + (1/6) c_{ijklmn}\eta_{ij}\eta_{ik}\eta_{mn} + \quad 2.37$$

where

$$c_{ijkl} = \rho_o \left(\frac{\partial^2 U(S,\eta)}{\partial\eta_{ij}\partial\eta_{kl}}\right)_{\eta=0} \qquad 2.38$$

and

$$c_{ijklmn} = \rho_o \left(\frac{\partial^3 U(S,\eta)}{\partial\eta_{ij}\partial\eta_{kl}\partial\eta_{mn}}\right)_{\eta=0} \qquad 2.39$$

The first two terms in the above energy expansion are the second order and third order adiabatic elastic constants respectively.

If a similar approach is adopted with the expression for Helmoltz free energy the expressions for the isothermal elastic constants are obtained

$$c_{ijkl} = \rho_o \left(\frac{\partial F(T,\eta)}{\partial\eta_{ij}\partial\eta_{kl}}\right)_{\eta=0} \qquad 2.40$$

$$c_{ijklmn} = \rho_o \left(\frac{\partial^3 F(T,\eta)}{\partial\eta_{ij}\partial\eta_{mn}}\right)_{\eta=0} \qquad 2.41$$

The form of these expansions is similar to that for potential energy in terms of interatomic displacement, and thus it is ultimately possible to relate the elastic constants to the interatomic forces in a solid.

Since the strains and the thermodynamic tensions are symmetric ie $\eta_{ij}=\eta_{ji}$ and $\Gamma_{ij}=\Gamma_{ji}$, only six of each set of nine variables are independent, and it is customary to use the Voigt notation:

11=1 : 22=2 : 33=3 : 23,32=4 :13,31=5 :12,21=6

By convention , in the contracted notation the strain η_{ij} is written as η_x. The magnitudes of the η_x are related to

the magnitudes of the η_{ij} by

$$\eta_{ij} = 1/2\ (1+\delta_{ij})\eta_I \qquad 2.42$$

Also by Brugger (1964)

$$r_{ij} = r_I \qquad 2.43$$

where lower case subscripts run from 1 to 3 and capital subscripts run from 1 to 6.

Applying this contracted notation to the elastic constants gives

$$c_{IJ} = c_{ijkl} \qquad 2.44$$

In the reduced notation the thermodynamic potential becomes

$$c_{JP} = \rho_o \left(\frac{\partial^2 U}{\partial\eta_J \partial\eta_P}\right)_{s,\eta=0} \qquad 2.45$$

$$c_{IJK} = \rho_o \left(\frac{\partial^3 U}{\partial\eta_I \partial\eta_J \partial\eta_K}\right)_{s,\eta=0} \qquad 2.46$$

The potentials U,F,H and G are extensive properties of the system , and so their n'th partial derivatives are independent of the order of differentiation ; ie the strain energy must be independent of the path by which the state of strain is attained. Thus all permutations of the contracted suffixes lead to the same constants, so for second order

$$c_{IJ}=c_{JI}$$

and third order

$$c_{IJK}=c_{IKJ}=c_{KJI}=c_{KIJ}=c_{JIK}=c_{JKI}$$

The maximum numbers of independent SOEC and TOEC are 21 and 56 respectively. These numbers are further reduced by crystal symmetry. Brugger (1965a) lists the

independent SOEC and TOEC for all of the crystallographic systems. For a crystal of monoclinic symmetry there are 13 second order elastic constants and 32 third order elastic constants. These are

$$C_{11}\ ,\ C_{12}\ ,\ C_{13}\ ,\ C_{15}\ ,\ C_{22}\ ,\ C_{23}\ ,\ C_{25}$$

$$C_{33}\ ,\ C_{35}\ ,\ C_{44}\ ,\ C_{46}\ ,\ C_{55}\ ,\ C_{66}$$

and

$$C_{111}\ ,\ C_{112}\ ,\ C_{113}\ ,\ C_{115}\ ,\ C_{122}\ ,\ C_{123}\ ,\ C_{125}\ ,$$

$$C_{133}\ ,\ C_{135}\ ,\ C_{144}\ ,\ C_{146}\ ,\ C_{155}\ ,\ C_{166}\ ,\ C_{222}$$

$$C_{223}\ ,\ C_{225}\ ,\ C_{233}\ ,\ C_{235}\ ,\ C_{244}\ ,\ C_{246}\ ,\ C_{255}$$

$$C_{266}\ ,\ C_{333}\ ,\ C_{335}\ ,\ C_{344}\ ,\ C_{346}\ ,\ C_{355}\ ,\ C_{366}$$

$$C_{445}\ ,\ C_{456}\ ,\ C_{555}\ ,\ C_{566}$$

2.4 Propagation of elastic waves in crystals

The SOEC of a crystal are determined from measurements of the velocity of ultrasonic waves propagating in that crystal. The wave motion is assumed to be adiabatic and to cause only infinitesimal displacements of volume elements in the crystal.

The equation of motion comes from the fundamental law of dynamics: force equals mass times acceleration. It can be shown that the force exerted on a unit volume of a stressed material is

$$f_i = \frac{\partial \sigma_{ij}}{\partial a_j} \qquad 2.47$$

When the effect of gravity and any other forces on the body are neglected, this force gives rise to an

acceleration along the i 'th axis for a unit volume of mass ρ_o.

$$\rho_o \frac{\partial^2 u_i}{\partial t^2} = \frac{\partial \sigma_{ij}}{\partial a_j} \qquad 2.48$$

From equations 2.8 and 2.17 the Lagrangian strain parameter is

$$\eta_{ij} = (u_{ij} + u_{ji} + u_{ki}u_{kj}) \qquad 2.49$$

but as u_{ij} are infinitesimal strains, $u_{ki}u_{kj}$ are second order infinitesimal , and in a first order approximation can be ignored. This leads to the usual infinitesimal strain definition

$$\epsilon_{ij} = (u_{ij} + u_{ji})/2 \qquad 2.50$$

$$\epsilon_{ij} = 1/2 \left(\frac{\partial u_i}{\partial a_j} + \frac{\partial u_j}{\partial a_i} \right) \qquad 2.51$$

by differentiating 2.1 with respect to a ,and comparing with 2.48, the equation of motion is obtained as

$$\rho_o \frac{\partial^2 u_i}{\partial t^2} = c_{ijkl} \frac{\partial^2 u_l}{\partial a_j \partial a_k} \qquad 2.53$$

Assuming a plane wave solution , travelling in the direction of a unit vector $\underline{N}$, where u_o is the particle displacement amplitude, then the particle displacement vector $\underline{a}$ at any point can be described by

$$u = u_o \exp i(wt - kN.a) \qquad 2.54$$

Substituting 2.54 into 2.53 and carrying out the differentiation

$$\rho V^2 u_i = c_{ijkl} N_j N_k u_l \qquad 2.55$$

Introducing the second rank tensor

$$\Gamma_{il} = c_{ijkl} N_j N_k \qquad 2.56$$

This is known as Christoffel equation. Rewriting 2.55

$$\Gamma_{il} u_l = \rho V^2 u_i \qquad 2.57$$

The velocities and particle polarization of those plane waves which propagate along a direction $\underline{N}$ in a crystal with elastic stiffness tensor c_{ijkl} are obtained by searching for the eigenvalues and eigenvectors of the tensor Γ_{il} . For a given propagation direction, there are three roots of the equation

$$\Gamma_{il} - \rho V^2 \delta_{il} = 0 \qquad 2.58$$

Each velocity obtained is related to an eigenvector which defines the particle displacement direction (ie the wave polarization). Since the eigenvalues must be real and positive , there are generally three waves propagating in the same direction with different velocities and mutually orthogonal polarizations. The particle displacement vector u is generally not parallel or perpendicular to the polarization direction N.

A pure mode occurs when the particle displacement vector $\underline{u}$ is parallel (for longitudinal modes) or perpendicular (for shear modes) to the wave propagation direction $\underline{N}$. If all three waves propagating in a direction $\underline{N}$ are pure, the direction is referred to as being a pure mode one. Brugger (1965a) investigated the necessary conditions for a pure mode direction to occur for most of the crystal classes. This was achieved by identifying the conditions necessary for the longitudinal mode to be pure (u.N=0). As the wave solutions are orthogonal, it automatically implies that the two shear modes are also pure and hence a pure mode direction is identified. Brugger (1965a) found that the number of pure

mode directions is dependent on the crystal symmetry. Pure mode directions are important as in these directions the energy flux vector is perpendicular to the plane wavefronts. When this occurs maximum energy is transferred from the transducer to the mode under measurement.

In monoclinic crystals there are very few pure mode directions (see Fig 2.1) only one of which, denoted as β , is directly determined by crystal symmetry. This occurs along the two fold symmetry axis (Y direction). Any other pure mode directions present are a function of the elastic stiffness of the material, not on crystal symmetry; these are termed accidental pure mode directions. It can be shown that there are two accidental pure mode directions which can be designated by α and γ in the XZ plane. Also in this plane for all directions the Y polarized shear is a pure mode. Other accidental pure mode directions may occur in monoclinic crystals, but these lie off any of the axial planes and are of little experimental use.

In general the waves propagated are quasi-pure modes ,for these the energy flux vector is not perpendicular to the plane wavefronts. Ideally one would use pure modes if at all possible , so that no energy is lost from the transducer in exciting modes which are not under measurement with the subsequent energy loss. Unfortunately it is not usually possible with monoclinic crystals to use pure modes as practically every mode is quasi-pure.

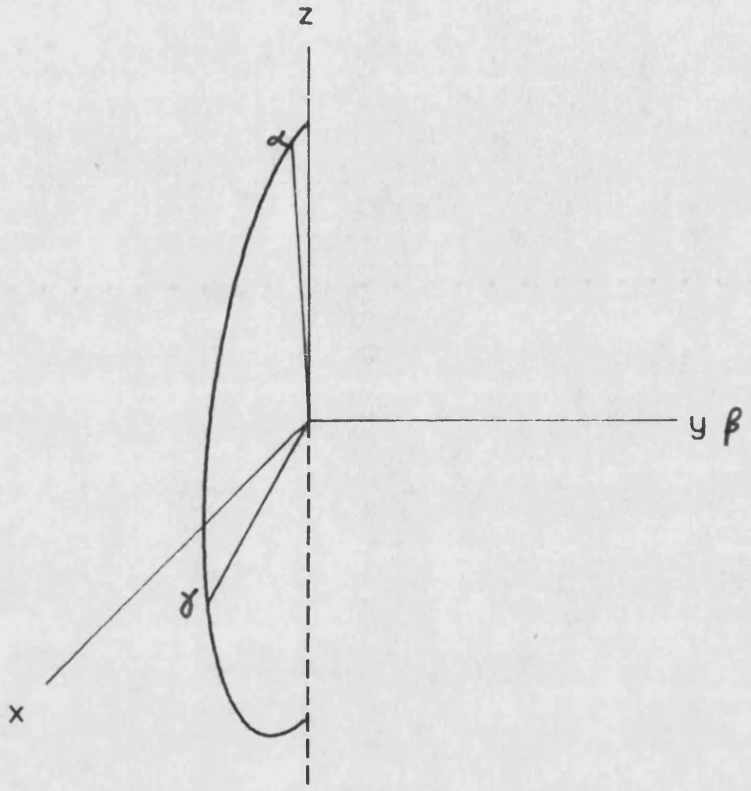

Fig 2.1 Pure mode directions for monoclinic crystal. β lies along the two fold y axis α and γ lie in the xz plane.

Expressions linking the wave velocities and elastic stiffness for monoclinic crystals are listed in table 2.1. The evaluation procedure used to obtain the elastic constants is rather lengthy; an example is discussed in chapter four.

2.5 Hydrostatic pressure derivatives of "effective" SOEC

Thurston and Brugger (1963) defined a "natural velocity" $W=l_o/t$, where l_o is the path length of the wave in the unstressed crystal and t is the measured experimentally measured transit time over the distance l_o. The product $\rho_o W^2$ being the measure of elastic stiffness in that direction.

The quantity $(\rho_o W^2)_{p=o}$ does not represent the actual pressure derivative of the SOEC as no correction has been applied to account for the increase in pressure altering the sample path length and density. Using a relationship developed by Thurston (1965) the pressure derivatives can be calculated , without the need to calculate the path length and density for each data point used. The equation is

$$\left[(\rho V^2)' - (\rho_o W^2)'\right]_{p=0} = \rho_o W_o^2 \left(S^T_{KKii} - 2N_K N_M S^T_{KMii}\right)_{p=0} \quad 2.59$$

Here W_o is the natural velocity, defined as the path length at zero pressure divided by the transit time at pressure p. The quantity in parentheses on the right is the volume compressibility minus twice the linear compressibility in the direction N. The volume compressibility component corresponds to the effects of changes of density and the linear compressibility part to

the pressure induced change in path length. It is the isothermal compliance coefficients which appear in 2.59 because the pressure derivatives are measured at constant temperature. The advantage of using the natural velocity is that $(\rho_o W^2)_{p=o}$ is directly related to the initial slope and intercept of the measured frequency versus pressure graph.

$$(\rho_o W^2)'_{p=o} = 2\rho_o V^2 f'/f_o \qquad 2.60$$

combining 2.59 and 2.60

$$(\rho V^2)_{p=o} = \frac{\partial c_{IJ}}{\partial p}_{p=o} = \rho_o V^2 (2f'/f_o + \chi^T - 2N_k N_m s_{kmi1}) \qquad 2.61$$

where χ^T is the volume compressibility, f' is the gradient of the least square line of a plot of frequency versus pressure and fo is the intercept at zero pressure.

From Nye (1957) the volume compressibility is

$$\chi = s_{11} + s_{12} + s_{13} + 2(s_{11} + s_{12} + s_{13}) \qquad 2.62$$

and the linear compressibility by

$$\beta = (s_{11} + s_{12} + s_{13})l_1 + (s_{12} + s_{22} + s_{23})l_2 + (s_{13} + s_{23} + s_{33})l_3 + (s_{15} + s_{25} + s_{35})l_3 l_1 \qquad 2.63$$

Strictly equation 2.61 is only true for modes where the pressure derivative of the particle displacement vector $\underline{u}$ and the propagation direction $\underline{N}$ are zero. These conditions are only true for the longitudinal mode propagating in the Y direction. As the errors in excluding this effect are small in comparison with the experimental error to a first order approximation they can be ignored and equation 2.61 used for all mode directions.

CHAPTER THREE

EXPERIMENTAL METHODS

3.1 Introduction

To obtain the SOEC and the associated pressure derivatives of a solid, it is usual to measure the transit time of an ultrasonic wave through the solid and the change of this transit time with pressure.

Prominent names in the early development of pulsed ultrasonic techniques are Huntington(1947), Mason and McSkimin (1947), Arenberg (1950), Roderick and Truell (1952), May (1958) and Papadakis (1964,1966,1967). Several variations of the basic technique have been described in the literature, the simple pulsed - echo method remains the most common type : a suitable equipment can easily be constructed from commercially available apparatus.

In this work the ultrasonic wave measurements were made using a single ended pulse echo method in which a transducer is bonded onto a sample which has flat and parallel faces. A radio frequency tone burst of 1 to 2 microseconds duration is applied to the transducer, which excites mechanical stress waves at the sample surface. Then stress waves propagate through the bulk and are reflected at the opposite face. This echo, and subsequent impinging echoes are detected by the same transducer which produces an electrical voltage in proportion to the amplitude of the stress wave. This voltage, after amplification, can be used to display the echoes on an oscilloscope from which the attenuation and the transit

time of propagation of the stress waves through the solid can be determined.

This chapter describes the pulse echo overlap technique used to measure the transit time of ultrasonic waves in TGS samples and the equipment used to stress hydrostatically these samples. The temperature dependences of the hydrostatic pressure derivatives of wave velocity for several directions have also been investigated. The method by which the temperature of the hydrostatic pressure cell was measured, varied and controlled is also described here.

3.2 Sample preparation

Large crystals of TGS can be grown from water solutions prepared by reacting an aqueous glycine solution with the correct amount of sulphuric acid. A suitable crystal growth rate can be achieved by slow evaporation of the solvent at constant temperature or by slowly lowering the temperature at constant supersaturation. The habit of the crystals obtained depends on the growth procedure and is generally quite complex owing to the presence of many faces in this material. Further details of the habits of TGS can be obtained by referring to Furuhata (1970), Konstantinova et al (1960) and Mitsui et al (1976). TGS crystals have a pronounced cleavage plane parallel to [010] direction, thus crystal plates orientated perpendicular to this polar axis can easily be obtained by cleavage of larger crystals without needing to know the directions of the

monoclinic a and c axes. The crystals used in this work were kindly provided by Dr R.J. Jones of R.S.R.E. Malvern.

Orientation of a monoclinic crystal by X-Ray methods alone can be rather difficult. With carefully grown crystals, where pronounced faces are present, the crystal morphology (see Fig 3.1) can be used to assist in the identification of the crystallographic axis. The TGS crystal used in this work was orientated by first identifying the two fold symmetry axes using the X-Ray back reflection Laue technique , then the a and c axes were identified by reference to the crystal morphology (Konstantinova et al (1960) corresponding to our crystal.

As shown in chapter 4, for monoclinic crystals it is possible to obtain all the SOEC's by propagating ultrasonic waves along six crystallographic directions, namely [001], [010], [100], [101], [110] and [011]. This required four rectangular parallelepipeds to be cut (with a diamond wheel) of dimensions about 1 cm x 1 cm x 1 cm, one with faces perpendicular to the [001], [010] and [100] directions and the other three such that they had a pair of faces perpendicular to the [101],[011] and [110] directions respectively. Faces were polished flat and parallel on a cast - iron plate, first with aloxite and water for a few seconds and finished with 14 μm diamond paste. The parallelism between the faces was checked by making several measurements at different points on the surface using a micrometer; parallelism was found to be

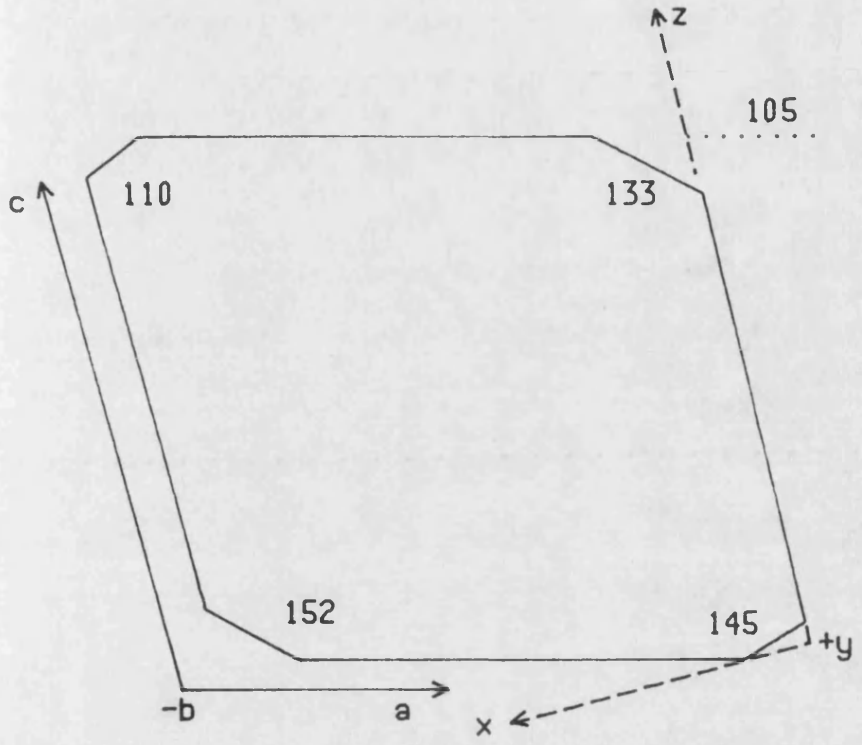

Fig 3.1 The Mythology of TGS viewed down -b axis. The crystallographic axes being due to Wood and Holden (1957) and the reference orthogonal axis due to Konstantinova et al (1960).

better than 10^{-3} radians.

Transducers are effectively phase sensitive devices, which places narrow tolerance upon the parallelism of the sample faces. For example if the phase of the wavefront striking the transducer is positive on one half and negative on the other due to path difference, then the net response of the transducer would be zero.

3.3 Transducers

The generation and detection of the ultrasonic waves was accomplished by the use of a gold plated piezoelectric quartz transducer with a diameter of 6 mm, attached by a bonding medium to one of the sample faces (see fig 3.2). The fundamental frequency of the transducers used in this work was 10 MHz. The resonant frequency of the transducer is determined by its thickness , the fundamental frequency is given by

$$d = \lambda/2$$

where d is the thickness and λ is the wavelength of the stress wave in quartz at the resonant frequency. For longitudinal modes the transducer thickness is 0.29 mm and for shear modes 0.19 mm.

The transducer acts as a piston source and generates a wave which is essentially plane and has a width equal to the diameter of the piston up to a distance (r) given by

$$r = a^2/\lambda$$

where a is the radius of the vibrating piston. The size of the transducer was chosen such that the vibrations were plane in nature but not large enough when it is

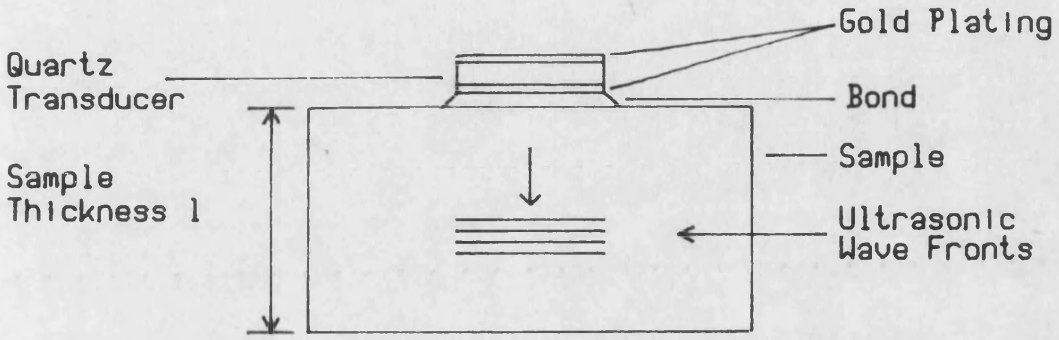

Fig 3.2 Schematic representation of sample bond and transducer which has gold plated electrodes with a guard ring.

compared with the crystal cross section to risk side-wall reflections (Waterman 1959).

This work required the generation of longitudinal and shear modes of vibration in TGS crystals. For longitudinal modes X-cut quartz transducers are employed, while Y-cut transducers were used for shear modes. The transducers were obtained commercially from Gooch and Housego Ltd, Ilminister, England.

3.4 Bonding materials and procedure

To attach the transducer to the sample, a bonding medium is required. The bonding medium will couple the acoustic energy from the transducer into the sample. The principle of making a good bond is based on the minimum loss of the acoustic energy converted by a transducer. For a bond to meet these requirements, the bond thickness should be small compared to the acoustic wavelength (this avoids losses due to reflection). It should also be uniform, and more importantly, it should not damage or react with either the sample surface or the transducer. A viscoelastic resin , Dow Resin 276-v9 (Dow - Corning Corp) meets these requirements and was used exclusively as a bonding medium. It was found that the bond resisted attack from the castor oil used as the pressure transmitting medium in the hydrostatic pressure bomb and remained usable for 4 to 5 days at least. For general information on bonding agents which can be used see Bateman (1966) or Farley (1973).

The essential procedure for bonding is to form a uniform thin bond between the transducer and sample without damaging either since the quartz transducer is fragile. The shear transducers have to be bonded with the polarization vector parallel to that of the ultrasonic waves required. The procedure for bonding the transducer to the sample was to ensure first that the faces of the transducer and sample were free from grease and dust by cleaning with acetone. A small amount of the bonding medium was placed on to the sample face. As the resin used has a high viscosity at room temperature, it was warmed using a hair-dryer to approximately 40° C; then the transducer was placed onto the resin and by gently rotating the transducer (use of a Q tip was efficacious) a thin film (2 to 3 μm) bond was produced. After the bond had cooled, any excess bonding material which had been extruded from the bond was removed. At the end of the experimental run, the transducers were easily removed by warming the sample and gently sliding off the transducer from the sample face.

3.5 Pulse echo overlap system

A pulse echo overlap system was used to measure the wave transit times and their temperature and pressure derivatives of TGS. This equipment is based on the development of a system first proposed by May (1958) and Papadakis (1964,1966,1967) and was constructed using commercially obtainable equipment from the Matec Corporation of America. A schematic diagram of the pulse

echo overlap system is shown in Fig 3.3. An accuracy of better than 1 part in 10^4 can be obtained using this equipment.

In the pulse echo overlap system used the pulse modulator and receiver (Matec model 6600) generate a tone burst containing 10 MHz cycles, which are at the resonant frequency of the transducer. The tone burst is generated at a rate derived from the high resolution frequency source (0.5Hz to 50 Mhz , Matec model 110) which has been divided by a factor of 100 or 1000 by the frequency divider , (Matec Model 122B and referred to as the divided sync line). The division ratio is chosen such that the repetition rate does not exceed 1000 Hz. If the x axis of the oscilloscope is triggered from the divided sync line , and the output from the transducer (after amplification) is connected to the Y input of the oscilloscope , the whole echo train can be displayed on the oscilloscope screen (see fig 3.4). The repetition rate of the r.f pulse generator is low enough to ensure that all echoes have decayed before the next tone burst is applied. By using the video output from the Matec pulse modulator and receiver , the rectified echoes can be coupled via an exponential generator (Matec model 1204B) to the oscilloscope so that attenuation can be measured manually.

By using the dual delay strobe generator (Matec model 122B), which produces two time variable square wave pulses, delayed from the divided sync pulse, which when linked to the Z modulation of the oscilloscope enable

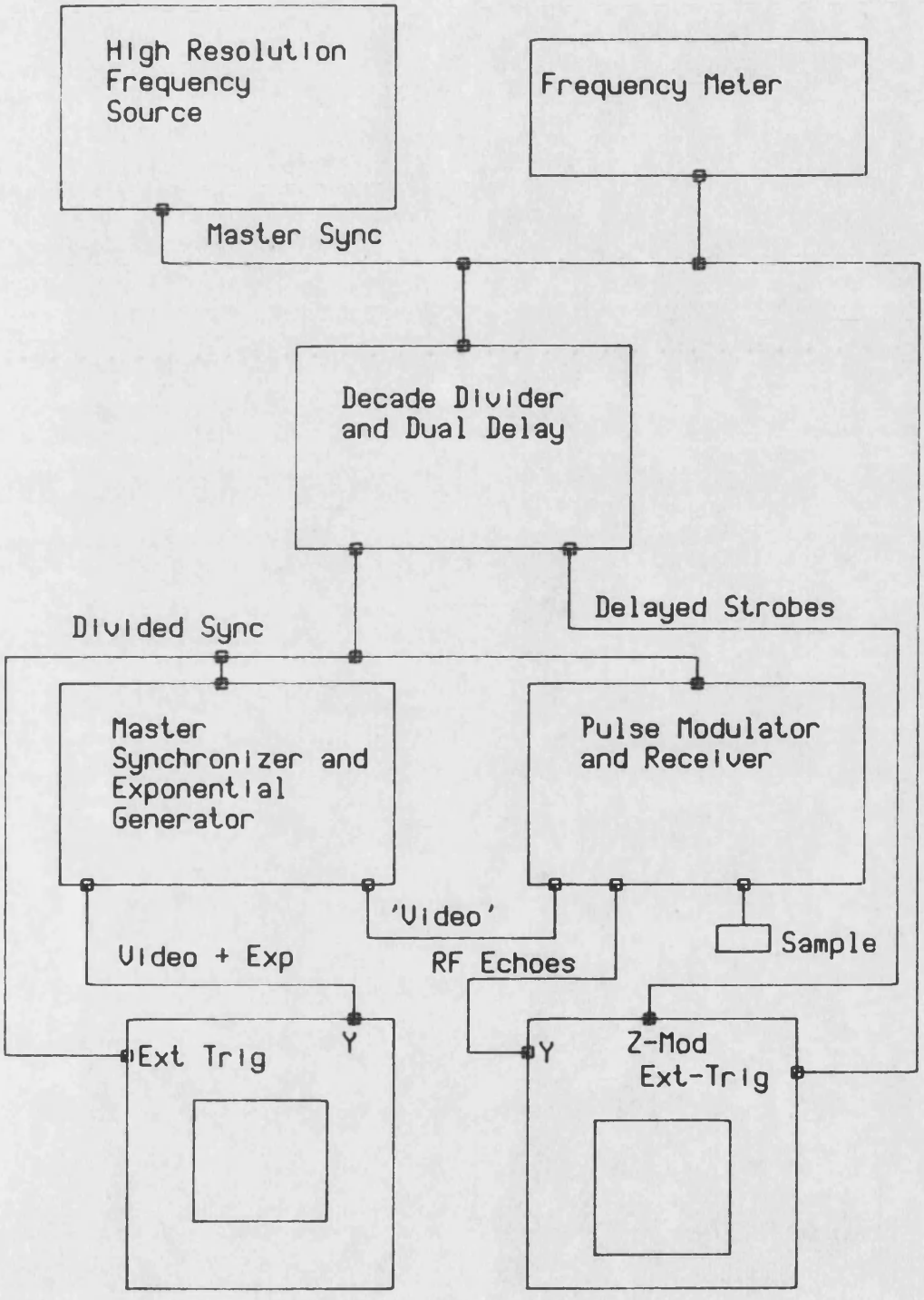

Fig 3.3 Schematic Diagram of the Pulse Echo Overlap Apparatus.

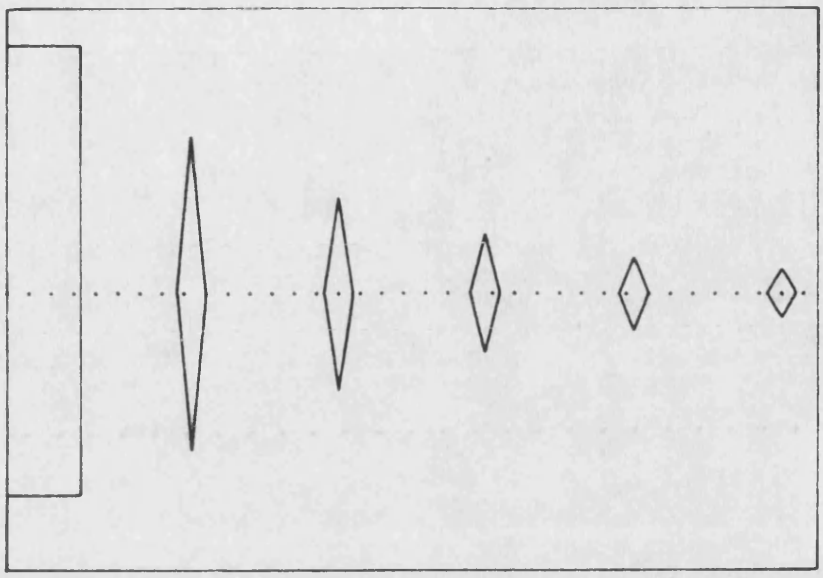

Fig 3.4 Schematic diagram of the echo train as viewed on an oscilloscope.

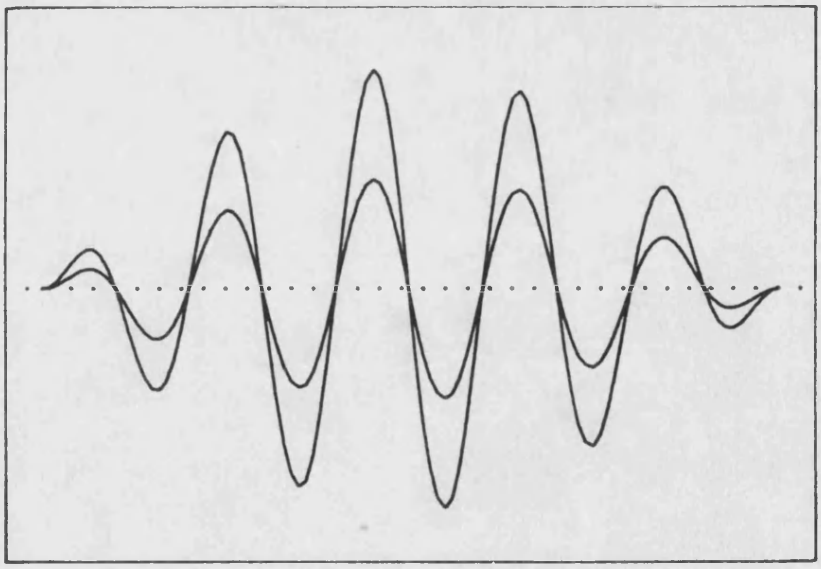

Fig 3.5 Schematic representation of two successive overlaped echoes as seen on an oscilloscope.

intensification of any two chosen sections of the echo train. By decreasing the oscilloscope brightness , it is then possible to eliminate all echoes but the two intensified ones. If the oscilloscope is now triggered from the master sync line, and the time between each sync pulse corresponds to the transit time, then the result is an illusion of the two intensified echoes superimposed on the display (see Fig 3.5), provided that the time base sweep of the oscilloscope is set to roughly the echo width. By careful adjustment of the high resolution frequency source, cycle-to-cycle matching can be obtained. The echo transit time is then given by the reciprocal of the oscillator frequency. The frequency is measured on a racal 9913 frequency counter. The typical repetition frequency is of the order 80 to 300Khz.

3.6 Hydrostatic pressure system

The pressure system used in this work is of the simple piston and cylinder type, using castor oil (for low pressure) as the pressure transmitting fluid.

A schematic diagram of this pressure system is shown in Fig 3.6. It consists of a cylinder and two pistons made from EN26 nickel alloy carbon steel. The dimensions of the cylinder are , diameter 127 mm, height 115 mm with a 25.4 mm bore. There are two pistons; the lower piston rests on the base of the pressure rig with the sample holder and the manganin coil gauge mounted on it. Electrical connections to the transducer , manganin coil and the thermocouple are made into the pressure bomb

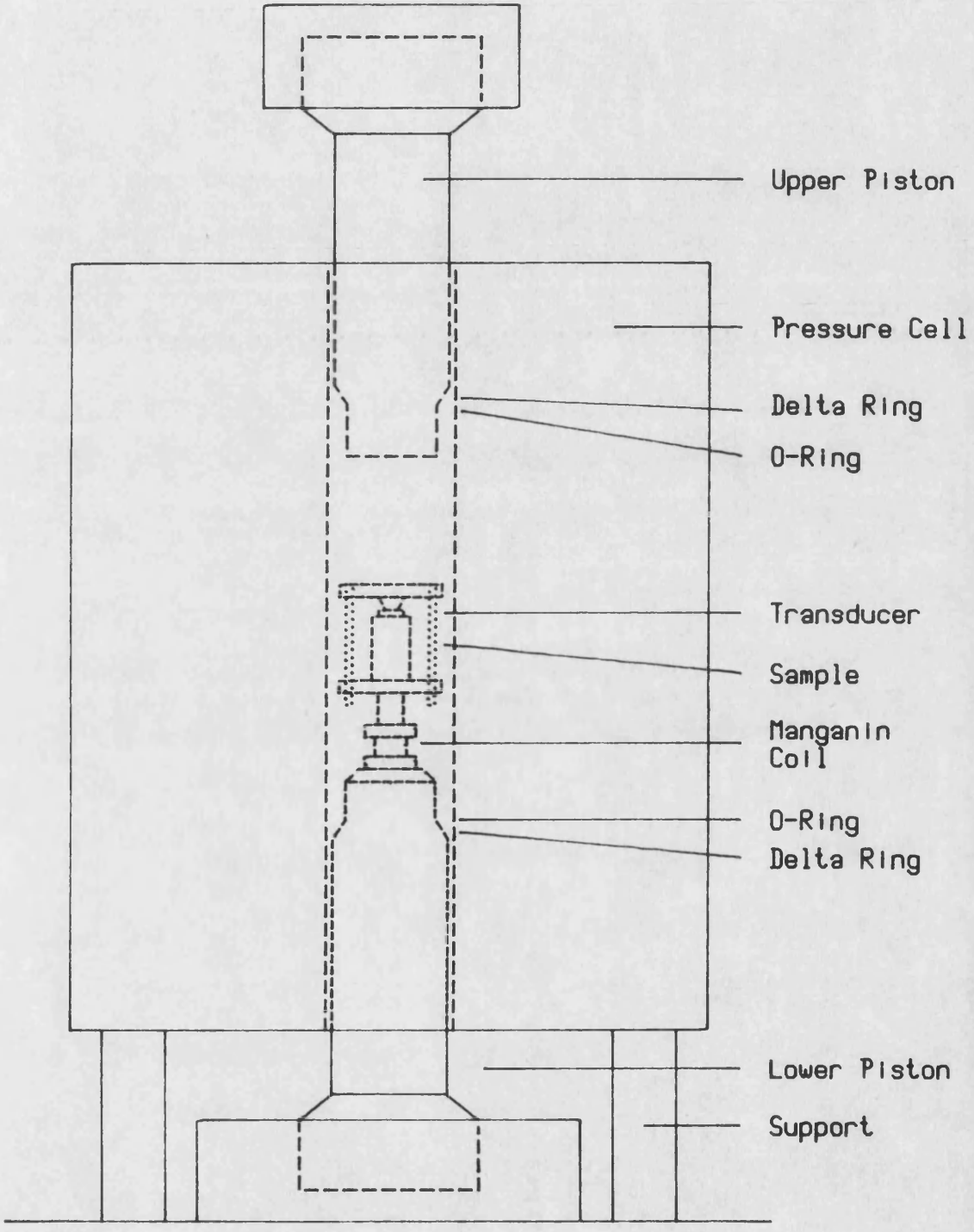

Fig 3.6 Schematic diagram of the hydrostatic pressure cell.

through beryllium - copper (2.0 to 2.5% Be, 0.3%Co, remainder Cu) plugs in ceramic insulators lapped into conical holes at the top of the lower piston. The top of the press drives down onto the top piston. Sealing between the pistons and the internal cylinder walls is achieved by using nylon delta rings and nylon O-rings on each piston. These seals were found to be satisfactory for pressures up to 2 Kbar and temperatures in the range 10°C to 70°C. The hydraulic press employed was built by Bishop Lifting Services (Bristol ,England) and is capable of supplying 50 tons. To satisfy safety requirements, the press and the pressure cell are contained within a 7mm thick steel cabinet.

The normal operational procedure was to seal the bomb and lightly pressurize the system (to about 0.2 Kbar) to test for leaks and to set the bond on the transducer. The system was then left to regain thermal equilibrium. This point was found to be particulary important when temperature runs were commenced because when the press made contact with the upper piston the heat loss mechanism altered (the mass of the press was then in thermal contact and acted as an extra heat sink) and resulted in a change of bomb temperature. After the system had regained thermal equilibrium, data acquisition commenced by pressurizing the system in steps of 0.2 Kbar. Changes in pressure caused the temperature in the pressure cell to alter. On average it took fifteen minutes for the system to return to its equilibrium temperature, at which time measurements of the pressure

and echo transit time were taken.

An important point to realize is that in some cases the change of the ultrasonic wave transit time due to a pressure increase of 0.2 Kbar is comparable to that obtained if the sample temperature changes by a few tenths of a degree C ; therefore for most modes it was necessary to keep the sample temperature stable during the course of the experiment.

During the course of the experiment , the data obtained was entered into a CBM 30XX series microcomputer (PET), running a programme hydroplot. This programme allowed, amongst other features the conversion of the resistance of the manganin coil to a pressure reading and permitted a low resolution plot of the data on the microcomputer's VDU. The data obtained could be saved on tape and transferred to another microcomputer, which was connected to a Philip's intelligent plotter, printer and disk drives. By using a programme HP ADV a plot and hardcopy of the data could be obtained. The data could be stored on floppy disc for further analysis.

3.7 Measurement of hydrostatic pressure

The measurement of the hydrostatic pressure within the pressure cell can be obtained by two methods. The first method which can be used provides an immediate but an approximately measurement of pressure. This is achieved by using the hydraulic pressure gauge situated on the pressure line between the pump and the press intensifier. When the reading of this gauge is multiplied by the

intensification factor of the intensifier and divided by the area of the piston, the result being the pressure inside the pressure cell.

The second method of pressure measurement used is based on the change of electrical resistance of a manganin wire with applied hydrostatic pressure. Manganin is an alloy, consisting of a face centred cubic solution of manganese in copper with an addition of nickel. The pressure properties of manganin were first reported by Lisell (1903) , and the alloy was first used as a pressure gauge by Bridgman (1911) and its use has become widespread since.

Manganin has several advantages for use as a pressure gauge, the principle advantages being (i) high sensitivity of resistance with pressure, (ii) low drift of the wire resistance with time or past history (Boren et al 1965) and a low hysteresis, (iii) a high degree of uniformity between coils prepared from the same batch of wire (providing they have undergone the Bridgman (1940) cycle), and (iv) a linear response with pressure.

It has been shown from static measurements that the change in manganin resistance with pressure is not far from linear up to approximately 150 Kbar (Montgomery (1963)); shock wave techniques have indicated that this behaviour extends up to 300 Kbar (Fuller (1962)). However manganin is known to be very sensitive to shear stress , and even in hydrostatic usage, the slightest strains can change its pressure coefficient by several percent.

Various values for the pressure coefficient for manganin wire have been quoted in the literature ranging from 2.1 $\times 10^{-3}$ to 2.5 $\times 10^{-3}$ Kbar^{-1}. Most of the recent work (Samara and Giardini (1964), S. Kume et al (1980), Wang (1967) indicates a value near 2.4 10^{-3} Kbar (to 2 significant figures) which is used in this work.

The pressure P within the pressure cell is given by

$$P = (\Delta R / R_{(atm)}) / 2.4 \times 10^{-3} \text{ Kbar}$$

where R(p) is the coil resistance at a pressure P , and

$$\Delta R / R_{(atm)} = (R_{(P)} - R_{(atm)}) / R_{(atm)}$$

Basically the pressure sensor used in this work consisted of a length of insulated manganin wire wound non - inductively onto a PTFE core . The coil was then subjected to the Bridgman (1940) cycle of seasoning , which involved heating the coil to 140 ^{o}C for 8 hours and then quenching in liquid nitrogen (-196 ^{o}C) for two hours. The Bridgman cycle was repeated several times. The final stage of the seasoning of the coil was to pressurize the gauge to the maximum operating pressure obtainable by the equipment (8.5 Kbar) for several hours. This had the effect of stablishing the pressure coefficient of resistance (Bridgman 1911).

The gauge used in this work had a resistance of approximately 50 ohms at atmospheric pressure , the resistance being measured by a digital multimeter with a sensitivites of 10^{-3} ohm in 100 ohms. A pressure change of 0.2 Kbar corresponded to a change in coil resistance of 0.024 Ω, which permitted the pressure to be measured to an accuracy of 0.01 Kbar. Manganin does not have

a zero temperature coefficient of resistance (Decker et al 1972). This means that all readings of pressure must be taken at the same temperature so that resistance changes due to the applied pressure are not significantly offset by variations in the coil temperature. Although the value of the temperature coefficient is dependent on temperature, it has been shown to increase with temperature. At the maximum temperature used of 65 °C a change of 1 °C causes a temperature induced change in resistance of 0.0017Ω ; this would correspond to a pressure change of 0.014 Kbar , which corresponds to the limit of resolution of the multimeter. In practice using a temperature controller stability can be obtained of 0.1 °C , so the errors due to temperature fluctuation are negligible.

It has been shown by Wang (1967) , Adams, Goranson and Gibson (1937) , Michels and Lenssen (1934) and Bridgman (1940a,b) that the pressure coefficient of manganin is independent of temperature at pressures below 10 Kbar up to about 120 °C, whereupon the pressure coefficient starts to increase with temperature. So if the gauge is operated at the same temperature , and $R_{<atm>}$ has been measured at the operational temperature, the pressure in the chamber can be measured accurately at elevated temperatures.

3.8 Temperature controller

In this work ultrasonic measurements were made in the temperature range from room temperature to 65 °C. The temperature of the pressure cell was increased by passing an electric current through a cylindrical heating element clamped onto the external walls of the pressure cylinder. Initially the temperature was controlled using a Eurotherm Ether mini 17-90B relay controller. The sensing element for the controller was a NiCr/NiAl thermocouple sandwiched between the heater element and the external walls of the pressure cylinder. The power supplied to the heater was controlled by a simple on-off operation of the relay (the power to the heater element being supplied via a variac). It was found that although the temperature at the external cylinder wall was held constant to a few degrees C, damping by the thermal mass of the system resulted in the sample temperature at the centre of the cylinder remaining constant to within 1 °C. As the temperature induced change of the ultrasonic wave velocity was greater than the contribution from the induced pressure change , this gave unsatisfactory experimental results: a different approach was required.

An alternative controller (see fig 3.7) was constructed based on the three term controller principle. The heart of this temperature controlling system was an Oxford Instrument three term controller EA 2349. This was orginally designed to use a carbon film resistance thermometer as its temperature sensing element, but was modified to accept the 1 mV per deg °C output from a

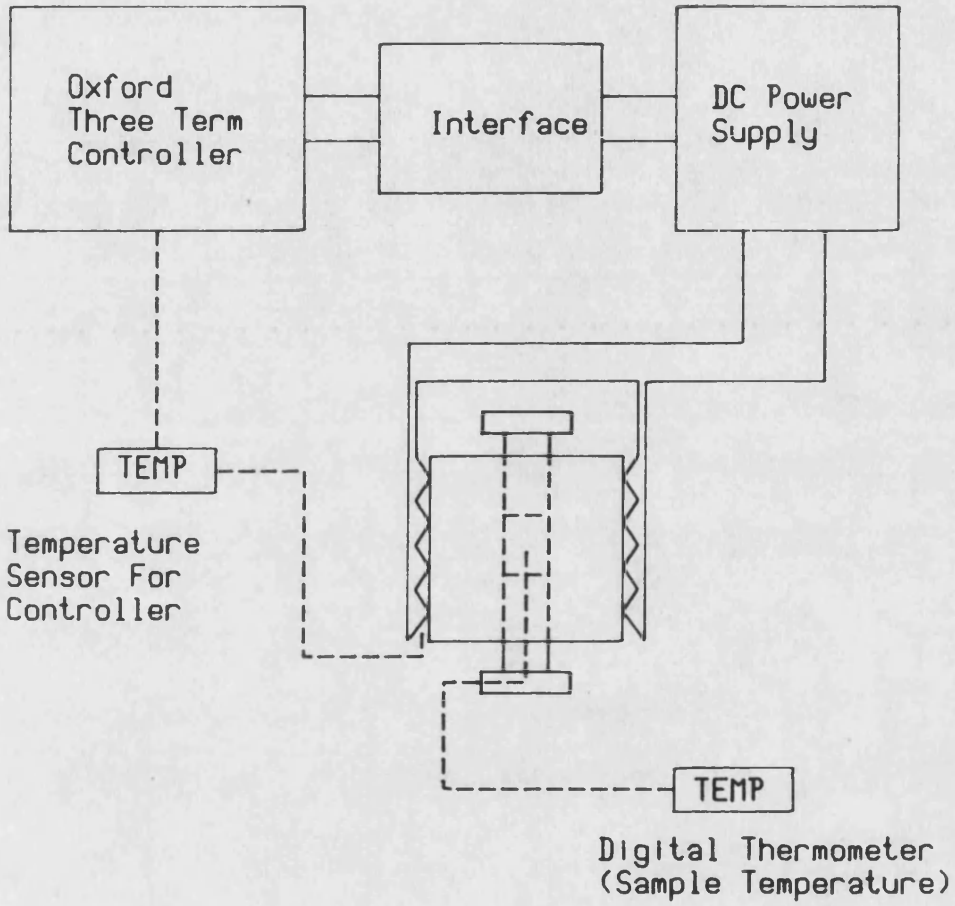

Fig 3.7 Schematic diagram of the pressure system temperature control.

digitron digital thermometer as its temperature sensing input (a NiCr/NiAl thermocouple connected to the digitron acted as the temperature sensing element). The advantage of using the output from the digitron was two fold: (i) the temperature compensating network inherent in the instrument could be ultized, (ii) the low noise amplifiers of the digitron could be used to amplify the small thermocouple voltage to a useable level. The Oxford controller was unable to supply enough power to drive the heating element directely so an interface unit was constructed to enable the controller heater output to control a 0 to 90 Volt DC power supply which was connected to the heater element. The use of the three term controller system permitted the pressure cell temperature to be held stable to within 0.1 °C.

When pressure runs where carried out at elevated temperatures, it generally took 3 to 4 hours for the pressure cell to reach and stabilize at the selected temperature starting from room temperature. It was usual practice to connect the whole controller system to a timer so that it switched on five hours before the experiment was due to begin. The hydrostatic experiment itself was performed in the usual way; after increasing the pressure the temperature was left to return to its equilibrum value before an echo transit time measurement was made. It was observed that during a pressure run the temperature of the pressure cell would gently drift downwards when pressure increased and upwards when pressure was decreased. This effect could be negated by

increasing or decreasing the controller set temperature as appropriate. It is probably due to the piston being pushed further into the pressure cylinder and increasing the heat loss path to the press, but as the controller's thermocouple is situated on the outside of the pressure cylinder walls, the controller is unable to compensate for this.

3.9 Experimental errors and their correction

There are several sources of experimental error which can affect the overall accuracy of an elastic constant measurement. These are discussed below ; the principle source of error is due to the accuracy with which the ultrasonic transit time and the relative changes in velocities can be measured.

(i) Measurement of sample dimensions

In all cases the sample dimensions were measured using a micro 2000 micrometer which has an accuracy of 0.002 mm. Several measurements were made at different points on the samples faces and the mean of these measurements was taken as the sample length. It can be shown that the error in velocity measurement δV due to an error in measurement of sample length δl is given by $\delta V = 2\delta l/t$ where δl is the error in measurement of the sample length and t is the measured transit time. Substituting typical numbers shows that this can give an error in velocity of approximately 0.5 ms^{-1} which corresponds to a percentage error of about 0.02%.

(ii) Transit time errors

The largest source of error in the determination of the SOEC arises from the measurement of the ultrasonic wave transit time. The largest component of this error being due to the delay in transit time caused by multiple internal reflections within the quartz transducer. Altman and Beyer (1976) considered a typical pulse incident on the transducer/sample boundary, which would be partially transmitted into the transducer and reflected back into the sample. The portion transmitted into the transducer will undergo multiple reflections inside the transducer; each time the waves hits the sample/transducer interface a wave will be transmitted into the sample, which is an image of the incident pulse (reduced in amplitude due to the reflections) and delayed by a time 1/fo for each reflection it has undergone in the transducer. Therefore the resulting pulse consists of a superposition of pulses of ever - diminishing amplitude whose "peak" is shifted by a time of 1/fo for each reflection in the transducer. The resulting reflected pulse is both lengthened and delayed with respect to a pulse which is totally reflected from the front surface in the absence of a transducer.

The delay due to this effect can be estimated by reference to calculations made by Kittinger (1977) which relate the estimated echo delay t (in units of the reciprocal fundamental transducer frequency) to the acoustic reflection coefficient r at the sample-transducer boundary. This reflection coefficient

is defined as

$$\Gamma = \frac{\rho_2 c_2 - \rho_1 c_1}{\rho_2 c_2 + \rho_1 c_1}$$

where is the density and c is the velocity of sound; the subscripts 1 denotes the sample, and 2 denotes the transducer medium. The quantity ρc is the acoustic impedance. The corresponding echo delay time δt can be found from Kittinger's experimental curve; the corrected ultrasonic wave transit time t_r is given by $t_r = t_m - \delta t$, where t_m is the measured transit time. This correction was of the order of a few percent, a programme "TRANS-CORR" (Brassington 1982) being used to make it.

These corrections do not take into account the effect of the gold plated electrodes on the transducer or the resin bond between the transducer and sample. Kittinger (1977) considers their contribution to the echo delay time to be small.

(iii) Diffraction and non-parallelism

The transducer can be regarded as a piston source producing plane ultrasonic waves. However some radiated energy may still be lost from the sides of the cylindrical region of acoustic flux because the transducer is finite in extent and has a diffraction field. Errors in transit time measurement can occur from these diffraction effects especially at low frequencies when small transducers are used. This effect has been investigated by Truell et al (1959) at various

frequencies. They came to the conclusion that when the ultrasonic wave is propagated along directions which have 2 or 4-fold symmetry , the transit time error due to diffraction is of the order 0.01%, providing the crystal orientation is accurate to within 0.5° and the area of the transducer is smaller than the sample.

A related source of error in the transit time is due to non-parallelism of the sample faces , which results in the transducer receiving different phases of the wave across its surface. This effect has been investigated by Truell (1954). It can be reduced to negligible proportions by ensuring the faces of each sample are parallel to 10^{-3} radians.

(iv) Errors due to temperature fluctuations

In most materials the velocity of sound and hence the SOEC are temperature dependent; therefore when measuring relative velocity changes due to applied hydrostatic pressure, the temperature must be maintained at a constant value. For the case of TGS, whose pressure coefficients are small , a change of 0.4°C corresponds to a pressure induced change of 0.2 Kbars. During the course of the experiment the temperature of the sample in the hydrostatic pressure cell was monitored by a thermocouple mounted in close proximity to it. Temperature control was stable to be within 0.1 °C.

CHAPTER 4

EVALUATION OF ELASTIC CONSTANTS

4.1 Introduction

The determination of the elastic properties of an anisotropic medium by a dynamic method requires the measurement of the velocities of elastic waves in several non-equivalent directions in the medium. From the measured values of the elastic wave velocities certain combinations of the elastic constants can be obtained with the aid of the Christoffel determinant. Aleksandrov (1958) showed that for a monoclinic crystal measurements of the ultrasonic wave velocities in six directions, namely [001], [010], [100], [101], [110] and [011] referenced to the orthogonal axis frame, sufficient experimental data can be obtained to enable the thirteen elastic constants to be determined. Only for certain directions are the velocities related to the elastic constants of the crystal by simple relationships.

This chapter describes in detail the evaluation procedure used (taking as an example the experimental data obtained in this work for TGS at 20°C) to obtain the elastic constants and their associated pressure derivatives.

4.2 Determination of the elastic constants

The propagation of an ultrasonic wave through an anisotropic medium is described by the Christoffel equation:

$$[\Gamma_{ij} - \rho v^2 \delta_{ij}][u_j] = 0 \qquad 4.1$$

where ρ is the density of the medium, v is the ultrasonic wave velocity, u_j is the particle displacement vector and δ_{ij} is the Kronecker delta. The elements of the Christoffel matrix Γ_{ij} are

$$\Gamma_{11} = c_{11}l_x^2 + c_{66}l_y^2 + c_{55}l_z^2 + 2c_{15}l_z l_x$$

$$\Gamma_{12} = (c_{46} + c_{25})l_y l_z + (c_{12} + c_{66})l_x l_y$$

$$\Gamma_{13} = c_{15}l_x^2 + c_{46}l_y^2 + c_{35}l_z^2 + (c_{13} + c_{55})l_z l_x$$

$$\Gamma_{22} = c_{66}l_x^2 + c_{22}l_y^2 + c_{44}l_z^2 + 2c_{46}l_z l_x$$

$$\Gamma_{23} = (c_{44} + c_{23})l_y l_z + (c_{25} + c_{46})l_x l_y$$

$$\Gamma_{33} = c_{55}l_x^2 + c_{44}l_y^2 + c_{33}l_z^2 + 2c_{35}l_z l_x$$

where l_x, l_y, l_z are components of a unit vector in the direction of wave propagation. The condition for a non-zero solution of the Christoffel equation is given by:-

$$\det[\Gamma_{ij} - \rho v^2 \delta_{ij}] = 0 \qquad 4.2$$

For each propagation direction three solutions are obtained to the Christoffel equation corresponding to a longitudinal mode and two transverse modes. Each solution of 4.2 yields the phase velocity of the ultrasonic wave expressed in terms of the medium's elastic constants and density but contains no information on the type of vibrational mode it belongs to. To identify which vibrational mode the solution refers to, it is necessary to substitute the solution into 4.1 and by examination of

the expressions for the particle displacement vectors, the mode of vibration can be identified.

The appropriate solutions to the Christoffel equation have been given by many workers (Luspin and Hauret 1977, Kameyama et al 1973); those for the [001], [010], [100], and [101] directions and are reproduced in table 4.1. No solutions for the [110] and [011] directions have been reported in the literature. The solutions for these directions require the extraction of roots from a complex third order algebraic equation; the resultant expression for each root would be rather lengthy. On the evaluation of 4.2 for the four directions [001], [010], [100] and [101], one root can easily be identified. The remaining two roots are obtained by the solution of a quadratic equation. In a procedure to obtain the elastic constants it is more useful to use relationships between roots and coefficients of the remaining quadratic equation than to solve uniquely for each root. These relationships are given below:-

for the [100] direction

$$\rho v_2^2 = c_{66} \qquad 4.3$$

$$\rho v_1^2 + \rho v_3^2 = c_{11} + c_{55} \qquad 4.4$$

$$\rho v_1^2 \rho v_3^2 = c_{11}c_{55} - c_{15}^2 \qquad 4.5$$

for the [010] direction

$$\rho v_5^2 = c_{22} \qquad 4.6$$

$$\rho v_4^2 + \rho v_6^2 = c_{44} + c_{66} \qquad 4.7$$

$$\rho v_4^2 \rho v_6^2 = c_{66}c_{44} - c_{46}^2 \qquad 4.8$$

Table 4.1 Ultrasonic wave velocity and elastic stiffness constant relationships for a monoclinic crystal.

Mode symbol	Direction of wave propagation	Polarisation vector	Relationship between elastic constant and wave velocity
v_1	[100]	[100]	$\rho v_1^2=\left[C_{11}+C_{55}+\sqrt{(C_{11}-C_{55})^2+4C_{15}^2}\right]/2$
v_2	[100]	[010]	$\rho v_2^2=C_{66}$
v_3	[100]	[001]	$\rho v_3^2=\left[C_{11}+C_{55}-\sqrt{(C_{11}-C_{55})^2+4C_{15}^2}\right]/2$
v_4	[010]	[100]	$\rho v_4^2=\left[C_{44}+C_{66}+\sqrt{(C_{44}-C_{66})^2+4C_{46}^2}\right]/2$
v_5	[010]	[010]	$\rho v_5^2=C_{22}$
v_6	[010]	[001]	$\rho v_6^2=\left[C_{44}+C_{66}-\sqrt{(C_{44}-C_{66})^2+4C_{46}^2}\right]/2$
v_7	[001]	[100]	$\rho v_7^2=\left[C_{33}+C_{55}-\sqrt{(C_{33}-C_{55})^2+4C_{35}^2}\right]/2$
v_8	[001]	[010]	$\rho v_8^2=C_{44}$
v_9	[001]	[001]	$\rho v_9^2=\left[C_{33}+C_{55}+\sqrt{(C_{33}-C_{55})^2+4C_{35}^2}\right]/2$
v_{10}	[101]	[$\bar{1}$01]	$\rho v_{10}^2=\left[(C_{11}+C_{33}+2(C_{15}+C_{35}+C_{55})-\sqrt{4(2C_{35}+C_{33}-C_{11}-2C_{15})^2+(C_{15}+C_{35}+C_{13}+C_{55})^2}\right]/4$
v_{11}	[101]	[010]	$\rho v_{11}^2=\frac{1}{2}(C_{66}+C_{44}+2C_{46})$
v_{12}	[$\bar{1}$01]	[101]	$\rho v_{12}^2=\left[(C_{11}+C_{33}+2(C_{15}+C_{35}+C_{55})+\sqrt{4(2C_{35}+C_{33}-C_{11}-2C_{13})^2+(C_{15}+C_{35}+C_{13}+C_{55})^2}\right]/4$
v_{13}	[110]	[110]	v_{13} to v_{18} obtained as a root of third order
v_{14}	[110]	[001]	algebraic equations including known
v_{15}	[110]	[1$\bar{1}$0]	stiffness constants. The resulting equations
v_{16}	[011]	[011]	are extensive.
v_{17}	[011]	[0$\bar{1}$1]	
v_{18}	[011]	[100]	

for the [001] direction

$$\rho v_8^2 = c_{44} \qquad 4.9$$

$$\rho v_7^2 + \rho v_9^2 = c_{55} + c_{33} \qquad 4.10$$

$$\rho v_7^2 \rho v_9^2 = c_{55}c_{33} - c_{35}^2 \qquad 4.11$$

and for the [101] direction

$$\rho v_{11}^2 = (c_{44} + c_{66} + 2c_{46})/2 \qquad 4.12$$

$$\rho v_{10}^2 + \rho v_{12}^2 = (c_{11} + c_{33} + 2(c_{15} + c_{35} + c_{55}))/2 \qquad 4.13$$

$$\rho v_{10}^2 \rho v_{12}^2 = ((c_{11} + c_{55} + 2c_{15})(c_{55} + c_{33} + c_{35}) - (c_{15} + c_{35} + c_{13} + c_{55})^2) \qquad 4.14$$

An additional relationship (equation 4.15) was obtained by substituting equations 4.4 and 4.10 into equation 4.13. This substitution has the effect of replacing three elastic constants c_{11}, c_{33} and c_{55} in terms of experimental measured velocities:

$$c_{15} + c_{35} = \rho(v_{10}^2 + v_{12}^2 - (v_1^2 + v_3^2 + v_4^2 + v_7^2)/2) \qquad 4.15$$

The procedure used to determine the elastic constants will now be described. The density of TGS was taken to be 1680 Kg/m^3 (Konstantinova et al 1960) and all measured ultrasonic wave velocities have been corrected for transducer delay (see section 3.9).

The first velocity measurements were made on a single parallelepiped sample with polished faces perpendicular to the [001] , [010] and [100] directions in the reference orthogonal frame. From the nine velocity measurements made on this cube the magnitude and sign of three elastic constants c_{44}, c_{66} and c_{22} can be obtained, along with the magnitude of c_{46}. The next sample to be prepared had a pair of faces polished perpendicular to the [101] direction. Then measurement of the velocity of

the [010] polarized shear mode permitted the sign and magnitude of c_{46} to be determined. After measurement of the velocities of the other two modes in the [101] direction there was sufficient velocity data, combined with elastic constants previously determined to enable a further six elastic constants c_{11}, c_{33}, c_{55}, c_{15}, c_{35} and c_{13} to be obtained.

Evaluation of the elastic constants from the velocity data began with the determination of c_{22}, c_{44} and c_{66}. These elastic constants were obtained directly from the measured velocities v_5, v_6 and v_2 respectively (equations 4.6, 4.9 and 4.3). Once c_{44} and c_{66} had been obtained, c_{46} was the next elastic constant to be determined. This could be obtained in two ways:

(i) using the equations for v_4 or v_6 from table 4.1 gave the magnitude of c_{46},

(ii) using the equation for v_{11} from table 4.1 (or equation 4.12) gave the magnitude and sign of c_{46}.

The next set of elastic constants to be obtained was c_{11}, c_{55}, c_{33}, c_{35} and c_{15}. These elastic constants were obtained from the solution of five equations (4.4, 4.5, 4.10, 4.11 and 4.15). The first step taken to solve these equations was to manipulate them in such a way that an expression containing c_{55} in terms of measured velocities was obtained. This was done in the following way:

(i) Substitution of 4.4 into 4.5 to eliminate c_{11}

$$c_{55}(\rho v_1^2 + \rho v_3^2 - c_{55}) - c_{15}^2 = \rho v_1^2 \rho v_3^2 \qquad 4.16$$

(ii) Substitution of 4.10 into 4.11 to eliminate c_{33}

$$c_{55}(\rho v_7^2 + \rho v_9^2 - c_{55}) - c_{35}^2 = \rho v_7^2 \rho v_9^2 \qquad 4.17$$

Equations 4.16 and 4.17 can be manipulated so that c_{13} and c_{33} can be expressed in terms of measured velocities and an elastic constant c_{55}

$$c_{13} = \pm (c_{55} (\rho v_1^2 + \rho v_3^2 - c_{55}) - \rho v_1^2 \rho v_3^2)^{1/2} \qquad 4.18$$

$$c_{33} = \pm (c_{55} (\rho v_7^2 + \rho v_9^2 - c_{55}) - \rho v_7^2 \rho v_9^2)^{1/2} \qquad 4.19$$

It should be noted that if the equations for c_{13} and c_{33} are substituted into 4.15 there would be an expression containing measured velocities and an unknown elastic constant c_{55}, but four different combinations of c_{13} and c_{33} would have to be considered which would lead to four values being obtained for c_{55}. If equation 4.15 is squared on both sides (4.20), it is shown below that only two different combinations of c_{13} and c_{33} need to be considered giving two possible values for c_{55}. This is best illustrated by the following example

$$(\pm c_{13} + \pm c_{33})^2 = (\rho(v_9^2 + v_{12}^2 - (v_1^2 + v_9^2 + v_7^2)/2)^2 \qquad 4.20$$

The four different permutations on the left hand side are (the right hand side being a constant):

(i) $-c_{13}$, $-c_{33}$ $\quad (-c_{13} - c_{33})^2 = c_{13}^2 + 2c_{13}c_{33} + c_{33}^2 \qquad 4.21$

(ii) c_{13} , c_{33} $\quad (c_{13} + c_{33})^2 = c_{13}^2 + 2c_{13}c_{33} + c_{33}^2 \qquad 4.22$

(iii) c_{13} , $-c_{33}$ $\quad (c_{13} - c_{33})^2 = c_{13}^2 - 2c_{13}c_{33} + c_{33}^2 \qquad 4.23$

(iv) c_{33} , $-c_{13}$ $\quad (c_{33} - c_{13})^2 = c_{33}^2 - 2c_{13}c_{33} + c_{13}^2 \qquad 4.24$

It can be seen that 4.21 and 4.22 are equivalent; 4.23 and 4.24 are also equivalent identities. Therefore we only need to consider the grouping of $(c_{13} + c_{33})$ or $(c_{13} - c_{33})$ in the solution of equation 4.20. Substituting c_{13} and c_{33} into equation 4.20 the following expression containing c_{55} in terms of measured velocities

was obtained:

$$\left(c_{55}\rho v_1^2 + \rho v_3^2 - c_{55} \right) - \rho v_1^2 \rho v_2^2 \Big)^{1/2}$$

$$\begin{matrix} + \text{ case 1} \\ - \text{ case 2} \end{matrix} \left(c_{55}\rho v_7^2 + \rho v_4^2 - c_{55} \right) - \rho v_7^2 \rho v_4^2 \Big)^{1/2}$$

$$= \left(\rho\left(V_{10}^2 + v_{12}^2 - \left(v_1^2 + v_3^2 + v_4^2 + v_7^2 \right)/2 \right)^2 \right. \qquad 4.25$$

The convention set up to analyse 4.25 is as follows, one solution for c_{55} was obtained by taking the "top" sign in the $\begin{matrix} + \text{ case 1} \\ - \text{ case 2} \end{matrix}$ and the second solution was obtained by using the "bottom" sign. In future equations of this type will be abbreviated to $\pm$ (or $\mp$) as appropriate. Equation 4.25 was solved numerically using Newtons method, the solution being given by

$$(c_{55})_{n+1} = (c_{55})_n - \frac{\left(A \begin{matrix} - \text{ case 2} \\ + \text{ case 1} \end{matrix} B - C^2 \right)}{\dfrac{\rho v_1^2 + \rho v_3^2 - 2c_{55}}{A} \begin{matrix} - \text{ case 2} \\ + \text{ case 1} \end{matrix} \dfrac{\rho v_7^2 + \rho v_4^2 - 2c_{55}}{B}}$$

where $A = \left(c_{55}\left(\rho v_1^2 + \rho v_3^2 - c_{55} \right) - \rho v_1^2 \rho v_3^2 \right)^{1/2}$

$B = \left(c_{55}\left(\rho v_7^2 + \rho v_4^2 - c_{55} \right) - \rho v_7^2 \rho v_4^2 \right)^{1/2}$

$C = \rho\left(v_{10}^2 + v_{12}^2 - \left(v_1^2 + v_3^2 + v_4^2 + v_7^2 \right)/2 \right)$

Evaluation of 4.26 revealed one solution for c_{55} for each case. By back substitution of c_{55} into 5.18 and 5.19 the magnitudes of c_{15} and c_{35} were found. The signs of c_{15} and c_{35} were obtained with the aid of equation 4.15, the signs being selected such that good agreement is obtained with the value of the velocity sum. c_{11} and c_{33} were obtained by back substituting the values obtained of c_{15}, c_{35} and c_{55} into 4.4 and 4.10.

The following results were obtained for the two cases

+ case	− ve case
$c_{55} = 1.08 \times 10^{10}$	$c_{55} = 1.43 \times 10^{10}$
$c_{11} = 4.41 \times 10^{10}$	$c_{11} = 4.06 \times 10^{10}$
$c_{33} = 2.73 \times 10^{10}$	$c_{33} = 2.38 \times 10^{10}$
$c_{15} + c_{35} = -0.41 \times 10^{10}$	$c_{15} + c_{35} = -0.37 \times 10^{10}$
$c_{35} = -1.8 \times 10^{7}$	$c_{35} = 7.0 \times 10^{7}$
$c_{15} = -2.1 \times 10^{7}$	$c_{15} = -1.04 \times 10^{10}$

all units are Nm^{-2}

To eliminate one set of solutions, the physical principles involved in the propagation of ultrasonic waves in the sample need to be considered. Huntington et al (1969) showed that c_{55} must be smaller than c_{11}, if this condition was not met, it would lead to the identification of the [100] propagating [001] polarized shear mode with the [100] propagating pseudo-longitudinal mode. In some cases this condition is enough to eliminate one set of solutions (and was used by Huntington et al (1969) in their work on anthracene), but unfortunately for TGS this did not turn out to be the case. To assist in the selection of a valid solution, the particle displacement vectors for the longitudinal mode in the xz plane were considered (note there will be no u_2 component for the particle displacement vector as the [010] polarized shear mode is pure).

For the [100] direction the ratio of the particle displacement vectors is given by

$$\frac{u_3}{u_1} = \frac{-c_{15}(c_{44} - \rho v^2)}{(c_{44} - \rho v^2)(c_{55} - \rho v^2)} \qquad 4.27$$

and for the [001] direction

$$\frac{u_3}{u_1} = \frac{-c_{33}(c_{44} - \rho v^2)}{(c_{44} - \rho v^2)(c_{33} - \rho v^2)} \qquad 4.28$$

where v is the velocity of the longitudinal mode. Substituting values for the elastic constants and longitudinal mode velocites gives for the +ve case

[100] longitudinal mode, $u_1 = 0.999$, $u_3 = 0.014$, $\theta = 0.8^\circ$

[001] longitudinal mode, $u_1 = -0.141$, $u_3 = 0.99$, $\theta = 8.1^\circ$

and for the -ve case

[100] longitudinal mode, $u_1 = 0.999$, $u_3 = 0.016$, $\theta = 0.9^\circ$

[001] longitudinal mode, $u_1 = 0.472$, $u_3 = 0.881$, $\theta = 28.2^\circ$

where θ is the angle between the propagation direction of the wavefronts and the particle displacement vector.

On inspection of the particle displacement vectors it can be seen that both solutions are plausible. For the [100] direction both solutions give a particle displacement vector which is close to the direction of propagation, but in the [001] direction there is a notable difference. The solution set which gave the least off-axis particle displacement vectors was considered to be the most likely. In this case the positive solution set with $c_{55} = 1.08 \times 10^{10}$Nm was selected. This can be justified on experimental grounds for TGS. If the longitudinal mode was off-axis by approximately 28° difficulty would be experienced in injecting ultrasonic waves into the sample; however this was found not to be the case.

The next elastic constant to be determined was c_{13}. By rearranging equation 4.14 an expression was obtained

expressing c_{13} as a function of measured velocities and known elastic constants:

$$c_{13} = c_{15} + c_{35} + c_{55} + \qquad 4.29$$

$$\pm((c_{11} + c_{55} + 2c_{15})(c_{55} + c_{33} + 2c_{35}) - 4\rho^2 v_{10}^2 v_{12}^2)^{1/2}$$

Two solutions for c_{13} were obtained. The selection of the correct solution was made by considering the particle displacement vectors of the longitudinal wave in the [101] direction. The ratio of the particle displacement vectors is given by

$$\frac{u_3}{u_1} = \frac{(c_{15}+c_{35}+c_{13}+c_{55})((c_{66}+c_{44}+2c_{46})/2 - \rho v^2)/-2}{((c_{66}+c_{44}+2c_{46})/2 - \rho v^2)((c_{55}+c_{33}+2c_{35})/2 - \rho v^2)} \qquad 4.30$$

It should be noted that as the [010] polarized shear mode is pure there will be no u_2 component of the particle displacement vector. A condition is imposed on this ratio of the particle displacement vectors (u_3/u_1) in that it must be positive. If this condition is not met, it results in the identification of a longitudinal mode with a shear mode. The two solutions obtained for c_{13} were

(i) $c_{13} = 1.67 \times 10^{10}$ Nm^{-2} , $u_3/u_1 = 0.685$

(ii) $c_{13} = -3.05 \times 10^{10}$ Nm^{-2} , $u_3/u_1 = -0.686$

The second solution was rejected as it is physically impossible.

A computer program was written to assist in the determination of the first ten elastic constants of a monoclinic crystal and is listed in appendix 2.A.

At this point I wish to pass on a warning to fellow workers evaluating elastic constants of a monoclinic crystal. If propagation of ultrasonic waves in the xz plane is considered, the following relationship is

obtained between the quasi-longitudinal and quasi-shear modes:

$$\rho v_L^2 + \rho v_S^2 = c_{11}l_x^2 + c_{55}(l_z^2 + l_x^2) + c_{33}l_z^2 + 2c_{15}l_z l_x + 2c_{35}l_z l_x \qquad 4.31$$

This expression contains 5 unknown elastic constants. At a first glance it suggests that if the velocities of the quasi-shear and quasi-longitudinal mode were to be measured for five directions in the plane, five equations linking the elastic constants would be obtained and that these could be solved to give unique solutions for the elastic constants without having to consider particle displacement vectors. Unfortunately this is not so, evaluation of the determinant of the components reveals it to be zero. This means that the equations are singular and that no unique solution exists. This is not a wild goose worth chasing .

4.3 Determination of the elastic constants c_{12}, c_{25} and c_{23}

Determination of the remaining three elastic constants c_{12}, c_{25} and c_{23} required the measurement of the quasi-longitudinal and quasi-shear modes for the [011] and [110] directions in the orthogonal reference frame. These measurements were performed on two samples with appropriately cut and polished faces. On the substitution of the relevant terms into the Christoffel determinant (4.2) a rather lengthy cubic equation is produced from which it would be difficult to isolate expressions for each root in terms of elastic constants; even if this

could be achieved it may be of little value. The relationships between the roots and coefficients of the cubic equation are more useful in a procedure to evaluate the elastic constants, these are given below.

for the [110] direction

$$4\rho^2(v_{13}^2v_{14}^2 + v_{13}^2v_{15}^2 + v_{14}^2v_{15}^2) = (c_{66} + c_{22})(c_{55} + c_{44}) + (c_{11} + c_{66})(c_{66} + c_{22} + c_{55} + c_{44}) - (c_{15} + c_{46})^2 - (c_{12} + c_{66})^2 - (c_{25} + c_{46})^2 \quad 4.32$$

$$\rho^3v_{13}^2v_{14}^2v_{15}^2 = 1/8\ (\ (c_{11} + c_{66})(c_{66} + c_{22})(c_{55} + c_{44}) 2(c_{15} + c_{46})(c_{25} + c_{46})(c_{12} + c_{66}) - (c_{11} + c_{66})(c_{25} + c_{46})^2 - (c_{55} + c_{44})(c_{12} + c_{66})^2 - (c_{15} + c_{46})^2(c_{66} + c_{22})\ ) \quad 4.33$$

$$\rho(v_{13}^2 + v_{14}^2 + v_{15}^2) = c_{66} + (c_{11} + c_{22} + c_{55} + c_{44}) \quad 4.34$$

and for the [011] direction

$$4\rho^2(v_{16}^2v_{17}^2 + v_{16}^2v_{18}^2 + v_{17}^2v_{18}^2) = (c_{22} + c_{44})(c_{44} + c_{33}) + (c_{22} + 2c_{44} + c_{33})(c_{66} + c_{55}) - (c_{46} + c_{35})^2 - (c_{46} + c_{25})^2 - (c_{44} + c_{23})^2 \quad 4.35$$

$$\rho^3v_{16}^2v_{17}^2v_{18}^2 = 1/8\ (\ (c_{66} + c_{55})(c_{22} + c_{44})(c_{44} + c_{33}) 2(c_{46} + c_{35})(c_{44} + c_{23})(c_{46} + c_{25}) - (c_{66} + c_{55})(c_{44} + c_{23})^2 - (c_{46} + c_{25})^2(c_{44} + c_{33} - (c_{22} + c_{44})(c_{46} + c_{35})^2\ ) \quad 4.36$$

$$\rho(v_{16}^2 + v_{17}^2 + v_{18}^2) = c_{44} + (c_{66} + c_{55} + c_{22} + c_{33})/2 \quad 4.37$$

On examination of equations 4.32 to 4.37 it can be seen that c_{25} is common to the [011] and [110] directions. The evaluation procedure adopted to obtain the values of the elastic constants c_{12}, c_{25}, c_{23} was to manipulate the equations for the [110] direction (equations 4.32 to

4.34) to obtain an expression for c_{25} in terms of known elastic constants and experimentally measured velocities. Once c_{25} was obtained, values for c_{23} and c_{12} could be obtained by back substituting and further manipulation of the relevant equations. Rearranging equation 4.32

$$RT = X^2 + Y^2 \qquad 4.38$$

where $RT = (c_{66} + c_{22})(c_{55} + c_{44}) + (c_{11} + c_{66})(c_{66} + c_{22} + c_{55} + c_{44}) - (c_{15} + c_{46})^2 - 4\rho^2(v_{13}^2v_{14}^2 + v_{13}^2v_{15}^2 + v_{14}^2v_{15}^2$

$Y = (c_{12} + c_{66}) \quad X = (c_{25} + c_{46})$

Rearranging equation 4.33

$$GA*X*Y - LM*X^2 - SD*Y^2 = RE \qquad 4.39$$

where $RE = 8\rho^3v_{13}^2v_{14}^2v_{15}^2 - (c_{15} + c_{46})^2(c_{66} + c_{22}) - (c_{11} + c_{66})(c_{66} + c_{22})(c_{55} + c_{44})$

$GA = 2(c_{15} + c_{46})$; $LM = c_{11} + c_{66}$; $SD = c_{55} + c_{44}$

Rearranging 4.38

$$Y = \pm(RT - X^2)^{1/2} \qquad 4.40$$

and substituting into 4.39, an expression containing c_{25} in terms of known elastic constants and measured velocities was obtained.

$$GA*X* \pm(RT - X^2)^{1/2} - LM*X^2 - SD*(RT - X^2) = RE \qquad 4.41$$

Equation 4.41 was evaluated numerically for the two solution cases ($-(RT-X^2)$ and $+(RT-X^2)$) using Newtons method to obtain a value for X, from which c_{25} can be extracted. The necessary formula is

$$X_{n+1} = X_n - \frac{f(X_n)}{f'(X_n)} \qquad 4.42$$

where $X_n = (c_{25} + c_{46})$

$f(X_n) = GA*X* \pm(RT - X^2)^{1/2} - LM*X^2 - SD*(RT - X^2) - RE$

$f'(X_n) = GA* \pm(RT - X^2)^{1/2} - GA*X^2 \pm(RT - X^2)^{-1/2}$

$-2*LM*X + 2*SD*X$

It was found on evaluation of 4.42 that no real solution could be obtained for c_{25} in either case. Finding real solutions to equations involving the last three elastic constants is a difficulty cited by numerous workers on monoclinic crystals. To find a solution for c_{25}, the procedure suggested by Krupnyi et al (1973) was followed. This involved finding the value of X such that df/dx = 0 (ie a minimum point) and adopting this value as the solution. This minimum point was found numerically using Newtons method. Where a solution of X^n corresponds to the condition $f' = 0$

$$X_{n+1} = X_n - \frac{f'(X_n)}{f''(X_n)} \qquad 4.43$$

where

$f''(X_n) = -GA*X* \pm(RT - X^2)^{-1/2} - X^3 \pm(RT - X^2)^{-3/2}*GA$

$- GA*2*X* \pm(RT - X^2)^{-1/2} - 2*LM + 2*SD$

$f'(X_n) = GA* \pm(RT - X^2)^{1/2} - GA*X^2* \pm(RT - X^2)^{-1/2}$

$- 2*LM*X + 2*SD*X$

The values of X obtained from 4.43 were confirmed to be minima by using f'' (the second derivative). Evaluation of 4.43 produced two solutions for c_{25}. Values for the elastic constant c_{12} were obtained by substituting the value obtained for c_{25} into 4.44 (rewritten 4.38):

$$c_{12} + c_{66} = \pm(RT - (c_{25} + c_{46})^2)^{1/2} \quad 4.44$$

It is obvious that each value of c_{25} substituted into equation 4.44 will result in two values being generated for c_{12} . The last remaining constant c_{23} is obtained by rewritting 4.35:

$$c_{44} + c_{23} = \pm(RX - (c_{46} + c_{25})^2)^{1/2} \quad 4.45$$

where $RX = (c_{22} + 2c_{44} + c_{33})(c_{66} + c_{55} - (c_{46} + c_{35})^2 + (c_{22} + c_{44})(c_{44} + c_{33}) - 4\rho^2(v_{16}^2v_{17}^2 + v_{17}^2v_{18}^2 + v_{16}^2v_{18}^2)$

For each value of c_{25} substituted into 4.45 two values for c_{23} will be generated.

At the present stage in the evaluation procedure two values for c_{25} and four values each for c_{23} and c_{12} have been obtained. The selection of the correct values for the elastic constants was made by using information obtained on the particle displacement vectors to eliminate physically impossible solutions. It can be shown that the following relationships exist between the ratios of the particle displacement vectors for the [110] direction:

$$\frac{u_3}{u_2} = \frac{\frac{1}{2}(c_{12}+c_{66})\frac{1}{2}(c_{25}+c_{46}) - \frac{1}{2}(c_{15}+c_{46})(\frac{1}{2}(c_{66}+c_{22})-\rho V^2)}{\frac{1}{2}(c_{15}+c_{46})\frac{1}{2}(c_{25}+c_{46}) - \frac{1}{2}(c_{12}+c_{66})(\frac{1}{2}(c_{55}+c_{44})-\rho V^2)}$$

Eq 4.46

$$\frac{u_3}{u_1} = \frac{\frac{1}{2}(c_{12}+c_{66})\frac{1}{2}(c_{25}+c_{46}) - \frac{1}{2}(c_{15}+c_{46})(\frac{1}{2}(c_{66}+c_{22})-\rho V^2)}{\frac{1}{2}(c_{66}+c_{22})-\rho V^2)(\frac{1}{2}(c_{55}+c_{44})-\rho V^2) - (\frac{1}{2}(c_{25}+c_{46}))^2}$$

Eq 4.47

and for the [011] direction:

$$\frac{u_3}{u_2} = \frac{\frac{1}{2}(c_{46}+c_{25})\frac{1}{2}(c_{44}+c_{23}) - \frac{1}{2}(c_{46}+c_{35})(\frac{1}{2}(c_{22}+c_{44})-\rho v^2)}{\frac{1}{2}(c_{46}+c_{35})\frac{1}{2}(c_{44}+c_{23}) - \frac{1}{2}(c_{46}+c_{25})(\frac{1}{2}(c_{44}+c_{33})-\rho v^2)}$$

Eq 4.48

$$\frac{u_3}{u_1} = \frac{\frac{1}{2}(c_{46}+c_{25})\frac{1}{2}(c_{44}+c_{23}) - \frac{1}{2}(c_{46}+c_{35})(\frac{1}{2}(c_{22}+c_{44})-\rho v^2)}{\frac{1}{2}(c_{22}+c_{44})-\rho v^2)(\frac{1}{2}(c_{44}+c_{33})-\rho v^2) - (\frac{1}{2}(c_{44}+c_{33}))^2}$$

Eq 4.49

The particle displacement vectors of a longitudinal mode propagating in the [011] and [110] directions produced by the solution sets for the elastic constants c_{25}, c_{12} and c_{23} are given in table 4.2 for an evaluation procedure started in the [110] direction.

On examination of the particle displacement vectors in Table 4.2 and eliminating physically impossible solutions, the following values were obtained for the last three elastic constants :-

$$c_{25} = -1.9 \times 10^{10}\ Nm^{-2}$$

$$c_{12} = 1.89 \times 10^{10}\ Nm^{-2}$$

$$c_{23} = 1.97 \times 10^{10}\ Nm^{-2}$$

To check the accuracy of the values obtained for the elastic constants c_{25}, $c_{12}$and c_{23}, the evaluation procedure was retraced for the [011] direction. This involved obtaining an expression for c_{25} using the relationships between products and roots (equations 4.35 to 4.37) for the [011] direction.

Equations 4.35 and 4.36 can be rewritten in the following form:

Table 4.2 Particle displacement vectors

positive case	negative case
$c_{25} = -1.9\times10^{7}$ Nm^{-2}	$c_{25} = 9.0\times10^{8}$ Nm^{-2}
c_{12} positive case	c_{12} positive case
$c_{12} = 1.89\times10^{10}$ Nm^{-2}	$c_{12} = 1.89\times10^{10}$ Nm^{-2}
particle displacement vectors	particle displacement vectors
u_1= 0.77 ; u_2= 0.636 ; u_3=-0.044	u_1= 0.772 ; u_2= 0.635 ; u_3=-0.008
propagation vectors	propagation vectors
l_x= 0.707 ; l_y= 0.707 ; l_z= 0.0	l_x= 0.707 ; l_y= 0.707 ; l_z= 0.0
c_{12} negative case	c_{12} negative case
$c_{12} = -3.11\times10^{10}$ Nm^{-2}	$c_{12} = -3.11\times10^{10}$ Nm^{-2}
particle displacement vectors	particle displacement vectors
u_1= 0.772 ; u_2=-0.636 ; u_3=-0.008	u_1= 0.77 ; u_2=-0.637 ; u_3=-0.044
propagation vectors	propagation vectors
l_x= 0.707 ; l_y= 0.707 ; l_z= 0.0	l_x= 0.707 ; l_y= 0.707 ; l_z= 0.0
c_{23} positive case	c_{12} positive case
$c_{23} = 1.97\times10^{10}$ Nm^{-2}	$c_{23} = 1.97\times10^{10}$ Nm^{-2}
particle displacement vectors	particle displacement vectors
u_1= 0.602 ; u_2= 0.592 ; u_3= 0.534	u_1=-0.993 ; u_2= 0.063 ; u_3= 0.100
propagation vectors	propagation vectors
l_x= 0.0 ; l_y= 0.707 ; l_z= 0.707	l_x= 0.0 ; l_y= 0.707 ; l_z= 0.707
c_{23} negative case	c_{12} negative case
$c_{23} = -4.05\times10^{10}$ Nm^{-2}	$c_{23} = -4.05\times10^{10}$ Nm^{-2}
particle displacement vectors	particle displacement vectors
u_1= 0.992 ; u_2= 0.063 ; u_3=-0.101	u_1=-0.603 ; u_2= 0.592 ; u_3= 0.535
propagation vectors	propagation vectors
l_x= 0.0 ; l_y= 0.707 ; l_z= 0.707	l_x= 0.0 ; l_y= 0.707 ; l_z= 0.707

$$X^2 + H^2 = KD \qquad 4.50$$

$$LA*X*H - OA*H^2 - JD*X^2 = NA \qquad 4.51$$

where $X=(c_{46}+c_{25})$ $H=(c_{44}+c_{23})$

$$KD = (c_{22}+2c_{44}+c_{33})(c_{66}+c_{55}) + (c_{22}+c_{44})(c_{44}+c_{33}) - (c_{46}+c_{35})^2 - 4\rho^2(v_{16}^2v_{17}^2+v_{16}^2v_{18}^2+v_{17}^2v_{18}^2)$$

$$NA = 8\rho^3v_{16}^2v_{17}^2v_{18}^2 - (c_{66}+c_{55})(c_{22}+c_{44})(c_{44}+c_{33}) + (c_{22}+c_{44})(c_{46}+c_{35})^2$$

$$LA = 2(c_{46}+c_{35}) \qquad OA = c_{66}+c_{55} \qquad JD = c_{44}+c_{33}$$

Equations 4.50 and 4.51 contain two unknown elastic constants c_{25} and c_{23}. By modifying 4.50 to obtain an expression for $(c_{44}+c_{23})$

$$H = \pm(KD-X^2)^{1/2} \qquad 4.52$$

and substituting the resulting equation (equation 4.52) into equation 4.51, the following expression was obtained:

$$LA*\pm(KD-X^2)^{1/2}*X - OA*(KD-X^2) - SD*X^2 = NA \qquad 4.53$$

This expression contains only one unknown elastic constant c_{25} expressed in terms of known elastic constants and velocities. A solution to 4.53 was sought numerically using Newtons method to obtain a value for X where

$$X_{n+1} = X_n - \frac{f(X_n)}{f'(X_n)} \qquad 4.54$$

where $X_n = (c_{46}+c_{25})$

$$f(X_n) = LA*\pm(KD-X^2)^{1/2}*X - OA*KD + OA*X^2 - JD*X^2 - NA$$

$$f'(X_n) = LA*\pm(KD-X^2)^{1/2} - LA*\pm X^2*(KD-X^2)^{-1/2} + 2*X*OA - 2*JD*X$$

No real solution could be found for X. As discussed earlier, if no real solution can be obtained for X, then the point at which X is a minimum can be adopted as the solution. This condition was obtained numerically using Newtons method where

$$X_{n+1} = X_n - \frac{f'(X_n)}{f''(X_n)} \qquad 4.55$$

where

$$f'(X_n) = LA*\pm(KD-X^2)^{1/2} - LA*\pm X^2*(KD-X^2)^{-1/2} + 2*X*OA - 2*JD*X$$

$$f''(X_n) = -LA*X*\pm(KD-X^2)^{-1/2} - LA*\pm(KD-X^2)^{-3/2}*X^3 - LA*2*X*\pm(KD-X^2)^{-1/2} + 2*OA - 2*JD$$

A solution for the elastic constant c_{25} was obtained for each case. Values for c_{23} were obtained by substituting the values obtained for c_{25} into equation 4.52

$$c_{44}+c_{23} = H = \pm(KD-X^2)^{1/2} \qquad 4.56$$

Note that each value of c_{25} will generate two values for c_{23}. The values for the remaining elastic constant c_{12} were obtained by using 4.40

$$c_{12}+c_{66} = Y\pm(RT-X^2)^{1/2} \qquad 4.57$$

Each value of c_{25} generates two possible values for c_{12}. The selection of the set of elastic constants as the valid solution was made by considering the information contained in the particle displacement vectors. On inspection of this information (Table 4.3) the negative case for c_{25} can be rejected as the solutions are physically impossible. The correct solutions for the elastic constants c_{25}, $c_{23}$and c_{12} obtained by starting the analysis in the [011] direction are

Table 4.3 Particle displacement vectors

positive case	negative case
$c_{25} = -2.4\times10^{7}$ Nm^{-2}	$c_{25} = 1.40\times10^{7}$ Nm^{-2}
c_{23} positive case	c_{23} positive case
$c_{23} = 1.90\times10^{10}$ Nm^{-2}	$c_{23} = 1.97\times10^{10}$ Nm^{-2}
particle displacement vectors	particle displacement vectors
$u_1 = 0.534$; $u_2 = 0.625$; $u_3 = 0.568$	$u_1 = -0.937$; $u_2 = 0.235$; $u_3 = 0.260$
propagation vectors	propagation vectors
$l_x = 0.0$; $l_y = 0.707$; $l_z = 0.707$	$l_x = 0.0$; $l_y = 0.707$; $l_z = 0.707$
c_{23} negative case	c_{23} negative case
$c_{23} = -4.05\times10^{10}$ Nm^{-2}	$c_{23} = -4.05\times10^{10}$ Nm^{-2}
particle displacement vectors	particle displacement vectors
$u_1 = 0.936$; $u_2 = 0.235$; $u_3 = -0.261$	$u_1 = -0.535$; $u_2 = 0.625$; $u_3 = -0.569$
propagation vectors	propagation vectors
$l_x = 0.0$; $l_y = 0.707$; $l_z = 0.707$	$l_x = 0.0$; $l_y = 0.707$; $l_z = 0.707$
c_{12} positive case	c_{12} positive case
$c_{12} = 1.89\times10^{10}$ Nm^{-2}	$c_{12} = 1.89\times10^{10}$ Nm^{-2}
particle displacement vectors	particle displacement vectors
$u_1 = 0.769$; $u_2 = 0.636$; $u_3 = -0.051$	$u_1 = 0.772$; $u_2 = 0.635$; $u_3 = -0.001$
propagation vectors	propagation vectors
$l_x = 0.707$; $l_y = 0.707$; $l_z = 0.0$	$l_x = 0.707$; $l_y = 0.707$; $l_z = 0.0$
c_{12} negative case	c_{12} negative case
$c_{12} = -3.11\times10^{10}$ Nm^{-2}	$c_{12} = -3.11\times10^{10}$ Nm^{-2}
particle displacement vectors	particle displacement vectors
$u_1 = 0.772$; $u_2 = -0.636$; $u_3 = 0.001$	$u_1 = 0.769$; $u_2 = -0.637$; $u_3 = -0.051$
propagation vectors	propagation vectors
$l_x = 0.707$; $l_y = 0.707$; $l_z = 0.0$	$l_x = 0.707$; $l_y = 0.707$; $l_z = 0.0$

$$c_{25} = -2.4 \times 9^{7}\ Nm^{-2}$$

$$c_{12} = 1.89 \times 10^{10}\ Nm^{-2}$$

$$c_{23} = 1.90 \times 10^{10}\ Nm^{-2}$$

These values compare favourably with the values obtained earlier from the procedure started in the [110] direction.

The most efficient way to determine values for the last three elastic constants is by first obtaining solutions for c_{25}. If this was not carried out, a larger number of possible solutions for the remaining elastic constants c_{23} and c_{12}would have to be considered. Consider the following case, if the equations were evaluated such that c_{23} was to be obtained first, then two values for c_{23} would be expected and substitution of these values into equation 4.50 would result in four values for c_{25}. c_{12} would then be obtained by substituting the known values of c_{25} into 4.38, each value of c_{25} generating two values for c_{12}. This would lead to a set of solutions containing two values for c_{23}, giving in turn four values for c_{25} followed by eight values for c_{12}. A similar argument holds if a solution was sought for c_{12} first. If the procedure described in this section is followed, two values for c_{25} are obtained generating four values each for c_{12} and c_{23}, a useful reduction in effort.

As the calculations progress the accuracy of the values obtained for the elastic constants deteriorates. In particular the values obtained for the last three elastic constants have a substantial error. The

deterioration in accuracy is caused by the lengthy expressions used involving experimental velocities which themselves contain errors.

A series of computer programs has been written to carry out the calculations described in this section and is listed in appendix 2.B and 2.C.

The evaluation procedure described here to obtain the elastic constants of a monoclinic crystal is not the only method which can be used. Prawer et al (1982) solved the necessary equations using a generalized Newton - Raphson algorithm. Alternatively Tylczynski (1981) describes a method to obtain values for c_{11}, c_{33}, c_{66}, c_{13}, c_{15}, c_{35} only.

4.3 Consistency checks on measured velocities and obtained elastic constants.

Cross checks on the accuracy of the velocity measurements were made using the trace identities described by Huntington (1969). These trace relationships are expressions containing only velocities which are obtained by the manipulation of equations 4.3 to 4.14 and are given below. The corresponding values obtained for TGS at 20°C are also included.

$$\rho v_4^2 + \rho v_6^2 = \rho v_2^2 + \rho v_8^2$$

1.65×10^{10} Nm^{-2} $\quad$ 1.65×10^{10} Nm^{-2}

$$\rho v_2^2 + \tfrac{1}{2}(\rho v_1^2 + \rho v_3^2 + \rho v_5^2 + \rho v_8^2) = \rho(v_{13}^2 + v_{14}^2 + v_{15}^2)$$

5.54×10^{10} Nm^{-2} $\quad$ 5.53×10^{10} Nm^{-2}

$$\rho v_8^2 + \tfrac{1}{2}(\rho v_2^2 + \rho v_5^2 + \rho v_7^2 + \rho v_9^2) = \rho(v_{16}^2 + v_{17}^2 + v_{18}^2)$$

4.92×10^{10} Nm^{-2} $\quad$ 4.87×10^{10} Nm^{-2}

$$\rho v_2^2 \rho v_8^2 - (\rho v_{11}^2 - \tfrac{1}{2}(\rho v_2^2 + \rho v_8^2))^2 = \rho v_4^2 \rho v_6^2$$

0.63×10^{20} (Nm^{-2})^2 $\quad$ 0.64×10^{20} (Nm^{-2})^2

The extent to which these checks are verified attests to the internal consistency of the experimental data. A programme was written to carry out the above checks and is listed in Appendix 2.D.

A less useful test for accuracy can be carried out on the calculated elastic constants by checking that they obey the crystal stability conditions. The stability conditions are obtained by considering the strained energy (E) of a crystal (Nye (1957) p137)

$$E = \tfrac{1}{2}c_{ij}S_iS_j \qquad 4.58$$

which must always be positive when the crystal is strained (or equal to zero in the unstrained state). If 4.58 is to be positive definite then the following conditions are true (see D.M. Bloom and F.E. Hohn 1978) :

(1) $c_{ii} > 0$

(2) Det $c_{ij} > 0$

(3) Every principle minor determinant of c_{ij} is positive

The necessary crystal stability conditions have been reported by Alers and Neighbours (1957) for crystals of higher symmetry and are given below for monoclinic crystals.

$$c_{11}>0 \; ; \; c_{22}>0 \; ; \; c_{33}>0 \; ; \; c_{44}>0 \; ; \; c_{55}>0 \; ; \; c_{66}>0$$

$$c_{11}c_{22}>c_{12}^2 \; ; \; c_{11}c_{33}>c_{13}^2 \; ; \; c_{11}c_{55}>c_{15}^2 \; ; \; c_{22}c_{33}>c_{23}^2$$

$$c_{22}c_{55}>c_{25}^2 \; ; \; c_{33}c_{55}>c_{35}^2 \; ; \; c_{44}c_{66}>c_{46}^2$$

$$c_{11}c_{22}c_{33} + 2c_{12}c_{13}c_{23} > c_{11}c_{23}^2 + c_{33}c_{12}^2 + c_{22}c_{13}^2$$

$$c_{11}c_{22}c_{55} + 2c_{12}c_{25}c_{12} > c_{11}c_{25}^2 + c_{55}c_{12}^2 + c_{22}c_{15}^2$$

$$c_{22}c_{33}c_{55} + 2c_{23}c_{35}c_{25} > c_{22}c_{35}^2 + c_{55}c_{23}^2 + c_{33}c_{35}^2$$

Another potential use of the crystal stability

conditions is to assist in the selection of the correct set of solutions in the evaluation procedure for the elastic constants c_{12}, c_{23} and c_{25}. The elastic constants derived in this work obeyed the crystal stability conditions.

4.4 A procedure for determination of the hydrostatic pressure derivatives of the elastic stiffness constants for a monoclinic crystal.

By measuring the hydrostatic pressure dependence of the ultrasonic wave velocities in the [001], [010], [100], [101], [110] and [011] directions the pressure derivatives of the elastic constants were obtained using the procedure described below.

The pulse echo overlap frequency was converted to a relative change $(\delta W/W_o - 1)$ in the natural velocity W (Thurston and Brugger 1964). The initial pressure derivatives of ρv^2 can be obtained using the following relationship due to Thurston (1965):

$$(\rho V^2)'_{p=0} = \rho V_o^2 (2f'/f_o + \chi^T - 2N_k N_m S^T_{kmii}) \quad 4.59$$

where χ^T is the isothermal volume compressibility, $N_k N_m S^T_{kmii}$ corresponds to the isothermal linear compressibility, f_o is the frequency required for pulse overlap at atmospheric pressure and f' is the associated pressure derivative determined as the gradient of the least square line of the frequency against pressure plot, normalized to f_o. The equation in this form holds strictly only for pure mode directions, where the pressure dependence of the particle displacement vector

is zero. In a monoclinic crystal this is true for only a few modes. However, if the effect of pressure on the particle displacement vector is small, equation 4.59 can be taken as a reasonable approximation. Although in a determination of $(\rho v^2)'_{P=0}$ through equation 4.59 the isothermal elastic constants should be used, the difference between isothermal and adiabatic elastic constants is not substantial compared with the experimental error and the adiabatic compliances will be employed. While determination of the elastic constants themselves leads to several possible solution sets (the correct one has been deduced by arguments based on the physics of ultrasonic wave propagation), a single solution is obtained for the pressure derivatives.

The argument used to obtain the pressure derivatives of the elastic constants follows a similar path to that described in section 4.1 for the determination of the elastic constants. The pressure derivatives are found by differentiation and manipulation of equations 4.3 to 4.15. The pressure derivative of c_{22}, c_{44} and c_{66} can be obtained by differentiating 4.6, 4.9 and 4.3 respectively to obtain.

$$\frac{\partial c_{22}}{\partial P} = \frac{\partial(\rho v_6^2)}{\partial P} \quad ; \quad \frac{\partial c_{44}}{\partial P} = \frac{\partial(\rho v_5^2)}{\partial P} \quad ; \quad \frac{\partial c_{66}}{\partial P} = \frac{\partial(\rho v_2^2)}{\partial P}$$

The next pressure derivative, which can be easily found is that of c_{46}, by differentiating 4.12

$$\frac{\partial \rho v_{11}^2}{\partial P} = \frac{1}{2}\frac{\partial c_{44}}{\partial P} + \frac{\partial c_{66}}{\partial P} + \frac{\partial c_{46}}{\partial P} \qquad 4.60$$

and substituting in known pressure derivatives, c'_{44} can be obtained.

The pressure derivatives of c_{11}, c_{55}, c_{15}, c_{33} and c_{35} can be obtained by taking derivatives of equations 4.4, 4.5,4.10, 4.11 and 4.15

$$\frac{\partial \rho v_1^2}{\partial P} + \frac{\partial \rho v_3^2}{\partial P} = \frac{\partial c_{11}}{\partial P} + \frac{\partial c_{55}}{\partial P} = A' \qquad 4.61$$

$$\rho v_1^2 \frac{\partial \rho v_3^2}{\partial P} + \rho v_3^2 \frac{\partial \rho v_1^2}{\partial P} = c_{11} \frac{\partial c_{55}}{\partial P} + c_{55} \frac{\partial c_{11}}{\partial P}$$

$$- 2c_{15} \frac{\partial c_{15}}{\partial P} = B' \qquad 4.62$$

$$\frac{\partial \rho v_7^2}{\partial P} + \frac{\partial \rho v_\varphi^2}{\partial P} = \frac{\partial c_{55}}{\partial P} + \frac{\partial c_{33}}{\partial P} = C' \qquad 4.63$$

$$\rho v_7^2 \frac{\partial \rho v_\varphi^2}{\partial P} + \rho v_\varphi^2 \frac{\partial \rho v_7^2}{\partial P} = c_{33} \frac{\partial c_{55}}{\partial P} + c_{55} \frac{\partial c_{33}}{\partial P}$$

$$- 2c_{35} \frac{\partial c_{35}}{\partial P} = D' \qquad 4.64$$

$$\frac{\partial}{\partial P}(\rho(v_{10}^2 + v_{12}^2 - \tfrac{1}{2}(v_1^2 + v_3^2 + v_7^2 + v_\varphi^2)) =$$

$$= \frac{\partial c_{15}}{\partial P} + \frac{\partial c_{35}}{\partial P} = E' \qquad 4.65$$

These equations do not contain a squared term: only one solution exists for each derivative. The pressure derivative of c'_{55} can be obtained by manipulating equations 4.61 to 4.65 to yield the following equation for the derivative of c_{55} in terms of known elastic constants and measured $(\rho v^2)'_{P=0}$:

$$\frac{\partial c_{55}}{\partial P} = \frac{2E'c_{15}c_{35} + B'c_{35} + D'c_{15} - c_{35}c_{55}A' - c_{15}c_{55}C'}{(c_{35}c_{11} - c_{35}c_{55} + c_{15}c_{33} - c_{15}c_{55})} \qquad 4.66$$

Then by back substitution into the relevant equations (4.61 to 4.65) the pressure derivatives of c'_{11}, c'_{33}, c'_{15} and c'_{35} were determined. The starting point for the determination of the pressure derivative c_{13} was equation 4.14 , which on differentiation by the product rule and rearranging gives:

$$\frac{\partial c_{13}}{\partial P} = \tfrac{1}{2}(c_{15}+c_{35}+c_{13}+c_{55})^{-1}\left[(c_{55}+c_{33}+2c_{35})\frac{\partial}{\partial P}(c_{11}+c_{55}+2c_{15})\right.$$

$$+ (c_{11}+c_{55}+2c_{15})\frac{\partial}{\partial P}(c_{55}+c_{33}+2c_{35})$$

$$\left. - 4\left(\rho v_{10}^2\frac{\partial}{\partial P}v_{12}^2 + \rho v_{12}^2\frac{\partial}{\partial P}v_{10}^2 - \frac{\partial}{\partial P}(c_{15}+c_{35}+c_{55})\right)\right] \qquad 4.67$$

The best method for obtaining the pressure derivatives of the remaining three elastic constants c_{25}, c_{12} and c_{13} is to substitute the measured velocities at different pressures into the equations (see section 4.2) for the [110] and [011] modes to obtain these elastic constants as a function of pressure. Then their derivatives can be obtained. Taking derivatives directly of these equations leads to serious cumulative errors in c'_{25}, c'_{12} and c'_{13}.

This provides a general procedure for determination of the hydrostatic pressure derivatives of the elastic constants for a monoclinic crystal and has been employed here.

CHAPTER FIVE

EXPERIMENTAL METHODS

5.1 Introduction

In this chapter the results of the experiments performed on crystals of TGS to obtain the ultrasonic wave velocity as a function of hydrostatic pressure and temperature are given. The experiments were carried out over a temperature range commencing at 20 °C (ie below the phase transition temperature) to a temperature of 65 °C which is above the phase transition. Experiments could not be performed at higher temperatures because the transducer - sample bond started to break down above 65 °C. From the measurements it was possible to obtain:

(1) Values for all of the elastic stiffness constants and their pressure derivatives at room temperature.

(2) Values for all of the elastic compliances at room temperature.

(3) The temperature dependence of most elastic stiffness constants (the exceptions being c_{25} , c_{12} , c_{13}) over the temperature range 20 to 65 °C.

(4) The pressure derivatives of most elastic stiffness constants at various temperatures over the range 20 - 65 °C (again with the exceptions of c_{25} , c_{12} , c_{13}).

Below its phase transition temperature, TGS is piezoelectric and this results in various vibrational modes been stiffened (see Auld (1973) or Dieulesaint and Royer (1980) for a more details). It can be shown that only modes 2,5,8,11 (see Table 5.1) are subject to piezoelectric stiffening. No corrections to the velocity

data were made to take account of piezoelectric effects as the necessary data to enable these corrections to be performed have not been reported, as yet, in the literature. Above the transition temperature TGS is not piezoelectric so no corrections are necessary.

5.2 Measurement of the elastic properties of TGS at room temperature

Ultrasonic wave velocities were measured for 18 different modes of vibration (table 5.1) in TGS at room temperature (20°C) and atmospheric pressure by using the pulse echo overlap system as described in section 3.5. The ultrasonic wave velocities quoted for each mode are the average value of several measurements. Velocity corrections due to multiple internal reflections at the transducer - sample boundary have been applied (see section 3.9) , the velocities quoted in table 5.1 are the corrected ones.

Using the velocity measurements from table 5.1 and following the evaluation procedure described in section 4.2, the 13 elastic stiffness constants were determined ; these are quoted in table 5.2 along with data obtained by other workers on this material (the data of Luspin and Hauret (1977) has been transferred to the axial set used by Konstantinova et al (1960) and in this work). In view of the accumulation of errors involved in the extraction of elastic stiffness constants, especially in c_{25}, c_{23} and c_{12}, the agreement between the sets of data is more than reasonable.

Table 5.1 Pressure derivatives of the normalized overlap frequency and mode velocities for TGS

Mode number	Direction of wave propagation	Polarization vector	Measured wave velocity(ms^{-2})	$f'/f_o \times 10^{-3}$ bar^{-1}*	$\left(\frac{\partial \rho v^2}{\partial P}\right)_{P=0}$
1	[100]	[100]	5130	9.50	9.51
2	[100]	[010]	1900	3.50	0.58
3	[100]	[001]	2520	4.28	1.18
4	[010]	[100]	2460	3.93	1.01
5	[010]	[010]	4460	19.0	13.4
6	[010]	[001]	1940	3.78	0.61
7	[001]	[100]	2510	6.49	1.35
8	[001]	[010]	2490	4.55	0.92
9	[001]	[001]	4050	10.6	5.78
10	[101]	[101]	2270	5.15	0.92
11	[101]	[010]	2280	4.51	0.821
12	[101]	[101]	4530	11.4	8.01
13	[110]	[110]	4560	12.8	9.73
14	[110]	[001]	2460	4.41	1.13
15	[110]	[1$\bar{1}$0]	2460	7.99	1.86
16	[011]	[011]	4550	12.8	9.26
17	[011]	[0$\bar{1}$1]	1840	7.41	0.896
18	[011]	[100]	2210	5.62	0.999

*1 bar=$10^5 Nm^{-2}$.

Table 5.2 The elastic stiffness constants of TGS in the orthogonal axial set used by Konstantinova et al (1960) at room temperature. The units are 10^{10} Nm^{-2}

C_{11}	C_{22}	C_{33}	C_{44}	C_{55}	C_{66}	C_{12}	C_{13}	C_{23}	C_{15}	C_{25}	C_{35}	C_{46}	Reference
4.41	3.34	2.73	1.04	1.08	0.61	1.89	1.67	1.97	-0.21	-0.19	-0.18	0.05	This work
4.55	3.21	2.63	0.95	1.11	0.62	1.72	1.98	2.08	-0.30	-0.036	-0.500	-0.026	Konstantinova et al
4.71	3.35	2.75	1.02	1.03	0.61	1.50	2.10	1.85	-0.18	-0.20	0.05	-0.02	Luspin & Hauret
4.61		2.79		1.12			2.10		-0.22		0.15		Tylczynski

The elastic compliances were determined using the derived elastic stiffness constants by following the procedure described in Appendix A and the values obtained are quoted in table 5.3 along with those determined from other workers data. It should be appreciated that the values obtained for the elastic compliances by this indirect method will not be as accurate as those obtained by experiments which measured the elastic compliances directly. This inaccuracy is due to a combination of factors , the principle ones being that we are using elastic stiffness constants which contain experimental error and also the loss of numerical accuracy inherent in the inversion of the tensor which involves a large number of terms.

Measurements were taken of the hydrostatic pressure derivatives of the ultrasonic wave velocity for 18 modes of vibration (the average values obtained from three experimental runs are quoted in table 5.1) from which values of the pressure derivatives of the elastic stiffness constants were obtained; these are given in table 5.4. It can be seen (table 5.1) that for every acoustic mode measured for TGS the ultrasonic wave velocity increased with pressure. Hence the pressure derivatives of the elastic stiffness constants are positive ; $\partial C_{16}/\partial P$ is an exception but in itself does not correspond to any normal mode - it is obtained only in combination with other derivatives $\partial C_{ij}/\partial P$.

Table 5.3 The elastic compliances of TGS in the orthogonal axial set used by Konstantinova et al (1960) at room temperature. The units are 10^{-11} m^2N

S_{11}	S_{22}	S_{33}	S_{44}	S_{55}	S_{66}	S_{12}	S_{13}	S_{23}	S_{15}	S_{25}	S_{35}	S_{46}	Reference
3.19	5.62	6.79	9.65	9.39	16.45	-1.13	-1.12	-3.35	0.23	0.21	0.32	-0.79	This work
3.29	6.98	10.85	10.53	10.73	16.15	-0.29	-2.27	-5.77	-0.14	-2.45	4.08	0.44	Konstantinova et al
3.27	4.87	7.74	9.81	10.11	16.40	-0.06	-2.47	-3.25	0.68	1.09	-1.44	0.32	Luspin & Hauret

Table 5.4 Hydrostatic presure derivatives of the elastic stiffness constants of TGS.

$$\left(\frac{\partial C_{11}}{\partial P}\right)_{P=0} = 9.5\ ; \qquad \left(\frac{\partial C_{12}}{\partial P}\right)_{P=0} = 8.9\ ; \qquad \left(\frac{\partial C_{13}}{\partial P}\right)_{P=0} = 6.0\ ;$$

$$\left(\frac{\partial C_{15}}{\partial P}\right)_{P=0} = -0.40; \qquad \left(\frac{\partial C_{22}}{\partial P}\right)_{P=0} = 13.4\ ; \qquad \left(\frac{\partial C_{23}}{\partial P}\right)_{P=0} = 6.9\ ;$$

$$\left(\frac{\partial C_{25}}{\partial P}\right)_{P=0} = 0\ ; \qquad \left(\frac{\partial C_{33}}{\partial P}\right)_{P=0} = 5.9\ ; \qquad \left(\frac{\partial C_{35}}{\partial P}\right)_{P=0} = 0.43;$$

$$\left(\frac{\partial C_{44}}{\partial P}\right)_{P=0} = 0.92; \qquad \left(\frac{\partial C_{46}}{\partial P}\right)_{P=0} = 0.07; \qquad \left(\frac{\partial C_{55}}{\partial P}\right)_{P=0} = 1.2\ ;$$

$$\left(\frac{\partial C_{66}}{\partial P}\right)_{P=0} = 0.58.$$

5.3 Measurement of the temperature dependence of the elastic stiffness constants.

The experimental procedure adopted to obtain the temperature dependence of the ultrasonic wave velocity involved placing the sample inside the pressure cell, which was then heated without pressure being applied to the system. The ultrasonic wave velocity was measured using the pulse echo overlap technique. Experimental readings were taken at appropriate temperature increments while the sample was being heated. The heating rate selected was generally 8°C per hour at temperatures removed from the phase transition, with the heating rate being reduced in the vicinity of the phase transition to permit any effects at the phase transition to be followed in greater detail.

The temperature dependence of the ultrasonic wave velocities were measured for vibrational modes numbers 1 to 12 over the temperature range 20 °C to 65 °C. The numeric label assigned to each mode relates to table 5.1 which provides a description of the wave propagation and polarization vectors. The temperature dependences of ultrasonic wave velocities for modes 1 to 12 are presented in the form of plots of relative change in natural velocity $\Delta W/W_o$ versus applied temperature (figures 5.1 to 5.12), where $\Delta W/W_o$ is defined as

$$\Delta W/W_o = (W_{(T)} - W_o)/W_o$$

To obtain the velocity of the ultrasonic waves at elevated temperatures from these data, corrections have

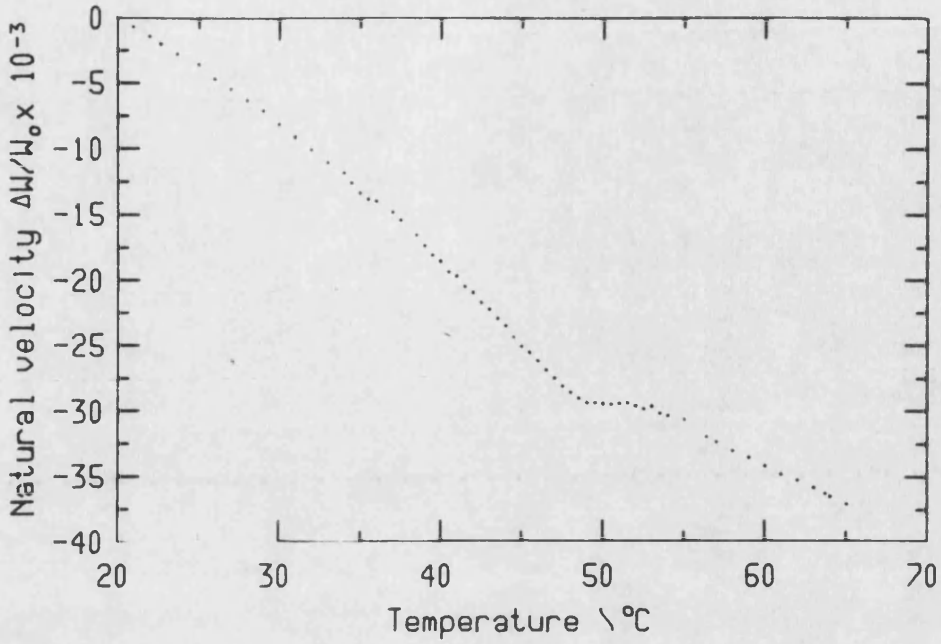

Fig 5.1 Temperature dependence of the ultrasonic wave velocity for the X propagated longitudinal mode.

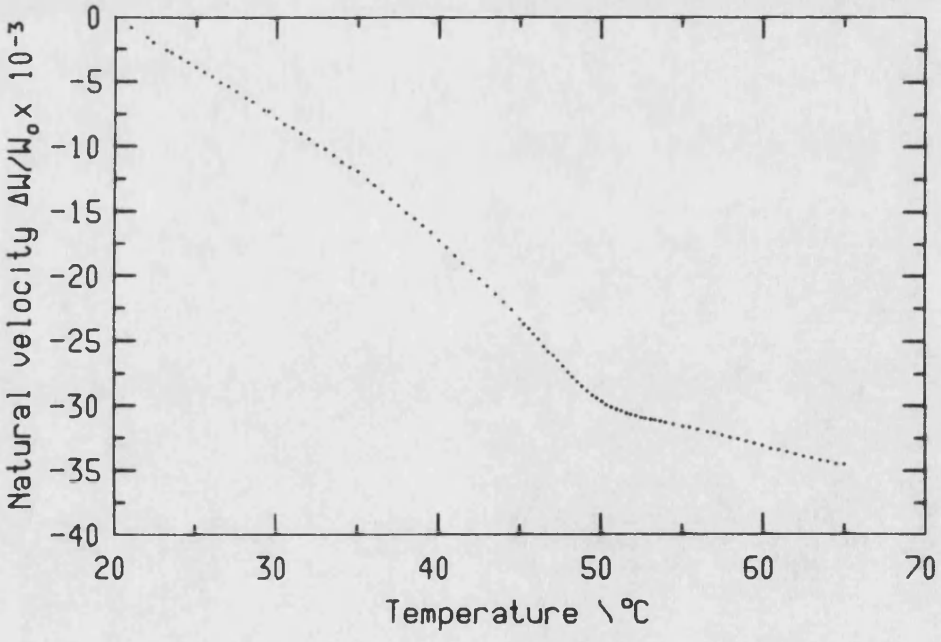

Fig 5.2 Temperature dependence of the ultrasonic wave velocity for the X propagated Y polarized shear mode.

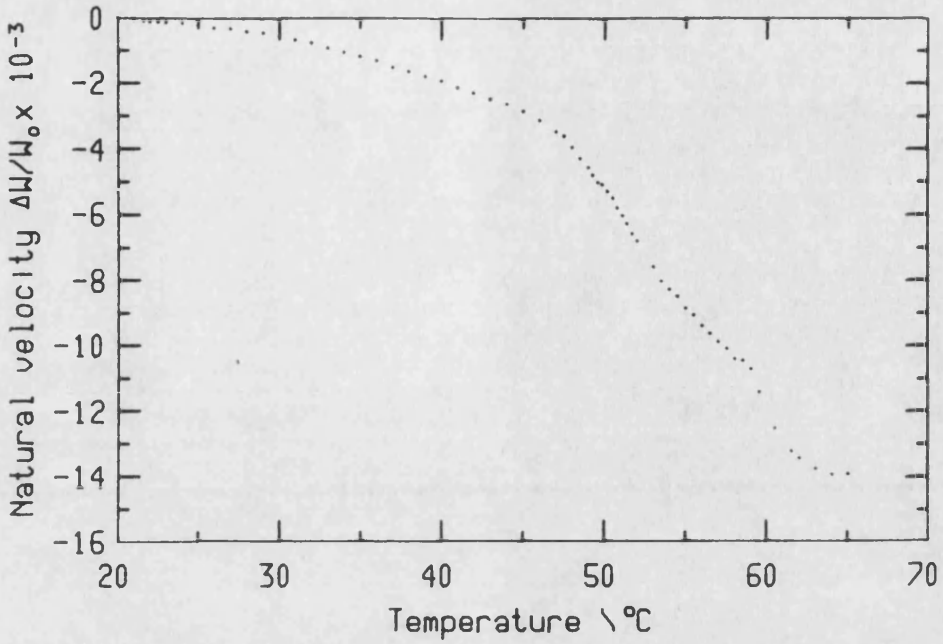

Fig 5.3 Temperature dependence of the ultrasonic wave velocity for the X propagated Z polarized shear mode.

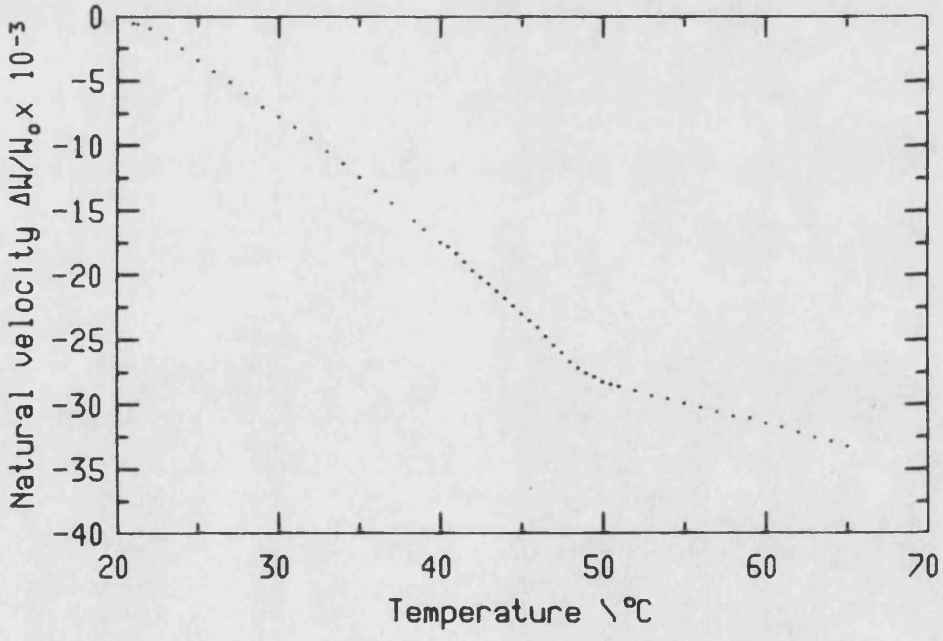

Fig 5.4 Temperature dependence of the ultrasonic wave velocity for the Y propagated X polarized shear mode.

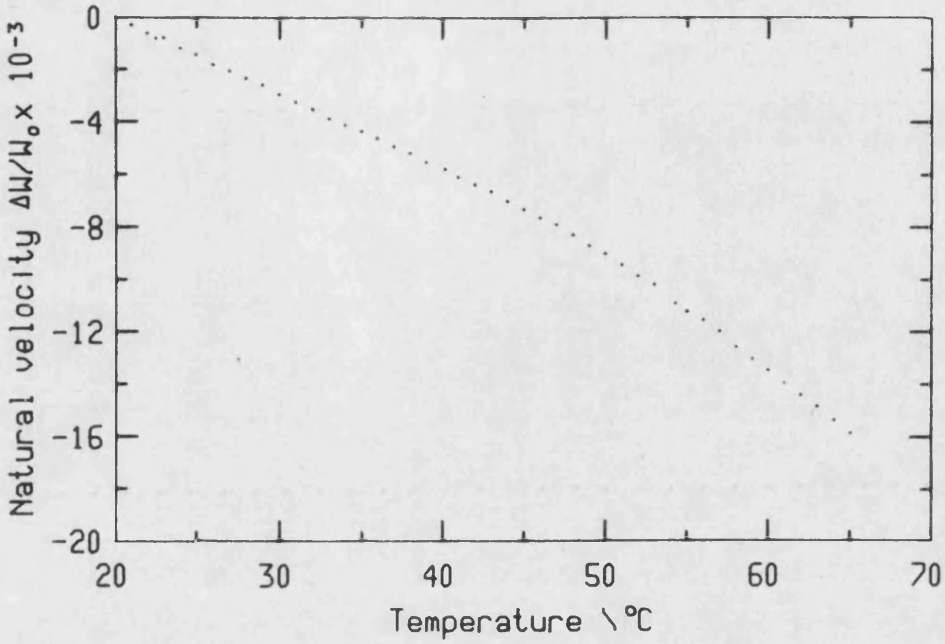

Fig 5.5 Temperature dependence of the ultrasonic wave velocity for the Y propagated longitudinal mode.

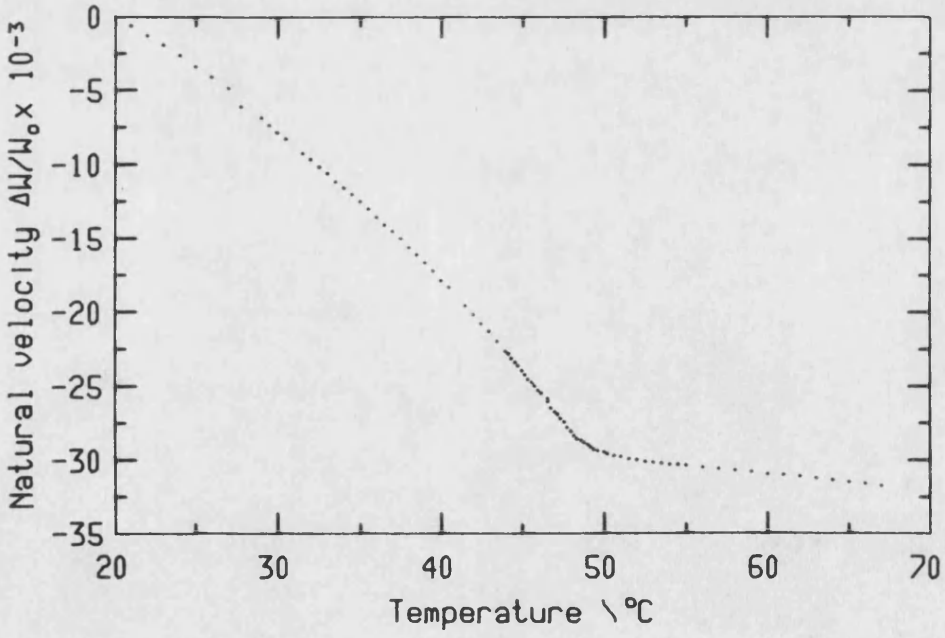

Fig 5.6 Temperature dependence of the ultrasonic wave velocity for the Y propagated Z polarized shear mode.

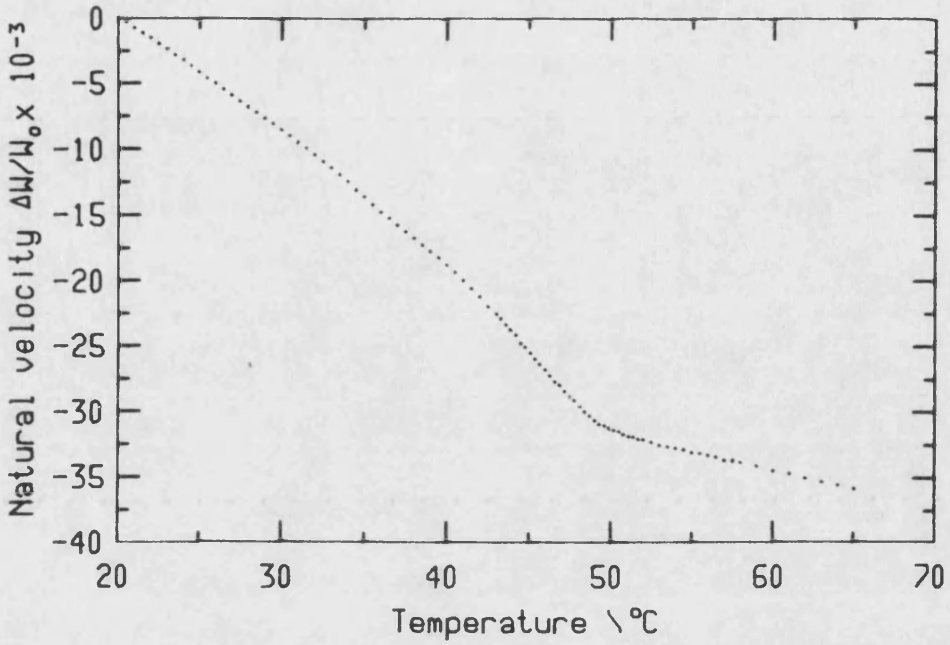

Fig 5.7 Temperature dependence of the ultrasonic wave velocity for the Z propagated X polarized shear mode.

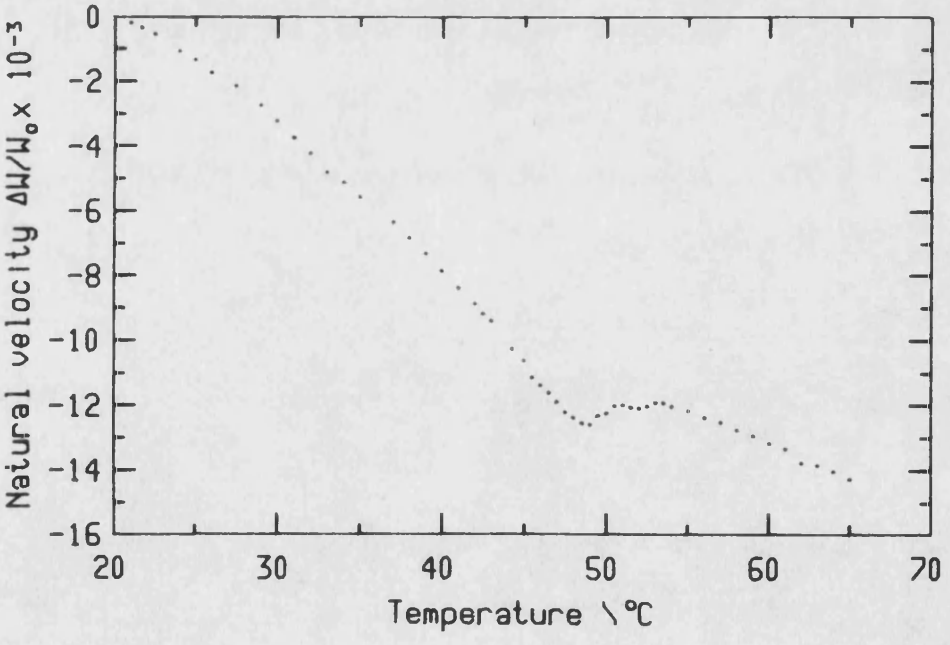

Fig 5.8 Temperature dependence of the ultrasonic wave velocity for the Z propagated Y polarized shear mode.

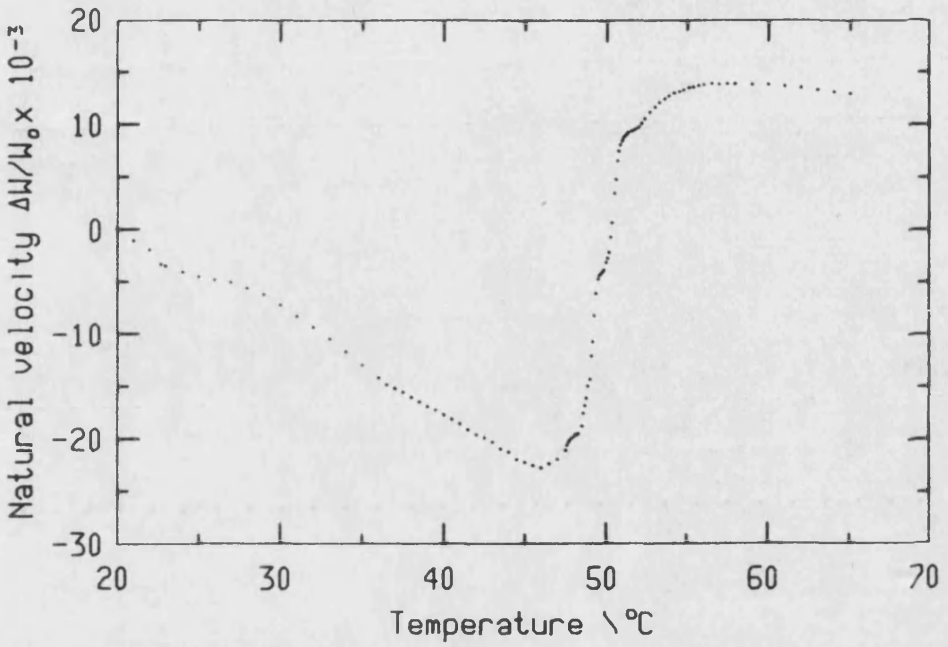

Fig 5.9 Temperature dependence of the ultrasonic wave velocity for the Z propagated longitudinal mode.

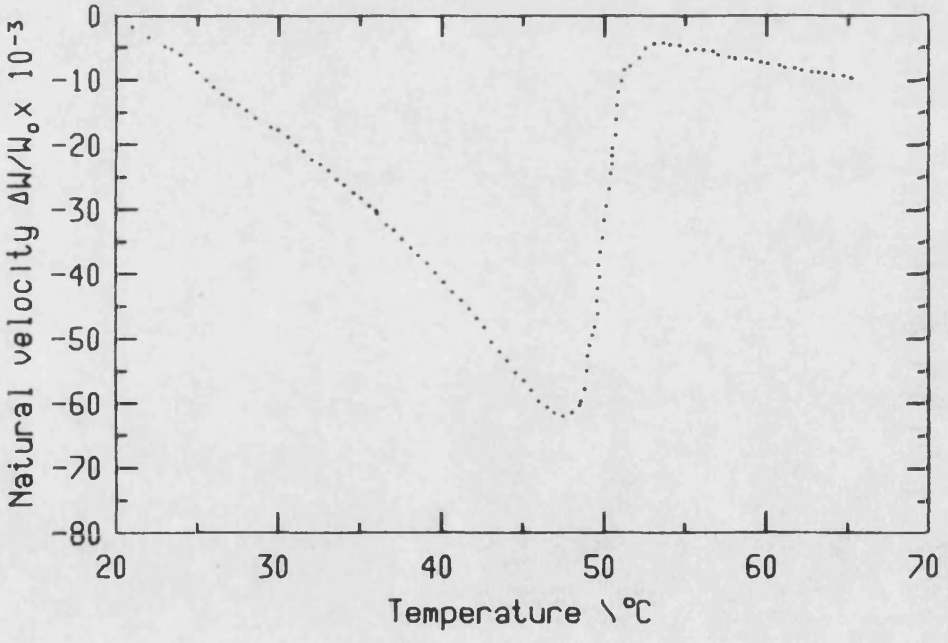

Fig 5.10 Temperature dependence of the ultrasonic wave velocity for the [1 0 1] propagated [-1 0 1] polarized shear mode.

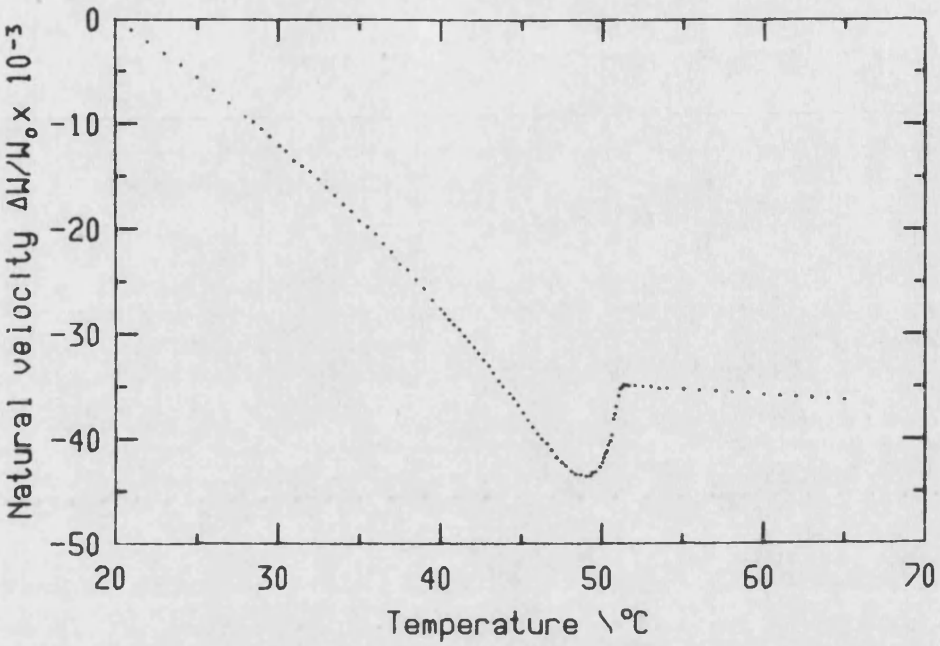

Fig 5.11 Temperature dependence of the ultrasonic wave velocity for the [1 0 1] propagated Y polarised shear mode.

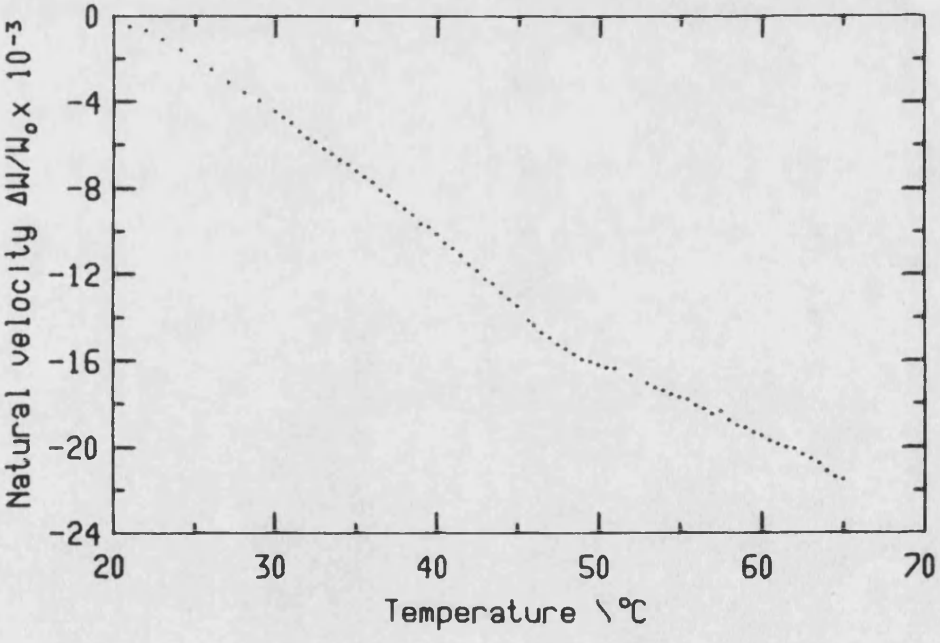

Fig 5.12 Temperature dependence of the ultrasonic wave velocity for the [1 0 1] propagated longitudinal mode.

to be applied to account for changes in sample path length and density (which can only be measured at room temperature) due to thermal expansion.

The thermal expansion properties of TGS have been investigated by several workers. Most of these workers concentrated their effort in a narrow region either close to the phase transition (Ehses et all (1978) , Gillespie et al (1974) , Deguchi and Nakamura (1977) , Deguchi (1979)) or investigated in detail the thermal expansion properties along one particular crystallographic direction (Imai (1977) , Ema et al (1979)). A few workers (Ganesan (1962) , Ezhkova et al (1959) and Stankowski and Malinowski (1980)) investigated the thermal expansion properties over a wide temperature range for several crystallographic directions. To carry out the corrections necessary to account for thermal expansion the data from Stankowski and Milinowski (1980) were used on the grounds that being the more recent work it was likely to be one of the more accurate determinations of the thermal expansion properties. Unfortunately they used a different orthogonal reference axial system so it was necessary to transfer their data to the frame of Konstantinova et al (1960) used throughout this work. Plots of $\Delta l/l_o$ against temperature are given in figures 5.13 to 5.16 for the directions investigated in this work, where $\Delta l = l - l_o$, l is the sample length at temperature T , l_o is the sample length at room temperature.

It was assumed in the calculation of the transducer

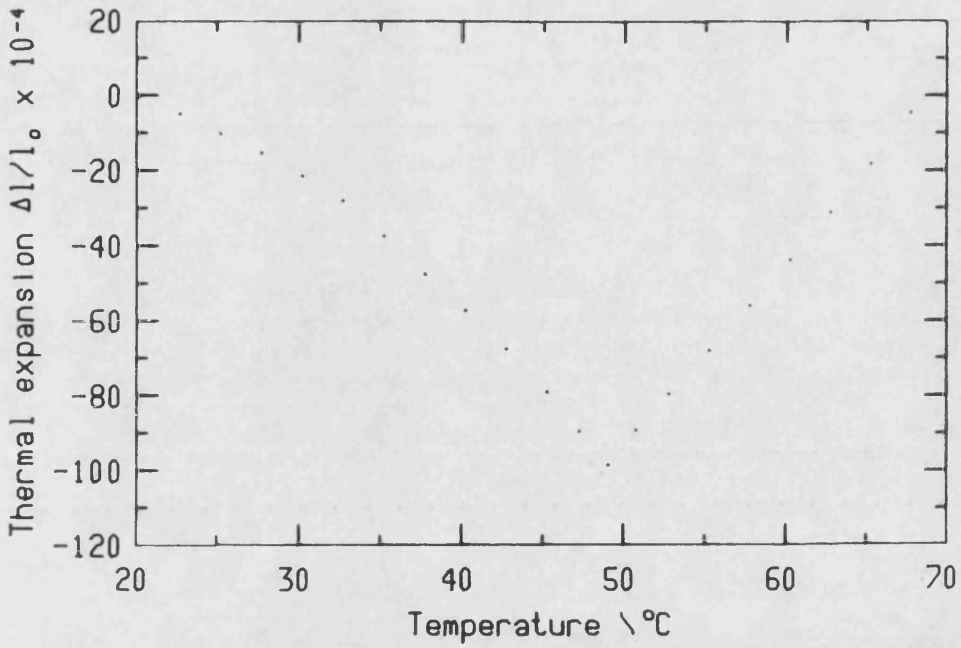

Fig 5.13 Temperature dependence of the relative change in length along the X axis.

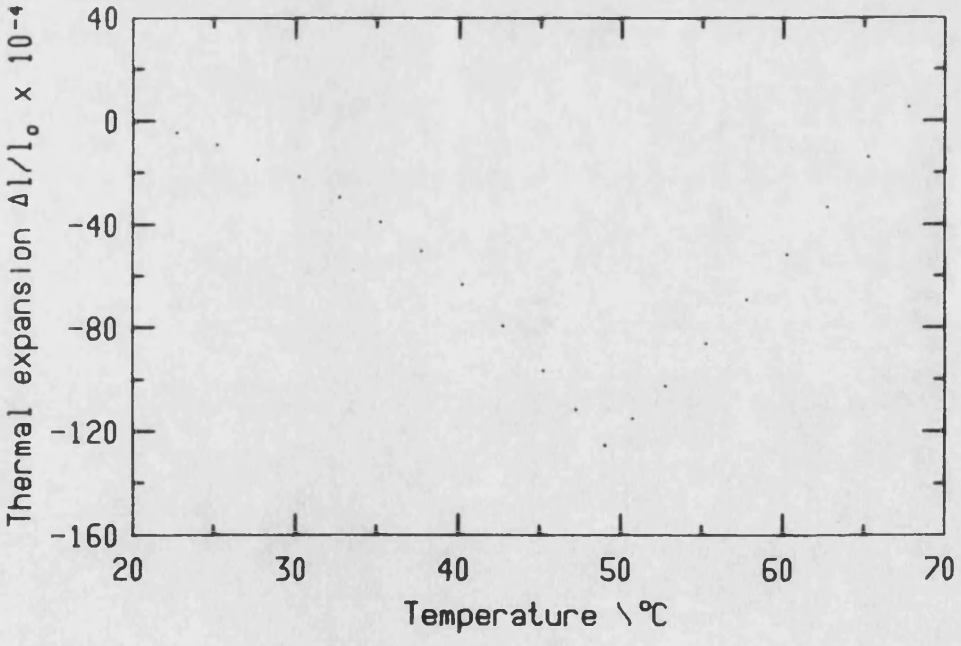

Fig 5.14 Temperature dependence of the relative change in length along the Y axis.

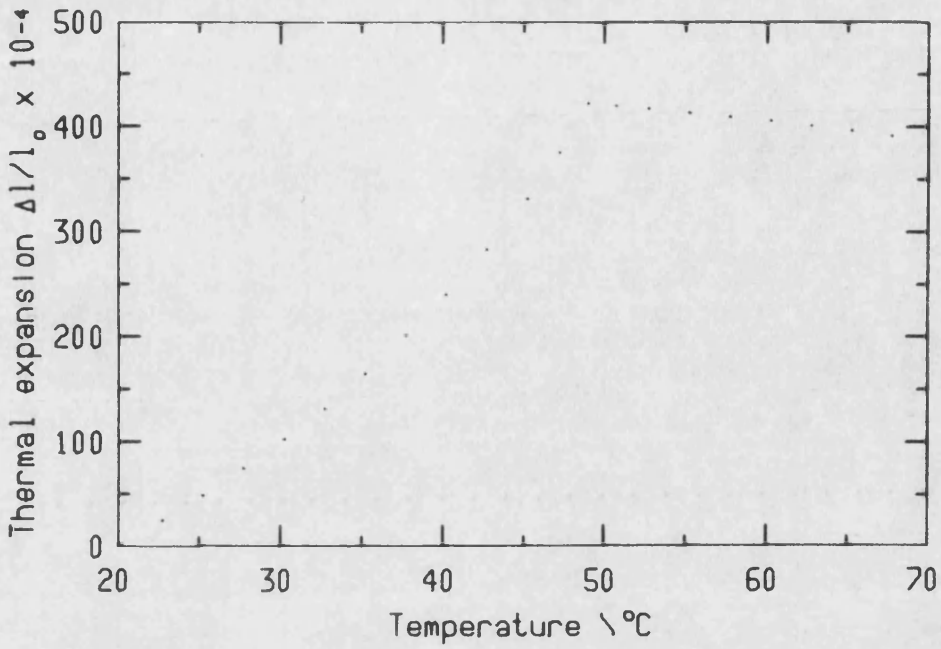

Fig 5.15 Temperature dependence of the relative change in length along the Z axis.

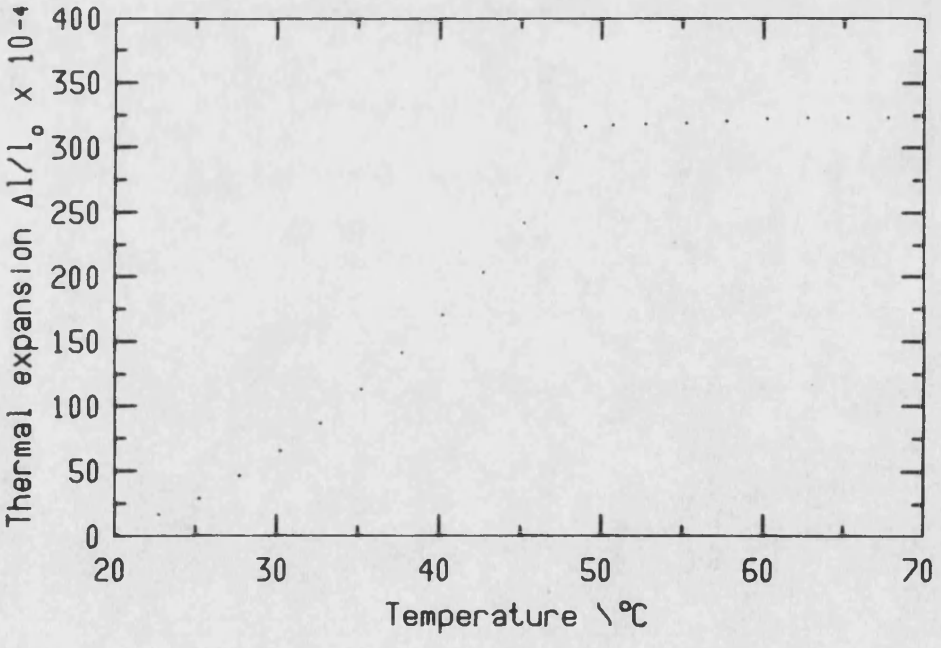

Fig 5.16 Temperature dependence of the relative change in length along the [1 0 1] axis.

delay that all properties except sample length were temperature independent. This is not an unreasonable assumption as any temperature induced changes are a correction to a correction, are second order and so can be ignored.

By applying corrections to the sample path length to account for thermal expansion and corrections to account for transducer delay to the data in figures 5.1 to 5.12 the ultrasonic wave velocities at elevated temperatures have been calculated and are presented in figures 5.17 to 5.28 in the form of velocity versus temperature plots. The velocities are also quoted in table 5.5 for modes 1 to 12 for 5 °C intervals. It can be seen that the ultrasonic wave velocity decreased as the temperature was increased. This trend continued above the phase transition. There are four more interesting modes (figures 5.24 to 5.27) where an anomaly occurs at the phase transition with the velocity increasing beyond the phase transition. The percentage change in velocity with temperature is more readily appreciated by examining the $\Delta W/W_o$ plots than the velocity against temperature plots.

From the velocity data obtained the elastic constants (with the exception of c_{12}, c_{13}, c_{25}) were calculated over the temperature range 20 °C to 65 °C in steps of 0.5 °C using the procedure described in section 4.2. Values for the density of TGS used in these calculations at elevated temperatures were determined by using the thermal expansion data along the principle axis to calculate the new sample volume at elevated temperature

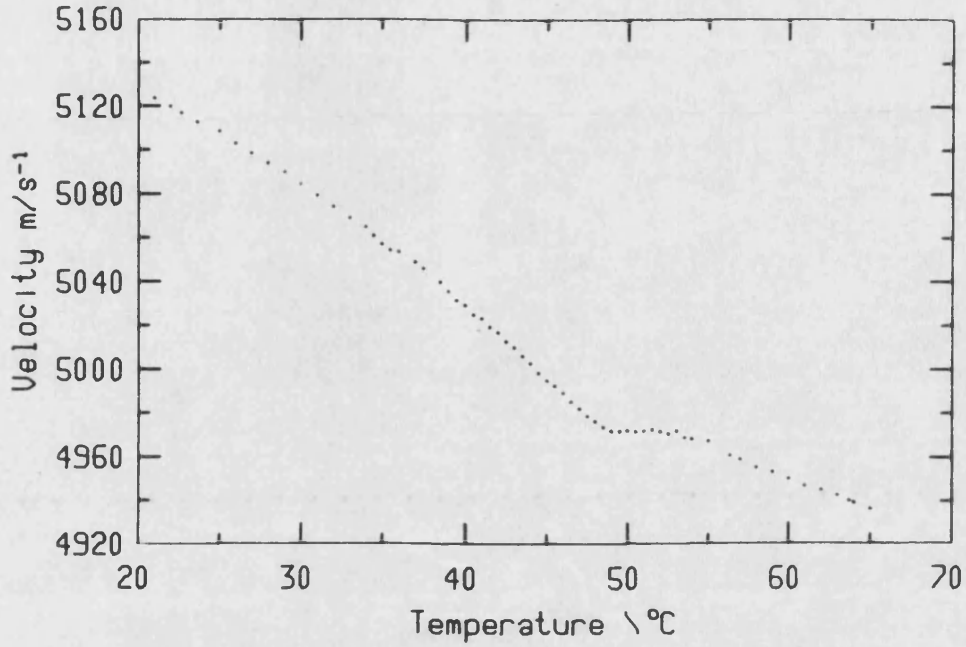

Fig 5.17 Temperature dependence of the ultrasonic wave velocity for the X propagated longitudinal mode corrected for transducer delay and thermal expansion.

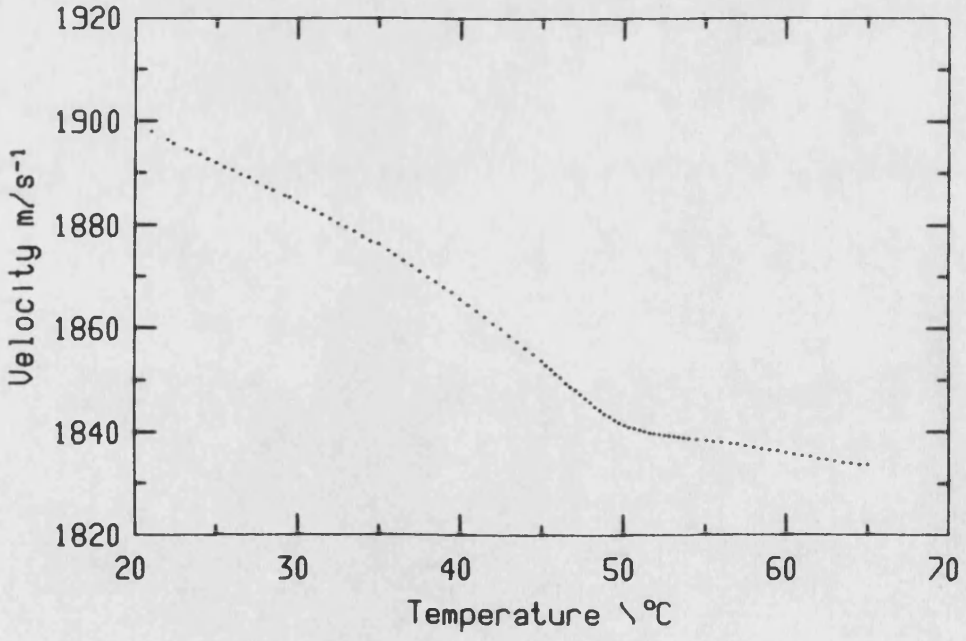

Fig 5.18 Temperature dependence of the ultrasonic wave velocity for the X propagated Y polarized shear mode corrected for transducer delay and thermal expansion.

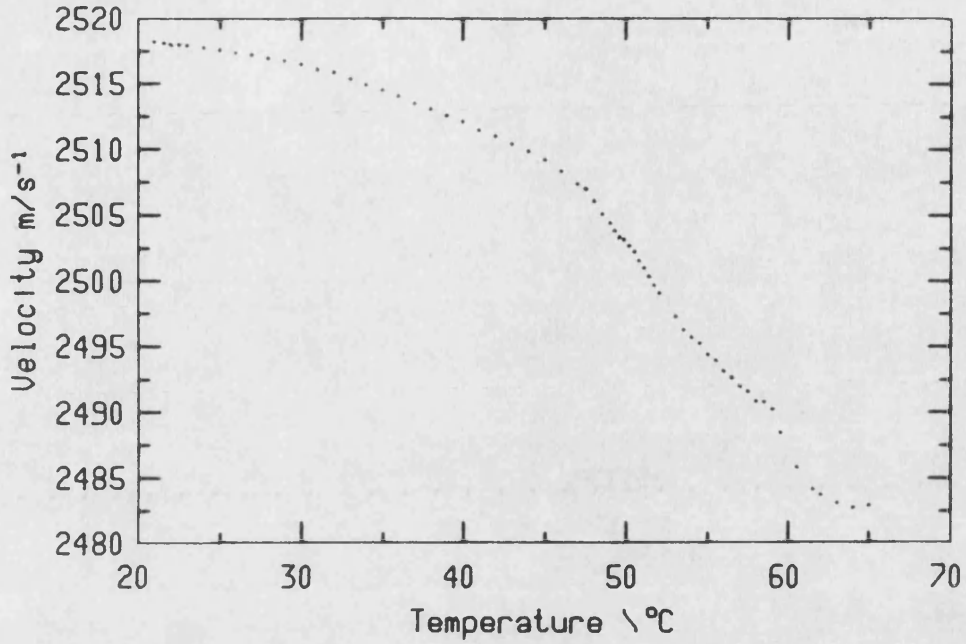

Fig 5.19 Temperature dependence of the ultrasonic wave velocity for the X propagated Z polarized shear mode corrected for transducer delay and thermal expansion.

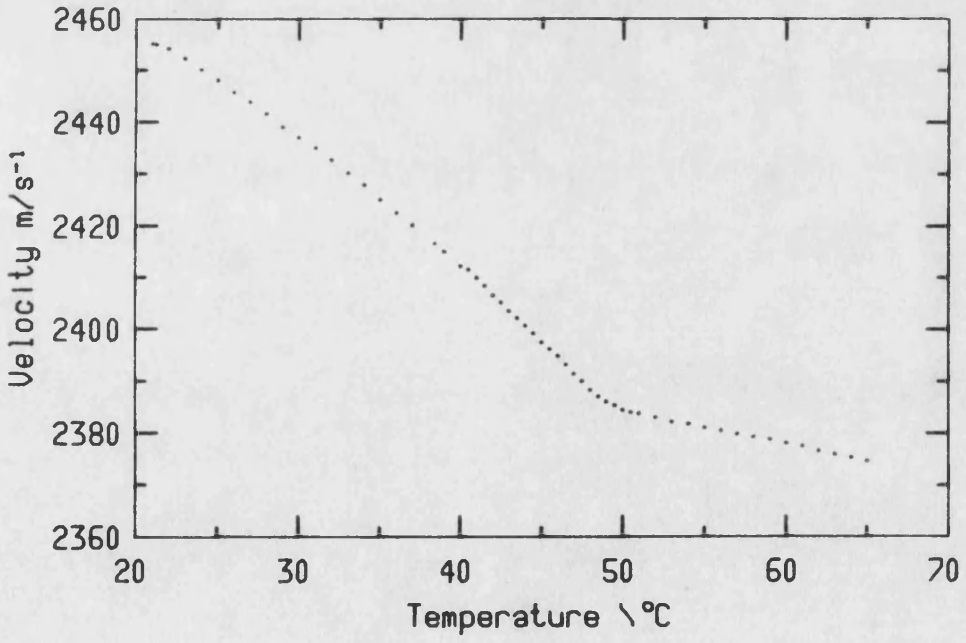

Fig 5.20 Temperature dependence of the ultrasonic wave velocity for the Y propagated X polarized shear mode corrected for transducer delay and thermal expansion.

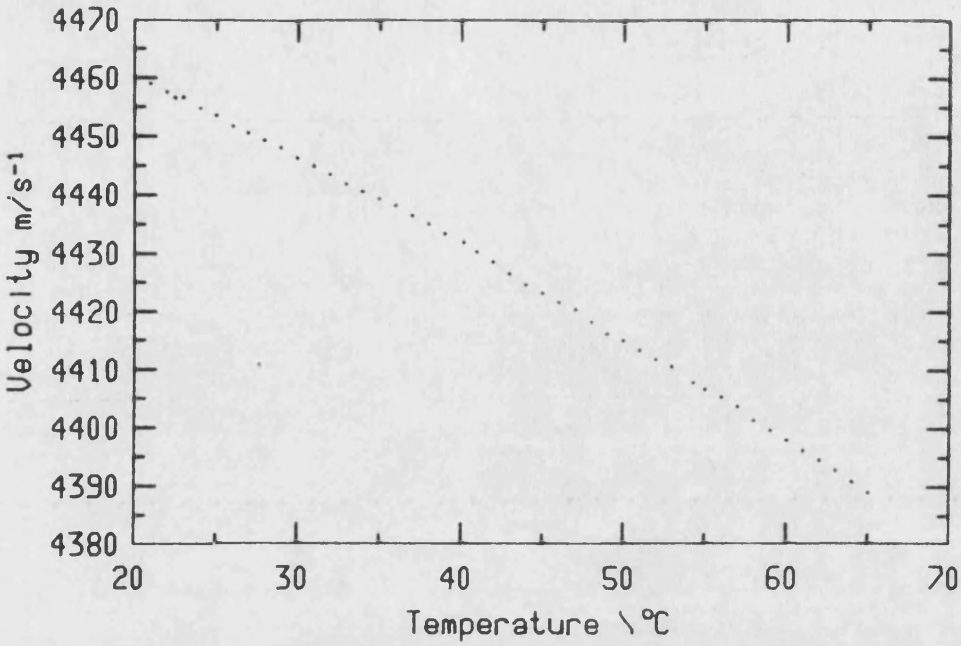

Fig 5.21 Temperature dependence of the ultrasonic wave velocity for the Y propagated longitudinal mode corrected for transducer delay and thermal expansion.

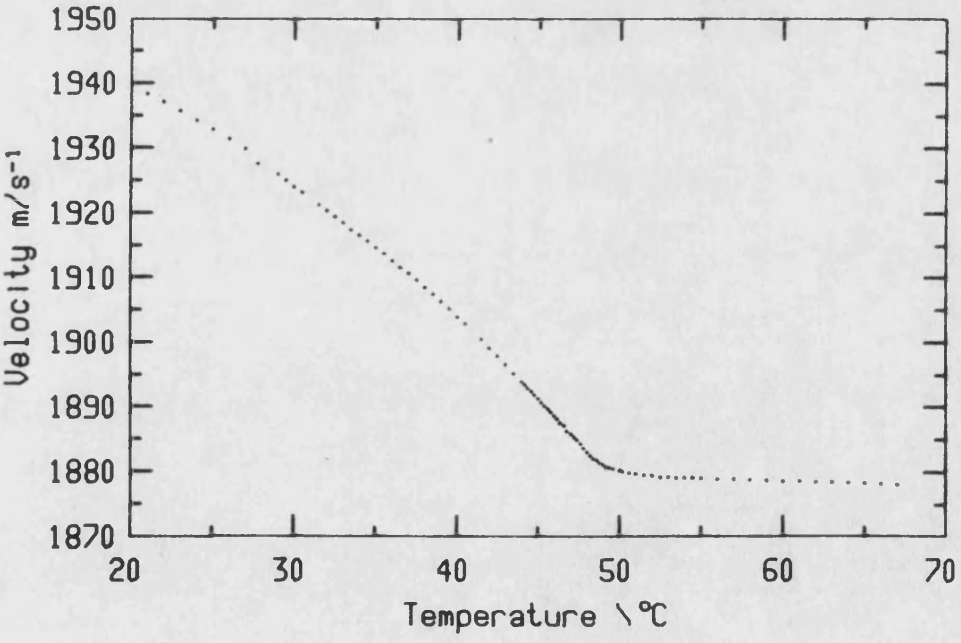

Fig 5.22 Temperature dependence of the ultrasonic wave velocity for the Y propagated Z polarized shear mode corrected for transducer delay and thermal expansion.

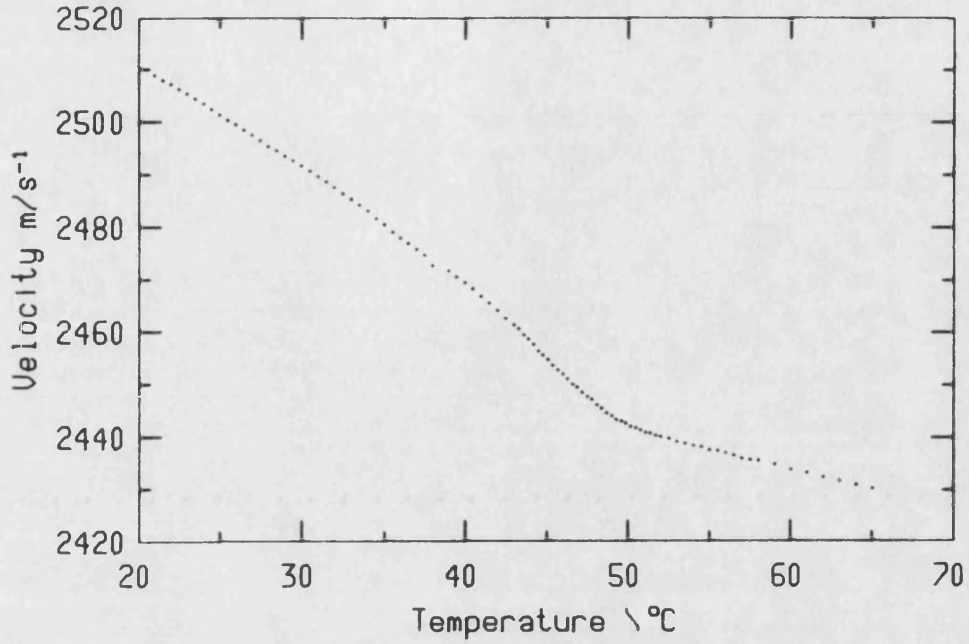

Fig 5.23 Temperature dependence of the ultrasonic wave velocity for the Z propagated X polarized shear mode corrected for transducer delay and thermal expansion.

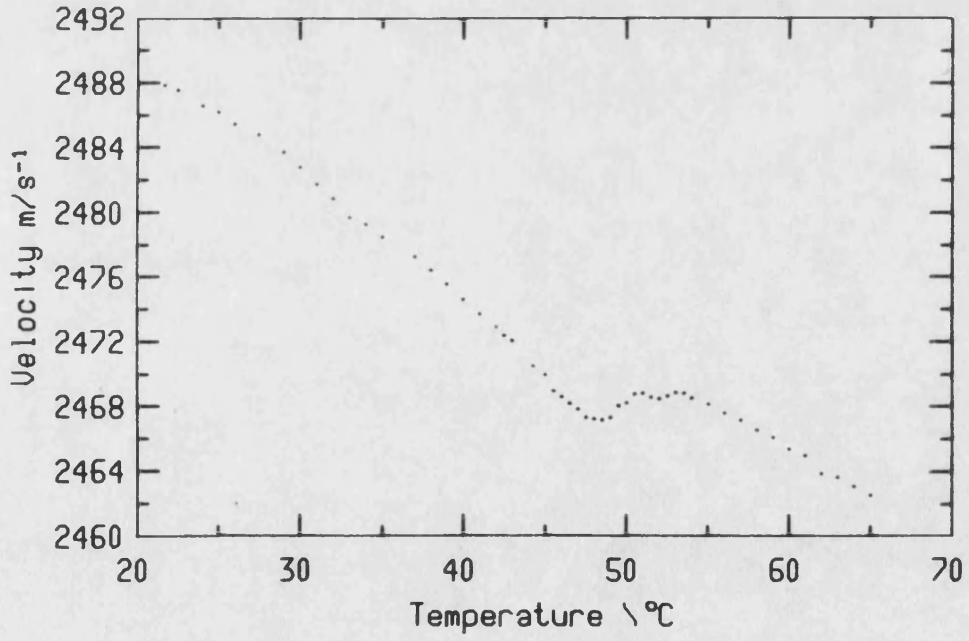

Fig 5.24 Temperature dependence of the ultrasonic wave velocity for the Z propagated Y polarized shear mode corrected for transducer delay and thermal expansion.

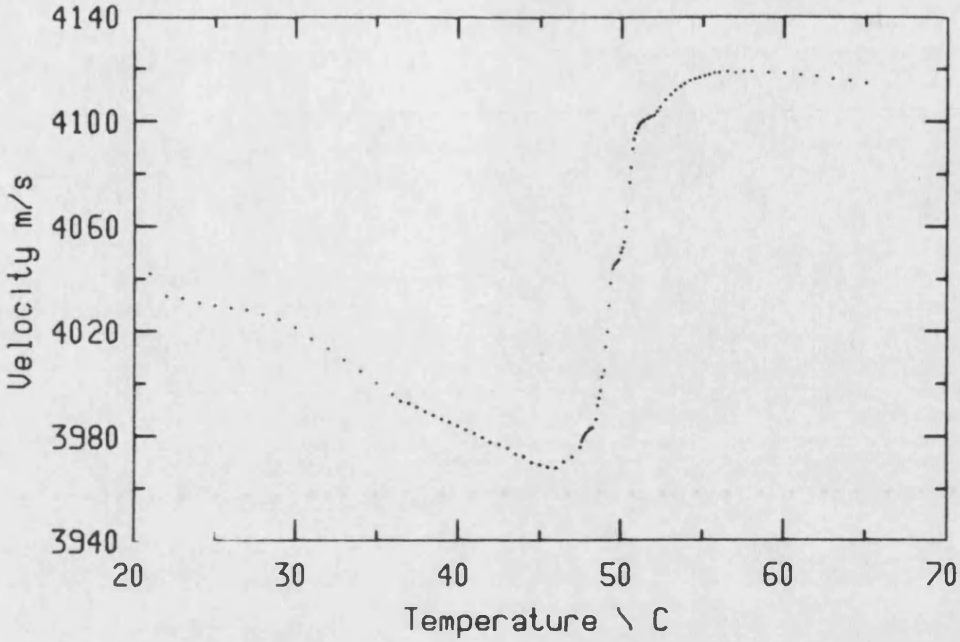

Fig 5.25 Temperature dependence of the ultrasonic wave velocity for the Z propagated longitudinal mode corrected for transducer delay and thermal expansion.

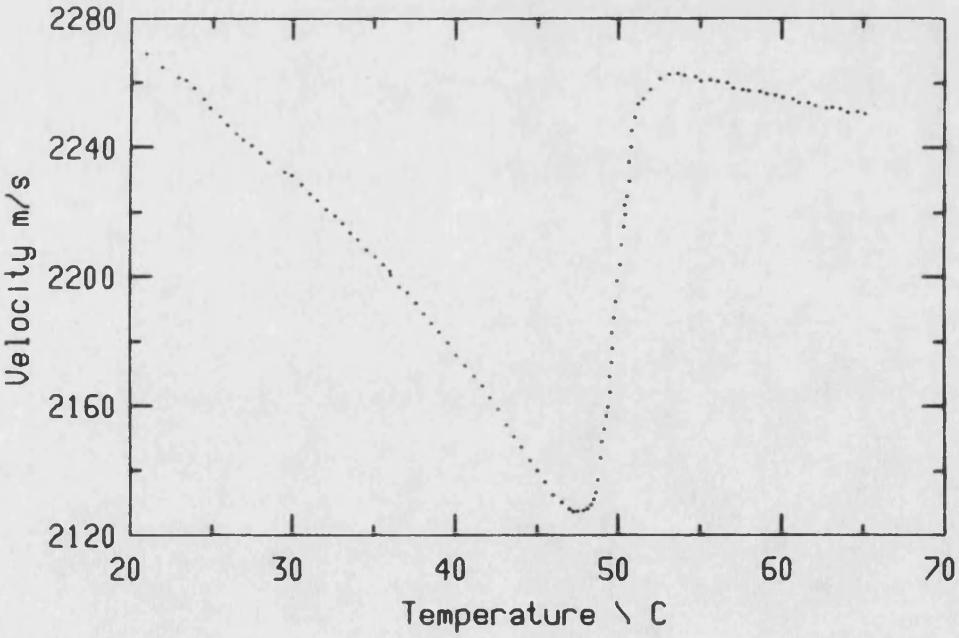

Fig 5.26 Temperature dependence of the ultrasonic wave velocity for the [1 0 1] propagated [-1 0 1] polarized shear mode corrected for transducer delay and thermal expansion.

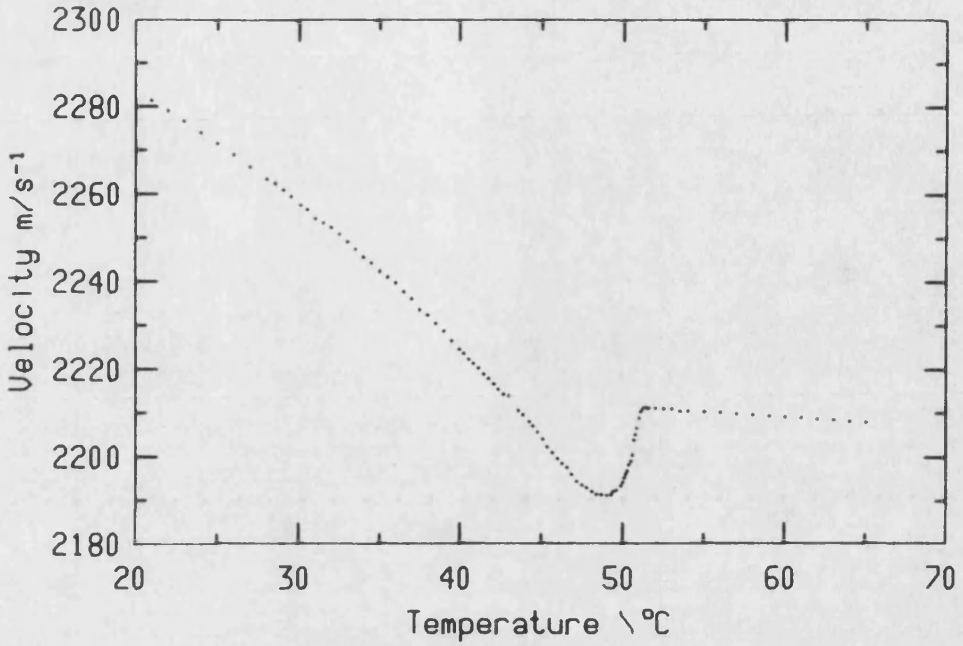

Fig 5.27 Temperature dependence of the ultrasonic wave velocity for the [1 0 1] propagated Y polarized shear mode corrected for transducer delay and thermal expansion.

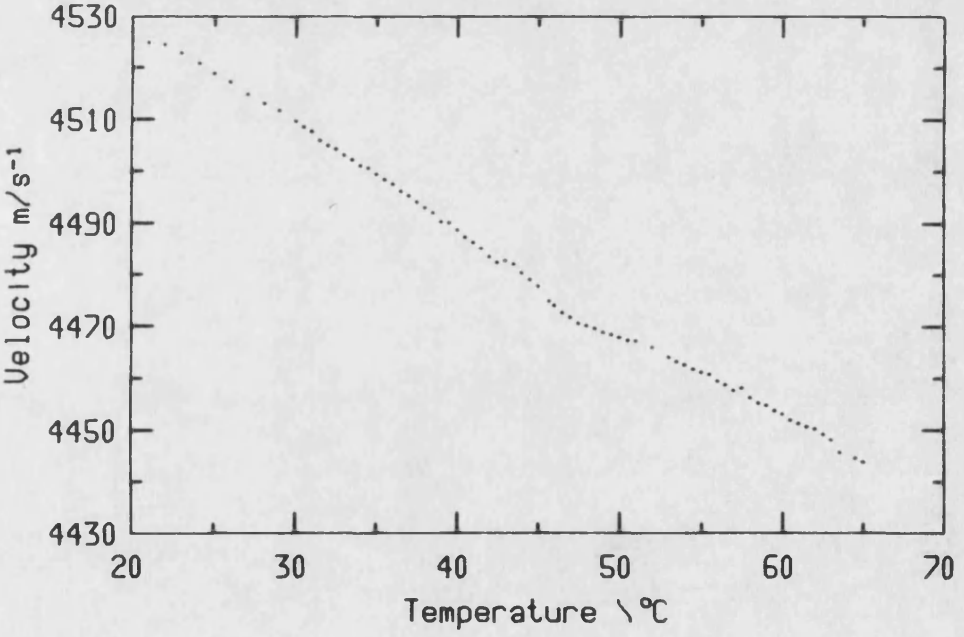

Fig 5.28 Temperature dependence of the ultrasonic wave velocity for the [1 0 1] propagated longitudinal mode corrected for transducer delay and thermal expansion.

Temperature	mode 1	mode 2	mode 3	mode 4	mode 5	mode 6	mode 7	mode 8	mode 9	mode 10	mode 11	mode 12
20	5127.60	1899.60	2518.40	2456.60	4460.40	1939.60	2510.60	2488.30	4045.80	2273.00	2283.60	4527.00
25	5108.69	1892.14	2517.57	2448.02	4453.63	1932.92	2501.36	2486.17	4029.73	2252.04	2271.58	4518.92
30	5084.78	1884.38	2516.47	2437.12	4446.29	1924.02	2491.71	2482.80	4021.17	2231.32	2257.91	4509.77
35	5057.15	1876.31	2514.51	2425.13	4439.23	1914.65	2480.46	2478.48	4000.23	2206.34	2242.29	4499.53
40	5029.51	1865.84	2512.11	2412.23	4432.06	1903.89	2469.31	2474.61	3983.84	2175.44	2224.48	4488.79
45	4994.97	1853.86	2509.21	2397.55	4423.15	1891.31	2454.90	2469.92	3968.98	2140.26	2204.54	4477.98
50	4971.90	1841.70	2503.04	2384.55	4414.96	1880.24	2442.31	2468.20	4050.17	2204.70	2194.34	4468.14
55	4967.07	1838.41	2494.37	2381.10	4406.58	1879.09	2437.55	2468.10	4117.18	2259.90	2210.31	4461.37
60	4949.94	1835.99	2487.13	2378.08	4397.98	1878.66	2433.85	2465.71	4118.22	2255.70	2209.06	4453.20
65	4936.40	1833.62	2482.87	2374.64	4388.95	1878.30	2430.22	2462.54	4114.55	2250.00	2207.80	4443.98

Table 5.5 Temperature variation of the ultrasonic wave velocity (corrected for thermal expansion and transducer delay) for TGS from 20 °C to 65 °C quoted for 5 °C steps. The units are ms^{-1}.

and as the samples mass remains constant the new density can hence be calculated. A plot of density against temperature is given in figure 6.29. The variations of the elastic constants with temperature are presented in figures 5.30 to 5.39. Values for the elastic constants at 5 °C intervals are also quoted in table 5.6.

The temperature derivatives of the elastic stiffness constants (Tc_{ij}) defined as

$$Tc_{ij} = \frac{1}{c_{ij}} \frac{\Delta c_{ij}}{\Delta T}$$

have been calculated in steps of 5 °C and are given in table 5.7.

Values for c_{13} are subject to a wide margin of experimental error.

5.4 Measurement of the temperature dependence of pressure derivatives of elastic stiffness constants.

The hydrostatic pressure dependence of the ultrasonic wave velocities are presented as a plot of the relative change in natural wave velocity versus applied hydrostatic pressure (units Kbar = 10^8 Pa). The parameter $\Delta W/W_o$ is defined as

$$\frac{\Delta W}{W_0} = \left(W_{(P)} - W_{(0)} \right) / W_0$$

where $W_{(P)}$ is the natural velocity at a pressure P. This provides a representation which is more easily interpreted and compared with other results than for example a plot of the raw echo overlap frequency versus

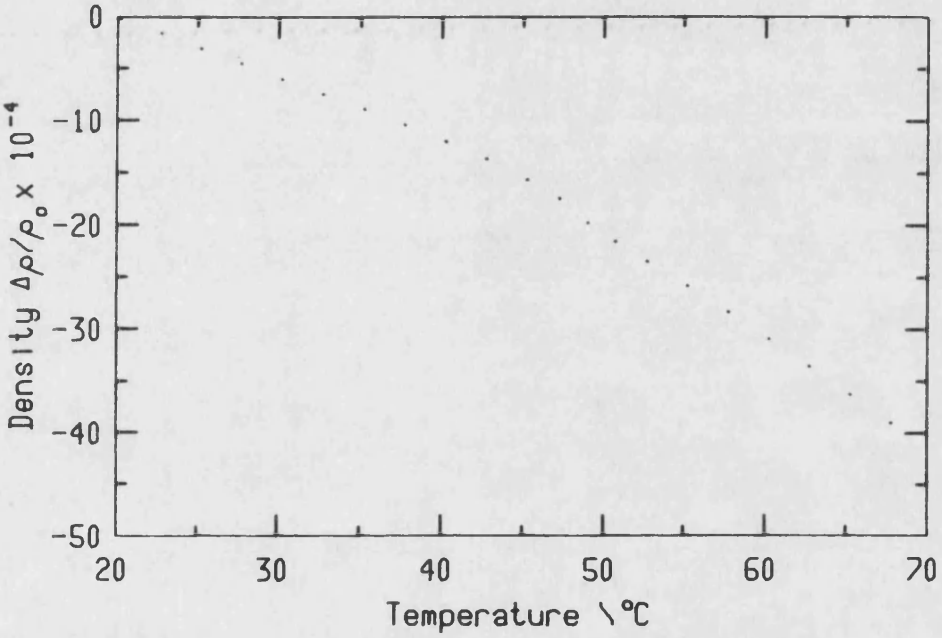

Fig 5.29 Temperature dependence of the density of TGS.

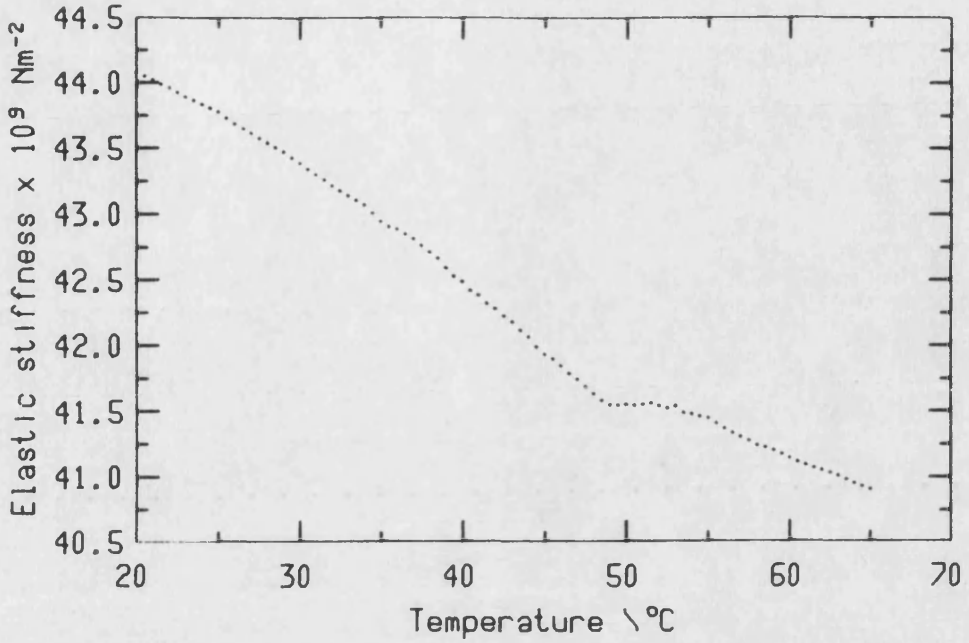

Fig 5.30 Temperature dependence of C_{11}

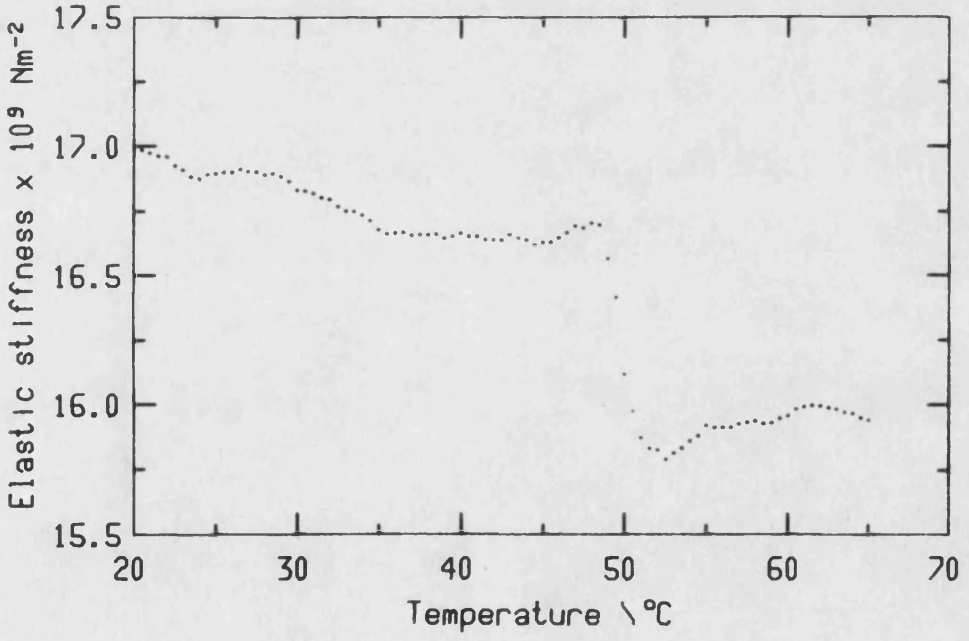

Fig 5.31 Temperature dependence of C_{13}

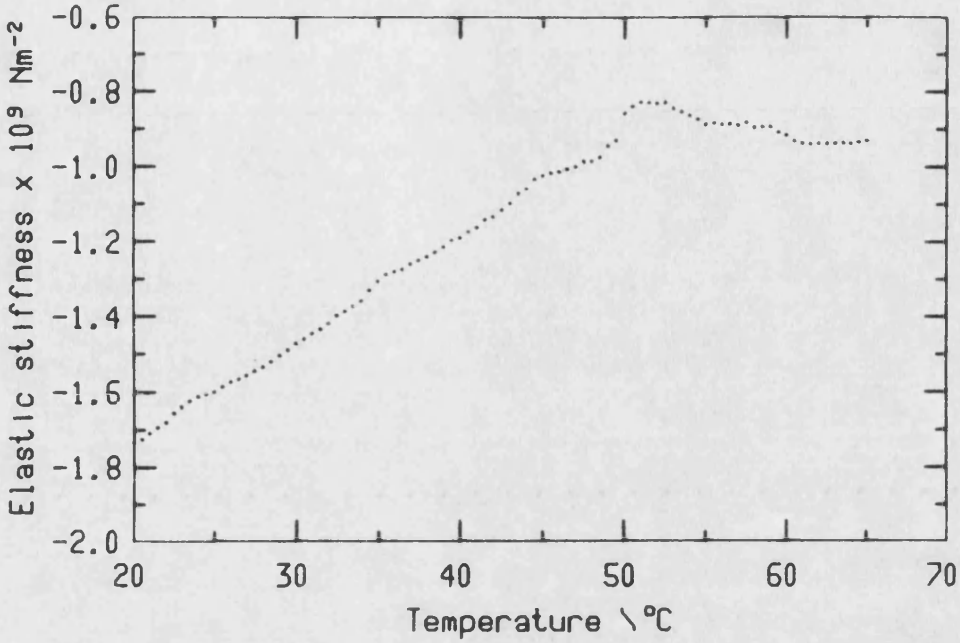

Fig 5.32 Temperature dependence of C_{15}

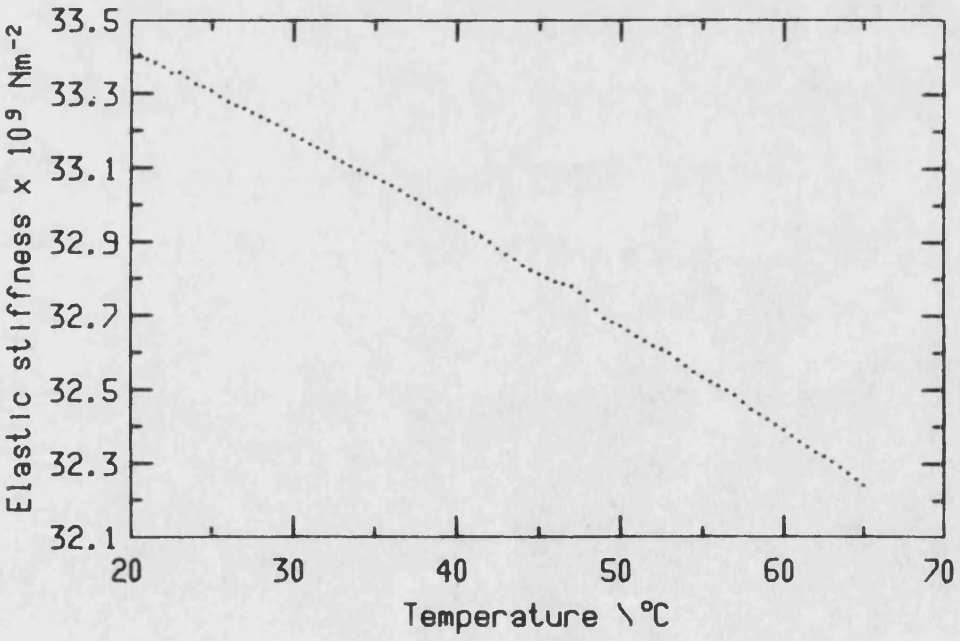

Fig 5.33 Temperature dependence of C_{22}

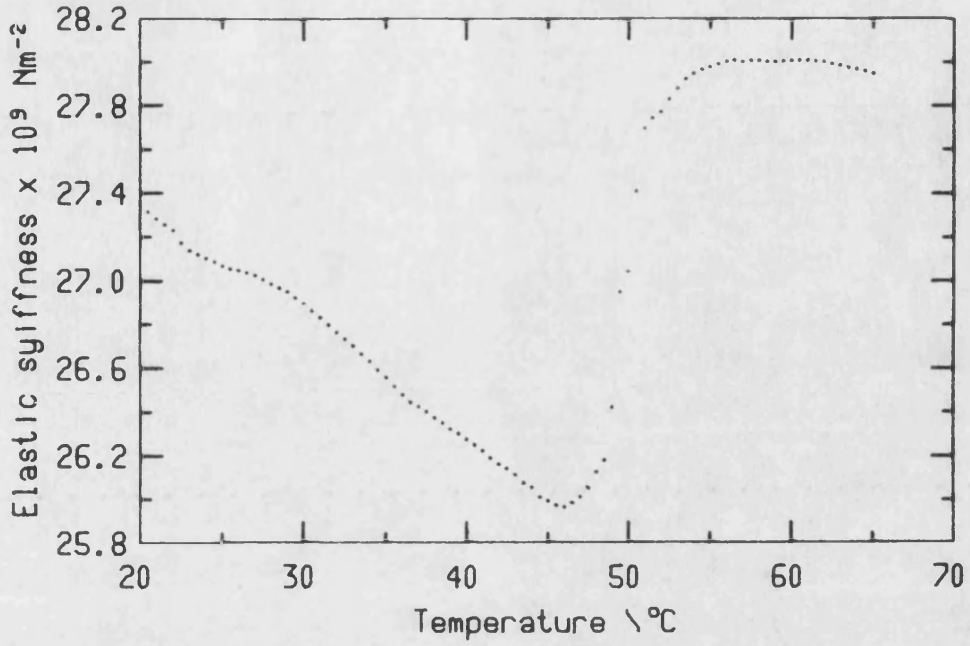

Fig 5.34 Temperature dependence of C_{33}

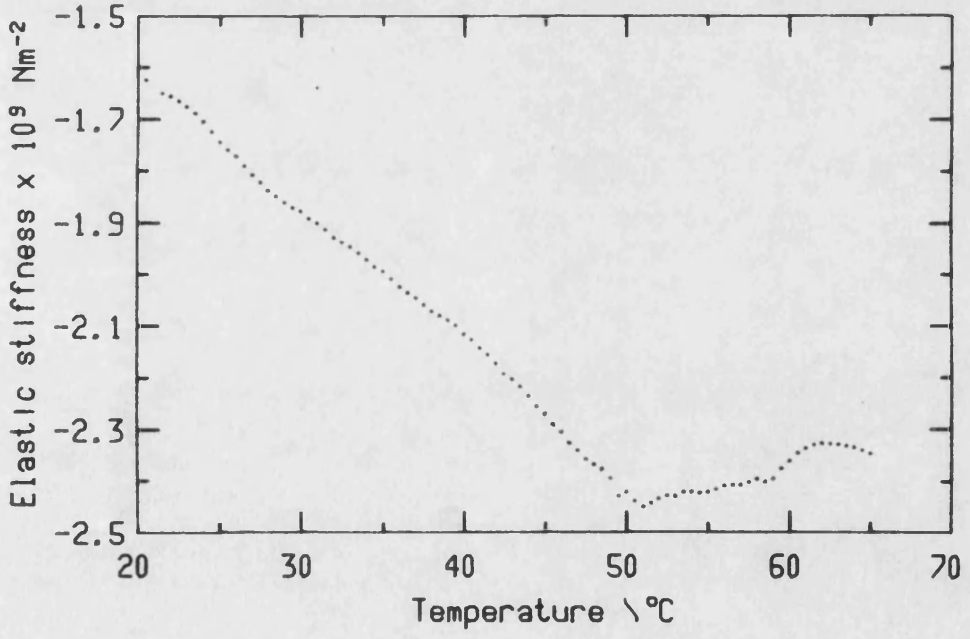

Fig 5.35 Temperature dependence of C_{35}

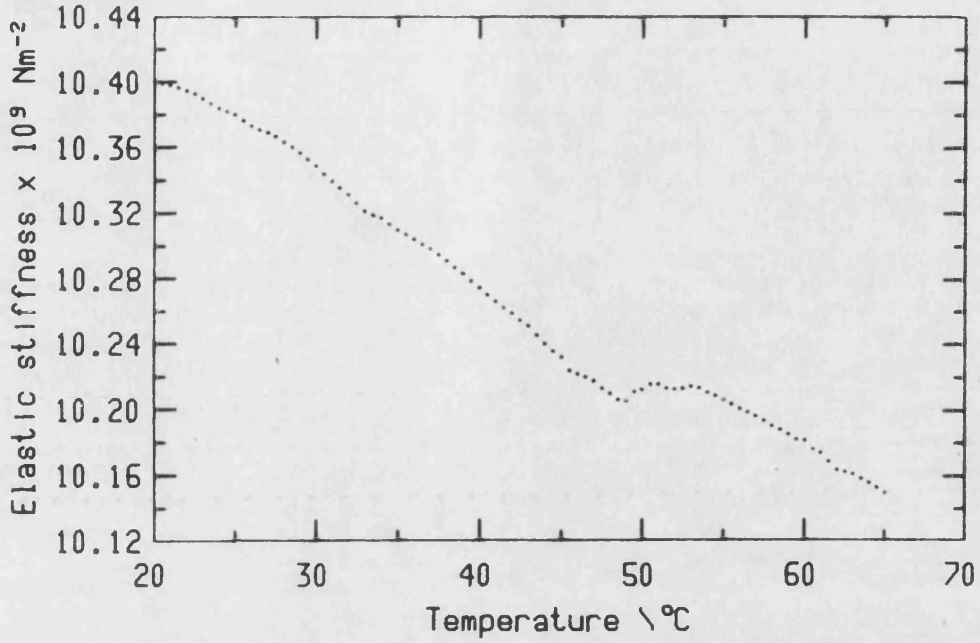

Fig 5.36 Temperature dependence of C_{44}

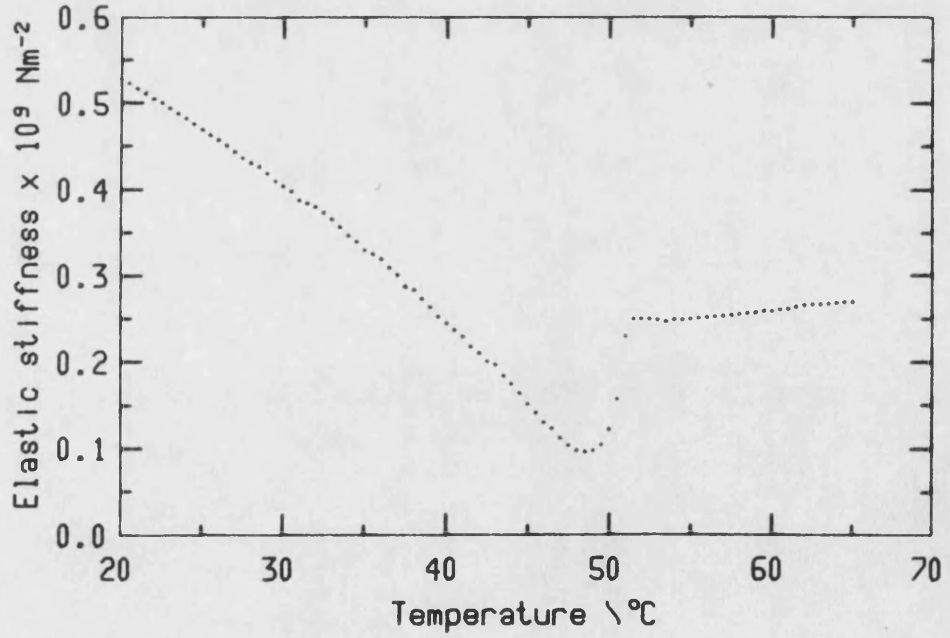

Fig 5.37 Temperature dependence of C_{46}

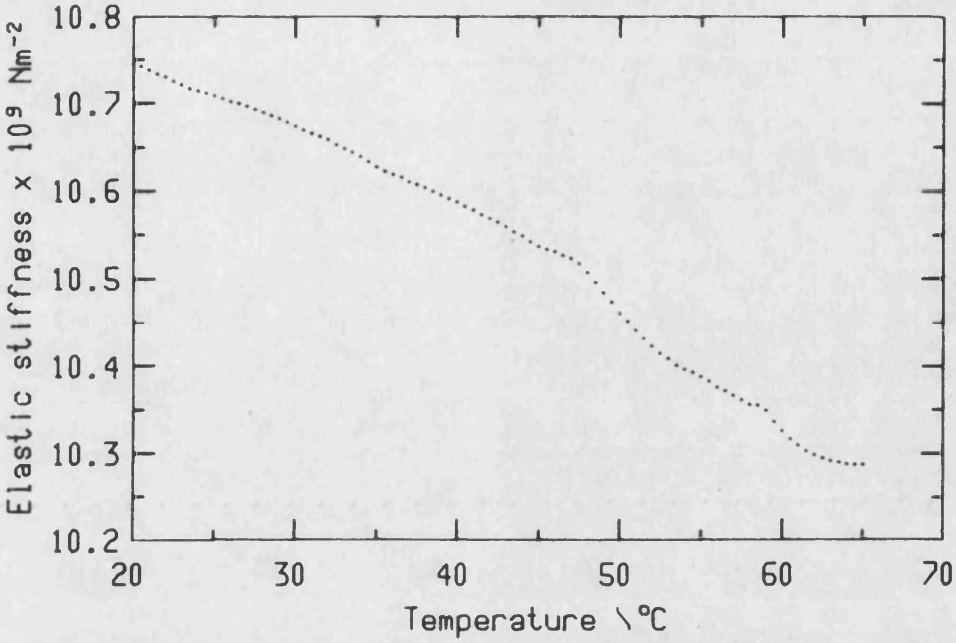

Fig 5.38 Temperature dependence of C_{55}

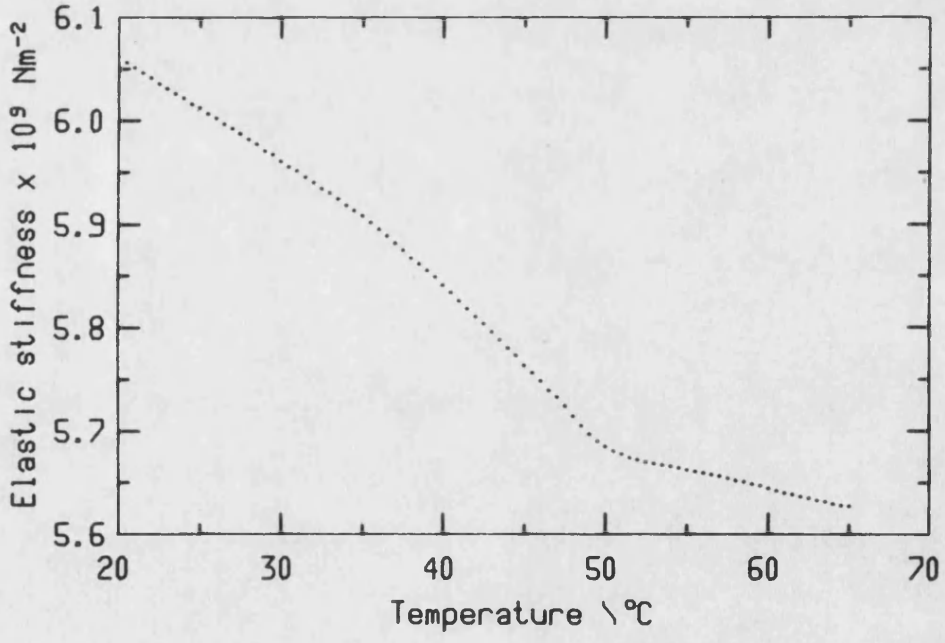

Fig 5.39 Temperature dependence of C_{66}

Temperature	C_{11}	C_{13}	C_{15}	C_{22}	C_{33}	C_{35}	C_{44}	C_{46}	C_{55}	C_{66}
20	44.081	16.995	-1.733	33.419	27.343	-1.615	10.401	0.529	10.745	6.062
25	43.776	16.900	-1.598	33.308	27.072	-1.743	10.380	0.469	10.709	6.012
30	43.386	16.833	-1.471	33.189	26.899	-1.877	10.349	0.404	10.674	5.961
35	42.941	16.680	-1.305	33.074	26.558	-1.993	10.309	0.329	10.628	5.909
40	42.488	16.666	-1.188	32.957	26.274	-2.116	10.274	0.245	10.587	5.841
45	41.928	16.632	-1.022	32.813	25.993	-2.268	10.232	0.153	10.537	5.764
50	41.548	16.118	-0.857	32.674	27.043	-2.419	10.212	0.123	10.460	5.686
55	41.446	15.922	-0.889	32.534	27.980	-2.419	10.206	0.251	10.387	5.663
60	41.144	15.958	-0.917	32.391	28.007	-2.360	10.181	0.259	10.325	5.645
65	40.902	15.940	-0.930	32.241	27.945	-2.349	10.150	0.270	10.287	5.628

Table 5.6 Temperature variation of elastic stiffness constants of TGS from 20 °C to 65 °C quoted for 5 °C steps. The units are $10^{10}\,Nm^{-2}$.

pressure. These are presented in figures 5.40 to 5.47 for modes 1 to 12 at 20 °C (below the phase transition temperature) and at 65 °C (above the phase transition temperature) on the same page. For modes 13 to 18 experiments were only performed at room temperature, results being given in figures 5.48 and 5.49.

To enable the pressure derivatives of the elastic constants to be obtained, it is necessary to calculate $(\dot{a}_o v^2)'_{p=o}$ for each mode (eq 2.59) where the values for f' are taken as the gradient of the least square lines and f_o as the intercept (ie at zero pressure). In calculating $(\dot{a}_o v^2)'_{p=o}$ it is assumed that values for linear compressibility and bulk modulus are independent of temperature. This is a reasonable assumption as any temperature corrections to these parameters will result in only second order corrections of $(\dot{a}_o v^2)'_{p=o}$ so can be ignored. The quantity $(\dot{a}_o v^2)'_{p=o}$ for modes 1 to 12 over the temperature range 20 to 65 °C are presented graphically in figures 5.50 to 5.61.

By using values for $(\dot{a}_o v^2)'_{p=o} = 0$ at selected temperatures the pressure derivatives of the elastic constants where calculated using the procedure described in section 4.5 and are tabulated in table 5.8.

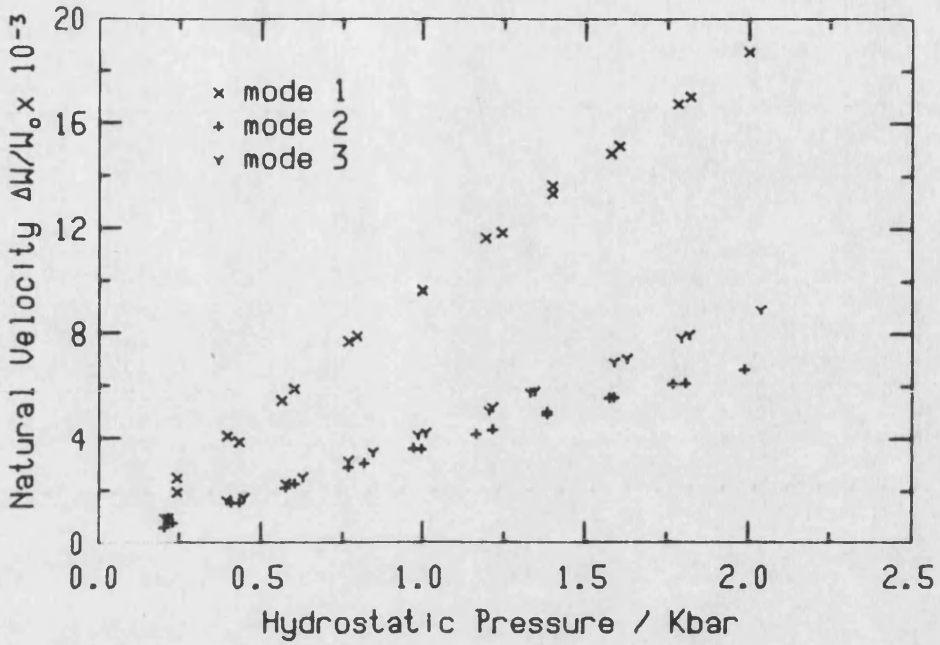

Fig 5.40 Results of hydrostatic pressure experiments on TGS for modes propagated in the X direction at room temperature.

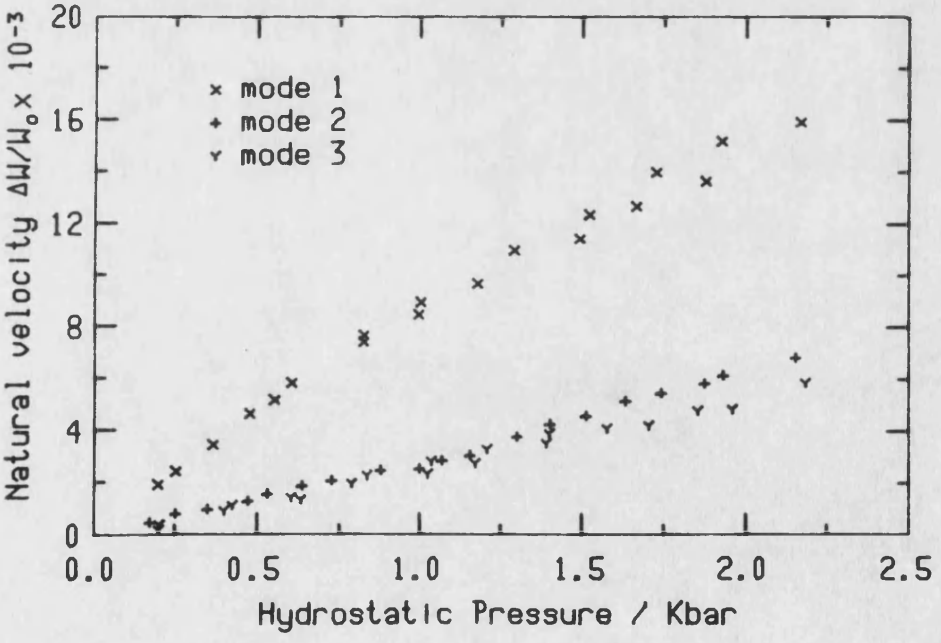

Fig 5.41 Results of hydrostatic pressure experiments on TGS for modes propagated in the X direction at 60 °C.

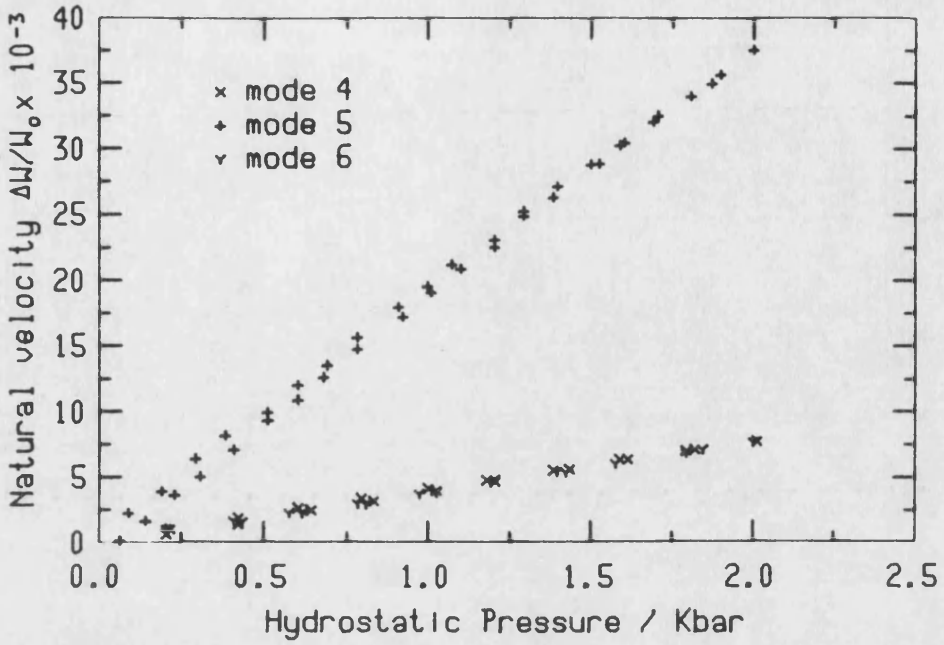

Fig 5.42 Results of hydrostatic pressure experiments on TGS for modes propagated in the Y direction at room temperature.

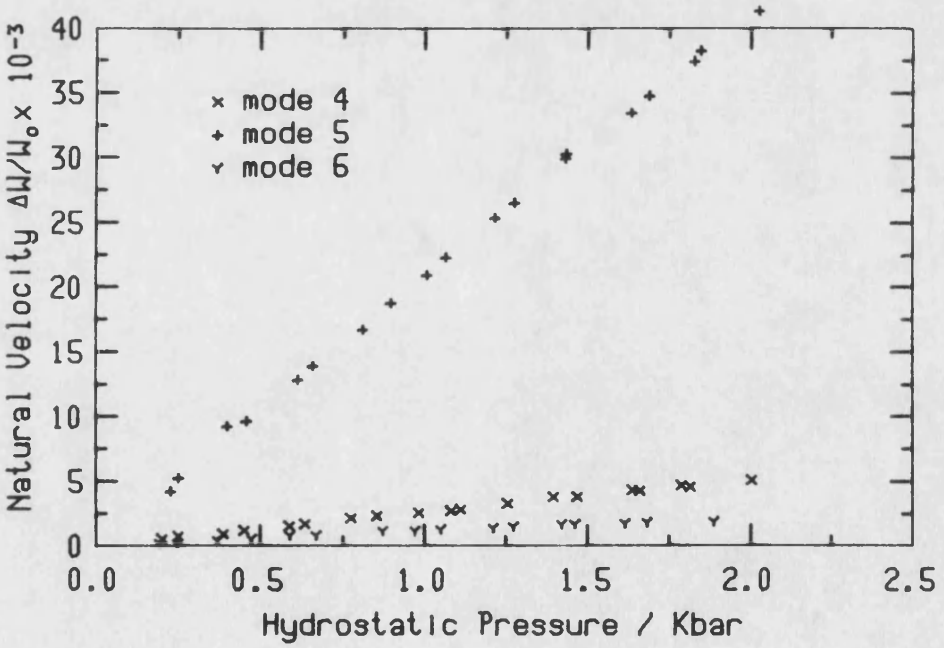

Fig 5.43 Results of hydrostatic pressure experiments on TGS for modes propagated in the Y direction at 60 °C.

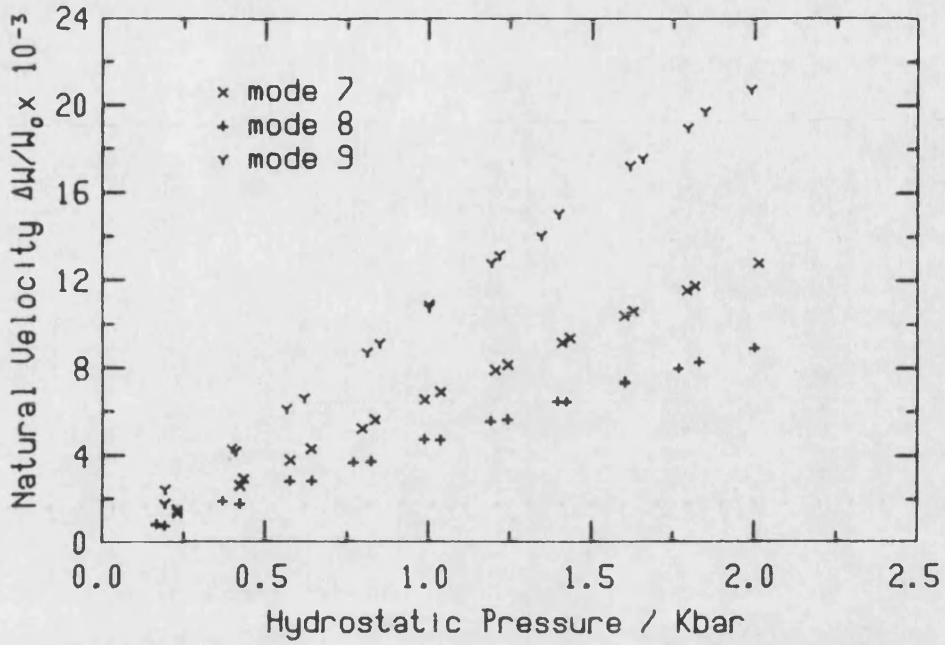

Fig 5.44 Results of hydrostatic pressure experiments on TGS for modes propagated in the Z direction at room temperature.

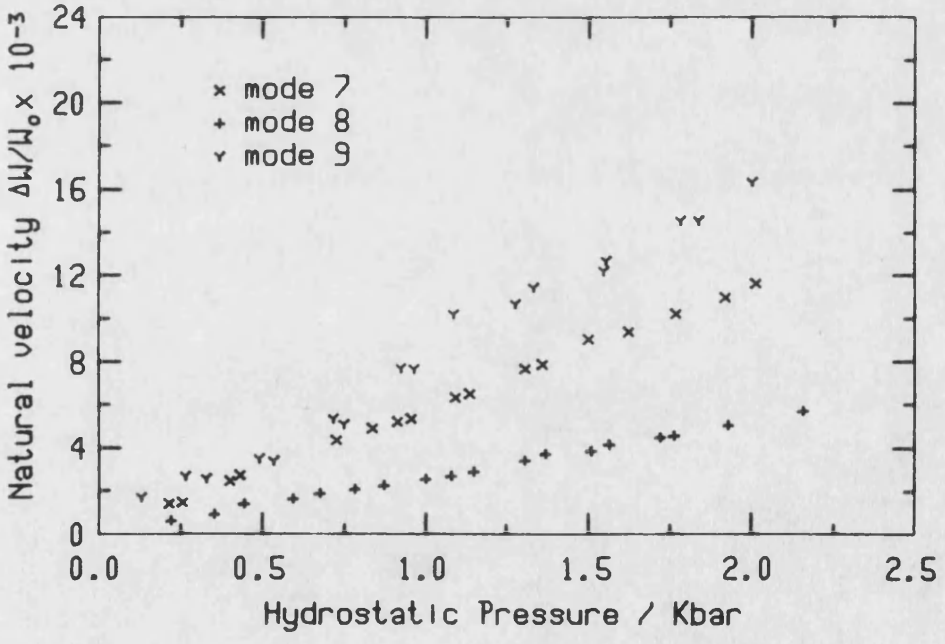

Fig 5.45 Results of hydrostatic pressure experiments on TGS for modes propagated in the Z direction at 60 °C.

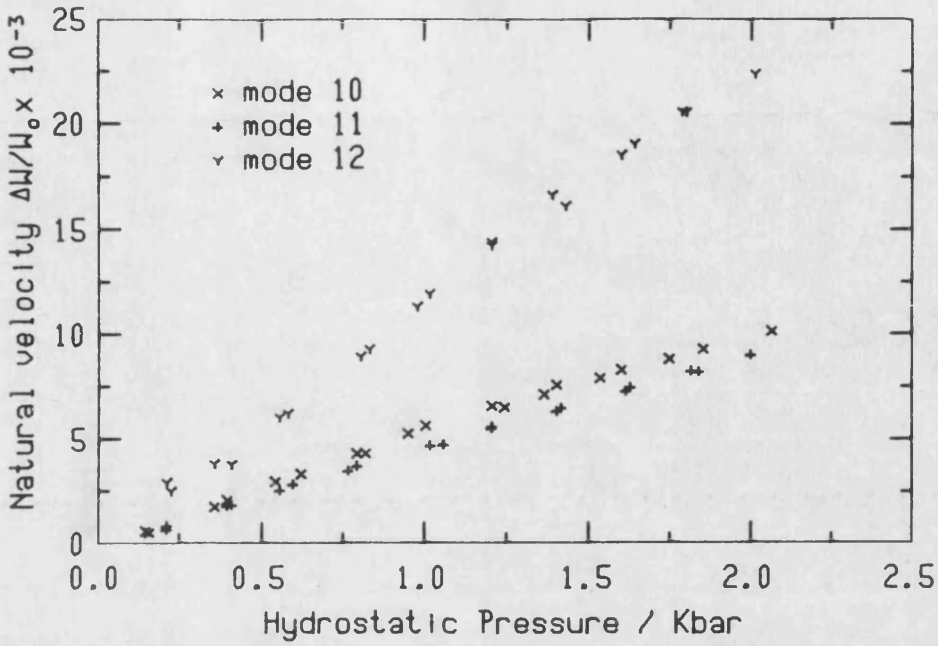

Fig 5.46 Results of hydrostatic pressure experiments on TGS for modes propagated in the [101] direction at room temperature.

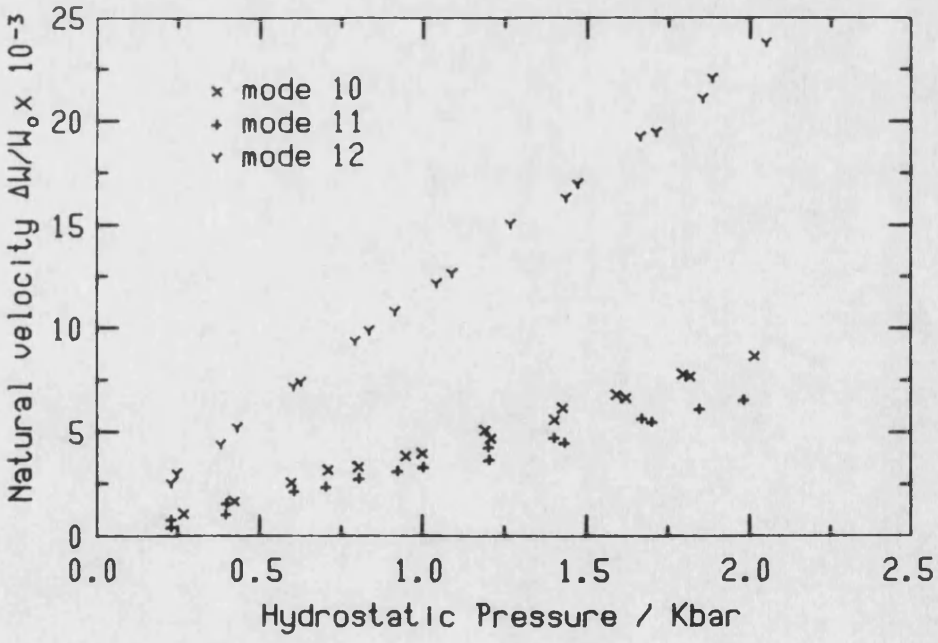

Fig 5.47 Results of hydrostatic pressure experiments on TGS for modes propagated in the [101] direction at 60 °C.

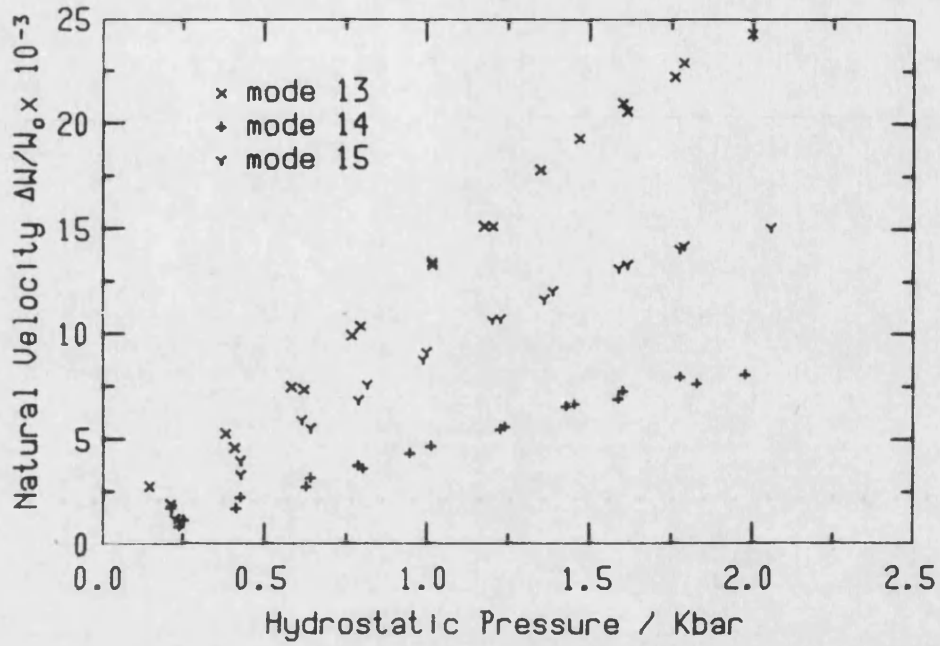

Fig 5.48 Results of hydrostatic pressure experiments on TGS for modes propagated in the [110] direction at room temperature.

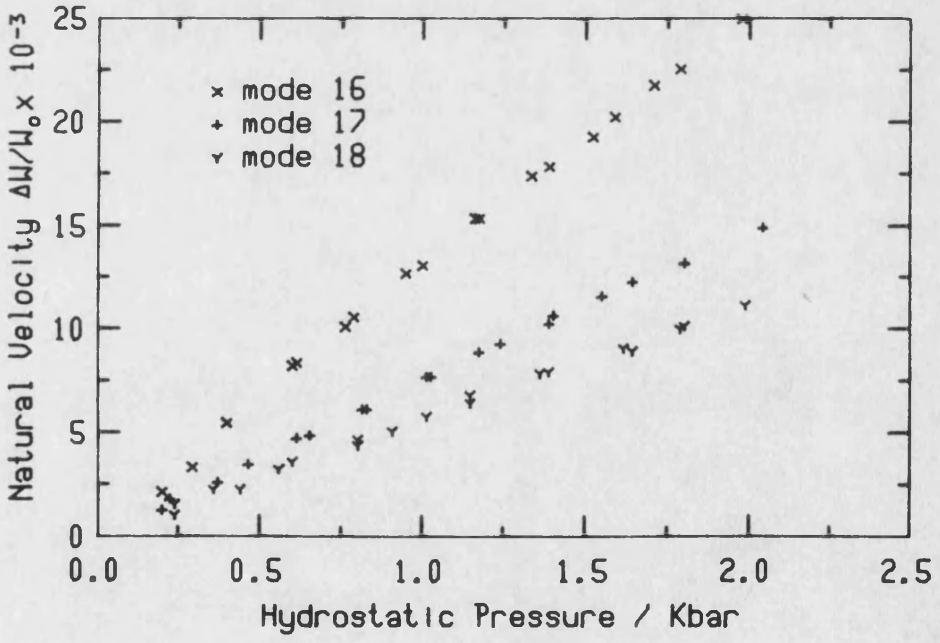

Fig 5.49 Results of hydrostatic pressure experiments on TGS for modes propagated in the [011] direction at room temperature.

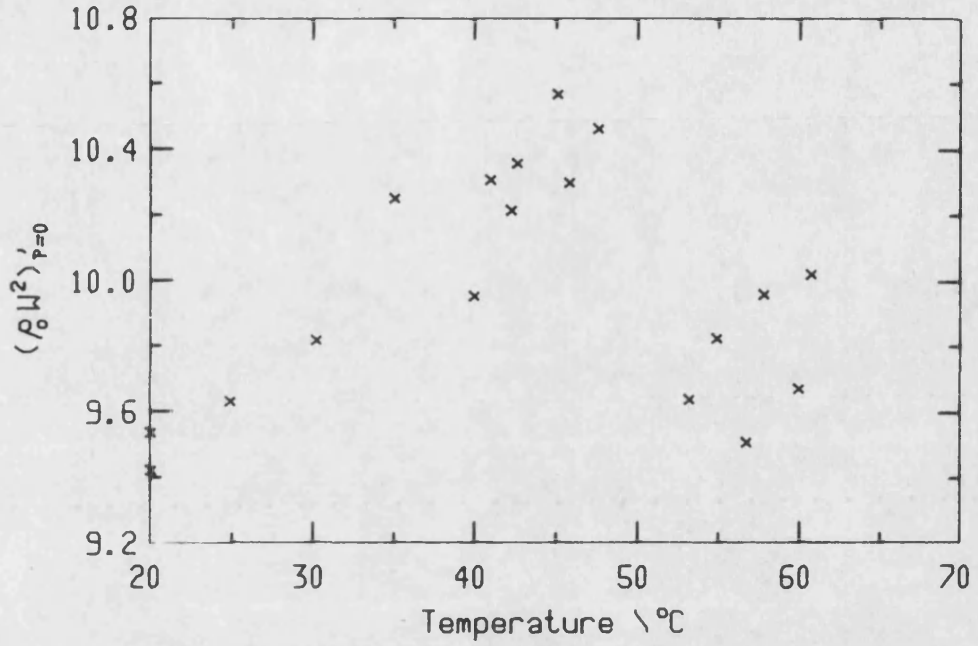

Fig 5.50 Temperature dependence of $(\rho_0 W^2)'_{P=0}$ for mode 1 in TGS.

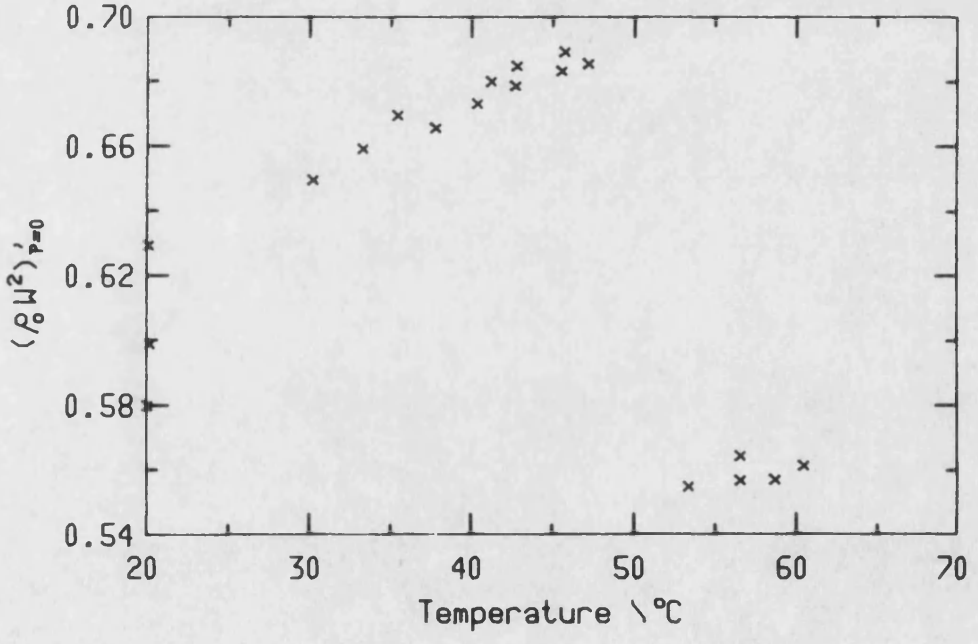

Fig 5.51 Temperature dependence of $(\rho_0 W^2)'_{P=0}$ for mode 2 in TGS.

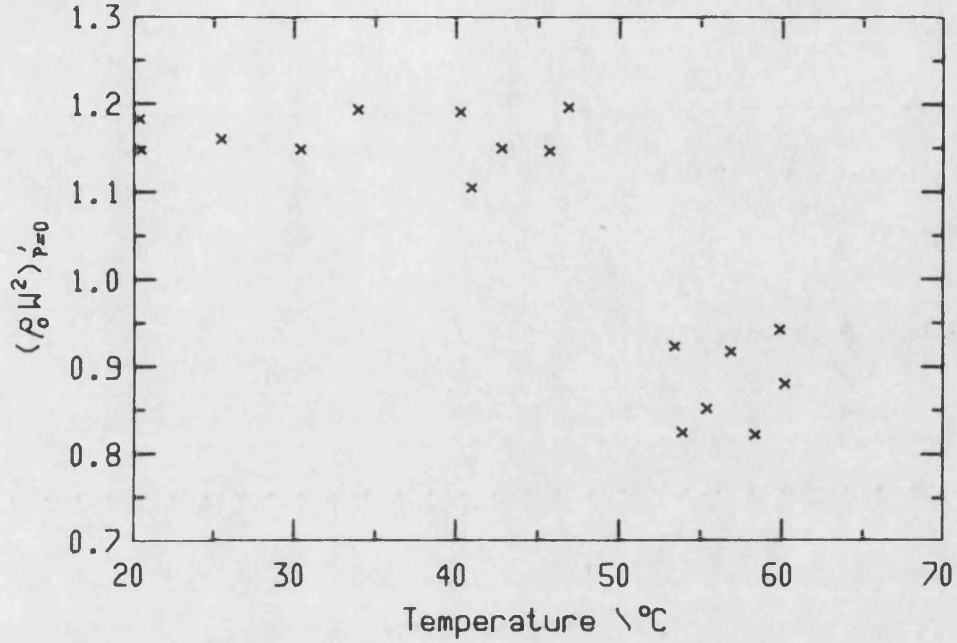

Fig 5.52 Temperature dependence of $(\rho_o W^2)'_{P=0}$ for mode 3 in TGS.

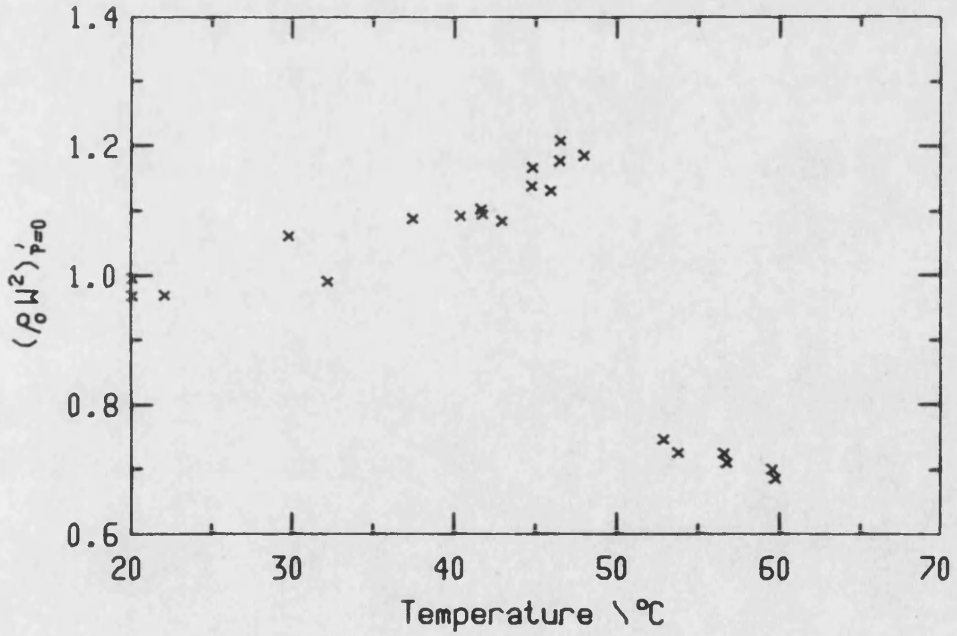

Fig 5.53 Temperature dependence of $(\rho_o W^2)'_{P=0}$ for mode 4 in TGS.

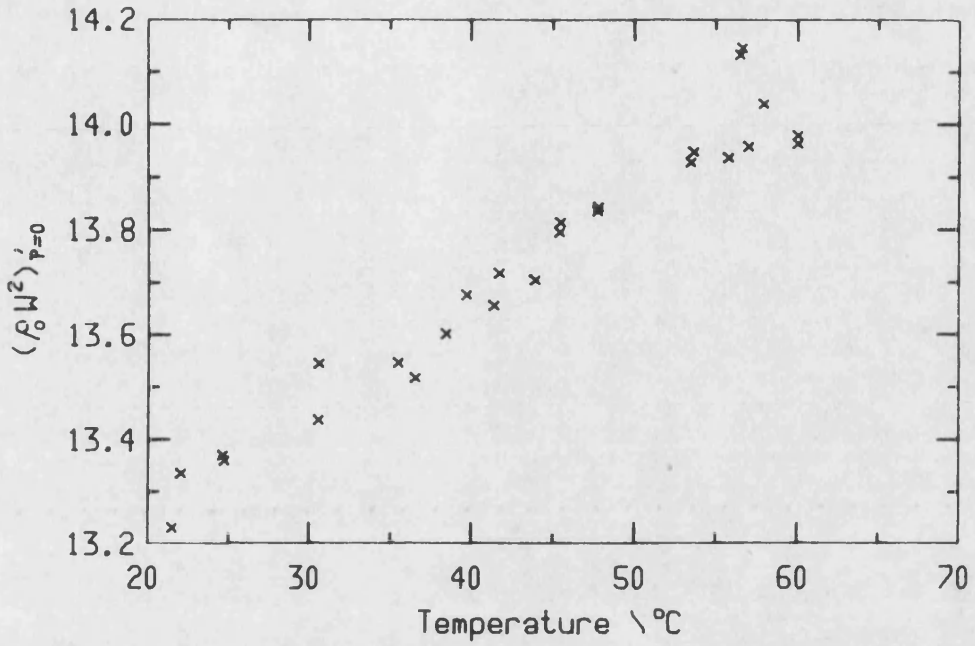

Fig 5.54 Temperature dependence of $(\rho_0 W^2)'_{P=0}$ for mode 5 in TGS.

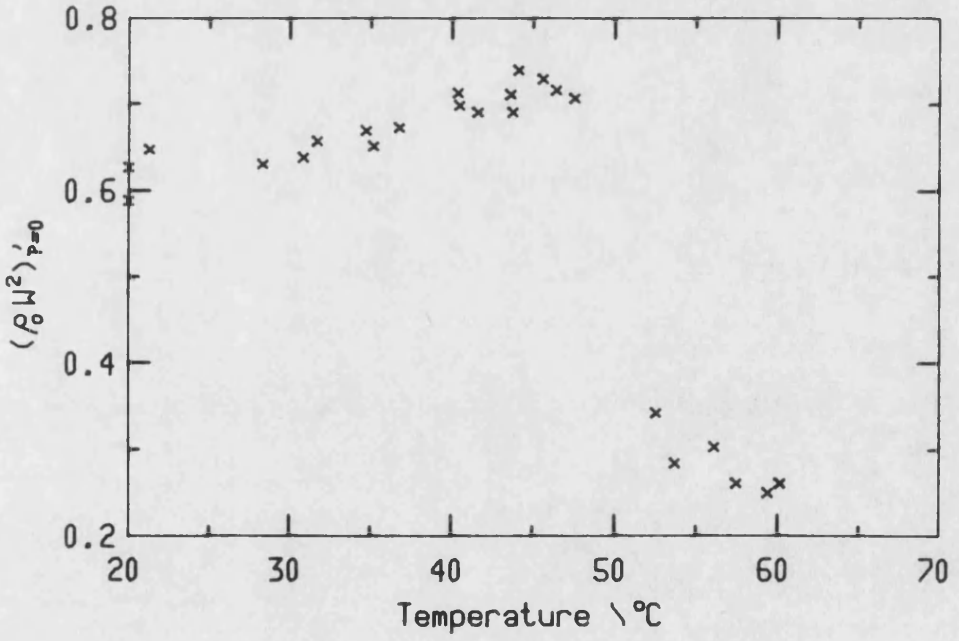

Fig 5.55 Temperature dependence of $(\rho_0 W^2)'_{P=0}$ for mode 6 in TGS.

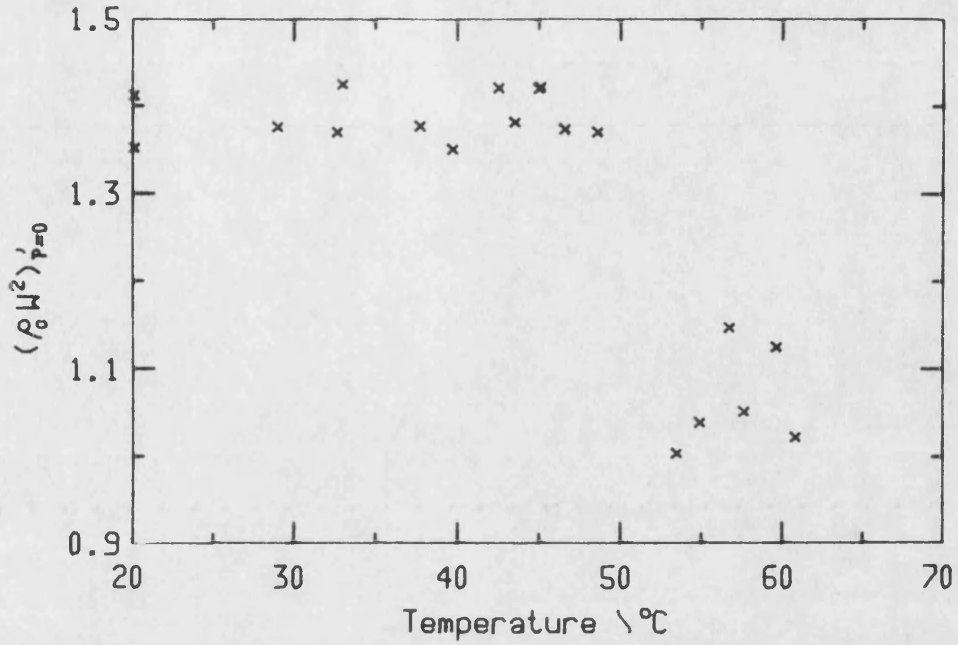

Fig 5.56 Temperature dependence of $(\rho_0 W^2)'_{P=0}$ for mode 7 in TGS.

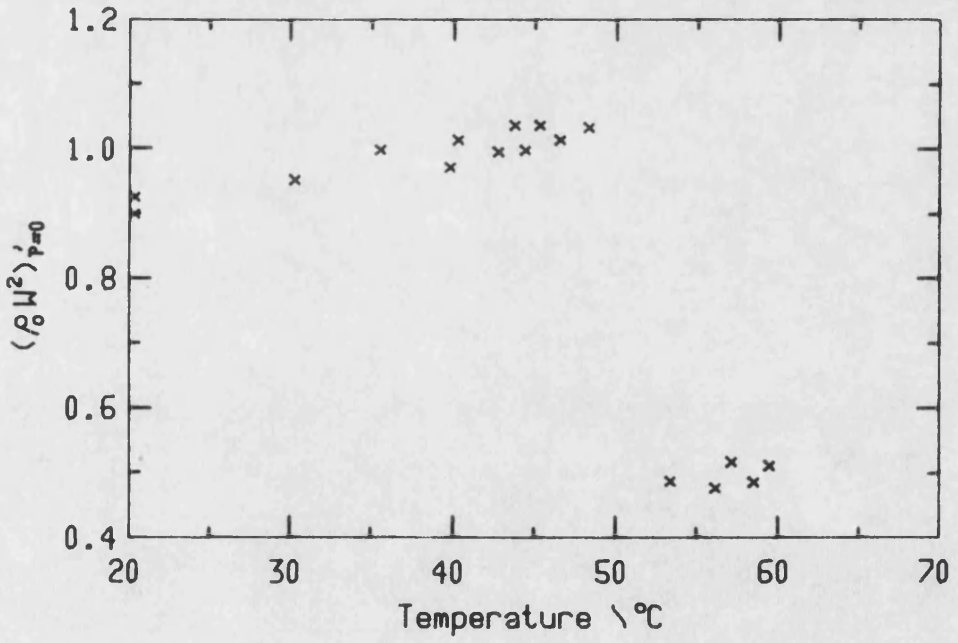

Fig 5.57 Temperature dependence of $(\rho_0 W^2)'_{P=0}$ for mode 8 in TGS.

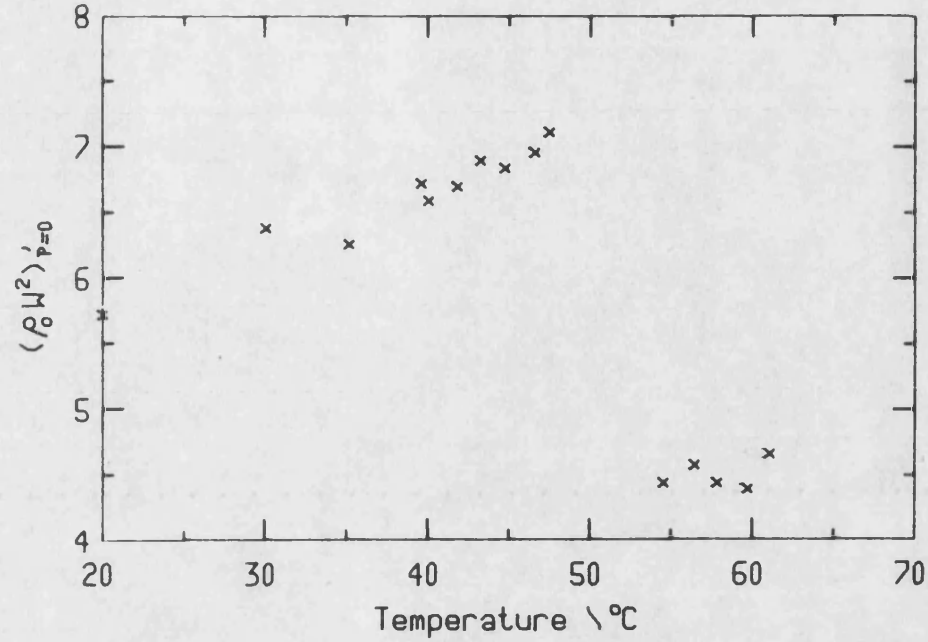

Fig 5.58 Temperature dependence of $(\rho_0 W^2)'_{P=0}$ for mode 9 in TGS.

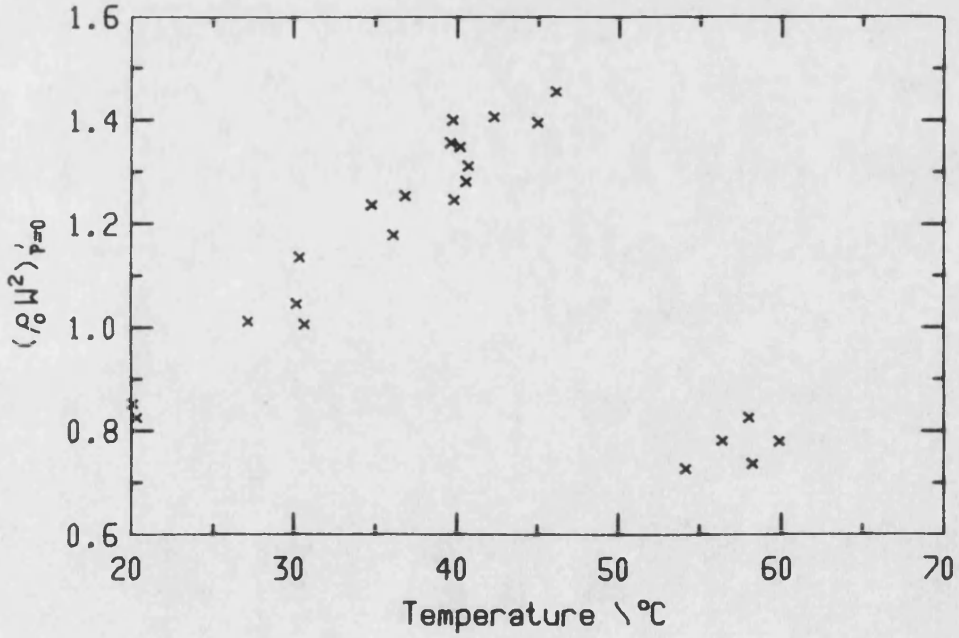

Fig 5.59 Temperature dependence of $(\rho_0 W^2)'_{P=0}$ for mode 10 in TGS.

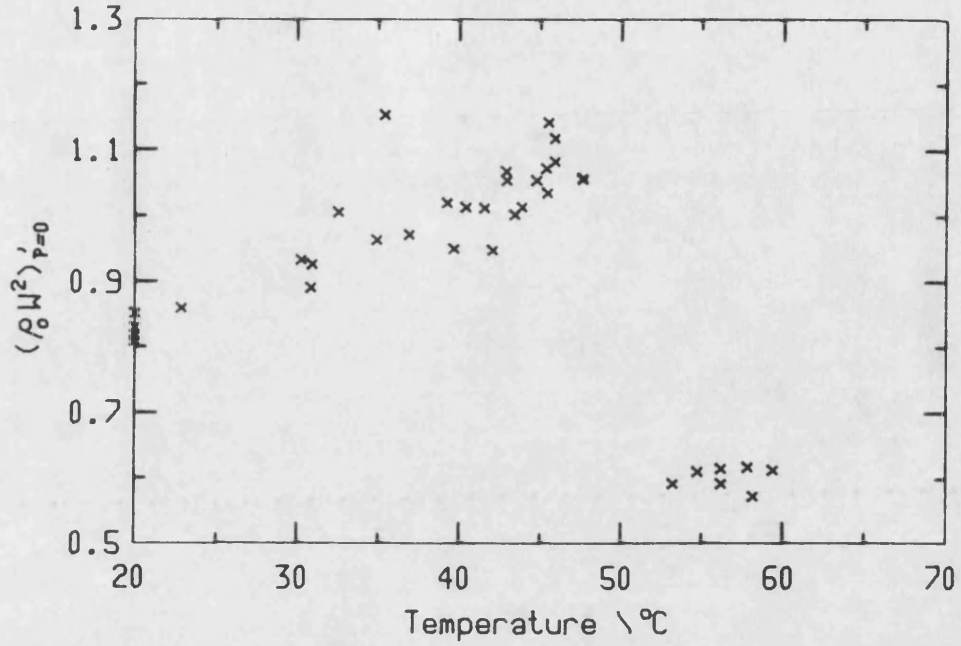

Fig 5.60 Temperature dependence of $(\rho_0 W^2)'_{P=0}$ for mode 11 in TGS.

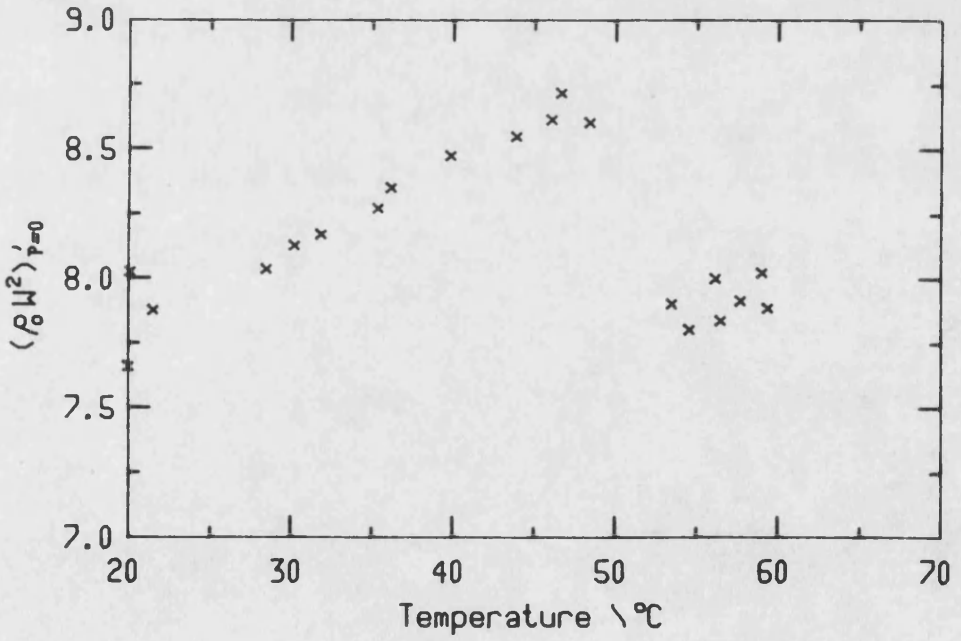

Fig 5.61 Temperature dependence of $(\rho_0 W^2)'_{P=0}$ for mode 12 in TGS.

Temperature	TC_{11}	TC_{13}	TC_{15}	TC_{22}	TC_{33}	TC_{35}	TC_{44}	TC_{46}	TC_{55}	TC_{66}
22.5	-13.5	-13.9	-177.3	-6.0	-20.5	146.1	-3.6	-234.5	-6.5	-15.8
27.5	-16.8	-5.7	-158.5	-6.3	-11.8	153.2	-5.1	-299.1	-5.7	-16.2
32.5	-19.2	-17.1	-228.7	-6.5	-24.8	120.9	-6.9	-387.0	-8.1	-17.4
37.5	-21.2	-1.3	-184.1	-6.7	-20.1	113.6	-6.2	-613.9	-6.9	-22.2
42.5	-25.3	-2.8	-304.1	-8.3	-21.1	142.1	-7.6	-891.7	-8.8	-25.6
57.5	-13.2	5.6	59.5	-8.2	2.0	-37.3	-4.1	67.9	-9.7	-5.3
62.5	-10.6	-3.6	14.1	-8.1	-3.6	-3.8	-4.9	77.8	-6.1	-5.2

Table 5.7 Temperature derivative TC_{ij} of elastic stiffness constants of TGS at selected temperatures. The units are $10^{-4}/°C$.

Temperature	$\partial c_{11}/\partial P$	$\partial c_{13}/\partial P$	$\partial c_{15}/\partial P$	$\partial c_{22}/\partial P$	$\partial c_{33}/\partial P$	$\partial c_{35}/\partial P$	$\partial c_{44}/\partial P$	$\partial c_{46}/\partial P$	$\partial c_{55}/\partial P$	$\partial c_{66}/\partial P$
20	9.397	6.441	-1.062	13.249	5.937	0.803	0.913	0.077	1.253	0.607
30	9.770	6.449	-0.929	13.455	6.456	0.783	0.955	0.128	1.239	0.640
40	10.149	6.425	-0.752	13.661	6.979	0.719	0.997	0.179	1.219	0.672
46	10.375	6.383	-0.600	13.785	7.292	0.636	1.022	0.211	1.208	0.691
53	9.644	5.272	0.288	13.933	4.598	0.317	0.483	0.079	0.865	0.556
60	9.854	5.382	0.159	13.987	4.726	0.416	0.506	0.071	0.888	0.561

Table 5.8 Pressure derivatives of the elastic stiffness constants of TBS at selected temperatures. The units are

CHAPTER SIX

DISCUSSION OF ULTRASONIC PROPERTIES AND ELASTIC BEHAVIOUR OF TGS.

6.1 Introduction

Considerable interest has been expressed by many workers over TGS, as it provides a convenient model system for the study of a second order ferroelectric phase transition of the order-dis-order type. TGS has a Curie temperature of 49 °C near which anomalies in a variety of physical properties are observed, including a jump in the acoustic wave velocity and a peak in the magnitude of the corresponding absorption coefficient. These anomalies are observed when the wave vector k of the ultrasonic wave is perpendicular to the direction of the spontanous polarization vector component P_z, ie for the quasi-longitudinal and quasi-shear modes propagated in the XZ plane (the anomaly is not present for the Y polarized shear mode). The anomalous behaviour is most pronounced for the quasi-longitudinal mode propagated in the Z axis.

All the work reported in the literature concerning the ultrasonic properties of TGS can be split into two principal groups. The first group of work was concerned with the measurement of the ultrasonic wave velocities for several crystallographic directions. The data obtained was then used to calculate the elastic stiffness constants. Later studies of this type measured the variation of the ultrasonic properties over a broad temperature range (usually 20 to 65 °C) from which the

temperature dependence of the elastic stiffness constants could be obtained along with their associated temperature derivatives. The second group of work was concerned with developing a therotical model to account for the anomalies observed in the ultrasonic properties at the phase transition. To substantiate any particular author's chosen theory, the ultrasonic properties of a single mode of vibration over a narrow temperature band centred at the phase transition were accurately measured. The experimental results obtained were compared with the predictions made by the selected theory. Two mechanisms have been put forward in the literature to account for the observed anomalies; one is based on a "relaxation" mechanism and the other on a "fluctuation" mechanism, these are briefly discussed in section 6.2. For a fluctuation model the Z axis longitudinal mode was generally chosen and for a relaxation model the Y longitudinal mode was selected.

The present work has been concerned with case one and presents the most comprehensive experimental data to date on the ultrasonic properties of TGS. The temperature dependence of the ultrasonic velocities for 12 modes of vibration over the temperature range 20 to 70 °C have been reported, from which the temperature derivatives of 10 elastic stiffness constants have been obtained. For the first time the pressure derivatives of the elastic stiffness constants at selected temperatures, above and below the phase transition are reported. No corrections have been made to take account of the dynamic

piezoelectric stiffening, as this effect is small when it is compared to experimental error. If piezoelectric corrections were to be made using the stiffened elastic theory (see Dieulesaint and Royer (1980) and Auld (1973) for a general introduction), then only modes 2,5,8 and 11 would be affected.

6.2 Theortical models of the phase transition.

The theortical base of much of the work concerned with the investigation of a second order phase transition is due to Landau. Landau theory states that the physical properties observed at a phase transition can be explained by postulating the existence of an order parameter which goes to zero at the phase transition point. In the case of TGS this order parameter is identified with the spontaneous polarization P_2, which disappears at the phase transition. Landau theory predicts that the relaxation time associated with the ordering parameter should increase hyperbolically as the phase transition temperature is approached.

The basic principal of relaxation theory is that, when an ultrasonic wave is propagating through a piezoelectric medium, the oscillations of the elastic strain produced by the acoustic waves can result in oscillations of the value of the spontaneous polarization by virtue of the piezoelectric effect (induced polarization is proportional to the elastic strain). It is the increasing magnitude of the relaxation time of this induced

polarization as the phase transition is approached which is the cause of the anomalies observed. For a more detailed explanation of relaxation theory as applicable to ultrasonic wave propagation see Landau and Khalatnikov (1954) , O'Brien and Litovitz(1964).

By studying the piezoelectric matrices it can be seen that the longitudinal strains along the three crystallographic axes are coupled to the spontaneous polarization P_z; that coupling will also be observed for modes of propagation which have a shear stress component in the XZ plane (Gilletta (1961)). Due to the magnitude of the components in the matrix of piezoelectric coefficients for TGS, longitudinal waves propagated along the Z axis produce the highest variation in spontanous polarization per unit strain compared to all other modes. Hence this particular mode shows the most anomalous behaviour.

From the above argument it would be expected that an anomaly should also be observed for a longitudinal mode propagated down the crystallographic Y axis. This is not the case. Lawson (1941) and Minaeva et al (1969) have shown that if the strains are set up by an ultrasonic wave with a wavelength short compared to the size of the crystal, then waves propagating along the ferroelectric axis are in fact decoupled from the spontaneous polarization, and hence no relaxation loss is to be expected for this direction of propagation.

Calculations by Geguzina and Krivoglaz (1968) find that the polarization relaxation time shows a strong

orientational dependence which depends on the angle between the ultrasonic wave vector k and the direction of the spontaneous polarization vector P_z. The net effect is that the anomalous reduction in the ultrasonic wave velocity will only be readily observed when the ultrasonic wave vector k is almost perpendicular to the polar axis. This strong orientational dependence can be seen in the work of Strukov et al (1976), who measured the ultrasonic wave velocity for a longitudinal mode propagated down the Z axis and for a mode propagated in a direction which was 4 degrees "off axis" in the XY plane. An increase of the ultrasonic wave velocity by 30 m/s was observed, which cannot be attributed solely to the usual anistropy of the elastic properties.

The relaxation theory does not predict any anomalous behaviour for modes of propagation involving YZ and XY shear strains as these cannot be coupled to the spontaneous polarization P_z. Michelson (1976) proposed a mechanism to account for anomalous behaviour involving these modes by suggesting that in the presence of an ultrasonic wave the microscopic state of the crystal is inhomgeneous and that the free energy expansion used in the Landau theory should also include terms to account for the spatial derivatives of polarization and stress. He predicted that the maximum absorption of the ultrasonic waves must occur at the phase transition, in contrast to the relaxation mechanism for which it occurs at a point removed from the Curie point. No data can be found in the literature to support this hypothesis, and

our data has insufficient resolution of temperature to enable this question to be resolved.

The second theory which has been developed (Minaeva et all (1967) and Levanyuk (1966)) to explain the physical effects observed at the phase transition is a "fluctuation" model. This theory was originally used by Todo and Tatsuzaki (1974), Minaeva et al (1969), Strukov et al (1976) , Zaporozhets et al (1970) and Kawashima et al (1976) to explain the anomolous behaviour observed for the Y propagated longitudinal mode, which according to relaxation theory should not have occurred. The "fluctuation" mechanism is based on the principle that as the vibrating ultrasonic wave causes changes in the temperature at a point then as the magnitude of the spontaneous polarization is temperature dependent, an oscillation of the spontanous polarization will occur. This effect is independent of the direction of propagation of the ultrasonic waves and will be present for all modes of propagation.

A contribution to the magnitude of the ultrasonic wave velocity observed will be expected from the fluctuation theory for modes which also suffer from the relaxation effect. It has been shown that the contribution from the fluctuation mechanism is small when compared to contributions from the relaxation mechanism. Strukov and Yakushkin (1978) have shown that the fluctuation contribution is small for temperatures outside the region $t-t_c>0.2\ ^{\circ}C$.

Explanations of the discrepancies in the predictions made by the relaxation and fluctuation theories when compared to experimental results are centred around the behaviour of the domains in TGS in the vicinity of the phase transition point. Strukov and Yakushkin (1978) have shown that the magnitude of the acoustic anomaly observed in TGS crystals is dependent upon the method of sample growth. For a crystal grown in the ferroelectric phase there will be domain structures localized on the intrinsic impurities. These will only disappear after a lengthy annealing period at a temperature greater than the Curie point (Distler and Constantinova 1968). Such domain structures do not exist in crystals grown in the paraelectric phase (Strukov and Yakushkin 1978). In principle the nature of the point defects, which are responsible for the formation of the "defect domains", should also be considered, but their interaction mechanism with the acoustic waves is unclear at present.

In connection with the investigation of the fluctuation mechanism, several workers have investigated the ultrasonic properties of TGS by propagating a longitudinal mode down the ferroelectric axis (relaxation effects are not expected to be present for this mode) and observing an anomalous change in the ultrasonic wave velocity at the phase transition point. The early work of Todo and Tatsuzaki (1974), Minaeva (1969), Strukov et al (1976) and Zaporozhets et al (1970) had attributed this anomaly to the fluctuation mechanism, but the later work of Strukov and Yakushkin (1978)

suggested that the interaction of the ultrasonic waves with the domain structures in TGS present in the phase transition region was responsible for the observed anomalies. Zaporozhets and Tikhonov (1981) results showed that the magnitude of the observed anomalies was strongly influenced by the thermal and electrical conditions of the crystal under experimentation, which will affect the domain structure. It has been reported by Strukov and Yakushkin (1978) that crystals grown in the paraelectric phase did not show any anomalous behaviour for the Y propagated longitudinal mode. In our work we find no anomalous behaviour for this mode.

The exact influence of the domain structures on the magnitude of the observed ultrasonic wave velocity is not clear at the present time and the reader is best referred to the papers cited and in turn their references so that he can form his own opinion.

6.3 Discussion of the present results

On examination of the experimental results reported here it can be seen that marked anomalous behaviour of the ultrasonic wave velocity for modes 8,9,10,11 at the region of the phase transition has been observed (see Table 5.1 for mode identification). For mode 1 only a slight anomaly has been seen in the ultrasonic wave velocity in that it remained constant over the temperature region straddling the phase transition. The anomalies observed for modes 1,9 and 10 can be accounted for by relaxation theory, but in the case of modes 8 and

11 (Y polarized shear modes propagated in the XZ plane) the anomalous behaviour cannot be accounted for by the relaxation model. The observed anomaly for these modes can be accounted for by either the fluctuation model or by the mechanism described by Micheleson (1976). In the case of mode 11 the ultrasonic wave velocity changes by 20 m/s, but for the quasi-shear mode, which is subject to relaxation effects, the observed change is 120 m/s. The net effect of the interaction mechanisms described is to depress the magnitude of the ultrasonic wave velocity as the phase transition is approached. As the magnitude of the elastic stiffnesss constants are directly related to the observed ultrasonic wave velocity via the Christoffel equations, anomalies are observed in the magnitude of the calculated elastic stiffness constants.

On examination of the Christoffel equations, and by considering the modes which are subject to anomalous behaviour, it can be seen that out of the ten elastic stiffnesss constants determined we would expect c_{22} and c_{66} to show no anomalous behaviour at the phase transition. The most notable change observed in the remaining elastic stiffnesss constants occurs for c_{33} which increases its magnitude by approximately 8% as the phase transition region is traversed. The elastic stiffnesss constant c_{46} also shows a similar effect but with an increase in magnitude by 100 %. This is not as significant as it first appears as the magnitude of c_{46} is considerably smaller than that of c_{33}. The elastic stiffness constant c_{44} shows similar behaviour, but is of

reduced magnitude compared to that of c_{33}. The only other significant anomaly is in the measurement of c_{13}, the magnitude of which shows a marked decrease of approximately 3% as the phase transition region is traversed. The properties of the remaining elastic stiffness constants show no measurable anomalous behaviour at the phase transition region.

On examination of the experimental data obtained at temperatures well removed from the phase transition, it can be seen that the temperature derivatives show differing characteristics in the ferroelectric phase as compared to those in the paraelectric phase. For c_{11},$c_{33}$and c_{66} the temperature derivatives' magnitude is decreased in the paraelectric phase compared to those in the ferroelectric phase, while for c_{13},c_{15},c_{35} and c_{46} the temperature derivative changes sign and becomes positive. The magnitudes of the temperature derivatives for c_{44} and c_{22} are identical within experimental limits on either side of the phase transition. The temperature derivatives of the elastic stiffness constants have been reported for the paraelectric phase by Haussuhl and Albers (1977) who used their own unique axial system.

The temperature dependences of the elastic stiffness constants have also been investigated by two other groups of workers. Luspin and Hauret (1977) used a Brillouin scattering method to determine the elastic stiffness constants c_{11},c_{22} and c_{33} while Tylczynski (1981) used an ultrasonic method and reported the temperature dependence

of c_{11},c_{33},c_{13},c_{55},c_{15} and c_{35}. On comparing these workers' experimental data with the present work it can be seen that we have good agreement for the behaviour of c_{33}, although the results of Tylczynski (1981) indicate that the anomaly observed for this elastic stiffness constant occurs over a very narrow temperature range, whereas Luspin and Hauret(1977) along with this work show that the change occurs over a broad temperature band of approximately 5°C.

For c_{11} Luspin and Hauret (1977) and Tylczynski (1981) found similar features, namely an anomaly at the phase transition, with the temperature derivative of the elastic stiffness constants in the parelectric phase reduced in magnitude. The present work shows a similar result, but we disagree over the behaviour at the phase transition: there is no anomaly in the magnitude of this elastic stiffness constant.

For the elastic stiffness constants c_{13},c_{55},c_{15} and c_{35} we find substantial disagreement with the work of Tylczynski (1981). Considering c_{55} first, Tylczynski (1981) shows that its magnitude decreases with temperature as the phase transition is approached, then increases as the phase transition region is traversed and then remains static in the paraelectric phase. The present work shows no such increase in magnitude at the phase transition, and in the paraelectric phase the magnitude decreases. Similarly for c_{13} there is little agreement. We both agree that the magnitude of the elastic stiffness constant decreases with temperature,

but over the phase transition region we show that the magnitude decrease as the temperature increases, while Tylczynski (1981) shows the opposite. In the paraelectric phase the temperature derivative is negative while our work shows a positive derivative. However it should be noted that the experimental error involved in determining this particular elastic constant is large. For c_{15} and c_{35} we find an entire disagreement, but since these elastic stiffness constants are small in magnitude anyway, the experimental error is substantantial.

It can be seen that generally the values for the pressure derivatives of the elastic stiffness constants increase with temperature, all derivatives show an anomaly at the phase transition varrying from a slight effect in $\partial c_{22}/\partial P$ to the more larger change in $\partial c_{44}/\partial P$.

6.4 Elastic properties of TGS

Using the elastic stiffness constant set obtained in this work, the three wave velocities have been calculated for propagation directions at 1° intervals around the YZ,ZX and XY planes by computation of the eigenvalues of the Christoffel equations. The resultant cross-sections of the three elastic wave velocity surfaces, presented in figures 6.1 to 6.3 follow the crystal Laue symmetry. Additional calculations show that the velocity surface features exhibit no discernible change over the temperature range investigated in this work.

In general, in a crystal three distinct, mutually orthogonal elastic plane waves propagate along a given

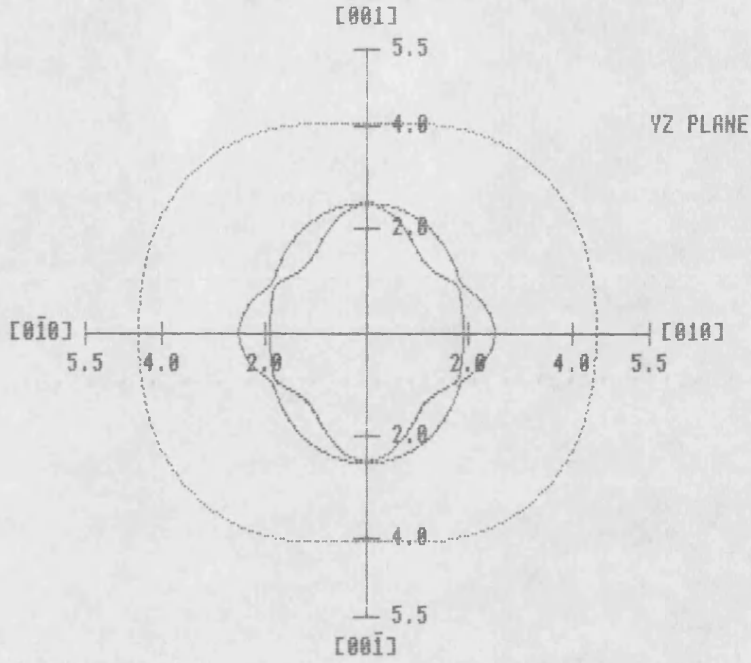

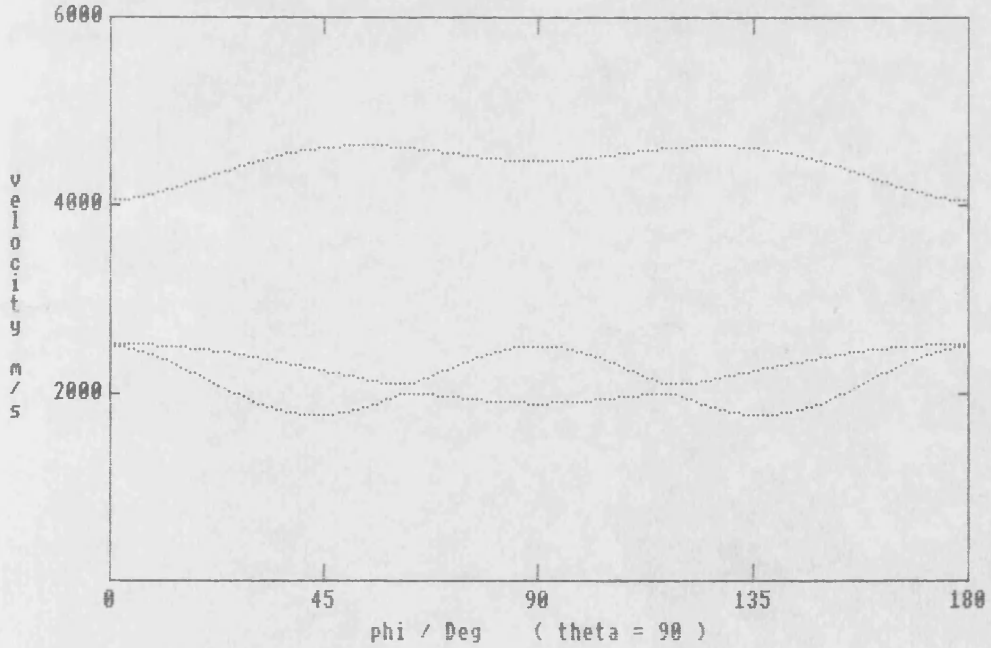

Fig 6.1 Velocity surface of TGS for the YZ plane.

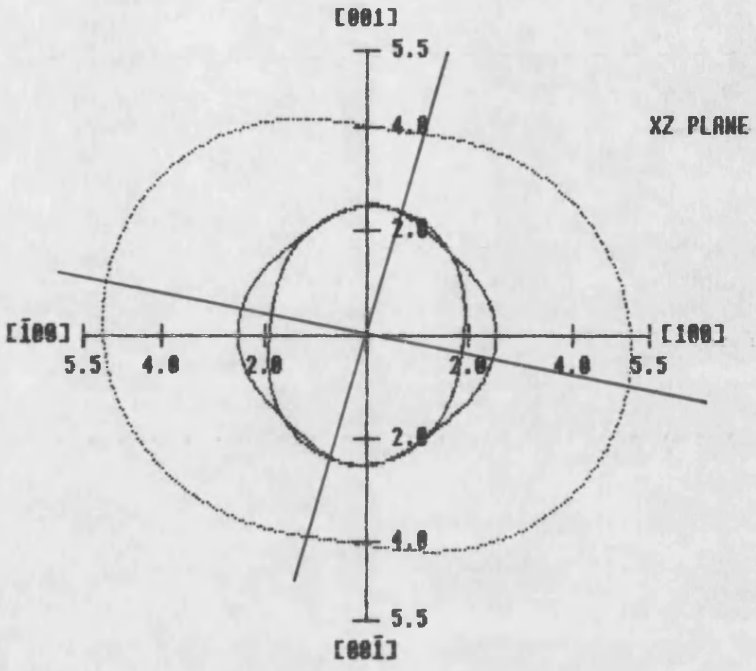

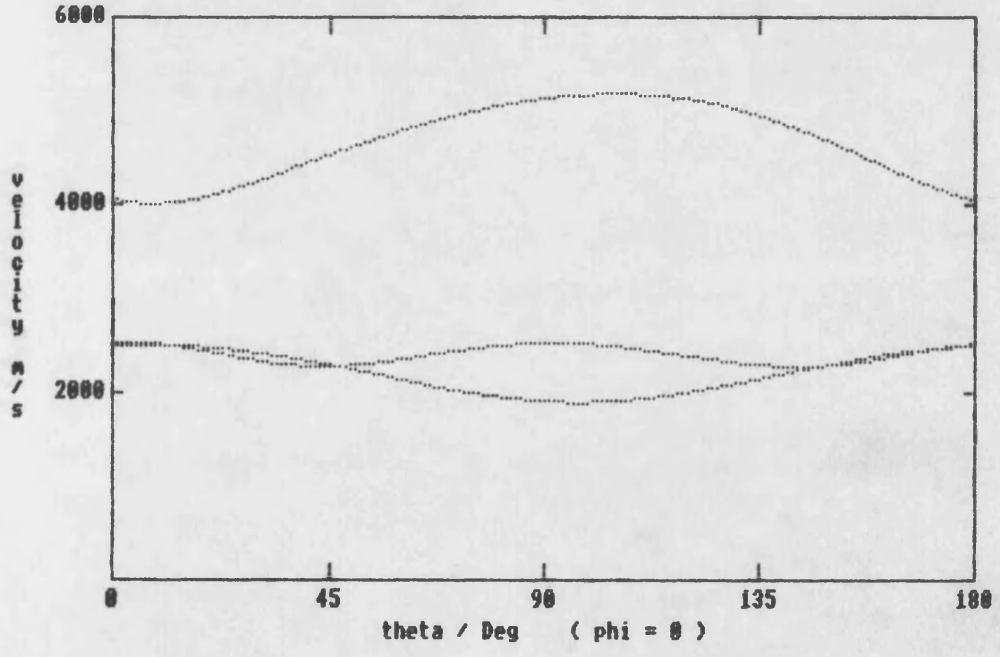

Fig 6.2 Velocity surface of TGS for the XZ plane.

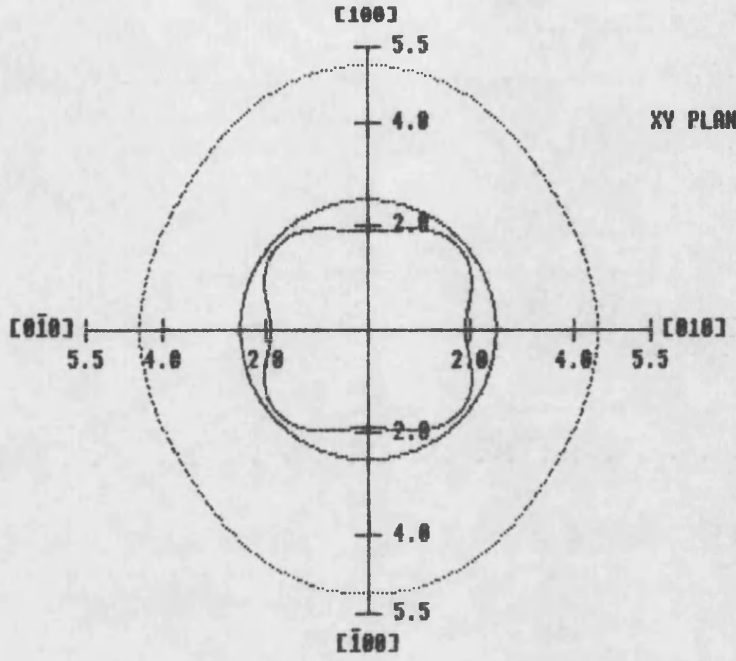

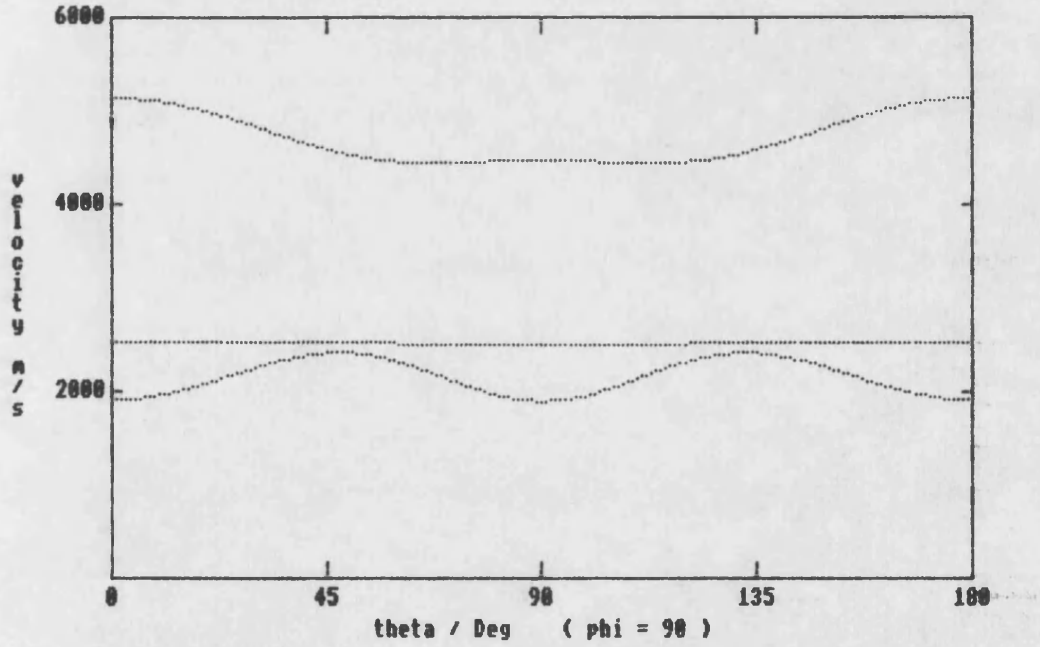

Fig 6.3 Velocity surface of TGS for the XY plane.

direction, these modes being neither pure longitudinal or pure transverse. However, along certain special directions, the pure mode directions (or acoustic axis), a pure longitudinal and two pure transverse waves do propagate. Knowledge of these directions can be useful because it is usually easier to excite such modes with X- or Y- cut transducers and also there is no deviation of the energy flux from the propagation direction - minimizing the possibility of sidewall reflections. The conditions for a pure mode direction are (Brugger (1965))

$$\epsilon_{ijk}\, C_{jirs}\, N_K\, N_J\, N_\Lambda\, N_S = 0$$

for a monoclinic crystal in the XZ plane this can be shown to take the form

$$N_1 N_3 [N_1^2 A_1 - N_3^2 C_1] + N_1^2 (3 N_3^2 - N_1^2) C_{15} - N_3^2 (3 N_1^2 - N_3^2) C_{35} = 0$$

or writing the direction cosine ratio N_1/N_2 as u

$$-u^4 C_{15} + A_1 u^3 + 3u^2 (C_{15} - C_{35}) - u_1 C_1 + C_{35} = 0$$

Here $A_1 = c_{11} - 2c_{55} - c_{13}$ and $C_1 = c_{33} - 2c_{55} - c_{13}$. Substituting the elastic constant values obtained from this work (Table 5.2) into this equation, shows that there is a pure mode axis for TGS in the XZ plane at 9.4° from the +Z axis towards the +X axis; this position is shown in Fig 6.2. A second pure mode axis occurs at 106.5° .

By using the known elastic stiffness constants, the particle displacement vectors for each of the three modes of vibration for a given direction can be calculated. By taking the vector dot product of the particle

displacement vector and the corresponding wave propagation vector, the angle of devation between these two vectors can be obtained. This operation has been carried out for modes propagated in the XY,XZ,YZ planes in TGS and the results are plotted in Figs 6.4 to 6.6 (note we have only plotted the moduls of the angle of deviation). These plots are useful as they can indicate the best experimental modes to be used if it is not possible to use pure mode directions. Ideally one would look for the smallest deviation angle so that most of the input energy is coupled into this operating mode and not into other spurious modes. It can be seen that the choice of the [101] direction was not amongst the better selection in this work as it is a high off-axis case.

For TGS there are significant changes in the wave velocity as the crystal goes from the ferroelectric to the parelectric phase. Hence it is useful to know how the polarisation vector deviations from propagation direction alter with temperature. The appropriate calculation have been carried out with the results plotted in figures 6.7 to 6.9. In fact the deviations are not very large and should have little influence on the design of ultrasonic experiments carried out in the phase transition.

Knowledge of the elastic stiffness tensor components enables determination of a material's response to any applied stress within the Hooke's law regime. Youngs modulus E, the measure of the ratio of an applied longitudinal stress to the resulting longitudinal strain,

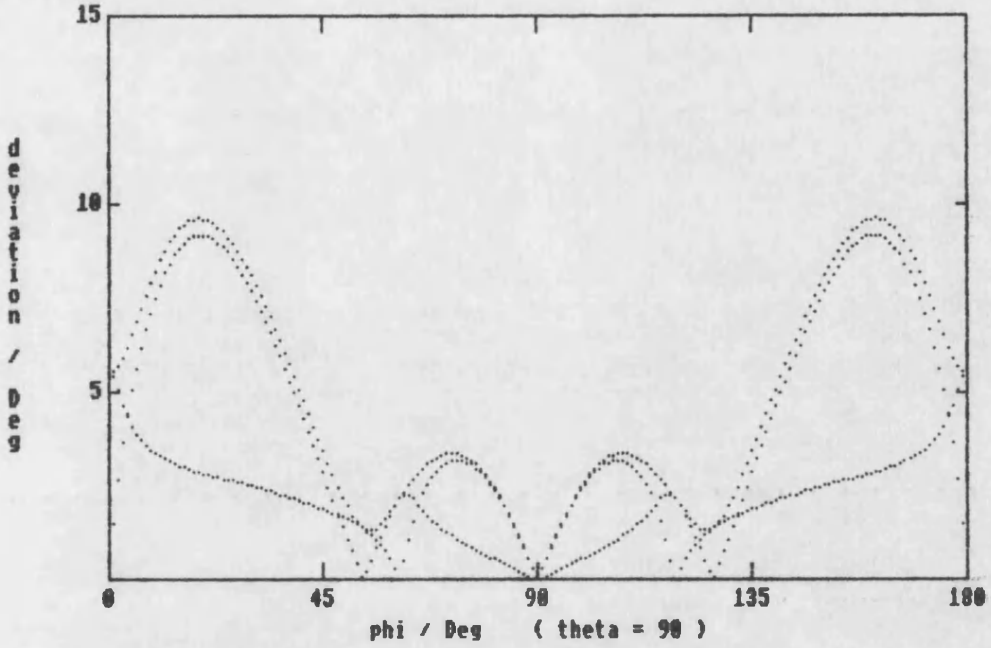

Fig 6.4 Deviation of the particle displacement vector from the wave propagation vector for TGS at 20 C for the YZ plane

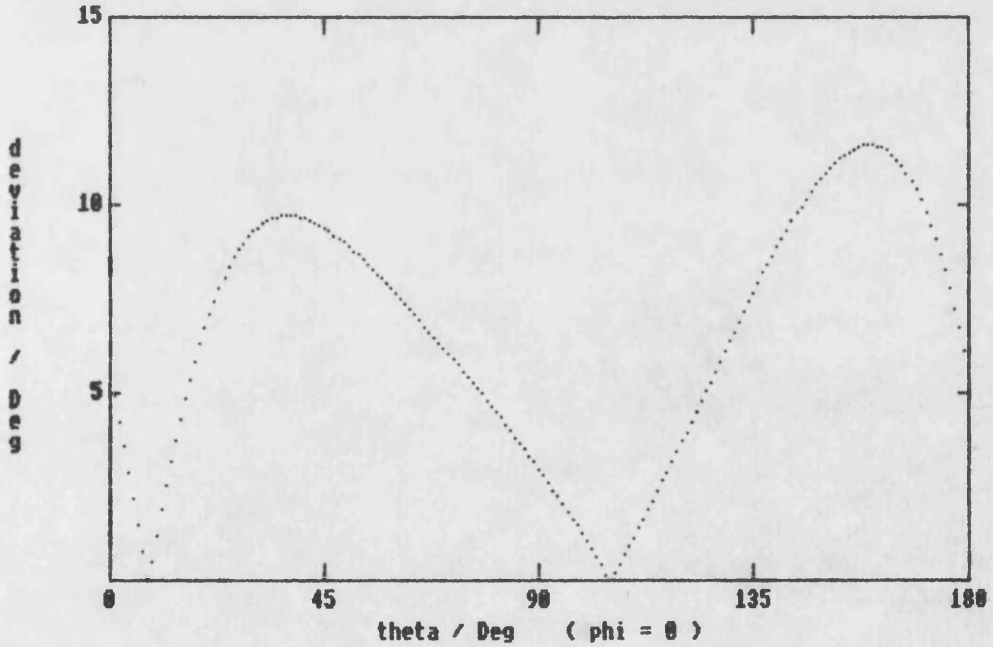

Fig 6.5 Deviation of the particle displacement vector from the wave propagation vector for TGS at 20 C for the XZ plane

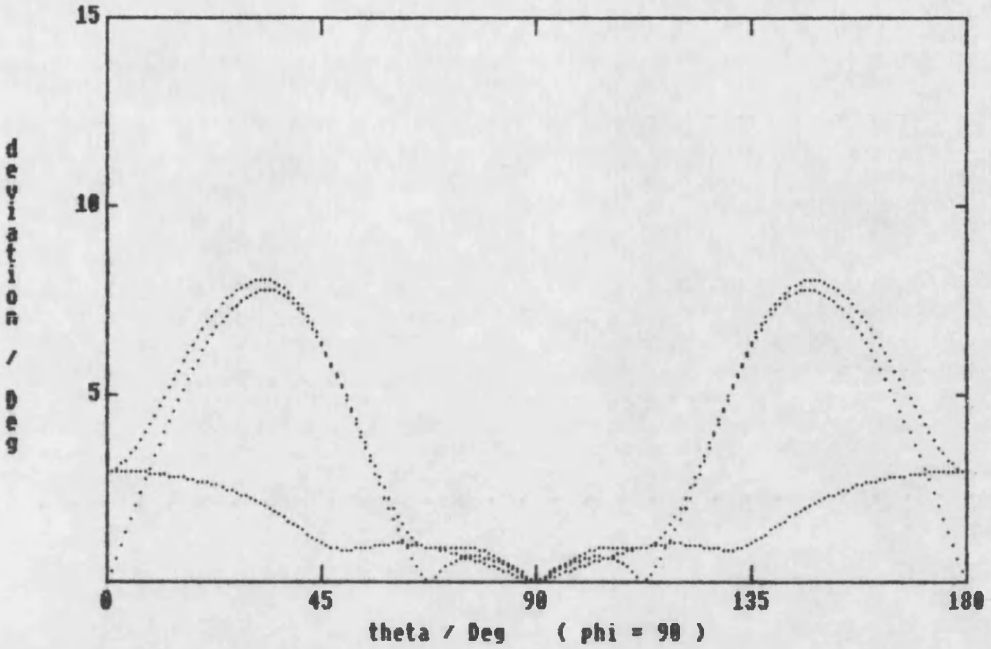

Fig 6.6 Deviation of the particle displacement vector from the wave propagation vector for TGS at 20 C for the XY plane

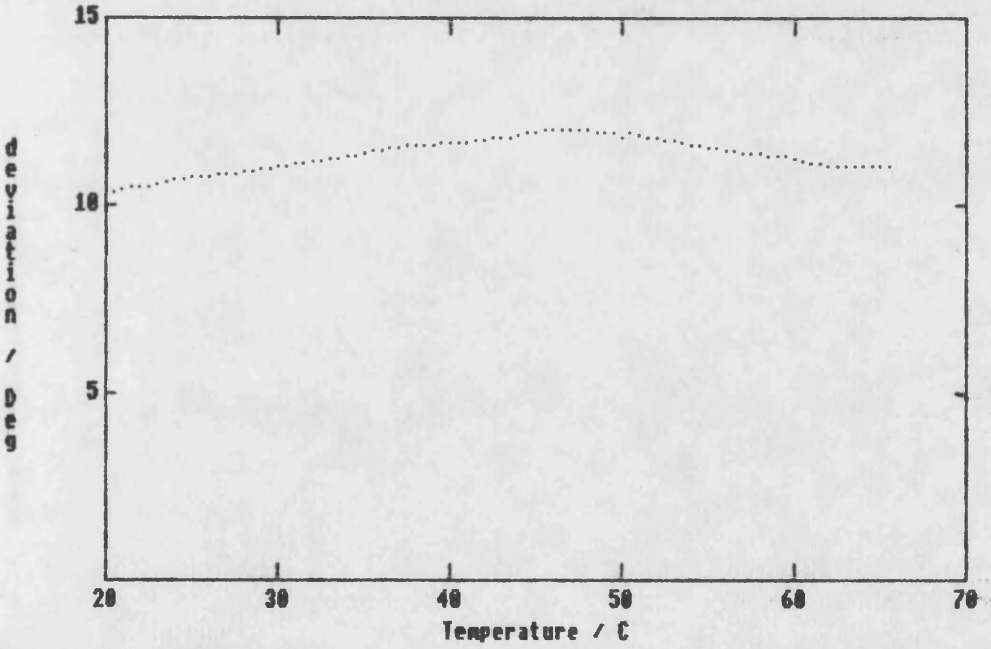

FIG 6.7 Variation of the angle between the propagation direction vector and the particle displacement vector with temperature for an ultrasonic wave propagated in the [101] direction.

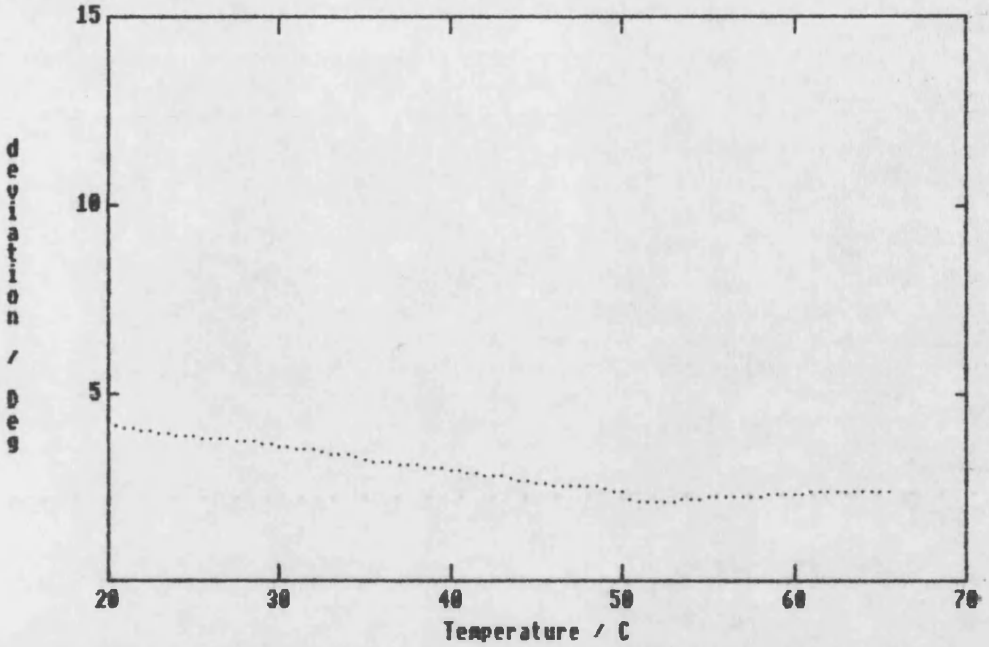

FIG 6.8 Variation of the angle between the propagation direction vector and the particle displacement vector with temperature for an ultrasonic wave propagated in the [100] direction.

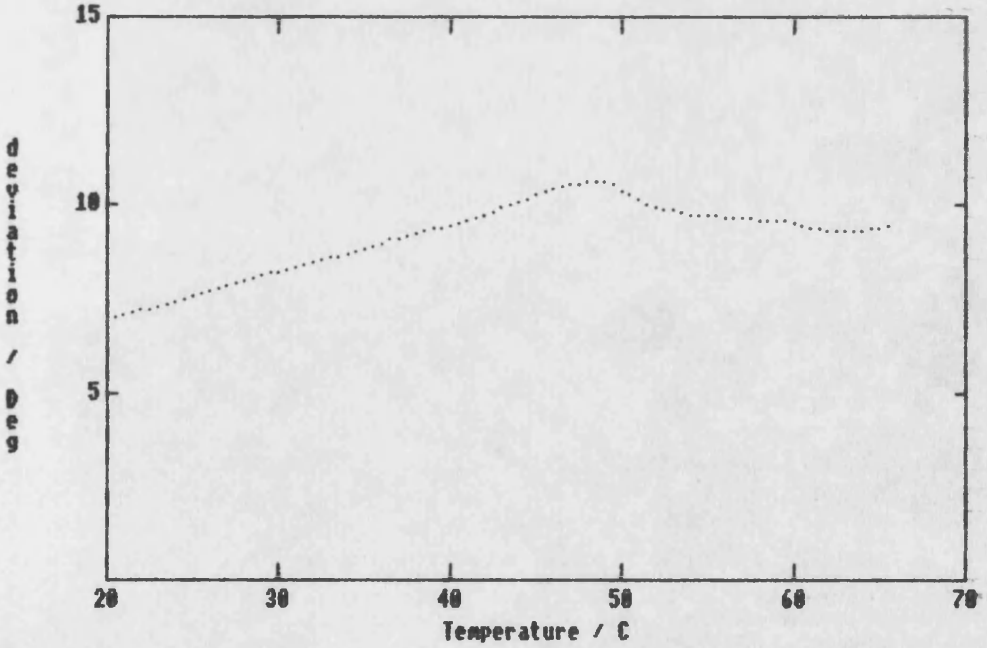

FIG 6.9 Variation of the angle between the propagation direction vector and the particle displacement vector with temperature for an ultrasonic wave propagated in the [001] direction.

for a monoclinic crystal (Nye (1957)) is

$$E = \{ l_1^4 S_{11} + 2 l_1^2 l_2^2 S_{12} + 2 l_1^2 l_3^2 S_{13} + 2 l_1^3 l_3 S_{15} + l_2^4 S_{22} + 2 l_3^2 l_3^3 S_{23} + 2 l_1 l_2^2 l_3 S_{25} + l_3^4 S_{33} + 2 l_1 l_2^3 S_{35} + l_2^2 l_3^2 S_{44} + 2 l_1 l_2^2 l_3 S_{46} + l_1^2 l_3^2 S_{55} + l_1^2 l_2^2 S_{66} \}^{-1}$$

for a stress in the direction labelled by the direction cosine l_1, l_2, l_3. Youngs modulus can be represented by a surface which gives a useful visual guide to the elastic behaviour of a crystal. Three plane (yz, xz and xy) cross-sections of this surface for TGS are presented in Fig 6.10 to 6.12. For a given stress applied along a crystallographic axis, the strain is greatest along the z-axis and least along the x-axis.

The volume compressibility $-\Delta/P$ (where Δ is the dilation) is S_{ijkl} (or in Voigt notation $S_{11}+S_{22}+S_{33}+2(S_{12}+S_{23}+S_{31})$) equal to 4.4×10^{-11} m^2N for TGS. Hence the bulk modulus, defined as the reciprocal of the compressibility is 2.27×10^{11} Nm^{-2} at 20 °C. Another elastic property commonly required is the linear compressibility, which is the relative decrease in length of a line when a crystal is subjected to hydrostatic pressure and is given by $S_{ijkl} l_i l_j$. Here l_i is a unit vector in the direction of the stretch of the line. For a monoclinic crystal the linear compressibility is (Nye (1957))

$$\beta = (S_{11} + S_{12} + S_{13}) l_1^2 + (S_{12} + S_{22} + S_{23}) l_3^2 + (S_{13} + S_{23} + S_{33}) l_3^2 + (S_{15} + S_{25} + S_{35}) l_3 l_1$$

The marked anisotropic behaviour of the linear compressibility of TGS can be seen in the YZ, XZ and XY plane plots of the property in Figs 6.13 to 6.15.

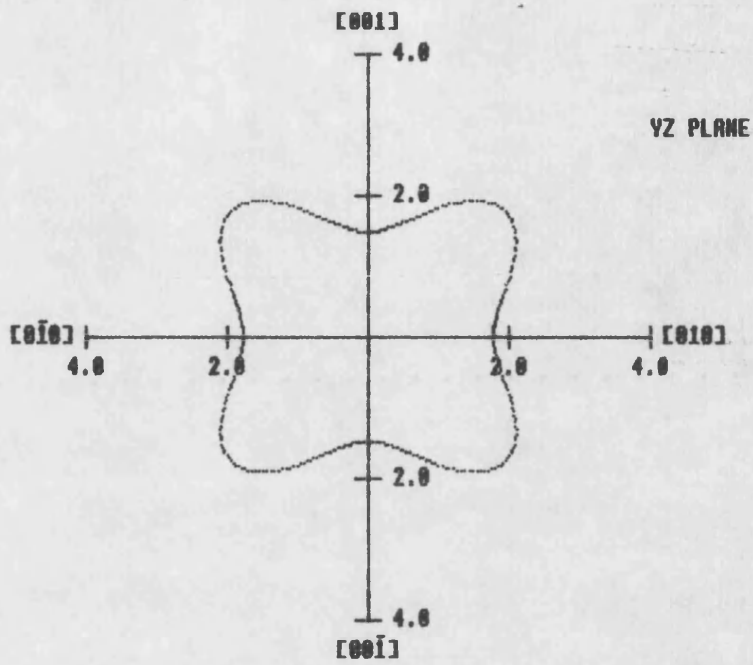

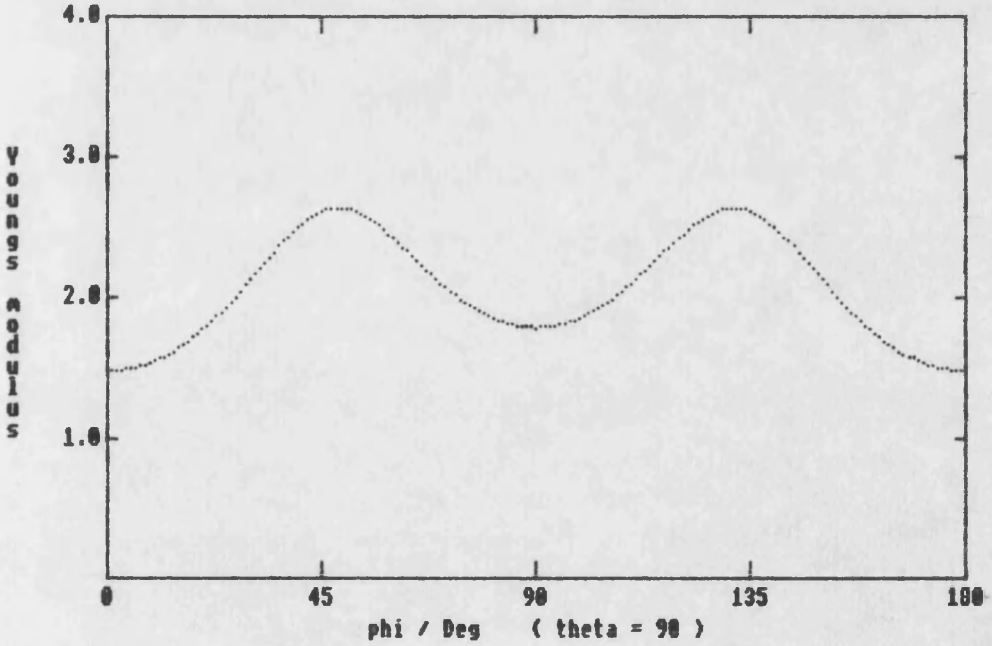

Fig 6.10 YZ plane cross-sections of the Young's modulus surface of TBS. Units are 10^{10} N m^{-2}.

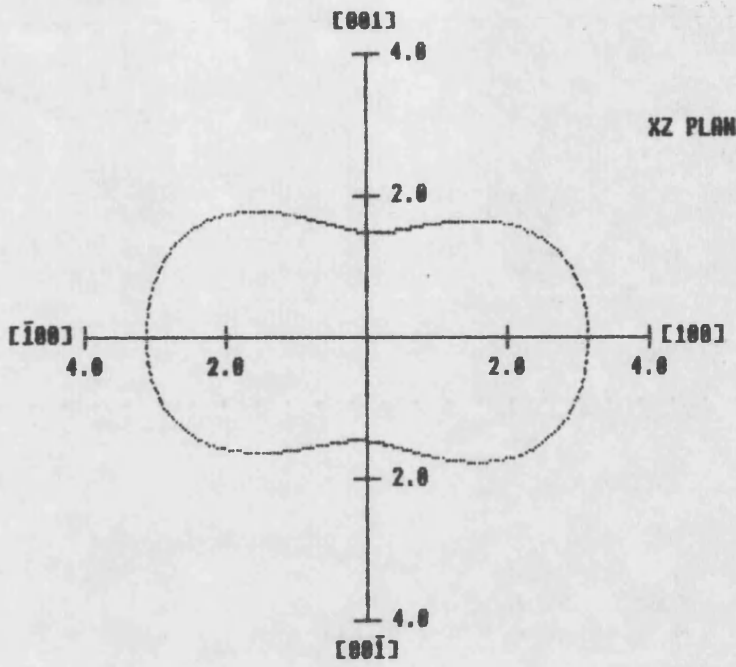

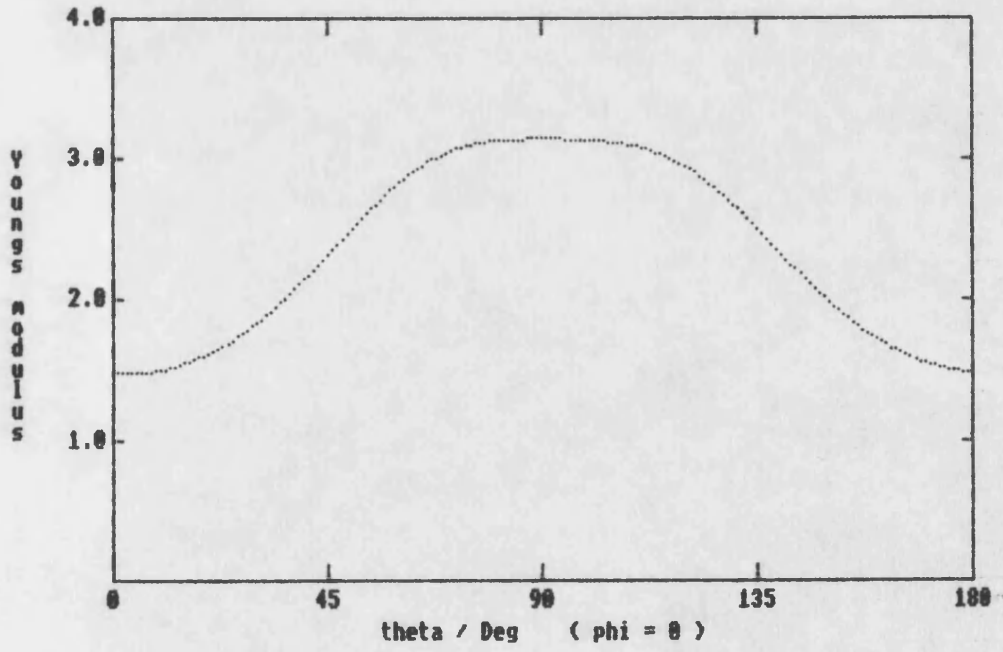

Fig 6.11 XZ plane cross-sections of the Young's modulus surface of TGS. Units are 10^{10} N m^{-2}.

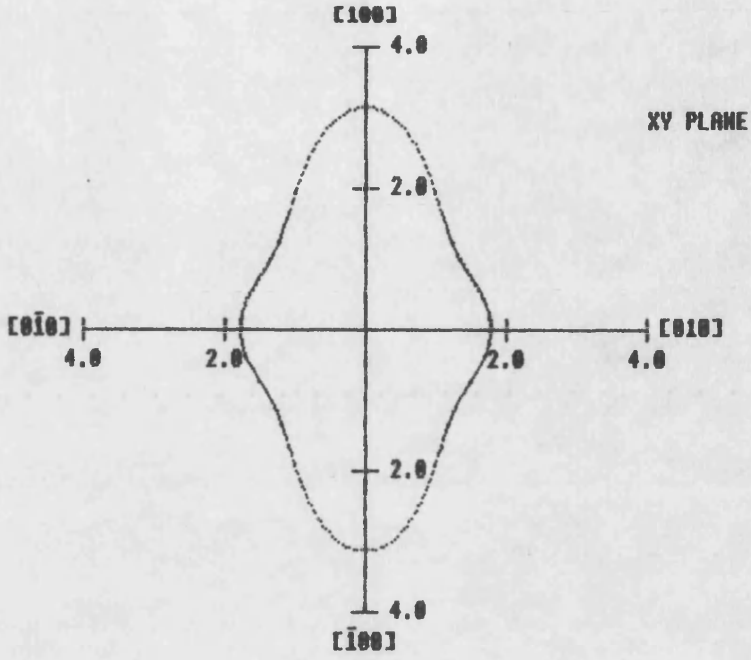

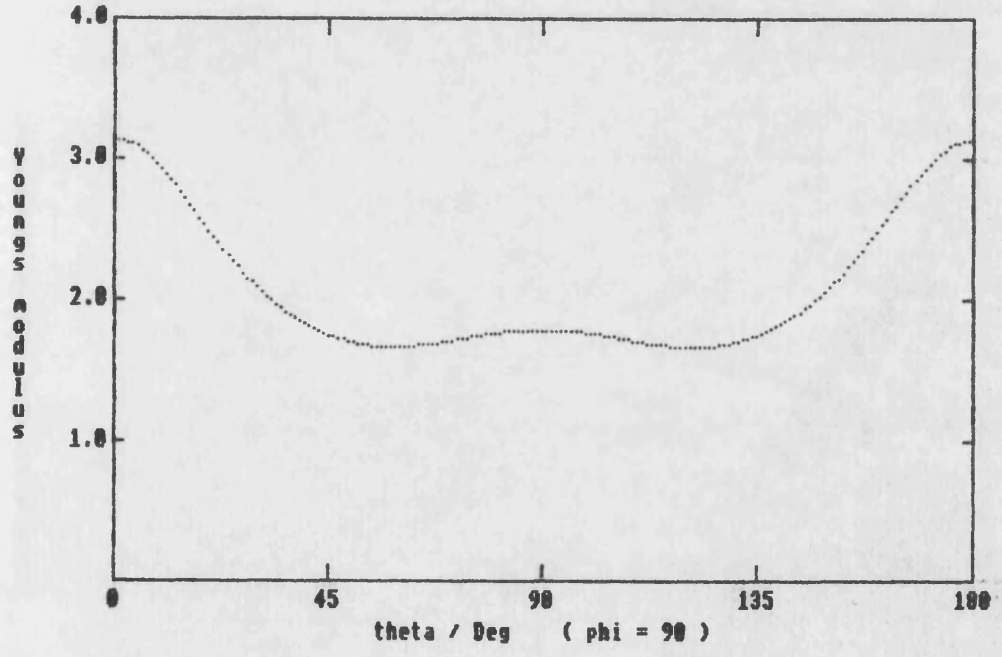

Fig 6.12 XY plane cross-sections of the Young's modulus surface of TGS. Units are 10^{10} N m^{-2}.

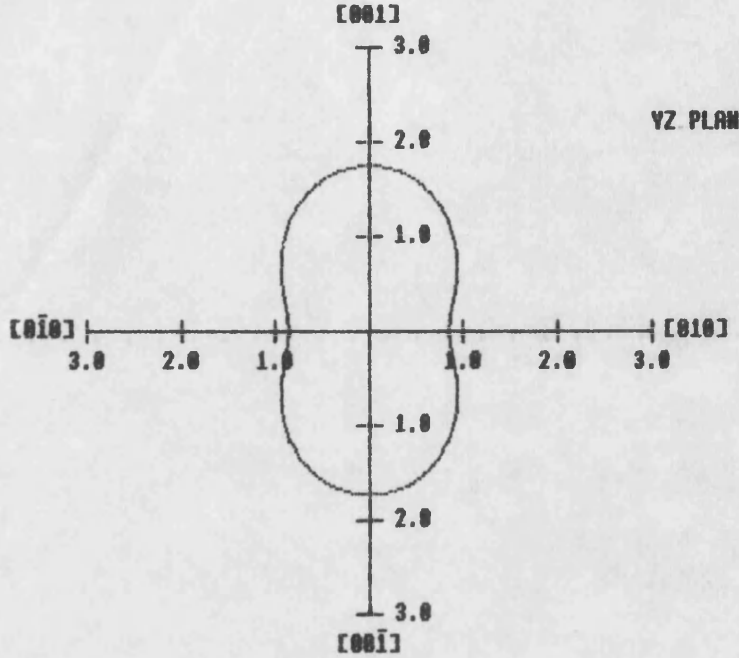

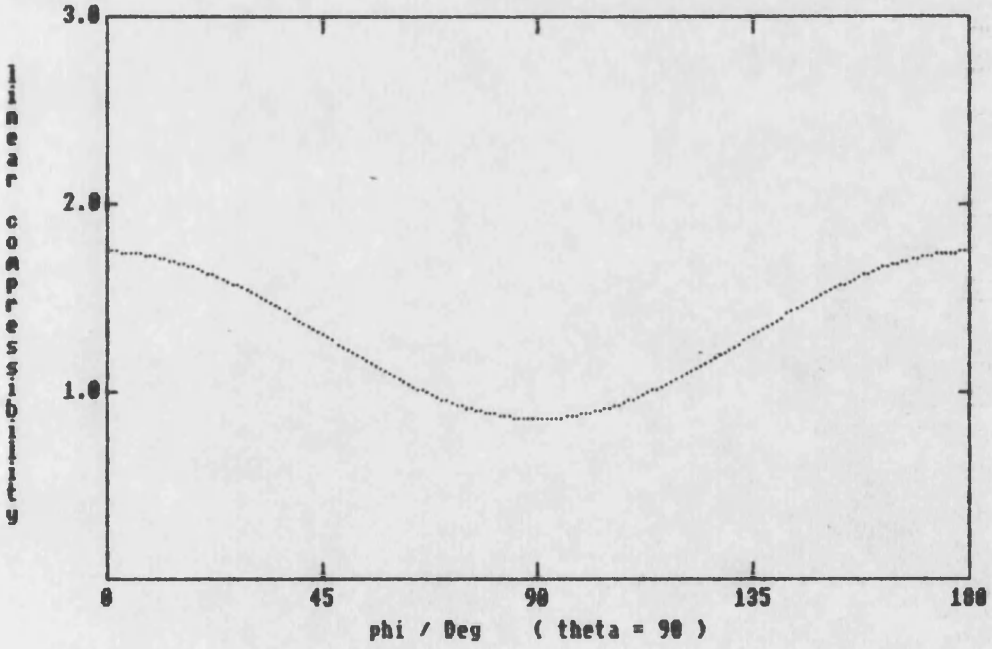

Fig 6.13 YZ plane cross-sections of the linear compressibility surface of TBS. Units are 10^{-10} m^2 N^{-1}.

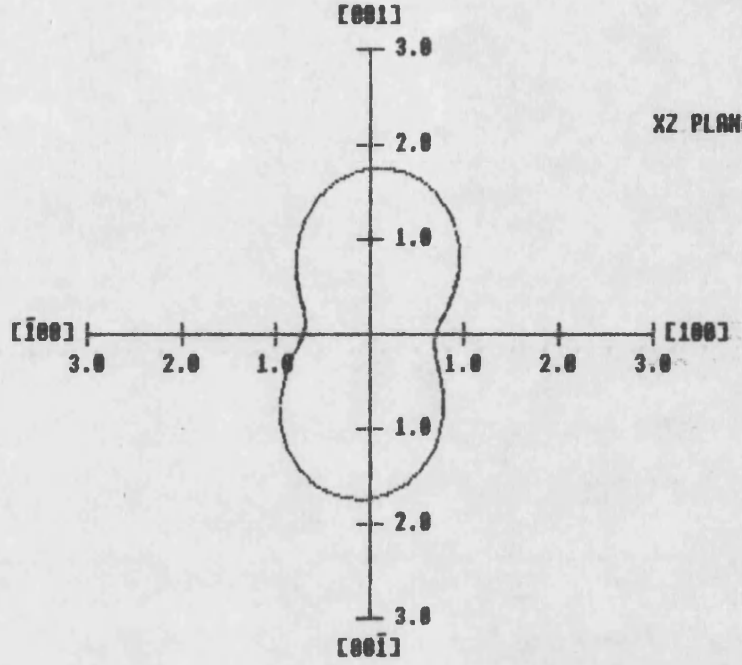

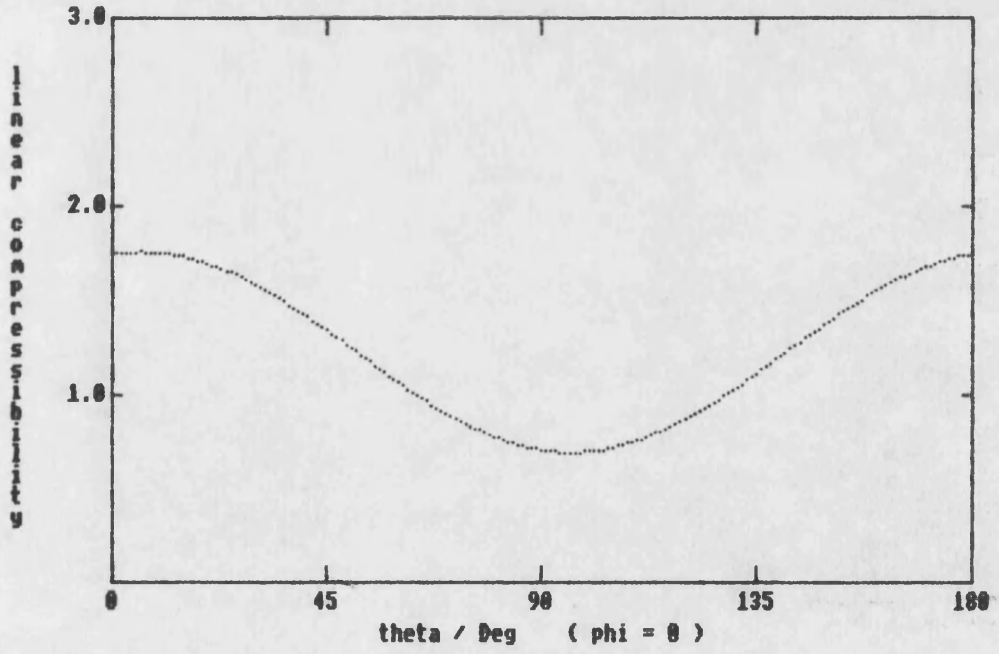

Fig 6.14 XZ plane cross-sections of the linear compressibility surface of TBS. Units are 10^{-10} m^2 N^{-1}.

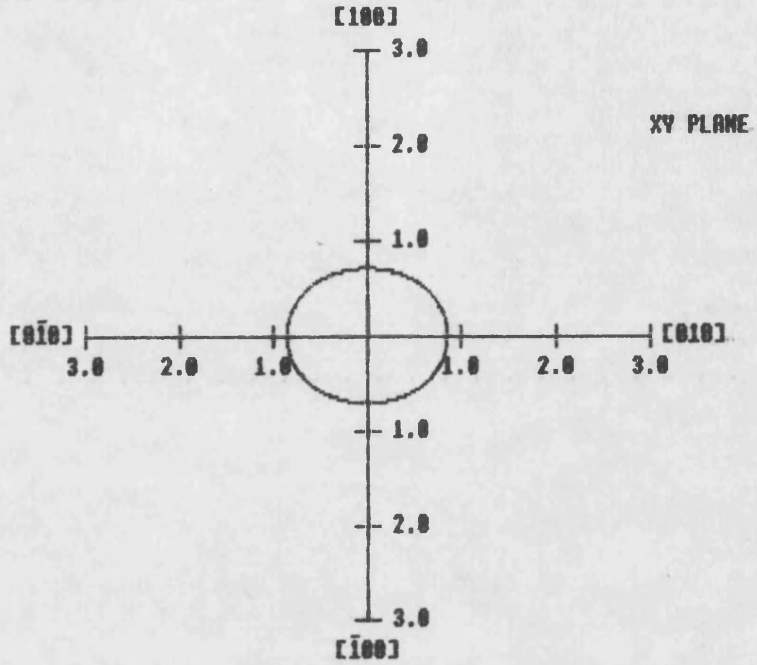

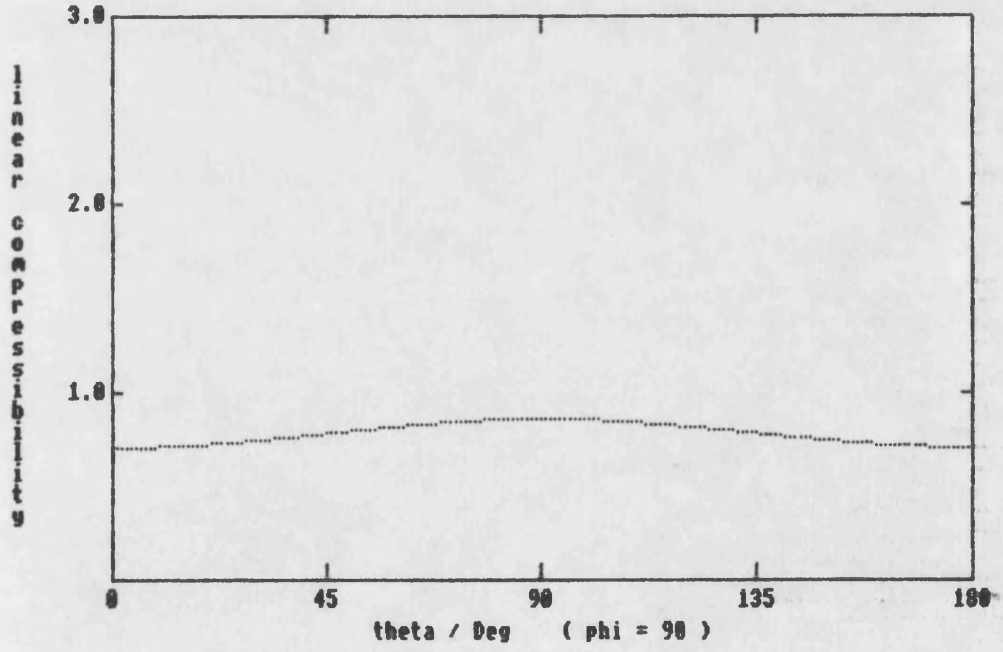

Fig 6.15 XY plane cross-sections of the linear compressibility surface of TGS. Units are 10^{-10} m^2 N^{-1}.

There is a simplifying feature of the elastic behaviour of TGS which is a helpful guide and may well be of practical value. This can be seen by considering the elastic stiffening constant matrix which collates the elastic constants. Now the elastic constants C_{15},C_{25},C_{35} and C_{46} are an order of magnitude smaller than the others (Table 5.2). If they were zero, the matrix would be that for an orthorhombic crystal. The wave velocity (Fig 6.1 to 6.3), Young's modulus (Fig 6.10 to 6.12) and compressibility surfaces (Fig 6.13 to 6.15) cross-sections, especially those of YZ and XY planes, show clearly this pseudo-orthorhombic elastic behaviour of TGS. In the XZ plane the surfaces are rotated away from the crystallographic X- and Z-axis to the acoustic axes; there is some distortion because the two acoustic axes in the xz plane are not perpendicular to each other.

The unit cell volume of TGS is 0.640 nm^3; there are two formula units, each comprising 37 atoms, per primitive unit cell (Wood and Holden (1957). Hence there are 3N (=222) degrees of freedom and therefore 3N phonon modes at the Brillouin zone centre. This complex vibrational spectrum makes for difficulties in quantitative analysis of lattice vibration properties. Thus it is useful to have an estimate of the elastic Debye temperature, θ_a, corresponding to the acoustic modes alone, which can be obtained from the measured elastic constants by integrating

$$\theta_d^{el} = \left(\frac{9N}{4\pi V}\right)^{1/3} \frac{h}{k} \Big/ \left[\int \left(\frac{1}{V_1^3} + \frac{1}{V_2^3} + \frac{1}{V_3^3}\right) \frac{d\Omega}{4\pi}\right]^{1/3}$$

over velocity space. Here the v_i (i= 1,2,3) are the three velocities obtained as the eigenvalues of the Christoffel equations for a given direction. This integration has been carried out over the whole of velocity space for all three modes (the curves in Fig 6.1 to 6.3 show only the YZ, XZ and XY plane cross-sections of these velocity surfaces). The integral over solid angle has been approximated by a sum taken at 10288 points each subtending an equal solid angle $\Delta\Omega$ of 1.218×10^{-3} steradians. The Debye temperature θ_d of TGS calculated from the room temperature elastic constants (table 5.2) is 170 K. Using the room temperature, rather than low temperature elastic constant data, can be expected to produce quite a large error (of the order of 10 k) in θ_d^{el}. Lawless (1976) found that the low-temperature specific heats of several ferroelectrics, including TGS, are complex and involve, in addition to the Debye T^3 term, a $T^{3/2}$ component, which he ascribed to a contribution from domain walls. He obtained a value of 107 K for θ_d for TGS. Thus there is a substantial difference between the Debye temperature obtained from the specific heat and elastic constants, perhaps not surprisingly in view of the complexities of the lattice dynamical behaviour and the domain wall effects which must be present in TGS.

APPENDIX 1

Determination of the elastic compliances.

The elastic compliances are determined from the elastic stiffness constants by using the following relationship (Nye 1957)

$$S_{qr} = \Delta c_{qr} / \Delta C$$

where Δc is the determinant of the elastic stiffness matrix and Δc_{qr} is the relevant minor determinant associated with S_{qr}. The expansion of the determinants has been carried out, so as to express each of the elastic compliances as a function of numerous elastic stiffness constants. The obtained relationships are given overleaf.

To check that no errors had occurred during the expansion of the determinants the values derived for the elastic compliances using the relationships overleaf were compared with those obtained using an alternative numerical method (which involved finding the inverse of the elastic stiffness matrix). There were found to be no differences in the magnitudes of the calculated elastic compliances.

$$\Delta C = (c_{66}c_{44} - c_{46}^2) \times [$$

$$c_{11}c_{22}(c_{33}c_{55} - c_{35}^2) - c_{11}c_{23}(c_{23}c_{55} - c_{35}c_{25})$$

$$+ \; c_{11}c_{25}(c_{23}c_{35} - c_{33}c_{25}) - c_{12}^2(c_{33}c_{55} - c_{35}^2)$$

$$+ \; c_{12}c_{23}(c_{13}c_{55} - c_{35}c_{15}) - c_{12}c_{25}(c_{13}c_{35} - c_{15}c_{33})$$

$$+ \; c_{13}c_{12}(c_{23}c_{55} - c_{35}c_{25}) - c_{22}c_{13}(c_{13}c_{55} - c_{35}c_{15})$$

$$+ \; c_{13}c_{25}(c_{13}c_{25} - c_{23}c_{15}) - c_{15}c_{12}(c_{23}c_{35} - c_{33}c_{25})$$

$$+ \; c_{15}c_{22}(c_{13}c_{35} - c_{33}c_{15}) - c_{15}c_{23}(c_{13}c_{25} - c_{23}c_{15}) \;]$$

$$S_{11} = (c_{44}c_{66} - c_{46}^2)[c_{22}(c_{33}c_{55} - c_{35}^2) -$$

$$c_{23}(c_{23}c_{55} - c_{25}c_{35}) + c_{25}(c_{23}c_{35} - c_{25}c_{33})] \; / \Delta C$$

$$S_{12} = (c_{46}^2 - c_{66}c_{44})[c_{12}(c_{33}c_{55} - c_{35}^2) -$$

$$c_{23}(c_{13}c_{55} - c_{35}c_{15}) + c_{25}(c_{13}c_{35} - c_{15}c_{23})] \; / \Delta C$$

$$S_{13} = (c_{44}c_{66} - c_{46}^2)[c_{12}(c_{23}c_{55} - c_{25}c_{35}) -$$

$$c_{22}(c_{13}c_{55} - c_{35}c_{15}) + c_{25}(c_{13}c_{25} - c_{23}c_{15})] \; / \Delta C$$

$$S_{15} = (c_{46}^2 - c_{66}c_{44})[c_{12}(c_{23}c_{35} - c_{33}c_{25}) -$$

$$c_{22}(c_{13}c_{35} - c_{15}c_{33}) + c_{23}(c_{13}c_{25} - c_{15}c_{23})] \; / \Delta C$$

$$S_{22} = (c_{44}c_{66} - c_{46}^2)[c_{11}(c_{33}c_{55} - c_{35}^2) -$$

$$c_{13}(c_{13}c_{55} - c_{15}c_{35}) + c_{15}(c_{13}c_{35} - c_{15}c_{33})] \; / \Delta C$$

$$S_{23} = (c_{46}^2 - c_{66}c_{44})[c_{11}(c_{23}c_{55} - c_{25}c_{35}) -$$

$$c_{12}(c_{13}c_{55} - c_{35}c_{15}) + c_{15}(c_{13}c_{25} - c_{23}c_{15})] \; / \Delta C$$

$$S_{25} = (C_{66}C_{44} - C_{46}^2)[C_{11}(C_{23}C_{35} - C_{25}C_{33}) -$$

$$C_{12}(C_{13}C_{35} - C_{33}C_{15}) + C_{13}(C_{13}C_{25} - C_{15}C_{23})] / \Delta C$$

$$S_{33} = (C_{44}C_{66} - C_{46}^2)[C_{11}(C_{22}C_{55} - C_{25}^2) -$$

$$C_{12}(C_{12}C_{55} - C_{15}C_{25}) + C_{15}(C_{12}C_{25} - C_{15}C_{22})] / \Delta C$$

$$S_{35} = (C_{46}^2 - C_{44}C_{66})[C_{11}(C_{22}C_{35} - C_{23}C_{25}) -$$

$$C_{12}(C_{12}C_{35} - C_{23}C_{15}) + C_{13}(C_{12}C_{25} - C_{22}C_{15})] / \Delta C$$

$$S_{44} = C_{66}C_{11}[C_{22}(C_{33}C_{55} - C_{35}^2) - C_{23}(C_{23}C_{55} - C_{25}C_{35}) +$$

$$C_{25}(C_{23}C_{35} - C_{33}C_{25})] - C_{12}C_{66}[C_{12}(C_{33}C_{55} - C_{35}^2) -$$

$$C_{23}(C_{13}C_{55} - C_{35}C_{15}) + C_{25}(C_{13}C_{35} - C_{33}C_{15})] +$$

$$C_{66}C_{13}[C_{12}(C_{23}C_{55} - C_{35}C_{25}) - C_{22}(C_{13}C_{55} - C_{35}C_{15}) +$$

$$C_{25}(C_{13}C_{25} - C_{23}C_{15})] - C_{15}C_{66}[C_{12}(C_{23}C_{35} - C_{25}C_{33}) -$$

$$C_{22}(C_{13}C_{35} - C_{15}C_{33}) + C_{23}(C_{13}C_{25} - C_{23}C_{15})] / \Delta C$$

$$S_{46} = - C_{46}C_{11}[C_{22}(C_{33}C_{55} - C_{35}^2) - C_{23}(C_{23}C_{55} - C_{35}C_{25}) +$$

$$C_{25}(C_{23}C_{35} - C_{33}C_{25})] + C_{46}C_{12}[C_{12}(C_{33}C_{55} - C_{35}^2) -$$

$$C_{23}(C_{13}C_{55} - C_{35}C_{15}) + C_{25}(C_{13}C_{35} - C_{33}C_{15})] -$$

$$C_{46}C_{13}[C_{12}(C_{23}C_{55} - C_{35}C_{25}) - C_{22}(C_{13}C_{55} - C_{35}C_{15}) +$$

$$C_{25}(C_{13}C_{25} - C_{23}C_{15})] + C_{46}C_{15}[C_{12}(C_{23}C_{35} - C_{33}C_{25}) -$$

$$C_{22}(C_{13}C_{35} - C_{15}C_{33}) + C_{23}(C_{13}C_{25} - C_{23}C_{15})] / \Delta C$$

$$S_{55} = (C_{66}C_{44} - C_{46}^2)[C_{11}(C_{22}C_{33} - C_{23}^2) -$$

$$C_{12}(C_{12}C_{33} - C_{23}C_{13}) + C_{13}(C_{12}C_{23} - C_{22}C_{13})] / \Delta C$$

$$S_{66} = c_{44}c_{11}[c_{22}(c_{33}c_{55} - c_{35}) - c_{23}(c_{23}c_{55} - c_{35}c_{25}) +$$

$$c_{25}(c_{23}c_{35} - c_{33}c_{25})] - c_{12}c_{44}[c_{12}(c_{33}c_{55} - c_{35}^2) -$$

$$c_{23}(c_{13}c_{55} - c_{15}c_{35}) + c_{25}(c_{13}c_{35} - c_{15}c_{33})] +$$

$$c_{13}c_{44}[c_{12}(c_{23}c_{55} - c_{25}c_{35}) - c_{22}(c_{13}c_{55} - c_{35}c_{15}) +$$

$$c_{25}(c_{13}c_{25} - c_{23}c_{15})] - c_{15}c_{44}[c_{12}(c_{23}c_{35} - c_{33}c_{25}) -$$

$$c_{22}(c_{13}c_{35} - c_{33}c_{15}) + c_{23}(c_{13}c_{25} - c_{15}c_{23})] / \Delta C$$

APPENDIX 2.A

The following computer program calculates the values of the 10 most readily obtained elastic stiffness constants for a monoclinic crystal using the sample density and the experimentally measured ultrasonic wave velocities for modes V_1 to V_{12} (for mode identification see Table 4.1).

```
   10 REM ***********************************************
   20 REM *** Determination of 10 elastic constants ***
   30 REM *** for a monoclinic crystal.              ***
   40 REM ***  c Solid State Physics                ***
   50 REM *** University of Bath   June 1983        ***
   60 REM ***********************************************
   70 FT=0:DIM C(10)
   80 MODE 7
   90 PRINT'''''"         Routine to find ten"''"
Elastic constants"''"         of a monoclinic crystal"''"
      c Solid State june 1983"
  100 TIME=0:REPEAT UNTIL TIME>500
  110 REM print out velocitys as user check
  120 REM velocity held in v1-vh using hex fornat
  130 READ DN:REM density
  140 DN=INT(DN*10)/10
  150 READ V1,V2,V3,V4,V5,V6,V7,V8,V9
  160 READ VA,VB,VC
  170 VA=INT(VA*10)/10:VB=INT(VB*10)/10
  180 VC=INT(VC*10)/10
  190 CLS:PRINT''"    how many significant "''"   figures
in the velocity"''"    range 1 to 5 ";
  200 REPEAT:A=GET:UNTIL A>48 AND A<56:BD=A-49
  210 DA=V1:GOSUB 2120:V1=DA
  220 DA=V2:GOSUB 2120:V2=DA
  230 DA=V3:GOSUB 2120:V3=DA
  240 DA=V4:GOSUB 2120:V4=DA
  250 DA=V5:GOSUB 2120:V5=DA
  260 DA=V6:GOSUB 2120:V6=DA
  270 DA=V7:GOSUB 2120:V7=DA
  280 DA=V8:GOSUB 2120:V8=DA
  290 DA=V9:GOSUB 2120:V9=DA
  300 DA=VA:GOSUB 2120:VA=DA
  310 DA=VB:GOSUB 2120:VB=DA
  320 DA=VC:GOSUB 2120:VC=DA
  330 CLS
  340 PRINT''"    density = ";DN;" kg/m^3"
  350 PRINT''"    v1 = ";V1;" m/s"
  360 PRINT''"    v2 = ";V2;" m/s"
  370 PRINT''"    v3 = ";V3;" m/s"
  380 PRINT''"    v4 = ";V4;" m/s"
```

```
  390 PRINT''"     v5 = ";V5;" m/s"
  400 PRINT''"     v6 = ";V6;" m/s":PRINT''"   Press any
key to continue":A=GET:CLS
  410 PRINT''"     v7 = ";V7;" m/s"
  420 PRINT''"     v8 = ";V8;" m/s"
  430 PRINT''"     v9 = ";V9;" m/s"
  440 PRINT''"    v10 = ";VA;" m/s"
  450 PRINT''"    v11 = ";VB;" m/s"
  460 PRINT''"    v12 = ";VC;" m/s"
  470 PRINT''"   Press any key to continue":A=GET:CLS
  480 REM evaluation of elastic constants c66,c22,c44,c46
  490 PRINT''"    How many significant figures"''"    are
the constants to be"''"     determined to (1 to 5)";
  500 REPEAT:A=GET:UNTIL A>48 AND A<56:BA=A-49
  510 REM determine c66
  520C6=DN*V2^2:CI=C6
  530GOSUB 2030
  540C6=CI:REM saving rounded elastic constants
  550REM calaculte c22
  560C2=DN*V5^2:CI=C2
  570GOSUB 2030
  580C2=CI
  590REM calculate c44
  600C4=DN*V8^2:CI=C4
  610GOSUB 2030
  620C4=CI
  630REM calculate c46
  640CC=0.5*(2*DN*VB^2-(C4+C6)):CI=CC
  650GOSUB 2030
  660CC=CI
  670REM the easy four now determined
  680CLS:PRINT''"       c22 = ";C2;" Nm"
  690PRINT''"       c44 = ";C4;" Nm"
  700PRINT''"       c66 = ";C6;" Nm"
  710PRINT''"       c46 = ";CC;" Nm"
  720PRINT''"  Press any key to
continue":OSCLI("FX21,0"):A=GET
  730CLS:PRINT''" i need to think this over for a bit"
  740REM using equations to get c55 first
  750REM in sheet a=pa, b=pd, d=pe ,f=pm, zx=zx
  760 PA=DN*(V1^2+V3^2):D7=1
  770PD=DN*DN*V1^2*V3^2
  780PE=DN*(V7^2+V9^2)
  790PM=DN*DN*V7^2*V9^2
  800DX=(VA^2+VC^2-0.5*(V1^2+V3^2+V9^2+V7^2))*DN
  810ZX=DX^2
  820REM set up system to search for root using newtons
method
  830FOR I=1 TO 100
  840CG=I*1.0E09
  850WQ=CG*(PA-CG)-PD:QP=CG*(PE-CG)-PM
  860IF WQ<0 OR QP<0 THEN 1010
  870IF FT=0 THEN U=SQR(WQ)+SQR(QP):GOTO 890
  880U=SQR(WQ)-SQR(QP):REM deals with negative case
  890TP=U^2-ZX
  900BF=(PA-2*CG)/SQR(WQ)
  910BK=(PE-2*CG)/SQR(QP)
  920BP=U*(BF+BK)
```

```
  930 CL=CG
  940 CG=CL-TP/BP:REM new cg
  950 IF ABS(CG-CL)>1.0E2 THEN 1000
  960CI=CG:GOSUB 2030:CG=CI:REM constant rounded
  970IF C(D7-1)<>CG THEN C(D7)=CG:D7=D7+1
  980REM elements same so continue
  990GOTO 1010
 1000GOTO 850: REM repeat iteration
 1010NEXT I
 1020REM need to check various solutions
 1030 IF C(1)=0.0 THEN 1060
 1040 IF C(2)<> 0.0 THEN 1070
 1050C5=C(1):TB=1:GOTO 1120:REM we have a single solution
so continue
 1060PRINT''"      no real solution for c55"''"
using exact solution":STOP
 1070 CLS:PRINT''"     their are two or more
solutions"''"     to the equations for c55"
 1080 *FX21,0
 1090 PRINT'"   Press any key to continue":A=GET
 1100FOR I=1 TO 10:IF C(I+1)=0 THEN TB=I:I=10
 1110NEXT I
 1120REM now calaculate c11, c15, c33,c35 from the
relevant equations
 1130FOR K=1 TO TB
 1140 C5=C(K)
 1150REM get c11
 1160C1=PA-C5:CI=C1:GOSUB 2030:C1=CI
 1170REM get c33
 1180C3=PE-C5:CI=C3:GOSUB 2030:C3=CI
 1190REM initial we can only obtain magnitude of c35 and
c15
 1200REM solve for c35
 1210CS=C5*C3-PM
 1220IF CS<0 THEN PRINT "     no real solution for
c35":GOTO 1250
 1230CF=SQR(CS)
 1240CI=CF:GOSUB 2030:CF=CI
 1250REM get c15
 1260CS=C1*C5-PD
 1270IF CS<0.0 THEN PRINT"no real solution for c15":GOTO
1300
 1280CX=SQR(CS)
 1290CI=CX:GOSUB 2030:CX=CI
 1300REM must deal with case of above to not known, +
sign problem
 1310REM user must make decision on sign of c15 and c35
 1320CLS:PRINT'"       *** user decision ***"
 1330PRINT'"      c15+c35 = ";:CI=DX:GOSUB
2030:DX=CI:PRINTDX
 1340PRINT'"         c15 = ";CX
 1350PRINT'"         c35 = ";CF
 1360PRINT'"   c15+c35 both -ve .........1"
 1370PRINT'"   c15+c35 both +ve .........2"
 1380PRINT'"   c15 -ve  c35 +ve .........3"
 1390PRINT'"   c15 +ve  c35 -ve .........4"
 1400 PRINT'"   Select option":*FX21,0
 1410A=GET
```

```
 1420IF A=49 THEN CX=-CX:CF=-CF:GOTO 1470
 1430IF A=50 THEN 1470
 1440IF A=51 THEN CX=-CX:GOTO 1470
 1450IF A=52 THEN CF=-CF:GOTO 1470
 1460PRINT'"     range 1 to 4 please":GOTO 1410
 1470PRINT:REM decision made
 1480IF FT=0 THEN CLS:PRINT'"   SOLVED FOR +VE CASE
SOLUTION";K:GOTO 1500
 1490CLS:PRINT'"   SOLVED FOR -VE CASE SOLUTION";K
 1500PRINT''"     c55=";C5;" nm"
 1510PRINT''"     c11=";C1;" nm"
 1520PRINT''"     c33=";C3;" nm"
 1530PRINT''"     c35=";CF;" nm"
 1540PRINT''"     c15=";CX;" nm"
 1550 PRINT'" Press a key to continue":A=GET:CLS
 1560REM calculate polarisation vectors for x axis
 1570PRINT''"  polarisation vectors":VT=V1*V1
 1580RU=-CC*(C6-DN*VT)/((C6-DN*VT)*(C5-DN*VT))
 1590PRINT''"  for x prop long u3/u1=";RU
 1600U1=1:U3=RU:NC=SQR(1+RU*RU):U1=U1/NC:U3=U3/NC:REM
NORMILIES POL VECTOR
 1610PRINT''"  normilsed vectors u1=";INT(1000*U1)/1000;
 1620PRINT" u3=";INT(1000*U3)/1000:VT=V9*V9:REM now do
for z axis
 1630RU=-CF*(C4-DN*VT)/((C4-DN*VT)*(C3-DN*VT))
 1640U3=1:U1=1/RU:NC=SQR(1+U1*U1):U1=U1/NC:U3=U3/NC
 1650 PRINT''"  for z prop long u3/u1=";RU
 1660 PRINT''"  normilsed vectors u1";INT(1000*U1)/1000;
 1670PRINT"  u3=";INT(1000*U3)/1000:REM polarisation
vectors are done"
 1680PRINT''"   press any key to continue":*FX21,0
 1690A=GET:CLS
 1700REM calculate c13
 1710ZT=(C1+C5+2*CX)*(C5+C3+2*CF)-4*DN^2*VA^2*VC^2
 1720PRINT'''"   solving for c13"
 1730PRINT''"      positive square root"
 1740 IF ZT<0 THEN PRINT"  no real solution for c13":END
 1750CU=SQR(ZT)-(CX+CF+C5):CI=CU:GOSUB 2030:CU=CI
 1760GOSUB 1960
 1770PRINT''"  c13=";CU;" n/m"
 1780PRINT'"  long mode prop [101]
u3/u1=";INT(RU*1000)/1000
 1790U1=1:U3=RU:NC=SQR(1+RU*RU):U1=U1/NC:U3=U3/NC
 1800 PRINT'"   normilsed vectors u1=";INT(1000*U1)/1000;
 1810PRINT"  u3=";INT(1000*U3)/1000
 1820 PRINT'"       negative square root"
 1830CU=-SQR(ZT)-(CX+CF+C5):CI=CU:GOSUB 2030:CU=CI
 1840GOSUB 1960
 1850PRINT'"  c13=";CU;"  n/m"
 1860PRINT'"   long mode prop [101]
u3/u1=";INT(RU*1000)/1000
 1870U1=1:U3=RU:NC=SQR(1+RU*RU):U1=U1/NC:U3=U3/NC
 1880PRINT'"   normilised vectors u1=";INT(1000*U1)/1000;
 1890PRINT" u3=";INT(1000*U3)/1000
 1900PRINT'"   press any key to continue":*fx21,0
 1910A=GET
 1920PRINT:NEXT K:REM looping for tb number of solutions
 1930IF FT=1 THEN END
```

```
 1940FT=1:D7=1:FOR J=1 TO 10:C(J)=0:NEXT:CLS:PRINT"   i
need to think this over"
 1950 FOR I=1 TO 10:C(I)=0:NEXT I:GOTO 830
 1960 YA=0.5*(CX+CF+CU+C5)
 1970YB=0.5*(C6+C4+2*CC)
 1980YC=0.5*(C5+C3+2*CF)
 1990VT=DN*VC*VC
 2000RU=-YA*(YB-VT)/((YB-VT)*(YC-VT))
 2010RETURN
 2020END
 2030REM rounding routine for elastic constants
 2040BB=BA+1
 2050IC=INT((CI*10^BB)/1.0E10)
 2060CD=INT((CI*10^BA)/1.0E10)
 2070B1=IC-10*CD
 2080IF B1<5 THEN 2100
 2090CD=CD+1
 2100CI=CD*1.0E10/(10^BA)
 2110RETURN
 2120REM rounding routine for velocitys
 2130BE=BD+1
 2140IC=INT((DA*10^BE)/1.0E03)
 2150CD=INT((DA*10^BD)/1.0E03)
 2160B1=IC-10*CD
 2170IF B1<5 THEN 2190
 2180CD=CD+1
 2190DA=CD*1.0E3/(10^BD)
 2200RETURN
 2210REM data input
 2220REM density
 2230DATA 1680
 2240REM      v1        v2          v3
 2250DATA  5127.6,  1899.6,   2518.4
 2260REM      v4        v5          v6
 2270DATA  2456.6,  4460.4,  1939.6
 2280REM      v7        v8          v9
 2290DATA  2510.6,  2488.3,  4045.8
 2300REM     v10       v11         v12
 2310DATA  2273.0,  2283.6,  4527.0
```

APPENDIX 2.B

The following computer program calculates the elastic stiffness constants c_{12}, c_{25} and c_{23} using the procedure described in section 4.3.

```
   50PRINT"          SOLVING FOR C25 USING (011)
DIRECTION"
   60FOR I=1 TO 5000:NEXT I
  100DIM C(10),D(100),B(100)
  110PRINT"            HOW MANY SIGNIFICANT FIGURES"
  120PRINT"       ARE THE CONSTANTS TO BE"
  130INPUT"       DETERMINED TO (RANGE 1-5)       ";BA
  140IF BA<1 OR BA>5 THEN 110
  150BA=BA-1
  160REM INPUT ELASTIC CONSTANTS AND VELOCITIES NEEDED
FROM DISC
  170E$="":BC=BC+1
  180INPUT"     DATA FILE NAME       ";A$
  190IF A$=" " THEN 180
  200INPUT"   DRIVE NUMBER OF DATA FILE       ";N
  210$O,N,"R",A$,E$
  220$R,A$:DN=VAL(A$)
  230$R,A$:C1=VAL(A$)
  240$R,A$:CU=VAL(A$)
  250$R,A$:CX=VAL(A$)
  260$R,A$:C2=VAL(A$)
  270$R,A$:C3=VAL(A$)
  280$R,A$:CF=VAL(A$)
  290$R,A$:C4=VAL(A$)
  300$R,A$:CC=VAL(A$)
  310$R,A$:C5=VAL(A$)
  320$R,A$:C6=VAL(A$)
  330$R,A$:VD=VAL(A$)
  340$R,A$:VE=VAL(A$)
  350$R,A$:VF=VAL(A$)
  360$R,A$:VG=VAL(A$)
  370$R,A$:VH=VAL(A$)
  380$R,A$:VI=VAL(A$)
  390$C
  391INPUT"        OUTPUT TO PRINTER       ";A$:IF A$=" "
THEN 391
  392IF LEFT$(A$,1)="Y" THEN N=4:GOTO 394
  393N=3
  394OPEN 1,N
  396PRINT" "
  400PRINT" ":PRINT£1,"":PRINT£1,"
DENSITY=";DN;"KG/M^3"
  410PRINT£1,"":PRINT£1,"          C11=";C1;" NM"
  420PRINT£1,"":PRINT£1,"          C13=";CU;" NM"
  430PRINT£1,"":PRINT£1,"          C15=";CX;" NM"
  440PRINT£1,"":PRINT£1,"          C22=";C2;" NM"
  450PRINT£1,"":PRINT£1,"          C33=";C3;" NM"
```

```
  460PRINT£1,"":PRINT£1,"          C35=";CF;" NM"
  470PRINT£1,"":PRINT£1,"          C44=";C4;" NM"
  480PRINT£1,"":PRINT£1,"          C46=";CC;" NM"
  490PRINT£1,"":PRINT£1,"          C55=";C5;" NM"
  500PRINT£1,"":PRINT£1,"          C66=";C6;" NM"
  510PRINT"     PRESS ANY KEY TO CONTINUE"
  520POKE158,0:REM EMPTY KEY BOARD
  530GET A$:IF A$="" THEN 530
  540PRINT" ":PRINT£1,"":PRINT£1,"          V13=";VD;"
M/S"
  550PRINT£1,"":PRINT£1,"          V14=";VE;" M/S"
  560PRINT£1,"":PRINT£1,"          V15=";VF;" M/S"
  570PRINT£1,"":PRINT£1,"          V16=";VG;" M/S"
  580PRINT£1,"":PRINT£1,"          V17=";VH;" M/S"
  590PRINT£1,"":PRINT£1,"          V18=";VI;" M/S"
  600PRINT"    PRESS ANY KEY TO CONTINUE"
  610POKE158,0
  620GET A$:IF A$="" THEN620
  630PRINT" "
  700KD=(C2+2*C4+C3)*(C6+C5)+(C2+C4)*(C4+C3)-(CC+CF)^2
  710KD=KD-4*DN^2*(VG^2*VH^2+VG^2*VI^2+VH^2*VI^2)

720NA=8*DN^3*VG^2*VH^2*VI^2-(C6+C5)*(C2+C4)*(C4+C3)+(C2+C
4)*(CC+CF)^2
  730LA=2*(CC+CF):OA=C6+C5:JD=C4+C3
  740REM SECTION TO FIND REGION WHERE WE HAVE + SOLUTION
  750A9=SQR(KD):REM ADJUST
  760A8=-A9:REM A9,A8 FIXES LIMIT FOR ITERATIONS
  770REM DO FOR POSITIVE SECTION
  780PRINT"          QUIET I'M TRYING TO THINK"
  790FOR I=1 TO 10:C(I)=0:NEXTI:D7=1:REM CLEARS HOLDING
ARRAY
  800X=A9:IF KD-X^2<0 THEN A9=A9-1.0E07:GOTO 800:REM
REDUCES A9 TO BOUNDRY
  810A8=-A9:X=A8:IZ=KD-X^2:GOSUB 2200:REM KICKS OUT IF
ERROR
  820REM WE HAVE NOW HOMED IN FROM THE TOP AND BOTTOM TO
GET ROOT NEAR BOUNDRY
  830FOR I=A8 TO A9 STEP 1.0E10
  840PRINT"+ CASE I=";I
  850X=I:GOSUB 2180:NEXT I:REM DEALING WITH POSITIVE CASE
  860X=A9:IZ=KD-X^2:GOSUB 2200:REM DOES HIGH CASE LAST TO
PREVENT DOUBILING
  870REM HUNT FOR POSITIVE SOLUTION TO C25
  880PRINT" "
  890IF C(1)=0 THEN GT=1:GOTO 940:REM NO SOLUTION
  900IF C(2)=0 THEN CT=1:GOTO 960:REM ONE SOLUTION
  910FOR I=2 TO 10
  920IF C(I)=0 THEN CT=I-1:I=10
  930NEXT I:GOTO  960
  940PRINT"     FOR THE POSITIVE CASE":GOSUB 2390
  950GOTO 980:REM JUMP TO -VE CASE C25 OF EXACT SOLUTION
FOR C25
  960PRINT£1,"":PRINT£1,"  SOLVING FOR C25 POSITIVE
CASE":B$="C25 POSITIVE CASE"
  970GOSUB 2450:REM FINDS CONSTANTS FOR CT SOLUTIONS
  980REM NOW DO FOR -VE CASE OF C25
  990REM NOTE LIMITS ARE SAME, SO CAN USE A9 AND A8 OF
LAST TIME
```

```
 1000PRINT"           QUIET PLEASE!"
 1010FOR I=1 TO 10:C(I)=0:NEXT I:D7=1:REMCLEARS HOLDING
ARRAY
 1020REM DO FOR LOW CASE
 1030X=A8:IZ=KD-X^2:GOSUB 2310
 1040REM HAVE NOW HOMED IN FROM TOP AND BOTTOM TO CAPTURE
ROOT,NOW CHECK MID
 1050FOR I=A8 TO A9 STEP 1.0E10
 1060PRINT" - CASE I=";I
 1070X=I:GOSUB 2290:NEXTI:REM DEALING WITH NEGATIVE CASE
 1080X=A9:IZ=KD-X^2:GOSUB 2310
 1090PRINT" "
 1100IF C(1)=0 THEN GX=1:GOTO 1150:REM NO SOLUTION FOUND
 1110IF C(2)=0 THEN CT=1:GOTO 1170:REM ONE SOLUTION
 1120FOR I=1 TO 10
 1130IF C(I)=0 THEN CT=I-1:I=10
 1140NEXT I:GOTO 1170
 1150PRINT"      FOR THE NEGATIVE CASE":GOSUB 2390
 1160GOTO 1190:REM NOW JUMP BEST FIR CASE
 1170PRINT"     SOLVING FOR C25 NEGATIVE CASE":B$="C25
NEGATIVE CASE"
 1180GOSUB 2450: REM CARRYS OUT EVALATION OF CONSTANTS
FOR C25 SOLUTIONS
 1190REM BEST FIT CASE +VE
 1200IF GT=0 THEN 1680:REM WE HAVE AN EXACT SOLUTION SO
BY PASS
 1210REM IF HERE TRYING BEST FIT
 1220PRINT"            QUIET I'M TRYING TO THINK"
 1230FOR I=1 TO 10:C(I)=0: NEXT I:D7=1:REM CLEARS HOLDING
ARRAY
 1240X=A8:IZ=KD-X^2:GOSUB 3230
 1250REM HAVE NOW HOMED IN FROM TOP AND BOTTOM TO CAPTURE
ROOT,NOW CHECK MIDDLE
 1260FOR I=A8 TO A9 STEP 1.0E10
 1270PRINT" BEST FIT +VE CASE I=";I
 1280X=I:GOSUB 3210:NEXT I
 1290X=A9:IZ=KD-X^2:GOSUB 3230
 1300PRINT" "
 1310IF C(1)=0 THEN 1360:REM NO SOLUTION FOUND
 1320IF C(2)=0 THEN CT=1: GOTO 1400:REM ONE SOLUTION
 1330FOR I=1 TO 10
 1340IF C(I)=0 THEN CT=I-1:I=10
 1350NEXT I:GOTO 1400
 1360PRINT"      FOR THE POSITIVE BEST"
 1370PRINT"      FIT CASE THEIR IS NO"
 1380PRINT"      MINIMUM POINT"
 1390GOTO 1690:REM TRY -VE BEST FIT CASE
 1400GOSUB 3700:REM SORTS OUT MAX POINTS
 1401PRINT"   PRESS ANY KEY TO CONTINUE":POKE 158,0
 1402GET A$:IF A$="" THEN 1402
 1403PRINT" "
 1405PRINT"    SOLVING FOR BEST FIT C25 +VE CASE":B$="C25
BEST FIT +VE CASE"
 1410GOSUB 2450:REM CARRYS OUT EVALATION OF CONSTANTS FOR
CT SOLUTIONS
 1420FOR I=A8 TO A9 STEP 1.0E09:REM STORES FOR PLOT OF
SOLUTION
```

```
 1430X=I:IZ=KD-X^2
 1440IF IZ<0 THEN 1470
 1450F=LA*SQR(IZ)*X-OA*IZ-JD*X^2-NA
 1460K=K+1:D(K)=(X-CC)/1.0E10:B(K)=F:REM PLOT DIRECTELY
C25
 1470NEXT I
 1480K=K+1
 1490D(K)=(A8-CC)/1.0E10:X=A8:B(K)=LA*SQR(IZ)*X-OA*IZ-JD*
X^2-NA
 1500DS=ABS(B(1))
 1510FOR I=2 TO K
 1520IF DS<ABS(B(I)) THEN DS=B(I)
 1530NEXT I
 1540REM DS HOLDS LARGEST TIME
 1550FOR I=1 TO K
 1560B(I)=B(I)/DS
 1570NEXT I:REM SCALED DATA
 1580A$=" 1"
 1590$O,2,"W","+VE",""
 1600$W,STR$(K)
 1610FOR I=1 TO K
 1620$W,STR$(D(I))
 1630$W,STR$(B(I))
 1640$W,A$
 1650$W,A$
 1660NEXT I
 1670$C
 1680REM BEST FIT NEGATIVE CASE
 1690IF GX=0 THEN
 1700REM IF HERE TRYING BEST FIT
 1710PRINT" "
 1720PRINT"            QUIET I'M TRYING TO THINK"
 1730FOR I=1 TO 10:C(I)=0:NEXT I:D7=1:REM CLEAR HOLDING
ARRAY
 1740X=A8:IZ=KD-X^2:GOSUB 3340
 1750REM HAVE NOW HOMED IN FROM TOP AND BOTTOM TO CAPTURE
ROOT NOW CHECK MID
 1760FOR I=A8 TO A9 STEP 1.0E10
 1770PRINT" BEST FIT CASE -VE I=";I
 1780X=I:GOSUB 3320:NEXT I:PRINT" "
 1790X=A9:IZ=KD-X^2:GOSUB 3340
 1800IF C(1)=0 THEN 1850:REM NO SOLUTION FOUND
 1810IF C(2)=0 THEN CT=1:GOTO 1890:REM ONE SOLUTION
 1820FOR I=1 TO 10
 1830IF C(I)=0 THEN CT=I-1:I=10
 1840NEXT I:GOTO 1890
 1850PRINT"     FOR THE NEGATIVE BEST"
 1860PRINT"      FIT CASE THEIR IS NO"
 1870PRINT"     MINIMUM POINT"
 1880
 1890GOSUB 5000:REM ROUTINE TO SORT OUT CORRECT VALUES
 1891PRINT"    PRESS ANY KEY TO CONTINUE":POKE158,0
 1892GET A$:IF A$="" THEN 1892
 1893PRINT" "
 1895PRINT"    SOLVING FOR BEST FIT C25 -VE CASE":B$="C25
BEST FIT -VE CASE"
 1900GOSUB 2450:K=0:REM CARRY OUT EVALATION FOR CT
SOLUTIONS
```

```
 1910FOR I=A8 TO A9 STEP 1.0E09:REM DUMP TO PLOTTER
 1920X=I:IZ=KD-X^2
 1930IF IZ<0 THEN 1960
 1940F=-LA*X*SQR(IZ)-0A*IZ-JD*X^2-NA
 1950K=K+1:D(K)=(X-CC)/1.0E10:B(K)=F:REM PLOT OUT AACTUAL
C25
 1960NEXT I
 1970K=K+1
 1980D(K)=(A8-CC)/1.0E10:X=A8:B(K)=-LA*X*SQR(IZ)-0A*IZ-JD
*X^2-NA
 1990DS=ABS(B(1))
 2000FOR I=2 TO K
 2010IF DS<ABS(B(I)) THEN DS=B(I)
 2020NEXT I
 2030REM DS HOLDS LARGEST TERM
 2040FOR I=1 TO K
 2050B(I)=B(I)/DS
 2060NEXT I:REM TERM CORRECTED TO 1
 2070A$=" 1"
 2080$O,2,"W","-VE",""
 2090$W,STR$(K)
 2100FOR I=1 TO K
 2110$W,STR$(D(I))
 2120$W,STR$(B(I))
 2130$W,A$
 2140$W,A$
 2150NEXT I
 2160$C
 2170
 2180IZ=KD-X^2
 2190IF IZ<0 THEN 2280
 2200TP=LA*SQR(IZ)*X-0A*IZ-JD*X^2-NA
 2210BP=LA*SQR(IZ)-LA*X^2/SQR(IZ)+0A*2*X-JD*2*X
 2220XL=X:REM NOW GET NEXT GUSS
 2230X=XL-TP/BP:REM NEW GUSS
 2240IF ABS(XL-X)>1.0E06 THEN 2180:REM REPEAR ITERATION
 2250CI=X:GOSUB 3440:X=CI:REM CONSTANT FOUND AND ROUNDED
 2260IF C(D7-1)<>X THEN C(D7)=X:D7=D7+1
 2270REM ELEMENT SAME SO CONTINUE
 2280RETURN
 2290IZ=KD-X^2
 2295REM ROUTINE CALACULATES X,WHERE X=C25+C46
 2300IF IZ<0 THEN2380
 2310TP=-LA*X*SQR(IZ)-0A*IZ-JD*X^2-NA
 2320BP=-LA*SQR(IZ)+(LA*X^2)/SQR(IZ)-2*JD*X+2*0A*X
 2330XL=X:REM NOW GET NEW GUESS
 2340X=XL-TP/BP:REM NEW GUESS
 2350IF ABS(XL-X)>1.0E06 THEN 2290:REM REPEAT ITTERATION
 2360CI=X:GOSUB 3440:X=CI:REM CONSTANT FOUND AND ROUNDED
 2370IF C(D7-1)<>X THENC(D7)=X:D7=D7+1
 2380RETURN
 2390PRINT"      USING (011) DIRECTION NO"
 2400PRINT"      SOLUTION CAN BE FOUND FOR C25":
 2410PRINT"       PRESS ANY KEY TO CONTINUE"
 2420POKE158,0
 2430GET A$:IF A$="" THEN 2430
 2440PRINT" ":RETURN
 2450FOR I=1 TO CT:REM REPEATS CALACULATIONS CT TIMES
```

```
 2460CA=C(I)-CC
 2480PRINT£1,"":PRINT£1," SOLUTION";I;"FOR THE";B$
 2490PRINT£1,"":PRINT£1,"    C25=";CA;" NM"
 2500PRINT£1,"":PRINT£1,"    C23 +VE CASE"
 2510REM NOW CALCULATE C23
 2520DZ=KD-(CA+CC)^2
 2530IF 0>DZ THEN 2860:REM NO SOLUTION FOR C23
 2540REM
 2550DZ=SQR(DZ)
 2560M1=DZ-C4:REM +VE CASE FOR C23
 2570M2=-DZ-C4:REM -VE CASE FOR C23
 2575CI=M1:GOSUB 3440:M1=CI:CI=M2:GOSUB 3440:M2=CI
 2580PRINT£1,"":PRINT£1,"    C23=";M1;" NM"
 2590REM NOW NEED POLARISATION VECTORS
 2600CB=M1:GOSUB 3080:REM GETS POLARISATION VECTORS
 2610PRINT£1,"":PRINT£1,"    C23 -VE CASE"
 2620PRINT£1,"":PRINT£1,"    C23=";M2;" NM"
 2630CB=M2:GOSUB 3080
 2640REM C23 AND C25 FOUND NOW GET C12
 2650EX=(C6+C2)*(C5+C4)+(C1+C6)*(C6+C2+C5+C4)-(CX+CC)^2-(
CA+CC)^2
 2660EX=EX-4*DN^2*(VD^2*VE^2+VD^2*VF^2+VE^2*VF^2)
 2670IF 0>EX THEN 2890
 2680EX=SQR(EX)
 2690M1=EX-C6:REM +VE CASE
 2700M2=-EX-C6:REM -VE CASE
 2710CI=M1:GOSUB 3440:M1=CI:CI=M2:GOSUB 3440:M2=CI
 2720PRINT£1,"":PRINT£1,"   C12 +VE CASE"
 2730PRINT£1,"":PRINT£1,"    C12=";M1;" NM":CE=M1
 2740REM NEED POLARISATION VECTORS
 2750GOSUB 2920
 2760PRINT£1,"":PRINT£1,"    C12 -VE CASE"
 2770PRINT£1,"":PRINT£1,"    C12=";M2;" NM":CE=M2
 2780REM NOW GET POLARISATION VECTORS
 2790GOSUB 2920:REM LOOKING AT (110)
 2800POKE 158,0:PRINT"     PRESS ANY KEY TO CONTINUE"
 2810GET A$:IF A$="" THEN 2810
 2820PRINT" "
 2830NEXT I
 2840PRINT"          PLEASE WAIT"
 2850RETURN
 2860PRINT£1,"":PRINT£1,"   NO REAL SOLUTION CAN BE"
 2870PRINT£1,"":PRINT£1,"   BE FOUND FOR C23"
 2880GOTO 2650:REM LOOK FOR C12 NOW
 2890PRINT£1,"":PRINT£1,"    NO REAL SOLUTION CAN"
 2900PRINT£1,"":PRINT£1,"    BE FOUND FOR C12"
 2910GOTO 2830
 2920REM SUBROUTINE TO GET POLARISATIONN VECTORS (110)
 29300Z=0.25*(CE+C6)*(CA+CC)-0.5*(CX+CC)*(0.5*(C6+C2)-DN*
VD^2):REM U3
 29400B=0.25*(CX+CC)*(CA+CC)-0.5*(CE+C6)*(0.5*(C5+C4)-DN*
VD^2):REM U2
 29500C=(0.5*(C6+C2)-DN*VD^2)*(0.5*(C5+C4)-DN*VD^2)-(0.5*
(CA+CC))^2
 2960REM U1 MUST BE POSITIVE
 2970U1=1.0
 2980U3=0Z/0C
 2990U2=0B*U3/0Z
```

```
 3000REM NORMILSE
 3010UT=U1^2+U2^2+U3^2:UT=SQR(UT)
 3020U1=U1/UT:U2=U2/UT:U3=U3/UT
 3025PRINT£1,""
 3030PRINT£1,"   U3/U2=";INT(OZ*1000/OB)/1000;"
U3/U1=";INT(OZ*1000/OC)/1000
 3040PRINT£1,"":PRINT£1,"     NORMILISED VECTORS ARE"
 3050PRINT£1,"":PRINT£1,"  U1=";INT(U1*1000)/1000;"
U2=";INT(U2*1000)/1000;
 3060PRINT£1,"  U3=";INT(U3*1000)/1000
 3065PRINT£1,"":PRINT£1,"  PROP VECT  X=0.707  Y=0.707
Z=0.0"
 3070RETURN
 3080REM SUBROUTINE TO GET POLARISATION VECTORS (011)
 30900D=0.25*(CC+CA)*(C4+CB)-0.5*(CC+CF)*(0.5*(C2+C4)-DN*
VG^2)
 31000E=0.25*(CC+CF)*(C4+CB)-0.5*(CC+CA)*(0.5*(C4+C3)-DN*
VG^2)
 31100F=(0.5*(C2+C4)-DN*VG^2)*(0.5*(C4+C3)-DN*VG^2)-(0.5*
(C4+CB))^2
 3120REM U2 ALWAYS POSITIVE
 3130U2=1.0:U3=OD/OE:U1=OF*U3/OD
 3140UT=U1^2+U2^2+U3^2:UT=SQR(UT):REM NORMILISED
 3150U1=U1/UT:U2=U2/UT:U3=U3/UT
 3155PRINT£1,""
 3160PRINT£1,"   U3/U2=";INT(OD*1000/OE)/1000;"
U3/U1=";INT(OD*1000/OF)/1000
 3170PRINT£1,"":PRINT£1,"     NORMILISED VECTORS ARE"
 3180PRINT£1,"":PRINT£1,"  U1=";INT(U1*1000)/1000;"
U2=";INT(U2*1000)/1000;
 3190PRINT£1,"  U3=";INT(U3*1000)/1000
 3195PRINT£1,"":PRINT£1,"  PROP VECT  X=0.0  Y=0.707
Z=0.707"
 3200RETURN
 3210IZ=KD-X^2
 3220IF IZ<0 THEN 3310
 3230TP=LA*SQR(IZ)-(LA*X^2)/SQR(IZ)-2*JD*X+2*OA*X
 3240BP=-LA*X/SQR(IZ)-LA*(IZ^-1.5)*X^3-LA*2*X/SQR(IZ)-2*J
D+2*OA
 3250XL=X:REM NOW GET NEW GUESS
 3260X=XL-TP/BP:REM NEW GUESS
 3270IF ABS(XL-X)>1.0E06 THEN 3210:REM REPEAT ITERATION
 3280CI=X:GOSUB 3440:X=CI:REM CONSTANT FOUNDED AND
ROUNDED
 3290IF C(D7-1)<>X THEN C(D7)=X:D7=D7+1
 3300REM ELEMENTS THE SAME SO CONTINUE
 3310RETURN
 3320IZ=KD-X^2:REM BEST FIT -VE CASE
 3330IF IZ<0 THEN 3420
 3340TP=-LA*SQR(IZ)+(LA*X^2)/SQR(IZ)-2*JD*X+2*OA*X
 3350BP=LA*X/SQR(IZ)+LA*(IZ^-1.5)*X^3+LA*2*X/SQR(IZ)-2*JD
+2*OA
 3360XL=X:REM NOW GET NEXT GUESS
 3370X=XL-TP/BP:REM NEW GUESS
 3380IF ABS(XL-X)>1.0E06 THEN 3320:REM REPEAT ITERATION
 3390CI=X:GOSUB 3440:X=CI:REM CONSTANT FOUND AND ROUNDED
 3400IF C(D7-1)<>X THEN C(D7)=X:D7=D7+1
 3410REM ELEMENTS THE SAME SO CONTINUE
```

```
 3420RETURN
 3430
 3440REM ROUNDING ROUTINE FOR ELASTIC CONSTANTS
 3450BB=BA+1
 3460IC=INT((CI*10^BB)/1.0E10)
 3470CD=INT((CI*10^BA)/1.0E10)
 3480B1=IC-10*CD
 3490IF B1<5 THEN 3510
 3500CD=CD+1
 3510CI=CD*1.0E10/(10^BA)
 3520RETURN
 3700PRINT"    FOR THE POSITIVE BEST FIT CASE"
 3710PRINT"   MINIMUM OR MAXIMUM POINT'S ARE"
 3720FOR I=1 TO CT
 3730PRINT"   POINT ";I;" AT C25=";(C(I)-CC)/1.0E10:REM
C(I) CONTAINS C46+C25
 3740NEXT I
 3750REM NOW ELIMINATE FALSE TERMS
 3760AU=AU+1:X=C(AU):IZ=KD-X^2
 3770DF=-LA*X/SQR(IZ)-LA*(IZ^-1.5)*X^3-LA*2*X/SQR(IZ)-2*J
D+2*0A
 3780DU=LA*X*SQR(IZ)-JD*X^2-0A*IZ-NA
 4030IF DU<0 THEN 4070:REM -VE CASE
 4040IF DF>0 THEN 4130:REM OK TRUE MIN POINT
 4050REM IF HERE WE HAVE A MAXIMUM SO DISCOUNT
 4060GOTO 4090:REM SHIFTER
 4070IF DF<0 THEN 4130:REM MIN POINT SO OK
 4090FOR I=AU+1 TO CT
 4100C(I-1)=C(I):NEXT I:REM THROWS OUT WRONG POINT
 4120CT=CT-1:AU=AU-1
 4130IF AU=CT THEN RETURN
 4140GOTO 3760
 4150RETURN
 5000PRINT"    FOR THE NEGATIVE BEST FIT CASE"
 5010PRINT"   MINIMUM OR MAXIMUM POINT'S ARE"
 5015AU=0
 5020FOR I=1 TO CT
 5030PRINT"   POINT ";I;" AT C25=";(C(I)-CC)/1.0E10:REM
C(I) CONTAINS C46+C25
 5040NEXT I
 5050REM NOW ELIMINATE FALSE TERMS
 5060AU=AU+1:X=C(AU):IZ=KD-X^2
 5070DF=LA*X/SQR(IZ)+LA*(IZ^-1.5)*X^3+LA*2*X/SQR(IZ)-2*JD
+2*0A
 5080DU=-LA*X*SQR(IZ)-JD*X^2-0A*(IZ)-NA
 5090IF DU<0 THEN 5130:REM -VE CASE
 5100IF DF>0 THEN 5190:REM OK TRUE MIN POINT
 5110REM IF HERE WE HAVE A MAXIMUM SO DISeR .7391120GOTO
5150:REM SHIFTER
 5130IF DF<0 THEN 5190:REM MIN POINT SO OK
 5150FOR I=AU+1 TO CT
 5160C(I-1)=C(I):NEXT I:REM THROWS OUT WRONG POINT
 5180CT=CT-1:AU=AU-1
 5190IF AU=CT THEN RETURN
 5200GOTO 5060
 5210RETURN
```

APPENDIX 2.C

The following computer program calculates the elastic stiffness constants c_{12}, c_{25} and c_{23} using the procedure described in section 4.3. This being the second method described in section 4.3.

```
   50PRINT"          FIND C25 USING [110] DIRECTION"
   60FOR I=1TO5000:NEXTI
  100DIM C(10),D(100),B(100)
  110PRINT"            HOW MANY SIGNIFICANT FIGURES"
  120PRINT"       ARE THE CONSTANTS TO BE"
  130INPUT"       DETERMINED TO (RANGE 1-5)       ";BA
  140IF BA<1 OR BA>5 THEN 110
  150BA=BA-1
  160REM INPUT ELASTIC CONSTANTS AND VELOCITIES NEEDED
FROM DISC
  170E$="":BC=BC+1
  180INPUT"     DATA FILE NAME       ";A$
  190IF A$=" " THEN 180
  200INPUT"   DRIVE NUMBER OF DATA FILE       ";N
  210$O,N,"R",A$,E$
  220$R,A$:DN=VAL(A$)
  230$R,A$:C1=VAL(A$)
  240$R,A$:CU=VAL(A$)
  250$R,A$:CX=VAL(A$)
  260$R,A$:C2=VAL(A$)
  270$R,A$:C3=VAL(A$)
  280$R,A$:CF=VAL(A$)
  290$R,A$:C4=VAL(A$)
  300$R,A$:CC=VAL(A$)
  310$R,A$:C5=VAL(A$)
  320$R,A$:C6=VAL(A$)
  330$R,A$:VD=VAL(A$)
  340$R,A$:VE=VAL(A$)
  350$R,A$:VF=VAL(A$)
  360$R,A$:VG=VAL(A$)
  370$R,A$:VH=VAL(A$)
  380$R,A$:VI=VAL(A$)
  390$C
  391INPUT"        OUTPUT TO PRINTER       ";A$:IF A$=" "
THEN 391
  392IF LEFT$(A$,1)="Y" THEN N=4:GOTO 394
  393N=3
  394OPEN 1,N
  396PRINT" "
  400PRINT" ":PRINT£1,"":PRINT£1,"
DENSITY=";DN;"KG/M^3"
  410PRINT£1,"":PRINT£1,"          C11=";C1;" NM"
  420PRINT£1,"":PRINT£1,"          C13=";CU;" NM"
```

```
  430PRINT£1,"":PRINT£1,"          C15=";CX;" NM"
  440PRINT£1,"":PRINT£1,"          C22=";C2;" NM"
  450PRINT£1,"":PRINT£1,"          C33=";C3;" NM"
  460PRINT£1,"":PRINT£1,"          C35=";CF;" NM"
  470PRINT£1,"":PRINT£1,"          C44=";C4;" NM"
  480PRINT£1,"":PRINT£1,"          C46=";CC;" NM"
  490PRINT£1,"":PRINT£1,"          C55=";C5;" NM"
  500PRINT£1,"":PRINT£1,"          C66=";C6;" NM"
  510PRINT"     PRESS ANY KEY TO CONTINUE"
  520POKE158,0:REM EMPTY KEY BOARD
  530GET A$:IF A$="" THEN 530
  540PRINT" ":PRINT£1,"":PRINT£1,"          V13=";VD;"
M/S"
  550PRINT£1,"":PRINT£1,"          V14=";VE;" M/S"
  560PRINT£1,"":PRINT£1,"          V15=";VF;" M/S"
  570PRINT£1,"":PRINT£1,"          V16=";VG;" M/S"
  580PRINT£1,"":PRINT£1,"          V17=";VH;" M/S"
  590PRINT£1,"":PRINT£1,"          V18=";VI;" M/S"
  600PRINT"    PRESS ANY KEY TO CONTINUE"
  610POKE158,0
  620GET A$:IF A$="" THEN620
  630PRINT" "
  640RT=(C6+C2)*(C5+C4)+(C1+C6)*(C6+C2+C5+C4)-(CX+CC)^2
  650RT=RT-4*DN^2*(VD^2*VE^2+VD^2*VF^2+VE^2*VF^2)

660RE=8*DN^3*VD^2*VE^2*VF^2-(C1+C6)*(C6+C2)*(C5+C4)+(CX+C
C)^2*(C6+C2)
  670GA=2*(CX+CC)
  680LM=C1+C6
  690SD=C5+C4
  700KD=(C2+2*C4+C3)*(C6+C5)+(C2+C4)*(C4+C3)-(CC+CF)^2
  710KD=KD-4*DN^2*(VG^2*VH^2+VG^2*VI^2+VH^2*VI^2)

720NA=8*DN^3*VG^2*VH^2*VI^2-(C6+C5)*(C2+C4)*(C4+C3)+(C2+C
4)*(CC+CF)^2
  730LA=2*(CC+CF):OA=C6+C5:JD=C4+C3
  740REM SECTION TO FIND REGION WHERE WE HAVE + SOLUTION
  750A9=SQR(RT):REM ADJUST
  760A8=-A9:REM A9,A8 FIXES LIMIT FOR ITERATIONS
  770REM DO FOR POSITIVE SECTION
  780PRINT"          QUIET I'M TRYING TO THINK"
  790FOR I=1 TO 10:C(I)=0:NEXTI:D7=1:REM CLEARS HOLDING
ARRAY
  800X=A9:IF RT-X^2<0 THEN A9=A9-1.0E07:GOTO 800:REM
REDUCES A9 TO BOUNDRY
  810A8=-A9:X=A8:IZ=RT-X^2:GOSUB 2200:REM KICKS OUT IF
ERROR
  820REM WE HAVE NOW HOMED IN FROM THE TOP AND BOTTOM TO
GET ROOT NEAR BOUNDRY
  830FOR I=A8 TO A9 STEP 1.0E10
  840PRINT"+ CASE I=";I
  850X=I:GOSUB 2180:NEXT I:REM DEALING WITH POSITIVE CASE
  860X=A9:IZ=RT-X^2:GOSUB 2200:REM DOES HIGH CASE LAST TO
PREVENT DOUBILING
  870REM HUNT FOR POSITIVE SOLUTION TO C25
  880PRINT" "
  890IF C(1)=0 THEN GT=1:GOTO 940:REM NO SOLUTION
  900IF C(2)=0 THEN CT=1:GOTO 960:REM ONE SOLUTION
```

```
  910FOR I=2 TO 10
  920IF C(I)=0 THEN CT=I-1:I=10
  930NEXT I:GOTO  960
  940PRINT"     FOR THE POSITIVE CASE":GOSUB 2390
  950GOTO 980:REM JUMP TO -VE CASE C25 OF EXACT SOLUTION
FOR C25
  960PRINT£1,"":PRINT£1,"  SOLVING FOR C25 POSITIVE
CASE":B$="C25 POSITIVE CASE"
  970GOSUB 2450:REM FINDS CONSTANTS FOR CT SOLUTIONS
  980REM NOW DO FOR -VE CASE OF C25
  990REM NOTE LIMITS ARE SAME, SO CAN USE A9 AND A8 OF
LAST TIME
 1000PRINT"           QUIET PLEASE!"
 1010FOR I=1 TO 10:C(I)=0:NEXT I:D7=1:REMCLEARS HOLDING
ARRAY
 1020REM DO FOR LOW CASE
 1030X=A8:IZ=RT-X^2:GOSUB 2310
 1040REM HAVE NOW HOMED IN FROM TOP AND BOTTOM TO CAPTURE
ROOT,NOW CHECK MID
 1050FOR I=A8 TO A9 STEP 1.0E10
 1060PRINT" - CASE I=";I
 1070X=I:GOSUB 2290:NEXTI:REM DEALING WITH NEGATIVE CASE
 1080X=A9:IZ=RT-X^2:GOSUB 2310
 1090PRINT" "
 1100IF C(1)=0 THEN GX=1:GOTO 1150:REM NO SOLUTION FOUND
 1110IF C(2)=0 THEN CT=1:GOTO 1170:REM ONE SOLUTION
 1120FOR I=1 TO 10
 1130IF C(I)=0 THEN CT=I-1:I=10
 1140NEXT I:GOTO 1170
 1150PRINT"     FOR THE NEGATIVE CASE":GOSUB 2390
 1160GOTO 1190:REM NOW JUMP BEST FIR CASE
 1170PRINT"    SOLVING FOR C25 NEGATIVE CASE":B$="C25
NEGATIVE CASE"
 1180GOSUB 2450: REM CARRYS OUT EVALATION OF CONSTANTS
FOR C25 SOLUTIONS
 1190REM BEST FIT CASE +VE
 1200IF GT=0 THEN 1680:REM WE HAVE AN EXACT SOLUTION SO
BY PASS
 1210REM IF HERE TRYING BEST FIT
 1220PRINT"           QUIET I'M TRYING TO THINK"
 1230FOR I=1 TO 10:C(I)=0: NEXT I:D7=1:REM CLEARS HOLDING
ARRAY
 1240X=A8:IZ=RT-X^2:GOSUB 3230
 1250REM HAVE NOW HOMED IN FROM TOP AND BOTTOM TO CAPTURE
ROOT,NOW CHECK MIDDLE
 1260FOR I=A8 TO A9 STEP 1.0E10
 1270PRINT" BEST FIT +VE CASE I=";I
 1280X=I:GOSUB 3210:NEXT I
 1290X=A9:IZ=RT-X^2:GOSUB 3230
 1300PRINT" "
 1310IF C(1)=0 THEN 1360:REM NO SOLUTION FOUND
 1320IF C(2)=0 THEN CT=1: GOTO 1400:REM ONE SOLUTION
 1330FOR I=1 TO 10
 1340IF C(I)=0 THEN CT=I-1:I=10
 1350NEXT I:GOTO 1400
 1360PRINT"     FOR THE POSITIVE BEST"
 1370PRINT"     FIT CASE THEIR IS NO"
 1380PRINT"     MINIMUM POINT"
 1390GOTO 1690:REM TRY -VE BEST FIT CASE.
```

```
 1400GOSUB 3700:REM SORTS OUT MAX POINTS
 1401PRINT"   PRESS ANY KEY TO CONTINUE":POKE 158,0
 1402GET A$:IF A$="" THEN 1402
 1403PRINT" "
 1405PRINT"    SOLVING FOR BEST FIT C25 +VE CASE":B$="C25
BEST FIT +VE CASE"
 1410GOSUB 2450:REM CARRYS OUT EVALATION OF CONSTANTS FOR
CT SOLUTIONS
 1420FOR I=A8 TO A9 STEP 1.0E09:REM STORES FOR PLOT OF
SOLUTION
 1430X=I:IZ=RT-X^2
 1440IF IZ<0 THEN 1470
 1450F=GA*SQR(IZ)*X-SD*IZ-LM*X^2-RE
 1460K=K+1:D(K)=(X-CC)/1.0E10:B(K)=F:REM PLOT DIRECTELY
C25
 1470NEXT I
 1480K=K+1
 1490D(K)=(A8-CC)/1.0E10:X=A8:B(K)=GA*SQR(IZ)*X-SD*IZ-LM*
X^2-RE
 1500DS=ABS(B(1))
 1510FOR I=2 TO K
 1520IF DS<ABS(B(I)) THEN DS=B(I)
 1530NEXT I
 1540REM DS HOLDS LARGEST TIME
 1550FOR I=1 TO K
 1560B(I)=B(I)/DS
 1570NEXT I:REM SCALED DATA
 1580A$=" 1"
 1590$O,2,"W","+VE",""
 1600$W,STR$(K)
 1610FOR I=1 TO K
 1620$W,STR$(D(I))
 1630$W,STR$(B(I))
 1640$W,A$
 1650$W,A$
 1660NEXT I
 1670$C
 1680REM BEST FIT NEGATIVE CASE
 1690IF GX=0 THEN
 1700REM IF HERE TRYING BEST FIT
 1710PRINT" "
 1720PRINT"            QUIET I'M TRYING TO THINK"
 1730FOR I=1 TO 10:C(I)=0:NEXT I:D7=1:REM CLEAR HOLDING
ARRAY
 1740X=A8:IZ=RT-X^2:GOSUB 3340
 1750REM HAVE NOW HOMED IN FROM TOP AND BOTTOM TO CAPTURE
ROOT NOW CHECK MID
 1760FOR I=A8 TO A9 STEP 1.0E10
 1770PRINT" BEST FIT CASE -VE I=";I
 1780X=I:GOSUB 3320:NEXT I:PRINT" "
 1790X=A9:IZ=RT-X^2:GOSUB 3340
 1800IF C(1)=0 THEN 1850:REM NO SOLUTION FOUND
 1810IF C(2)=0 THEN CT=1:GOTO 1890:REM ONE SOLUTION
 1820FOR I=1 TO 10
 1830IF C(I)=0 THEN CT=I-1:I=10
 1840NEXT I:GOTO 1890
 1850PRINT"     FOR THE NEGATIVE BEST"
 1860PRINT"      FIT CASE THEIR IS NO"
```

```
 1870PRINT"     MINIMUM POINT"
 1880
 1890GOSUB 5000:REM ROUTINE TO SORT OUT CORRECT VALUES
 1891PRINT"    PRESS ANY KEY TO CONTINUE":POKE158,0
 1892GET A$:IF A$="" THEN 1892
 1893PRINT" "
 1895PRINT"    SOLVING FOR BEST FIT C25 -VE CASE":B$="C25
BEST FIT -VE CASE"
 1900GOSUB 2450:K=0:REM CARRY OUT EVALATION FOR CT
SOLUTIONS
 1910FOR I=A8 TO A9 STEP 1.0E09:REM DUMP TO PLOTTER
 1920X=I:IZ=RT-X^2
 1930IF IZ<0 THEN 1960
 1940F=-GA*X*SQR(IZ)-SD*IZ-LM*X^2-RE
 1950K=K+1:D(K)=(X-CC)/1.0E10:B(K)=F:REM PLOT OUT AACTUAL
C25
 1960NEXT I
 1970K=K+1
 1980D(K)=(A8-CC)/1.0E10:X=A8:B(K)=-GA*X*SQR(IZ)-SD*IZ-LM
*X^2-RE
 1990DS=ABS(B(1))
 2000FOR I=2 TO K
 2010IF DS<ABS(B(I)) THEN DS=B(I)
 2020NEXT I
 2030REM DS HOLDS LARGEST TERM
 2040FOR I=1 TO K
 2050B(I)=B(I)/DS
 2060NEXT I:REM TERM CORRECTED TO 1
 2070A$=" 1"
 2080$O,2,"W","-VE",""
 2090$W,STR$(K)
 2100FOR I=1 TO K
 2110$W,STR$(D(I))
 2120$W,STR$(B(I))
 2130$W,A$
 2140$W,A$
 2150NEXT I
 2160$C
 2170
 2180IZ=RT-X^2
 2190IF IZ<0 THEN 2280
 2200TP=GA*SQR(IZ)*X-SD*IZ-LM*X^2-RE
 2210BP=GA*SQR(IZ)-GA*X^2/SQR(IZ)+LM*2*X-SD*2*X
 2220XL=X:REM NOW GET NEXT GUSS
 2230X=XL-TP/BP:REM NEW GUSS
 2240IF ABS(XL-X)>1.0E06 THEN 2180:REM REPEAR ITERATION
 2250CI=X:GOSUB 3440:X=CI:REM CONSTANT FOUND AND ROUNDED
 2260IF C(D7-1)<>X THEN C(D7)=X:D7=D7+1
 2270REM ELEMENT SAME SO CONTINUE
 2280RETURN
 2290IZ=RT-X^2
 2295REM ROUTINE CALACULATES X,WHERE X=C25+C46
 2300IF IZ<0 THEN2380
 2310TP=-GA*X*SQR(IZ)-SD*IZ-LM*X^2-RE
 2320BP=-GA*SQR(IZ)+(GA*X^2)/SQR(IZ)-2*LM*X+2*SD*X
 2330XL=X:REM NOW GET NEW GUESS
 2340X=XL-TP/BP:REM NEW GUESS
 2350IF ABS(XL-X)>1.0E06 THEN 2290:REM REPEAT ITTERATION
```

```
2360CI=X:GOSUB 3440:X=CI:REM CONSTANT FOUND AND ROUNDED
2370IF C(D7-1)<>X THENC(D7)=X:D7=D7+1
2380RETURN
2390PRINT"      USING (110) DIRECTION NO"
2400PRINT"      SOLUTION CAN BE FOUND FOR C25":
2410PRINT"       PRESS ANY KEY TO CONTINUE"
2420POKE158,0
2430GET A$:IF A$="" THEN 2430
2440PRINT" ":RETURN
2450FOR I=1 TO CT:REM REPEATS CALACULATIONS CT TIMES
2460CA=C(I)-CC
2480PRINT£1,"":PRINT£1," SOLUTION";I;"FOR THE";B$
2490PRINT£1,"":PRINT£1,"    C25=";CA;" NM"
2500PRINT£1,"":PRINT£1,"    C12 +VE CASE"
2510REM NOW CALCULATE C12
2520DZ=RT-(CA+CC)^2
2530IF 0>DZ THEN 2860:REM NO SOLUTION FOR C12
2540REM
2550DZ=SQR(DZ)
2560M1=DZ-C6:REM +VE CASE FOR C12
2570M2=-DZ-C6:REM -VE CASE FOR C12
2575CI=M1:GOSUB 3440:M1=CI:CI=M2:GOSUB 3440:M2=CI
2580PRINT£1,"":PRINT£1,"    C12=";M1;" NM"
2590REM NOW NEED POLARISATION VECTORS
2600CE=M1:GOSUB 2920:REM GETS POLARISATION VECTORS
2610PRINT£1,"":PRINT£1,"    C12 -VE CASE"
2620PRINT£1,"":PRINT£1,"    C12=";M2;" NM"
2630CE=M2:GOSUB 2920
2640REM C12 AND C25 FOUND NOW GET C23
2650EX=(C2+2*C4+C3)*(C6+C5)+(C2+C4)*(C4+C3)-(CC+CF)^2-(C
C+CA)^2
2660EX=EX-4*DN^2*(VG^2*VH^2+VH^2*VI^2+VG^2*VI^2)
2670IF 0>EX THEN 2890
2680EX=SQR(EX)
2690M1=EX-C4:REM +VE CASE
2700M2=-EX-C4:REM -VE CASE
2710CI=M1:GOSUB 3440:M1=CI:CI=M2:GOSUB 3440:M2=CI
2720PRINT£1,"":PRINT£1,"   C23 +VE CASE"
2730PRINT£1,"":PRINT£1,"    C23=";M1;" NM":CB=M1
2740REM NEED POLARISATION VECTORS
2750GOSUB 3080
2760PRINT£1,"":PRINT£1,"    C23 -VE CASE"
2770PRINT£1,"":PRINT£1,"    C23=";M2;" NM":CB=M2
2780REM NOW GET POLARISATION VECTORS
2790GOSUB 3080
2800POKE 158,0:PRINT"     PRESS ANY KEY TO CONTINUE"
2810GET A$:IF A$="" THEN 2810
2820PRINT" "
2830NEXT I
2840PRINT"          PLEASE WAIT"
2850RETURN
2860PRINT£1,"":PRINT£1,"   NO REAL SOLUTION CAN BE"
2870PRINT£1,"":PRINT£1,"   BE FOUND FOR C12"
2880GOTO 2650:REM LOOK FOR C23 NOW
2890PRINT£1,"":PRINT£1,"    NO REAL SOLUTION CAN"
2900PRINT£1,"":PRINT£1,"    BE FOUND FOR C23"
2910GOTO 2830
2920REM SUBROUTINE TO GET POLARISATIONN VECTORS (110)
```

```
 29300Z=0.25*(CE+C6)*(CA+CC)-0.5*(CX+CC)*(0.5*(C6+C2)-DN*
VD^2):REM U3
 29400B=0.25*(CX+CC)*(CA+CC)-0.5*(CE+C6)*(0.5*(C5+C4)-DN*
VD^2):REM U2
 29500C=(0.5*(C6+C2)-DN*VD^2)*(0.5*(C5+C4)-DN*VD^2)-(0.5*
(CA+CC))^2
 2960REM U1 MUST BE POSITIVE
 2970U1=1.0
 2980U3=0Z/0C
 2990U2=0B*U3/0Z
 3000REM NORMILSE
 3010UT=U1^2+U2^2+U3^2:UT=SQR(UT)
 3020U1=U1/UT:U2=U2/UT:U3=U3/UT
 3025PRINT£1,""
 3030PRINT£1,"   U3/U2=";INT(0Z*1000/0B)/1000;"
U3/U1=";INT(0Z*1000/0C)/1000
 3040PRINT£1,"":PRINT£1,"      NORMILISED VECTORS ARE"
 3050PRINT£1,"":PRINT£1,"  U1=";INT(U1*1000)/1000;"
U2=";INT(U2*1000)/1000;
 3060PRINT£1,"  U3=";INT(U3*1000)/1000
 3065PRINT£1,"":PRINT£1,"  PROP VECT  X=0.707  Y=0.707
Z=0.0"
 3070RETURN
 3080REM SUBROUTINE TO GET POLARISATION VECTORS (011)
 30900D=0.25*(CC+CA)*(C4+CB)-0.5*(CC+CF)*(0.5*(C2+C4)-DN*
VG^2)
 31000E=0.25*(CC+CF)*(C4+CB)-0.5*(CC+CA)*(0.5*(C4+C3)-DN*
VG^2)
 31100F=(0.5*(C2+C4)-DN*VG^2)*(0.5*(C4+C3)-DN*VG^2)-(0.5*
(C4+CB))^2
 3120REM U2 ALWAYS POSITIVE
 3130U2=1.0:U3=0D/0E:U1=0F*U3/0D
 3140UT=U1^2+U2^2+U3^2:UT=SQR(UT):REM NORMILISED
 3150U1=U1/UT:U2=U2/UT:U3=U3/UT
 3155PRINT£1,""
 3160PRINT£1,"   U3/U2=";INT(0D*1000/0E)/1000;"
U3/U1=";INT(0D*1000/0F)/1000
 3170PRINT£1,"":PRINT£1,"      NORMILISED VECTORS ARE"
 3180PRINT£1,"":PRINT£1,"  U1=";INT(U1*1000)/1000;"
U2=";INT(U2*1000)/1000;
 3190PRINT£1,"  U3=";INT(U3*1000)/1000
 3195PRINT£1,"":PRINT£1,"  PROP VECT  X=0.0  Y=0.707
Z=0.707"
 3200RETURN
 3210IZ=RT-X^2
 3220IF IZ<0 THEN 3310
 3230TP=GA*SQR(IZ)-(GA*X^2)/SQR(IZ)-2*LM*X+2*SD*X
 3240BP=-GA*X/SQR(IZ)-GA*(IZ^-1.5)*X^3-GA*2*X/SQR(IZ)-2*L
M+2*SD
 3250XL=X:REM NOW GET NEW GUESS
 3260X=XL-TP/BP:REM NEW GUESS
 3270IF ABS(XL-X)>1.0E06 THEN 3210:REM REPEAT ITERATION
 3280CI=X:GOSUB 3440:X=CI:REM CONSTANT FOUNDED AND
ROUNDED
 3290IF C(D7-1)<>X THEN C(D7)=X:D7=D7+1
 3300REM ELEMENTS THE SAME SO CONTINUE
 3310RETURN
 3320IZ=RT-X^2:REM BEST FIT -VE CASE
```

```
 3330IF IZ<0 THEN 3420
 3340TP=-GA*SQR(IZ)+(GA*X^2)/SQR(IZ)-2*LM*X+2*SD*X
 3350BP=GA*X/SQR(IZ)+GA*(IZ^-1.5)*X^3+GA*2*X/SQR(IZ)-2*LM
+2*SD
 3360XL=X:REM NOW GET NEXT GUESS
 3370X=XL-TP/BP:REM NEW GUESS
 3380IF ABS(XL-X)>1.0E06 THEN 3320:REM REPEAT ITERATION
 3390CI=X:GOSUB 3440:X=CI:REM CONSTANT FOUND AND ROUNDED
 3400IF C(D7-1)<>X THEN C(D7)=X:D7=D7+1
 3410REM ELEMENTS THE SAME SO CONTINUE
 3420RETURN
 3430
 3440REM ROUNDING ROUTINE FOR ELASTIC CONSTANTS
 3450BB=BA+1
 3460IC=INT((CI*10^BB)/1.0E10)
 3470CD=INT((CI*10^BA)/1.0E10)
 3480B1=IC-10*CD
 3490IF B1<5 THEN 3510
 3500CD=CD+1
 3510CI=CD*1.0E10/(10^BA)
 3520RETURN
 3700PRINT"    FOR THE POSITIVE BEST FIT CASE"
 3710PRINT"   MINIMUM OR MAXIMUM POINT'S ARE"
 3720FOR I=1 TO CT
 3730PRINT"   POINT ";I;" AT C25=";(C(I)-CC)/1.0E10:REM
C(I) CONTAINS C46+C25
 3740NEXT I
 3750REM NOW ELIMINATE FALSE TERMS
 3760AU=AU+1:X=C(AU):IZ=RT-X^2
 3770DF=-GA*X/SQR(IZ)-GA*(IZ^-1.5)*X^3-GA*2*X/SQR(IZ)-2*L
M+2*SD
 3780DU=GA*X*SQR(RT-X^2)-LM*X^2-SD*(RT-X^2)-RE
 4030IF DU<0 THEN 4070:REM -VE CASE
 4040IF DF>0 THEN 4130:REM OK TRUE MIN POINT
 4050REM IF HERE WE HAVE A MAXIMUM SO DISCOUNT
 4060GOTO 4090:REM SHIFTER
 4070IF DF<0 THEN 4130:REM MIN POINT SO OK
 4080REM SHIFTER
 4090FOR I=AU+1 TO CT
 4100C(I-1)=C(I):NEXT I:REM THROWS OUT WRONG POINT
 4110REM
 4120CT=CT-1:AU=AU-1
 4130IF AU=CT THEN RETURN
 4140GOTO 3760
 4150RETURN
 5000PRINT"    FOR THE NEGATIVE BEST FIT CASE"
 5010PRINT"   MINIMUM OR MAXIMUM POINT'S ARE"
 5015AU=0
 5020FOR I=1 TO CT
 5030PRINT"   POINT ";I;" AT C25=";(C(I)-CC)/1.0E10:REM
C(I) CONTAINS C46+C25
 5040NEXT I
 5050REM NOW ELIMINATE FALSE TERMS
 5060AU=AU+1:X=C(AU):IZ=RT-X^2
 5070DF=GA*X/SQR(IZ)+GA*(IZ^-1.5)*X^3+GA*2*X/SQR(IZ)-2*LM
+2*SD
 5080DU=-GA*X*SQR(RT-X^2)-LM*X^2-SD*(RT-X^2)-RE
 5090IF DU<0 THEN 5130:REM -VE CASE
```

```
5100IF DF>0 THEN 5190:REM OK TRUE MIN POINT
5110REM IF HERE WE HAVE A MAXIMUM SO DISCOUNT
5120GOTO 5150:REM SHIFTER
5130IF DF<0 THEN 5190:REM MIN POINT SO OK
5140REM SHIFTER
5150FOR I=AU+1 TO CT
5160C(I-1)=C(I):NEXT I:REM THROWS OUT WRONG POINT
5170REM
5180CT=CT-1:AU=AU-1
5190IF AU=CT THEN RETURN
5200GOTO 5060
5210RETURN
```

APPENDIX 2.D

The following computer program was used to perform the consistency checks on measured velocities and obtained elastic stiffness constants as described in section 4.4.

```
100POKE 144,49
110PRINT"                  TRACE RELATIONS"
120PRINT"             OR PUT ANOTHER WAY"
130PRINT"             IS YOUR DATA ANY GOOD"
140PRINT"      C SOLID STATE JAN 1982"
150FOR I =1 TO 5000:NEXT
160REM PRINT OUT VELOCITYS AS USER CHECK
170REM VELECITY HELD IN V1-VH USING HEX FORMAT
180READ DN:REM DENSITY
190DN=INT(DN*10)/10
200READ V1,V2,V3,V4,V5,V6,V7,V8,V9
210V1=INT(V1*10)/10:V2=INT(V2*10)/10
220V3=INT(V3*10)/10:V4=INT(V4*10)/10
230V5=INT(V5*10)/10:V6=INT(V6*10)/10
240V7=INT(V7*10)/10:V8=INT(V8*10)/10
250V9=INT(V9*10)/10
260READ VA,VB,VC,VD,VE,VF,VG,VH,VI
270VA=INT(VA*10)/10:VB=INT(VB*10)/10
280VC=INT(VC*10)/10:VD=INT(VD*10)/10
290VE=INT(VE*10)/10:VF=INT(VF*10)/10
300VG=INT(VG*10)/10:VH=INT(VH*10)/10
310VI=INT(VI*10)/10
320PRINT" "
330PRINT"      DENSITY=";DN;" KG/M^3"
340PRINT"       V1=";V1;" M/S"
350PRINT"       V2=";V2;" M/S"
360PRINT"       V3=";V3;" M/S"
370PRINT"       V4=";V4;" M/S"
380PRINT"       V5=";V5;" M/S"
390PRINT"       V6=";V6;" M/S"
400PRINT"       V7=";V7;" M/S"
410PRINT"       V8=";V8;" M/S"
420PRINT"    PRESS ANY KEY TO CONTINUE"
430POKE158,0
440GET A$:IF A$="" THEN 440
450PRINT" "
460PRINT"       V9=";V9;" M/S"
470PRINT"      V10=";VA;" M/S"
480PRINT"      V11=";VB;" M/S"
490PRINT"      V12=";VC;" M/S"
500PRINT"      V13=";VD;" M/S"
510PRINT"      V14=";VE;" M/S"
520PRINT"      V15=";VF;" M/S"
530PRINT"      V16=";VG;" M/S"
540PRINT"      V17=";VH;" M/S"
550PRINT"      V18=";VI;" M/S"
560PRINT"     PRESS ANY KEY TO CONTINUE"
```

```
  570POKE 158,0
  580GETA$:IF A$="" THEN 580
  590PRINT"           HOW MANY SIGNIFICANT "
  600PRINT"       FIGURES IN THE VELOCITY"
  610INPUT"       RANGE 1-5       ";BD:BD=BD-1
  620IF BD>4 OR BD<0 THENPRINT"   OUT OF RANGE":GOTO 610
  630DA=V1:GOSUB 1030:V1=DA:DA=V2:GOSUB 1030:V2=DA
  640DA=V3:GOSUB 1030:V3=DA
  650DA=V4:GOSUB 1030:V4=DA
  660DA=V5:GOSUB 1030:V5=DA
  670DA=V7:GOSUB 1030:V7=DA
  680DA=V8:GOSUB 1030:V8=DA
  690DA=V9:GOSUB 1030:V9=DA
  700DA=VA:GOSUB 1030:VA=DA
  710DA=VB:GOSUB 1030:VB=DA
  720DA=VC:GOSUB 1030:VC=DA
  730DA=VE:GOSUB 1030:VE=DA
  740DA=VF:GOSUB 1030:VF=DA
  750DA=VG:GOSUB 1030:VG=DA
  760DA=VH:GOSUB 1030:VH=DA
  770DA=VI:GOSUB 1030:VI=DA
  780DA=V6:GOSUB 1030:V6=DA
  790DA=VD:GOSUB 1030:VD=DA
  800REM WE NOW USE THE FOUR CHECK RELATIONSHIPS TO TEST
GOODNESS OF DATA
  810PRINT"              CHECK 1"
  820PRINT"           V6+V4=V2+V8"
  830MA=V6^2+V4^2:MA=INT(MA*1000/1.0E07)/1000
  840MB=V2^2+V8^2:MB=INT(MB*1000/1.0E07)/1000
  850PRINT"      ";MA;"   VS  ";MB
  860PRINT"              CHECK 2"
  870PRINT"   V2+0.5*(V5+V8+V1+V3)=V13+V14+V15"
  880MC=VD^2+VE^2+VF^2:MC=INT(MC*1000/1.0E07)/1000

890MD=V2^2+0.5*(V5^2+V8^2+V1^2+V3^2):MD=INT(MD*1000/1.0E0
7)/1000
  900PRINT"       ";MC;"  VS  ";MD
  910PRINT"              CHECK 3"
  920PRINT"   V16+V17+V18=V8+0.5*(V2+V5+V9+V7)"
  930ME=VG^2+VH^2+VI^2:ME=INT(ME*1000/1.0E07)/1000

940MF=V8^2+0.5*(V2^2+V5^2+V9^2+V7^2):MF=INT(MF*1000/1.0E0
7)/1000
  950PRINT"       ";ME;"  VS  ";MF
  960PRINT"              CHECK 4"
  970PRINT"   V6*V4=V2*V8-(V11-0.5*(V2+V8))^2"
  980MG=V6^2*V4^2:MG=INT(MG*1000/1.0E14)/1000
  990MH=V2^2*V8^2-(VB^2-0.5*(V2^2+V8^2))^2
 1000MH=INT(MH*1000/1.0E14)/1000
 1010PRINT"        ";MG;"  VS  ";MH
 1020POKE144,46:
 1030REM ROUNDING ROUTINE FOR VELOCITYS
 1040BE=BD+1
 1050IC=INT((DA*10^BE)/1.0E03)
 1060CD=INT((DA*10^BD)/1.0E03)
 1070B1=IC-10*CD
 1080IF B1<5 THEN 1100
 1090CD=CD+1
```

```
1100DA=CD*1.0E03/(10^BD)
1110RETURN
1120REM DATA INPUT
1130REM DENSITY
1140DATA  1680
1150REM     V1       V2        V3
1160DATA 5127.6 ,1899.6, 2518.4
1170REM     V4       V5        V6
1180DATA 2456.6, 4460.4, 1939.6
1190REM     V7       V8        V9
1200DATA 2510.6, 2488.3, 4045.8
1210REM    V10      V11       V12
1220DATA 2273.0, 2283.6, 4527.0
1230REM    V13      V14       V15
1240DATA 4555.6, 2457.6, 2443.9
1250REM    V16      V17       V18
1260DATA 4551.6, 1843.9, 2205.3
```

APPENDIX 2.E

The following computer program calculates the pressure derivatives of the elastic stiffness constants for a monoclinic crystal. To perform the required calculations, the program requires the following data: elastic stiffness constants, elastic compliances, sample density, experimentally measured ultrasonic wave velocities and the f'/f_o values.

```
   10 REM CALCULATION OF PRESSURE DERIVATIVES FOR FIRST
TEN ELASTIC CONSTANTS
   20 REM NEED ELASTIC CONSTANTS, COMPLIENCES + INITIAL
VELOCITYS AND F'/FO
   30  MODE 7
   40 READ C1,CU,CX,C2,C3,CF,C4,CC,C5,C6
   50 CLS
   60 @%=&01050B
   70 PRINTCHR$(141)+CHR$(157)+CHR$(132);"    Elastic
Constants N/m^2"
   80 PRINTCHR$(141)+CHR$(157)+CHR$(132);"    Elastic
Constants N/m^2"
   90 PRINT'"        C11 = ";C1;" N/m^2"
  100 PRINT'"        C13 = ";CU;" N/m^2"
  110 PRINT'"        C15 = ";CX;" N/m^2"
  120 PRINT'"        C22 = ";C2;" N/m^2"
  130 PRINT'"        C33 = ";C3;" N/m^2"
  140 PRINT'"        C35 = ";CF;" N/m^2"
  150 PRINT'"        C44 = ";C4;" N/m^2"
  160 PRINT'"        C46 = ";CC;" N/m^2"
  170 PRINT'"        C55 = ";C5;" N/m^2"
  180 PRINT'"        C66 = ";C6;" N/m^2"
  190 PROCpause
  200 REM NOW INPUT COMPLIENCES
  210 READ S1,SE,SU,SX,S2,SB,SA,S3,SF,S4,SC,S5,S6
  220 CLS
  230  PRINTCHR$(141)+CHR$(157)+CHR$(132)+"     Elastic
Compliances m^2/N"
  240  PRINTCHR$(141)+CHR$(157)+CHR$(132)+"     Elastic
Compliances m^2/N"
  250 PRINT'"      S11 = ";S1;" m^2/N"
  260 PRINT'"      S12 = ";SE;" m^2/N"
  270 PRINT'"      S13 = ";SU;" m^2/N"
  280 PRINT'"      S15 = ";SX;" m^2/N"
  290 PRINT'"      S22 = ";S2;" m^2/N"
  300 PRINT'"      S23 = ";SB;" m^2/N"
  310 PRINT'"      S25 = ";SA;" m^2/N"
  320 PROCpause
  330 CLS
```

```
  340 PRINTCHR$(141)+CHR$(157)+CHR$(132)+"     Elastic
Compliances m^2/N"
  350 PRINTCHR$(141)+CHR$(157)+CHR$(132)+"     Elastic
Compliances m^2/N"
  360 PRINT'"      S33 = ";S3;" m^2/N"
  370 PRINT'"      S35 = ";SF;" m^2/N"
  380 PRINT'"      S44 = ";S4;" m^2/N"
  390 PRINT'"      S46 = ";SC;" m^2/N"
  400 PRINT'"      S55 = ";S5;" m^2/N"
  410 PRINT'"      S66 = ";S6;" m^2/N"
  420 PROCpause
  430 REM NOW READ IN VELOCITYS AND DENSITY
  440 READ DN,V1,V2,V3,V4,V5,V6,V7,V8,V9,VA,VB,VC
  450 CLS
  460  @%=&020207
  470 PRINTCHR$(141)+CHR$(157)+CHR$(132);"   Ultrasonic
Wave velocity m/s"
  480 PRINTCHR$(141)+CHR$(157)+CHR$(132);"   Ultrasonic
Wave velocity m/s"
  490 PRINT'" X prop long         V1 = ";V1;" m/s^2"
  500 PRINT'" X prop Y pol shear V2 = ";V2;" m/s^2"
  510 PRINT'" X prop Z pol shear V3 = ";V3;" m/s^2"
  520 PRINT'" Y prop X pol shear V4 = ";V4;" m/s^2"
  530 PRINT'" Y prop long         V5 = ";V5;" m/s^2"
  540 PRINT'" Y prop Z pol shear V6 = ";V6;" m/s^2"
  550 PROCpause
  560 CLS
  570 PRINTCHR$(141)+CHR$(157)+CHR$(132);"   Ultrasonic
Wave velocity m/s"
  580 PRINTCHR$(141)+CHR$(157)+CHR$(132);"   Ultrasonic
Wave velocity m/s"
  590 PRINT'" Z prop X pol shear V7 = ";V7;" m/s^2"
  600 PRINT'" Z prop Y pol shear V8 = ";V8;" m/s^2"
  610 PRINT'" Z prop long         V9 = ";V9;" m/s^2"
  620 PRINT'" 101 prop -101 shear V10 = ";VA;" m/s^2"
  630 PRINT" 101 prop Y shear  V11 = ";VB;" m/s^2"
  640 PRINT'" 101 prop long     V12 = ";VC;" m/s^2"
  650 PROCpause
  660 REM NOW READ IN F'/Fo VALUES f'/fo  f'=khz/Kbar
fo=khz
  670  REM EFFECTIVE UNITS ARE KBAR-1
  680 READ F1,F2,F3,F4,F5,F6,F7,F8,F9,F10,F11,F12
  690  @%=&020608
  700 CLS
  710 PRINTCHR$(141)+CHR$(157)+CHR$(132);"        Values
for f'/fo"
  720 PRINTCHR$(141)+CHR$(157)+CHR$(132);"        Values
for f'/fo"
  730 PRINT'"X prop long         F1 = ";F1;" KBar -1"
  740 PRINT'"X prop Y pol shear F2 = ";F2;" KBar -1"
  750 PRINT'"X prop Z pol shear F3 = ";F3;" KBar -1"
  760 PRINT'"Y prop X pol shear F4 = ";F4;" KBar -1"
  770 PRINT'"Y prop longit       F5 = ";F5;" KBar -1"
  780 PRINT'"Y prop Z pol shear F6 = ";F6;" KBar -1"
  790 PROCpause
  800  CLS
  810  PRINTCHR$(141)+CHR$(157)+CHR$(132);"        Values
for f'/fo"
```

```
  820 PRINTCHR$(141)+CHR$(157)+CHR$(132);"        Values
for f'/fo"
  830 PRINT'"Z prop X pol shear F7 = ";F7;" KBar -1"
  840 PRINT'"Z prop Y pol shear F8 = ";F8;" KBar -1"
  850 PRINT'"Z prop longit      F9 = ";F9;" KBar -1"
  860 PRINT'"101 prop -101 shear F10 = ";F10;" KBar -1"
  870 PRINT'"101 prop Y pol shear F11 = ";F11;" KBar -1"
  880 PRINT'"101 prop longit      F12 = ";F12;" KBar -1"
  890 PROCpause
  900 REM NOW CALCULATE pV'- the corrected velocity
derivatives
  910 BM=S1+S2+S3+2*(SE+SB+SU):REM BULK MODULUS
  920 BA=S1+SE+SU:BB=SE+S2+SB:BC=SU+SB+S3:BD=SX+SA+SF
  930 LC=BA:REM LC IS STORE FOR LINEAR COMPRESSIBILITY
  940 REM DERIVITIVES OF DN*V^2 IS PUT BACK INTO F
  950 REM NOTE /1.0E8 CONVERTS FROM KBAR TO NEWTONS/METER
  960 REM DO FOR X DIRECTION
  970 F1=DN*V1*V1*(2*F1/1.0E08+BM-LC*2)
  980 F2=DN*V2*V2*(2*F2/1.0E08+BM-LC*2)
  990 F3=DN*V3*V3*(2*F3/1.0E08+BM-LC*2)
 1000 REM NOW FOR Y DIRECTION
 1010 LC=BB
 1020 F4=DN*V4*V4*(2*F4/1.0E08+BM-LC*2)
 1030 F5=DN*V5*V5*(2*F5/1.0E08+BM-LC*2)
 1040 F6=DN*V6*V6*(2*F6/1.0E08+BM-LC*2)
 1050 REM NOW DO FOR Z DIRECTION
 1060 LC=BC:REM LINEAR COMPRESIBILITY
 1070 F7=DN*V7*V7*(2*F7/1.0E08+BM-LC*2)
 1080 F8=DN*V8*V8*(2*F8/1.0E08+BM-LC*2)
 1090 F9=DN*V9*V9*(2*F9/1.0E08+BM-LC*2)
 1100 REM NOW DO FOR (101) DIRECTION
 1110 LC=BA*0.5+BC*0.5+BD*0.5
 1120 F10=DN*VA*VA*(2*F10/1.0E08+BM-LC*2)
 1130 F11=DN*VB*VB*(2*F11/1.0E08+BM-LC*2)
 1140 F12=DN*VC*VC*(2*F12/1.0E08+BM-LC*2)
 1150 REM NOW GRADIENTS ARE CORRECTED FOR PRESSURE
CHANGES
 1160 CLS
 1170 PRINTCHR$(141)+CHR$(157)+CHR$(132);"   Velocity
derivitives (p*v^2)'"
 1180 PRINTCHR$(141)+CHR$(157)+CHR$(132);"   Velocity
derivitives (p*v^2)'"
 1190 @%=&020306
 1200 PRINT'"      X prop longit      F1 = ";F1
 1210 PRINT'"      X prop Y pol shear F2 = ";F2
 1220 PRINT'"      X prop Z pol shear F3 = ";F3
 1230 PRINT'"      Y prop X pol shear F4 = ";F4
 1240 PRINT'"      Y prop longit      F5 = ";F5
 1250 PRINT'"      Y prop Z pol shear F6 = ";F6
 1260 PROCpause
 1270 CLS
 1280 PRINTCHR$(141)+CHR$(157)+CHR$(132);"   Velocity
derivitives (p*v^2)'"
 1290 PRINTCHR$(141)+CHR$(157)+CHR$(132);"   Velocity
derivitives (p*v^2)'"
 1300 PRINT'"      Z prop X pol shear F7 = ";F7
 1310 PRINT'"      Z prop Y pol shear F8 = ";F8
 1320 PRINT'"      Z prop long        F9 = ";F9
```

```
 1330 PRINT'"    101 prop -101 shear F10 = ";F10
 1340 PRINT'"    101 prop Y pol shear F11 = ";F11
 1350 PRINT'"    101 prop long        F12 = ";F12
 1360  PROCpause
 1370 CLS
 1380 PRINTCHR$(141)+CHR$(157)+CHR$(132);"
Pressure derivitives"
 1390 PRINTCHR$(141)+CHR$(157)+CHR$(132);"
Pressure derivitives"
 1400 REM Z DESIGNITATION IS A PRESSURE DERIVITIVE
 1410 Z6=F2:Z2=F5:Z4=F8:REM C66,C22,C44 CALCULATED
 1420 ZC=(2*F11-Z4-Z6)/2:REM C46 DERIVITIVE
 1430 VDU28,0,24,39,2:REM SET WINDOW
 1440  PRINT'"           d(C22)/dp = ";Z2
 1450  PRINT'"           d(C44)/dp = ";Z4
 1460  PRINT'"           d(C66)/dp = ";Z6
 1470  PRINT'"           d(C46)/dp = ";ZC
 1480 PROCpause
 1490  CLS
 1500  REM CALCULATE REMAINING DERIVITIVES BY EXACT MEANS
 1510 REM P PREFIXES EQUATIONS IN NOTES
 1520 PA=F1+F3
 1530 PB=DN*V1*V1*F3+DN*V3*V3*F1
 1540 PC=F7+F9
 1550 PD=DN*V7*V7*F9+DN*V9*V9*F7
 1560 PE=F10+F12-0.5*(F1+F3+F9+F7)
 1570 REM NOW GET DERIVITIVE OF C55
 1580
Z5=(PE*2*CX*CF+PB*CF+PD*CX-CF*C5*PA-CX*C5*PC)/(CF*C1-CF*C
5+CX*C3-CX*C5)
 1590 Z1=PA-Z5:REM DERIVITIVE OF C11
 1600 Z3=PC-Z5:REM DERIVITIVE OF C33
 1610 ZX=(C1*Z5+C5*Z1-PB)/(2*CX):REM DERIVITIVES OF C15
 1620 ZF=(C3*Z5+C5*Z3-PD)/(2*CF):REM DERIVITIVE OF C35
 1630 REM NOW GET DERIVITIVE OF C13
 1640 M1=(C5+C3+2*CF)*(Z1+Z5+2*ZX)
 1650 M2=(C1+C5+2*CX)*(Z5+Z3+2*ZF)
 1660 M3=-4*(DN*VA*VA*F12+DN*VC*VC*F10)
 1670 M4=2*(CX+CF+CU+C5)
 1680 ZU=(M1+M2+M3)/M4
 1690  ZU=ZU-(ZX+ZF+Z5)
 1700 REM NOW PRINT LAST SIX DERIVITIVES
 1710 CLS
 1720 PRINT'"           d(C11)/dp = ";Z1
 1730 PRINT'"           d(C33)/dp = ";Z3
 1740 PRINT'"           d(C55)/dp = ";Z5
 1750 PRINT'"           d(C15)/dp = ";ZX
 1760 PRINT'"           d(C35)/dp = ";ZF
 1770 PRINT'"           d(C13)/dp = ";ZU
 1780 PROCpause
 1790 REM DATA AREA HERE
 1800 REM ELASTIC CONSTANTS  units NM-2
 1810 DATA 4.4081E10 :REM C11
 1820 DATA 1.6994E10 : REM C13
 1830 DATA -.1733E10 :REM C15
 1840 DATA 3.3424E10 : REM C22
 1850 DATA 2.7343E10 : REM C33
 1860 DATA -.1615E10 : REM C35
```

```
1870 DATA 1.0402E10 : REM C44
1880 DATA 0.0529E10 : REM C46
1890 DATA 1.0745E10 : REM C55
1900 DATA .6062E10  : REM C66
1910 REM NOW COMPLIENCES units 1/nm-2
1920 DATA  3.2160E-11 : REM S11
1930 DATA -1.1296E-11 : REM S12
1940 DATA -1.1804E-11 : REM S13
1950 DATA  1.2229E-12 : REM S15
1960 DATA  5.5932E-11 : REM S22
1970 DATA -3.2903E-11 : REM S23
1980 DATA  4.0755E-12 : REM S25
1990 DATA  6.7648E-11 : REM S33
2000 DATA  1.8853E-12 : REM S35
2010 DATA  9.6140E-11 : REM S44
2020 DATA -8.3896E-13 : REM S46
2030 DATA  9.4337E-11 : REM S55
2040 DATA  1.6497E-10 : REM S66
2050 REM NOW READ IN DENSITY AND VELOCITIES
2060 DATA 1680      : REM DENSITY
2070 DATA 5127.6    : REM V1
2080 DATA 1899.6    : REM V2
2090 DATA 2518.4    : REM V3
2100 DATA 2456.6    : REM V4
2110 DATA 4460.4    : REM V5
2120 DATA 1939.6    : REM V6
2130 DATA 2510.6    : REM V7
2140 DATA 2488.3    : REM V8
2150 DATA 4045.8    : REM V9
2160 DATA 2273.0    : REM V10
2170 DATA 2283.6    : REM V11
2180 DATA 4527.0    : REM V12
2190 REM NOW READ IN f'/fo  units KBar-1
2200 DATA 9.5008E-03 : REM F1
2210 DATA 3.5035E-03 : REM F2
2220 DATA 4.2808E-03 : REM F3
2230 DATA 3.9285E-03 : REM F4
2240 DATA 1.8990E-02 : REM F5
2250 DATA 3.7818E-03 : REM F6
2260 DATA 6.4870E-03 : REM F7
2270 DATA 4.5545E-03 : REM F8
2280 DATA 1.0610E-02 : REM F9
2290 DATA 5.1498E-03 : REM F10
2300 DATA 4.5116E-03 : REM F11
2310 DATA 1.1428E-02 : REM F12
2320  @%=10:STOP
2330  DEF PROCpause:*FX21,0
2340  PRINT'CHR$(136);"       Press a key to continue"
2350  A=GET:ENDPROC
```

REFERENCES.

Adams,L.H., Goranson,R.W. and Gibson,R.E. 1937. Rev. Sci. Instrum., 8, 230

Aleksandrov,K.S. 1958. Sov. Phys. Cryst., 3, 630

Alers,G.A. and Neighbours,J.R. 1957. J. Appl. Phys., 28, 1514

Altman,H.E. and Beyer,R.T. 1976. J. Acoust. Soc. Am., 59, 545

Arenberg,D.L. 1950. J. Appl. Phys., 21, 941

Auld,B.A. 1973. Acoustic fields and waves in solids. John Wiley & Sons

Bateman,T.B. 1966. J. Acoust. Soc. Am., 41, 1011

Bloom,D.M. and F.E. Hohn 1978. Mathematical Methods. Wiley.

Boren,M.D., Babb,S.E. and Scott,G.J. 1965. Rev. Sci. Instrum., 36, 1456

Brassington,M.P. 1982. Phd thesis, University of Bath

Bridgman,P.W. 1911. Proc. Amer. Acad. Arts Sci., 47, 321

Bridgman,P.W. 1940. Phys. Rev., 57, 535

Bridgman,P.W. 1940a. Proc. Amer. Acad. Arts Sci., 74,1

Bridgman,P.W. 1940b. Phys. Rev., 57, 235

Brugger,K. 1964. Phys. Rev., 133, A1611

Brugger,K. 1965. Phys. Rev., 137, A1826

Brugger,K. 1965a. J. Appl. Phys., 36, 759

Decker,D.L., Bassett,W.A., Merrill,L., Hall,H.T. and Barnett,J.D. 1972. J. Phys. Chem. Ref. Data, 1, 3

Deguchi,K. 1979. J. Phys. Soc. Jpn. 47, 153

Deguchi,K. and Nakamura,E. 1977. Phys. Letts., 60A, 351

Dieulesaint and Royer. 1980. Elastic waves in solids - application to signal processing. Pub John Wiley & Sons 1980

Distler,G.J. and Constantinova,W.P. 1968. Nature 218, 762

Ema,K., Katayama,M., Ikeda,Y. and Hamano,K. 1979. J. Phys. Soc. Jap., 46, 347

Ehses,K.H, Meister,H.and Zeyen,C. 1978. Ferroelectrics. 20, 287

Ezhkova,Z.I., Zhdanov,G.S. and Umanskii, M.M. 1959. Sov. Phys. Cryst., 4, 249

Farley,J.M. 1973. Ph.D Theseis (University of Durham)

Fuller,P.J.A. and Price,J.H. 1962. Nature, 193, 262

Furuhata,Y. 1970. J. Phys. Soc. Jpn., 28, 425

Ganesan,S. 1962. Acta Cryst., 15, 81

Geguzina,S.Y. and Krivoglaz,M.A., 1968. Sov. Phys. Solid State, 9,11

Gillespie,S., Schurmann,H.K. and Gilletta,J. 1961. Compt Rend, 1556

Gunton,J.D, and Mihalisin,T. 1974. Solid State Comm., 15, 1753

Haussuhl,S. and Albers,J. 1977. Ferroelectrics, 15, 73

Hoshino,S., Okaya, Y. and Pepinsky,R. 1959. Phys. Rev., 115, 323

Huntington,H.B. 1947. Phys. Rev., 72, 321

Huntington,H.B. 1958. Solid State Physics, 7, 214

Huntington,H.B., Grangoli,S.G. and Mills,J.L. 1969. J. Chem. Phys., 50, 3844

Imai,K., 1977. J.Phys. Soc. Jpn., 43, 1320

Itoh,K. and Mitsui,T. 1973. Ferroelectrics, 5, 235

Kameyama,H., Ishabashi,Y. and Takagi,Y. 1973. J. Phys. Soc. Jpn., 35, 1450

Kawashima,R., Tokunaga,M., and Tatsuzaki,I. 1977. J. Phys. Japan. 42, 903

Kittinger,E. 1977. Ultrasonics, 15, 30

Konstantinova,V.P., Sil'vestrova,I.M. and Aleksandrov,K.S. 1960. Sov. Phys. Cryst., 4, 63

Krupnyi,A.I, Al'chikov,V.V., and Aleksandrov,K.S. 1973. Sov. Phys. Cryst., 16, 692

Kume,S., Machida,M., Mizukusa,S., Taguchi,A. and Nakayama,N. 1980. Rep. Gov. Ind. Res. Inst. Nagoya(Japan), 29, 211

Landau,L.D. and Khalatnikov,I.M. 1954. Dokl. Akad. Nauk SSSR, 96, 469

Lawson,A.W. 1941. Phys Rev 59, 838

Levanyuk,A.P. 1965. Sov. Phys. JEPT. 49, 1304

Lisell,E. 1903. Diss., Upsala

Luspin,Y. and Hauret,G. 1977. Ferroelectrics, 15, 43

Mason, W.P. and McSkimin,H.J. 1947. J. Acoust. Soc. Am., 19, 464

May,J.R. 1958. IRE Nat. Conv. Rec., 6, 134

Michelson,A. 1976. Physical Review B. 14, 4121

Michels,A. and Lenssen,M. 1934. J. Sci. Instrum., 11, 345

Minaeva,K.A., Strukov,B.A., and Varnstorff,K. 1968. Sov. Phys. Solid State, 10, 1665

Minaeva,K.A., Levanyuk,A.P., Strukov,B.A. and Koptsik,V.A. 1967. Sov. Phys. Solid State, 9, 950

Minaeva,K.A., Strukov,B.A. and Thu,C.H. 1970. Sov. Phys. Solid State, 12,5

Minaeva,K.A., Strukov,B.A. and Varnstorff,K. 1969, Sov. Phys. Solid State. 10, 1665

Mitsui,T., Tatsuzaki,I. and Nakamura,E. 1976. An introduction to the physics of ferroelectrics. Gordon and Breach.

Montgomery,P.W., Stromberg,H.D., Jura,G.A. and Jura,G. 1963. High Pressure Measurement. Butterworths

Murnaghan,F.D. 1951. Finite Deformation of an Elastic Solid. Wiley.

Nye,J.F. 1957. Physical Properties of Crystals. Clarendon Press, Oxford

O'Brien,E.J. and Litovitz,T.A., 1964. J. Appl. Phys. 35, 180

Papadakis,E.P. 1964. J. Appl. Phys., 35, 1474

Papadakis,E.P. 1966. J. Acoust. Soc. Am., 40, 863

Papadakis,E.P. 1967. J. Acoust. Soc. Am., 42, 1045

Prawer,S., Smith,T.F. and Finlayson,T.R. 1982, Aust. J. Physics

Roderick,R.L. and Truell,R. 1952. J. Appl. Phys., 23, 267

Samara,G.A. and Giardini,A.A. 1964. Rev. Sci. Instrum., 35,989

Stankowski,J. and Malinowski,W. 1980. Acta Physica Polonica, A58, 773

Strukov,B.A., Kkhanna,S.K. and Minaeva,K.A. 1976. Sov. Phys. Solid State. 18, 1934

Strukov,K.A. and Yakushkin, E.D. 1978. JEPT Lett., 28, 14

Truell,R., Elbaum,C. and Chick,B.B. 1959. Ultrasonic Methods in Solid State Physics. Academic Press, New York.

Thurston,R.N. and Brugger,K. 1964. Phys. Rev., 133, A1604

Thurston,R.N. 1965. Proc. IEEE, 53, 1320

Todo,J. and Tatsuzaki,J. 1976. J. Phys. Soc. Jpn., 37, 1477.

Tylczynski,Z. 1981. Physica, 111B, 267

Wood,E.A. and Holden,A.N. 1957. Acta Cryst., 10, 145

Wallace,D.C. 1972. Thermodynamics of Crystals. Wiley

Wang,C.Y. 1967. Rev. Sci. Instrum., 38, 24

Waterman,P.C. 1959. Phys. Rev., 113, 1247

Zaporozhets,O.I, Lyakhovitskaya,V.A. Pekar,S.I., Polotskii,I.G., and Silvestrova,I.M. 1970. Sov. Phys. Solid State, 12, 523

Zaporozhets,O.I., Tikhonov,L.V. 1981. Sov. Phys. Solid State, 23 ,7